

**RHEOLOGICAL EVALUATION OF CHITONATED FATTY
ACID LIPOSOME IN CARBOHYDRATE-BASED GEL**

TAN HSIAO WEI

**FACULTY OF SCIENCE
UNIVERSITY OF MALAYA
KUALA LUMPUR**

2014

**RHEOLOGICAL EVALUATION OF CHITONATED FATTY
ACID LIPOSOME IN CARBOHYDRATE-BASED GEL**

TAN HSIAO WEI

**THESIS SUBMITTED IN FULFILLMENT OF
THE REQUIREMENTS FOR THE DEGREE OF
DOCTOR OF PHILOSOPHY**

**DEPARTMENT OF CHEMISTRY
FACULTY OF SCIENCE
UNIVERSITY OF MALAYA
KUALA LUMPUR**

2014

ABSTRACT

Liposome in gel preparation has opened up a new dimension in pharmaceutical formulation especially topical application as gels usually have longer contact time with the skin. In this study, the liposomal gel was prepared by mixing surface modified oleic acid (OA) liposomes into a carbohydrate based gel. The surface of oleic acid liposomes was modified using different molecular weight of chitosan (Ch1 and Ch2) and *N*-palmitoyl chitosan with different degree of acylation (Ch2P1 and Ch2P2) thereby providing a cloak structure on the surface of the liposomes.

The surface modification of the OA liposomes by the Chs (Ch1 and Ch2) and Ch2Ps (Ch2P1 and Ch2P2) was characterized using microscope images and physicochemical properties such as zeta potential and the size of the liposomes. The micrographs obtained from the transmission electron microscope (TEM) showed that the Chs-modified and Ch2Ps-modified OA liposomes were spherical in shape and appeared to be dark in colour. It was mainly due to the present of the Chs and Ch2Ps on the lipid surface of the OA liposome that thickened the lipid layer and increased its opacity. The surface modification has also enhanced the OA liposome rigidity. After surface modification, the size of the Chs- and Ch2Ps-modified OA liposomes was decreased by at least 20 nm as compared to the unmodified OA liposomes. The decrease in the liposome size was also accompanied with the increase of their zeta potential. The increase of the zeta potential of the surface modified OA liposome from -86 mV to -60 mV indicated that the Chs and Ch2Ps had successfully modified the surface of OA liposomes.

The carbohydrate based gel was prepared from the mixture of iota carrageenan (*ι*C) and carboxymethyl cellulose (CMC). The presence of CMC in *ι*C gel showed the improvement of the flexibility and cohesive energy of the gel. The gel mixture with 5:5

ι C to CMC ratio has been found to be the optimum composition. Under this optimum composition, the gel matrix showed optimum flexibility and elasticity. The liposomal gels were prepared by dispersing the liposomes into the optimized gel matrix. Based on the rheological results, the presence of liposomes enhanced the elasticity and viscosity of the liposomal gel. The liposomal gels showed greater shear thinning effect indicating a better spreading ability of the liposomal gels as compared to the pure 5:5 ι C-CMC mixed gel. However, the changes in the viscous modulus (G'') and the n value obtained from creep test that described the physical entanglements within the liposomal gel were negligible. These results indicated that the liposomes do not alter the internal gel network structure, but accommodated in the void spaces in the gel. At the same time, the gel matrix could act as a protective layer for the liposomes towards disruption effect from the environment.

ABSTRAK

Pengenalan liposom ke dalam gel telah membuka suatu dimensi yang baru dalam formulasi farmaseutikal terutamanya untuk applikasi topikal kerana pada umumnya gel mempunyai masa pendedahan terhadap kulit yang lebih panjang. Dalam kajian ini, gel liposom disediakan dengan mencampurkan liposom asid oleik (OA) yang permukaannya diubahsuai. Pengubahsuaian permukaan liposom asid oleik dilakukan dengan menggunakan kitosan yang mempunyai berat molekul yang berlainan (Ch1 dan Ch2) dan *N*-palmitoyl kitosan yang mempunyai darjah penghasilan yang berlainan (Ch2P1 dan Ch2P2) untuk menghasilkan suatu lapisan yang meliputi permukaan liposom tersebut.

Sifat-sifat liposom OA yang permukaannya diubahsui dengan menggunakan Chs (Ch1 dan Ch2) dan Ch2Ps (Ch2P1 dan Ch2P2) telah dikenalpasti dengan menggunakan imej mikroskop elektron dan sifat fizikokimia seperti keupayaan Zeta dan saiz liposom. Imej liposom yang diperolehi dengan menggunakan mikroskop pancaran elektron (TEM) menunjukkan bahawa liposom OA yang diubahsuaikan dengan Ch dan Ch2P adalah berbentuk sfera dan legap. Ini disebabkan oleh kehadiran Ch dan Ch2P pada permukaan lipid liposom OA yang telah menambahkan ketebalan lapisan lipid dan kelegapan liposom tersebut. Pengubahsuaian liposom OA dengan Ch dan Ch2P juga dapat mempertingkatkan ketegaran liposom tersebut. Setelah pengubahsuaian permukaan dilakukan, saiz bagi liposom OA yang permukaannya diubahsuai dengan Ch dan Ch2P tersebut telah menurun sebanyak 20 nm berbanding dengan liposom OA. Selain itu, keupayaan Zeta bagi liposom OA yang permukaannya diubahsuai meningkat dari -86 mV ke -60 mV. Keputusan ini menunjukkan Ch dan Ch2P telah berjaya mengubahsuaikan permukaan liposom tersebut.

Dalam kajian ini, gel kabohidrat disediakan dari campuran iota karagenan (ι C) dan karboksimetil selulosa (CMC). Kehadiran CMC di dalam gel ι C telah meningkatkan kekenyalan dan tenaga jeleketan bagi gel tersebut. Gel campuran yang disediakan dengan nisbah 5:5 (ι C:CMC) merupakan komposisi optimum. Di bawah komposisi optimum tersebut, matriks gel ini telah menunjukkan keterlenturan dan kekenyalan yang optimum. Gel liposom telah disediakan dengan menyebarkan liposom ke dalam matriks gel dengan komposisi optimum. Mengikut hasil kajian reologi, kehadiran liposom dalam gel telah mempertingkatkan kekenyalan dan kelikatan gel liposom. Gel liposom ini juga mempamerkan sifat pencairan ricihan yang lebih tinggi berbanding dengan gel 5:5 (ι C:CMC) dan menunjukkan gel liposom ini boleh disebar dengan lebih mudah. Walaubagaimanapun, perubahan dalam modulus kelikatan dan nilai n yang diperolehi dari ujian rayap yang menggambarkan keadaan berbelit antara rantaian polimer bagi gel didapati tiada perubahan untuk gel liposom. Hasil kajian ini menunjukkan kehadiran liposom dalam gel tidak mengganggu struktur rangkaian gel, tetapi hanya menepatkan diri di dalam ruang kekosongan di dalam gel. Pada masa yang sama, gel matriks tersebut juga dapat menjadi suatu lapisan perlindungan bagi liposom terhadap gangguan dari sekitaran.

ACKNOWLEDGEMENT

I would like to take the opportunity to express my appreciation to many people that have made this dissertation possible. First of all, I would like to express my sincere gratitude to my supervisor Prof. Dr. Misni Misran for his valuable guidance, brilliant discussion, supervision and patience throughout the course of this research.

Special thanks to the Ministry of Science, Technology and Innovation (MOSTI) and the University of Malaya that have generously been giving financial support towards my PhD study. My heartfelt gratitude also goes out to all lecturers and staffs in the Department of Chemistry for their assiduous dedication and also the University of Malaya management.

I would like to render my appreciation to my colleagues for their experiences, advices and guidance on theories and operation of the instruments. I would also like to thank the members of Colloid and Surfaces Laboratory for their encouragement and assistance throughout the research.

Last but not least, I would like to extend my deepest gratitude to my beloved parents, my sister and my husband Dr. Tay Kheng Soo for encouraging and inspiring me all these years.

Table of Contents

ABSTRACT	ii
ABSTRAK	iv
ACKNOWLEDGEMENTS	vi
TABLE OF CONTENTS	vii
LIST OF FIGURES	x
LIST OF TABLES	xvi
LIST OF ABBREVIATIONS	xviii
LIST OF PUBLICATIONS	xx

Chapter 1	Introduction	Page
1.0	Gels and their application in cosmetic and pharmaceutical industries.....	1
1.1	Type of carrier in drug delivery systems.....	3
1.1.1	Liposome in gel.....	6
1.2	Liposomes as drug carrier.....	10
1.2.1	Surface modified liposomes.....	13
1.2.2	Chitosan modified liposomes.....	19
1.2.2.1	Chitosan.....	21
1.2.2.2	Solubility of chitosan in aqueous solution.....	22
1.3	Fatty acid liposomes.....	24
1.4	Potential application of liposomes in dermal/transdermal delivery systems.....	27
1.5	Rheology of gel and its topical applications.....	30
1.6	Objective.....	32

Chapter 2 Materials and Methods

2.0	Materials	33
2.1	Preparation of depolymerized chitosan.....	33
2.2	Preparation of <i>N</i> -acylated chitosan.....	34
2.3	Preparation of oleic acid liposome and chitosan-modified oleic acid liposomes.....	34

2.4	Preparation of γ C and CMC gel.....	35
2.5	Preparation of liposomal gels.....	36
2.6	Instrumentation.....	36
2.6.1	Centrifugation	36
2.6.2	Chitosan structural analysis.....	36
2.6.2.1	Fourier transform infrared spectroscopy (FT-IR) ...	36
2.6.2.2	^1H -NMR.....	37
2.6.3	Average molecular weight determination.....	37
2.6.4	Determination of chitosan solubility by UV-Vis spectroscopy...	39
2.6.5	Surface tension measurement.....	40
2.6.6	Size and Zeta potential.....	40
2.7	Morphological study.....	40
2.7.1	Optical polarizing microscope imaging.....	40
2.7.2	Confocal microscope.....	41
2.7.3	Atomic force microscope (AFM) imaging.....	41
2.7.4	Transmission electron microscope (TEM) imaging.....	41
2.8	Rheological study.....	42
2.8.1	Dynamic oscillation measurement.....	42
2.8.2	Temperature sweep.....	43
2.8.3	Creep-recovery test.....	44
2.8.4	Steady flow measurement.....	48
2.8.5	Thixotropic behavior study.....	50
2.9	Statistic.....	51

Chapter 3 Results and Discussion

3.1	Characterization of chitosan.....	52
3.1.1	FT-IR analysis	52
3.1.2	^1H -NMR analysis	53
3.1.3	Average molecular weight determination.....	55
3.1.4	Determination of chitosan solubility	56
3.2	Characterization of OA and Chitosan-modified OA liposomes.....	57
3.2.1	Titration curve.....	57
3.2.2	Surface tension.....	61
3.2.3	Morphology of liposomes.....	63
3.2.3.1	Optical polarizing micrographs.....	63

3.2.3.2	TEM and AFM micrographs.....	65
3.2.4	Size of liposomes.....	68
3.2.5	Zeta potential of liposomes.....	71
3.2.6	Liposome stability.....	72
3.3	Rheological study of ι C-CMC mixed gel.....	74
3.3.1	Rheological behavior of ι C and CMC pure gel	74
3.3.2	Gelation temperature of ι C-CMC mixed gel.....	78
3.3.3	Dynamic behavior of ι C-CMC mixed gel	79
3.3.4	Creep and recovery of ι C-CMC mixed gel.....	84
3.3.5	Flow behavior of ι C-CMC mixed gel.....	90
3.3.6	Thixotropic behavior of ι C-CMC mixed gel.....	92
3.4	Liposomal gels.....	94
3.4.1	Morphology of liposomal gels.....	95
3.4.2	Rheological properties of liposomal gels.....	96
3.4.2.1	Gelling temperature of liposomal gels	96
3.4.2.2	Dynamic behavior of liposomal gels	97
3.4.2.3	Creep and recovery of liposomal gels	101
3.4.2.4	Flow behavior of liposomal gels.....	107
3.4.2.5	Thixotropic behavior of liposomal gels.....	110
4.0	Conclusion	112
4.1	Future work.....	113
5.0	References	115
	Appendix	139

List of Figures

Chapter 1	Introduction	Page
Figure 1.1	Molecular structure of (a) carboxymethyl cellulose (CMC) and (b) <i>ι</i> -carrageenan (<i>ι</i> C).....	7
Figure 1.2	Unilamellar liposome showing the enclosed structure of the liposome.....	10
Figure 1.3	Different types of liposomes classified based on the liposomal structure and their fluorescence micrographs. (a) Fluorescence micrograph of unilamellar liposome; (b)(i) and (ii) shows the appearance of multilamellar liposomes; and (c) Fluorescence micrograph of multivesicular or oligomer liposomes.....	12
Figure 1.4	Surface modified liposome. The presence of the polymers on the surface of the liposome can act as steric shield that decreases the accessibility of the proteins which mark the liposome for recognition and removal by phagocyte system.....	14
Figure 1.5	Hydrophobic moieties from the polysaccharide backbone anchored into the lipid bilayer of liposome.....	19
Figure 1.6	The molecular structure of chitosan with n is the number of repeating unit where $R = H$ or $COCH_3$	21
Figure 1.7	The sequence of <i>N</i> -acetyl-D-glucosamine and D-glucosamine residues at chitosan chains. (a) Random-type distribution of <i>N</i> -acetyl-D-glucosamine and D-glucosamine residues which can be prepared from alkaline treatment under dissolved state. (b) Block-type distribution of <i>N</i> -acetyl-D-glucosamine and D-glucosamine residues which can be prepared at high temperatures under solid-state reaction conditions.....	23
Figure 1.8	(a) Images of the physical appearance of (i) micelles, (ii) liposomes, and (iii) emulsions. (b) Titration curve indicating the regions for the formation of (I) micelles, (II) coexistence of micelle and liposomes, (III) liposomes, (IV) coexistence of liposomes and emulsion, and (V) emulsion.....	25

Figure 1.9	The possible penetration route of the drug-loaded liposome through the stratum corneum, (A) the loaded drug release on the surface of the stratum corneum, (B) liposome adsorption or fusion with the stratum corneum and release the drug payload, (C) liposome penetration through intercellular diffusion in the stratum corneum, and (D) liposome penetration via transcellular diffusion through keratinocytes and lipid lamellae.....	27
Chapter 2	Materials and Methods	
Figure 2.1	The linear viscoelastic region (LVR) of gels.....	43
Figure 2.2	Sinusoidal stress response which shifted by an amount of δ to the sinusoidal strain deformation for viscoelastic material...	43
Figure 2.3	(I) Constant moduli showing the thermal stability of the gel ($G' > G''$). (II) Deformation of the internal gel network structure at high temperature ($G'' > G'$). The cross point between the G' and G'' profiles show the gelling temperature of the examined gel.....	44
Figure 2.4	Creep and recovery curves for (i) an ideal elastic material, (ii) an ideal viscous material, and (iii) a viscoelastic material.....	45
Figure 2.5	Creep and recovery profile for Burger's model.....	46
Figure 2.6	Burger's model which consists of Maxwell model and Kelvin-Voigt model in series.....	47
Figure 2.7	(a) Typical viscosity curve of pseudoplastic gel that showing shear thickening behavior at low shear rate. When the applied shear rate exceeded the yield point, the viscosity of the gel started to decrease with increasing shear rate and shows shear thinning behavior. (b) Yield stress determination from shear viscosity versus shear stress curve.....	49
Figure 2.8	Time dependent viscosity profile of (a) rheopectic systems for shear thickening materials, (b) thixotropic for shear thinning materials, and (c) the hysteresis loop of thixotropic gel.....	50

Chapter 3 Results and Discussion

Figure 3.1	FT-IR spectra of (a) Ch2, (b) Ch2P1 (DA= 8 ± 2 %), and (c) Ch2P2 (DA= 18 ± 2 %).	52
Figure 3.2	NMR spectra for (a) Ch2, (b) Ch2P1, and (c) Ch2P2 where D is the glucosamine group and A is the <i>N</i> -acetyl or <i>N</i> -acyl glucosamine group of the chitosan.	54
Figure 3.3	Chemical equation of the depolymerization of chitosan by sodium nitrite.	56
Figure 3.4	Formation of NO^+ from the salt of nitrous acid for the depolmerization process.	56
Figure 3.5	Water solubility of Ch1, Ch2, Ch2P1, and Ch2P2.	57
Figure 3.6	Equilibrium titration curve of oleate/oleic acid and the buffering effect (from pH 10-9) when the oleate and OA were coexists (a). The changes of the OA solution appearance with decreasing pH from (b)(i) the clear micellar region ($> \text{pH } 10$) to the formation of liposomes showing turbid appearance (pH 10 - 8.0) (b)(ii) and finally to milky appearance of emulsion ($< \text{pH } 8$) (b)(iii). The equilibrium titration curves for (c) OA + Ch1, (d) OA + Ch2, (e) OA + Ch2P1, and (f) OA + Ch2P2. All the titration curves were obtained at room temperature.	58
Figure 3.7	Surface tensions profile of the (■) OA, (○) OACH1 (0.20%), (▲) OACH2 (0.20%), (●) OACH2P1 (0.20%), and (▼) OACH2P2 (0.20%) liposome solutions respectively as a function of \ln concentration at pH 8.8 ± 0.1 in 0.05 mol dm^{-3} borate buffer solution at 25°C .	62
Figure 3.8	The optical polarizing micrograph of (a) OA liposome which showed birefringence effect, (b) OA liposome under dark field which showed Maltese cross, (c) OACH1 liposome, (d) OACH2 liposome, (e) OACH2P1, and (f) OACH2P2 liposome.	64
Figure 3.9	TEM image of the (a) OA liposomes, (b) OACH1 liposomes, (c) OACH2 liposomes, (d) OACH2P1 liposomes, and (e) OACH2P2 liposomes. The amount of chitosan used in the preparation of the OACH2 liposome was 0.20%.	65

Figure 3.10	AFM image of (a) OA liposome, (b) OACH1, (c) OACH2, (d) OACH2P1, and (e) OACH2P2. All the chitosan modified OA liposomes were prepared with 0.20 % (w/v) of chitosan and its derivatives. (The liposomes were indicated by the black arrows).....	67
Figure 3.11	Effect of the amount of Ch1, Ch2, Ch2P1, and Ch2P2 on the size and zeta potential of the OA liposome. The data was taken at day seventh after the liposome solutions were prepared.....	69
Figure 3.12	(a) The typical size distribution of the OA liposome showing its polydispersity. (b) The polydispersity index for the OA liposome and chitosan-modified OA liposomes.....	70
Figure 3.13	The effect of (\square) Ch1, (\circ) Ch2, (\blacktriangle) Ch2P1, and (\blacktriangledown) Ch2P2 amount of the zeta potential of the OA liposome.....	72
Figure 3.14	Variation of size of (a) OACH1, (b) OACH2, (c) OACH2P1, and (d) OACH2P2 liposomes.....	73
Figure 3.15	The rheological behavior of the (\blacksquare) ιC and (\bullet) CMC obtained at 25°C where (a) the strain sweep profile, (b) the variation of G' (solid symbol) and G'' (open symbol) as a function of frequency, (c) the $\tan \delta$, and (d) the flow curve.....	76
Figure 3.16	Gelation temperature of mixed gel. (a) pure ιC gel, (b) pure CMC solution, and (c) gelation temperature of the mixed gels as a function of the ιC weight fraction.....	79
Figure 3.17	The dynamic mode rheology of the mixed gel with ιC -CMC ratio of (\blacklozenge)3:7, (\blacktriangledown)4:6, (\blacktriangle)5:5, (\bullet)7:3, and (\blacksquare)8:2 mixed gels obtained at 25°C where (a) is the strain sweep profile, (b) is the plot of shear stress versus strain to determine the γ_c , (c) is the variation of G' (solid symbol) and G'' (open symbol) as a function of frequency, and (d) is the $\tan \delta$ of the mixed gels.....	81
Figure 3.18	Creep and recovery profiles for the mixed gels with ιC -CMC ratio of (\blacklozenge)3:7, (\blacktriangledown)4:6, (\blacktriangle)5:5, (\circ)7:3, and (\blacksquare)8:2 performed under 0.1 Pa constant stresses at 25°C.....	85
Figure 3.19	$\ln J(t)$ versus $\ln t$ plot (solid symbol) and $\ln G(t)$ versus $\ln t$ plot (open symbol) for the mixed gels with ιC -CMC ratio of (\blacklozenge)3:7, (\blacktriangledown)4:6, (\blacktriangle)5:5, (\bullet)7:3, and (\blacksquare)8:2 mixed gels that showed the reciprocal relationship between the $J(t)$ and $G(t)$	87

Figure 3.20	The flow behavior of the mixed gel with ι C-CMC ratio of (♦)3:7, (▼)4:6, (▲)5:5G, (●)7:3, and (■)8:2 where (a) is the shear viscosity profile of the mixed gels with increasing shear rate and (b) is the shear stress versus shear rate profile for the determination of yield stress (σ_p) of the mixed gels.....	91
Figure 3.21	Thixotropic plot for mixed gel.....	94
Figure 3.22	The fluorescence images of (a) OA in solution, (b) LG-OA, (c) LG-OACh1, and (d) LG-OACh2P1. The liposomes were indicated with arrows.....	96
Figure 3.23	The strain sweep profile of the (■)5:5 ι C-CMC mixed gel where (●)LG-OA, (▲)LG-OACh1, (▼)LG-OACh2, (◄)LG-OACh2P1, and (►)LG-OACh2P2 LGs that obtained at 25°C.	99
Figure 3.24	The variation of G' (solid symbol) and G'' (close symbol) as a function of frequency of the (■)5:5 ι C-CMC mixed gel where (●)LG-OA, (▲)LG-OACh1, (▼)LG-OACh2, (◄)LG-OACh2P1, and (►)LG-OACh2P2 LGs that obtained at 25°C...	99
Figure 3.25	The $\tan \delta$ of the (■)5:5 ι C-CMC mixed gel where (●)LG-OA, (▲)LG-OACh1, (▼)LG-OACh2, (◄)LG-OACh2P1, and (►)LG-OACh2P2 LGs that obtained at 25°C.....	100
Figure 3.26	Creep and recovery profiles for (■)5:5 ι C-CMC mixed gel, (□)LG-OA, (▼)LG-OACh1, (○)LG-OACh2, (◊)LG-OACh2P1, and (◻)LG-OACh2P2 that performed at 0.1 Pa constant stresses at 25 °C.....	101
Figure 3.27	(a) Gel matrix representing internal network structure of blank gel and liposomal gels before creep; (b) during creep, the pure 5:5 ι C-CMC mixed gel deformed more as compared to the liposomal gel where the $\theta > \theta'$	102
Figure 3.28	The (a) $\ln J(t)$ versus $\ln t$ plot and (b) $\ln G(t)$ versus $\ln t$ plot of the pure 5:5 ι C-CMC mixed gel and liposomal gels showing the reciprocal relationship between the $J(t)$ and $G(t)$	103
Figure 3.29	Schematic network structure of the 5:5 ι C-CMC mixed gel matrix (a) loaded with OA liposome and (b) chitosan-modified OA liposomes. They grey area is the possible hydrogen bonding zone between the gel network structure and the liposomes.....	106

Figure 3.30	(a) Viscosity curves of the liposomal gels. (b) The flow curve of the (■)5:5 ι C-CMC mixed gel, (●)LG-OA, (▲)LG-OACh1, (▼)LG-OACh2, (◀)LG-OACh2P1, and (◆)LG-OACh2P2.....	109
Figure 3.31	Thixotropic plot for liposomal gels.....	110

List of Table

Chapter 1	Introduction	Page
Table 1.1	The classification of liposomes and their size	11
Table 1.2	Polymers used for the modification of liposome surface.....	16
Chapter 2	Materials and Methods	
Table 2.1	Volume of NaNO ₂ used in the depolymerisation reaction of chitosan.....	34
Table 2.2	The final concentration of the gel mixtures.....	36
Chapter 3	Results and Discussion	
Table 3.1	Average molecular weight of the depolymerized chitosan with different amount of sodium nitrite and the degree of deacetylation.....	55
Table 3.2	p <i>K_a</i> of the pure OA and its mixture with Ch1, Ch2, Ch2P1, and Ch2P2.....	60
Table 3.3	CVC of OA, OACH1, OACH2, OACH2P1, and OACH2P2 liposome solutions at constant temperature of 25 °C.....	63
Table 3.4	The critical strain (γ_c), break point (γ_b), elastic modulus (G'), cohesive energy (CE), and yield stress (σ_p) of the ιC and CMC that determined from their dynamic and steady rheological behaviors.....	76
Table 3.5	The Critical strain (γ_c), break point (γ_b), elastic modulus (G'), cohesive energy (CE), and yield stress (σ_p) of the mixed gels determined from respective dynamic rheological behaviors.....	83
Table 3.6	Strain corresponded to Maxwell element (γ_0), strain correspond to Kelvin-Voigt element (γ_I), G_0 , G_I , η_0 , η_I , and delay time, λ_{ret} for ιC -CMC mixed gels. The percentage of deformation of each element in the Burger's model (J_{SM} , J_{KV} , and J_∞) and the percentage of recovery for the entire gel system ($R\%$) at $t=300$ s, the strength of junction zone, and degree of entanglement for ιC -CMC mixed gels.....	88

Table 3.7	Shear viscosity, Power Law Index (<i>PLI</i>), and yield stress (σ_p) of the mixed gels which determined from their steady rheological behaviors.....	90
Table 3.8	Degree of thixotropy, pseudoplastic index, and thixotropic index of the mixed gels.....	93
Table 3.9	Gelation temperature of liposomal gels.....	97
Table 3.10	The critical strain (γ_c), break point (γ_b), elastic modulus (G'), cohesive energy (CE), and yield stress (σ_p) of the liposomal gels which determined from their dynamic and steady rheological behaviors.....	100
Table 3.11	Strain corresponds to Maxwell element (γ_0), strain corresponds to Kelvin-Voigt element (γ_1), G_0 , G_1 , η_0 , η_1 , and delay time, λ_{ret} for the liposomal gels. The percentage of deformation of each element in the Burger's model (J_{SM} , J_{KV} , and J_∞), the percentage of total recovery ($R\%$) at $t=300$ s, the strength of junction zone, and degree of entanglement for liposomal gels.....	107
Table 3.12	Shear viscosity, Power Law Index (<i>PLI</i>), and yield stress (σ_p) of the liposomal gels which determined from their steady rheological behaviors.....	108
Table 3.13	Degree of thixotropy, pseudoplastic index, and thixotropic index of liposomal gels.....	111

List of Abbreviations

ABC	accelerated blood clearance
AFM	Atomic Force Microscope
<i>CE</i>	Cohesive force
Ch1	Water soluble chitosan with 10 kDa of average molecular weight
Ch2	Water soluble chitosan with 25 kDa of average molecular weight
Ch2P1	Water soluble chitosan with 25 kDa of average molecular weight and 8% of degree of acylation
Ch2P2	Water soluble chitosan with 25 kDa of average molecular weight and 18% of degree of acylation
Chs	Ch1 and Ch2
Ch2Ps	Ch2P1 and Ch2P2
CMC	carboxymethylcellulose
CVC	Critical vesicular concentration
DA	Degree of acylation
FT-IR	Fourier transform infrared spectroscopy
¹ H-NMR	Proton Nuclear magnetic resonance
<i>ι</i> C	iota carrageenan
LVR	linear viscoelastic region
OA	Oleic acid
OACH1	Ch1-coated oleic acid liposome
OACH2	Ch2-coated oleic acid liposome
OACH2P1	Ch2P1-coated oleic acid liposome
OACH2P2	Ch2P2-coated oleic acid liposome
PEG	polyethylene glycol
<i>PLI</i>	Power Law Index
SLS	Static Light Scattering
TEM	Transmission Electron Microscope
UV-Vis	Ultraviolet-visible
<i>G'</i>	elastic modulus
<i>G''</i>	viscous modulus
<i>T_{gel}</i>	Gelling temperature
δ	Phase in radian

γ	Shear strain
γ_c	Critical strain
γ_b	Break point where the $G' < G''$ (strain sweep profile)
η	Shear viscosity
$\dot{\gamma}$	Shear rate
σ_p	Yield stress
J	compliance
λ_{ret}	retardation time
G_o	instantaneous elastic modulus from the Maxwell model in the Burger's model
η_o	residual viscous flow from the Maxwell model in the Burger's model
G_I	retarded elastic from the Kelvin-Voigt model in the Burger's model
η_I	internal viscosity from the Kelvin-Voigt model in the Burger's model
J_{max}	maximum compliance
J_{KV}	Retarded recovery
J_{SM}	Instantaneous recovery
J_{∞}	permanent deformation
$\% J_e$	Contribution of the four elements in Burger's model to the total deformation ($e = SM, KV$, and ∞)
$\% R_e$	recovery percentage ($e = SM, KV$, and ∞)
n	Degree of entanglement
S	Strength of junction zone

List of Publications

Tan, H.W. and Misran, M. (2012) Characterization of fatty acid liposome coated with low molecular weight chitosan. *Journal of Liposome Research* 22:329-335.

Tan, H.W. and Misran, M. (2013) Polysaccharide-anchored fatty acid liposome. *International Journal of Pharmaceutics* 441:414-423.

Tan, H.W. and Misran, M. (2014) Effect of chitosan-modified fatty acid liposomes on the rheological properties of the carbohydrate-based gel. *Applied Rheology* (accepted).

CHAPTER 1

1.0 Gels and their application in cosmetic and pharmaceutical industries

Gels are soft solid masses composed of a three-dimensional macroscopic network of structures that can entrap large volumes of solvent within the network (Ajayaghosh et al., 2008). Gels are classified as soft solids because they can withstand their own weight without collapsing and at the same time exert some degree of flexibility (Estroff and Halmilton, 2003). In general, gels can be classified into two categories based on their gelling mechanism; colloidal gel and polymeric gel (Partlow and Yoldas, 1981). For a colloidal gel system, its gelling ability is a result of the electrostatic effects of the colloidal particles. These colloidal particles can link together via attractive bond or floc to form an interlaced network (Barlett et al., 2012; Ilg and Gado, 2011; Pemetti et al., 2007). Polymeric gels, however, are a cross-linked network of polymer chains. They can be formed via covalent cross-link or physical entanglement of the polymer chains (Grillet et al., 2012; Picout and Ross-Murphy, 2002). Polymeric gels are commonly used as the matrix in the pharmaceutical and cosmeceutical industries as carrier in which medicinal or cosmetic active ingredients are incorporated. This is because the fluid filling interstitial space within the polymer gel network not only provides continuous moisturising effect to the skin, it also effectively disperses the medicinal or cosmetically active ingredients homogeneously throughout the gel matrix (Kumar et al., 2009; Kwon and Gong, 2006; Saha and Bhattacharya, 2010).

Although polymeric gels can be prepared from synthetic polymers such as silicon and poly(*N*-isopropylacrylamide), the concept of using natural biopolymers such as polysaccharides in the preparation of polymeric gels for cosmetic and pharmaceutical applications has attracted growing interest over the recent years (Peppas and Huang,

2002; Singh, 2011). This is due to the characteristics of the polysaccharides as they are biocompatible, biodegradable, edible, and they are available from natural sources such as plants and living organisms (Klein, 2009). Traditionally, polysaccharides were used as viscosity modifiers, thickening agents, hair conditioners, moisturisers, hydrates, and emollients in various cosmetic and pharmaceutical products (Gruber, 1999). However, polysaccharides have played an even more important role in the modern cosmetic and pharmaceutical formulations, especially as drug carriers. Due to their adhesive property, polymer gels can also become the supporting layer in the topical and transdermal patch delivery systems such as DuoDERM[®], CitruGel[®], and Hydrocoll[®] (Kim et al., 2013; Munarin et al., 2012; Wokovich et al., 2006; Xi et al., 2013). This supporting layer not only helps to protect the dispersed drugs from the environment, but also helps to deliver the dispersed drugs through the skin into the body. Besides biocompatible and biodegradable, the polysaccharide gels such as pectin (Morris et al., 2010), carrageenan (Miyazaki et al., 2011), and carboxymethyl cellulose (Palmer et al., 2011) that are used as drug carriers and supporting matrix in controlled release drug delivery systems have also been reported to exhibit bioadhesive characteristics (Dew et al., 2009; Mourtas et al., 2009; Qiu and Park, 2001).

The delivery of drugs from gel matrix into the skin requires successful penetration of the drugs through the main skin barrier, stratum corneum, as it limits permeation of many active therapeutic agents because of its highly organised structure (Osborne et al., 2013; Touitou and Godin, 2007). For this reason, skin penetration enhancers such as sulphoxides, azones, pyrrolidones, alcohols, glycols, surfactants, and terpenes were used in topical and transdermal applications in order to increase the delivery efficiency through the percutaneous route (Gwak and Chun, 2002; Karande et al., 2005; Williams and Barry, 2004). They are known to induce structural changes in the stratum corneum by disrupting the tightly packed lipid layer, which consequently

increases the drug penetration through the skin (Barry, 1987; Moghadam et al., 2013). However, the use of skin penetration enhancers has often triggered undesired immune system reactions such as irritation, allergy or inflammation. Most skin penetration enhancers are also not specific and allow the penetration of small lipophilic compounds. This is particularly observed in cosmetic formulations where the fragrance compounds and preservatives will penetrate along with the active ingredients through the skin (Dayan, 2005). These problems can be minimised by encapsulating the drugs or active ingredients into carriers such as colloidal particles and liposomes and at the same time can also improve the percutaneous absorption of the drugs from the gel matrix (Mezei and Gulasekharam, 1980).

1.1 Type of carriers in drug delivery systems

Several particulate drug carriers such as colloidal particle systems and lipid-based drug delivery systems have been widely developed in order to improve the drug therapeutic efficacy by enhancing the specific targeted ability of the drug carrier systems (Peer et al., 2007). The colloidal particle systems can be inorganic-based, polymer-based or lipid-based particles (Gaumet et al., 2008). These colloidal particle systems consist of small colloidal particles with diameters ranging from hundreds to thousands of micrometers (Abraham et al., 2011; Zamiri and Gemeinhart, 2006). Of these colloidal particle systems, the inorganic-based particles such as silica nanoparticles, carbon nanoparticles and gold nanoparticles, which can be porous in nature, are known to be physically and chemically stable and exhibit a prolonged drug release profile (Anitha et al., 2012; Bianco et al., 2005; He et al., 2004; Prakash et al., 2011). For effective drug delivery applications, the drugs or active ingredients are loaded into the pores of these particles via adsorption or capillary filling, and their release profiles can be altered by controlling

the pore size and pore surface chemistry (Jiang and Brinker, 2006; Liu et al., 2009). Such inorganic particles can also be designed as hollow particles (Im et al., 2005; Koike et al., 2013; Zhang et al., 2009). The hollow structures were also used in drug delivery application due to the presence of a large fraction of void within the particle that could accommodate large amounts of drugs and active ingredients (Fuji et al., 2007; Lou et al., 2008; Yang et al., 2013). Besides, the surface of the hollow particles can be further modified using amino acids or polymers for controlled released and targeted delivery (You et al., 2013; Zhu et al., 2011).

Compared with the inorganic-based particle, the polymeric colloidal particles are used to load both small molecule drugs as well as biomacromolecules such as proteins and peptides (Leong et al., 2011; Teng et al., 2013; Zhang and Ma, 2013). Poly(lactic-co-glycolic acid) (PLGA) is currently one of the most frequently used polymers in the preparation of polymeric particle drug delivery systems (Choi et al., 2012; Klose et al., 2008; Samadder et al., 2013; Zeng et al., 2013). It is also one of the US FDA approved polymers for medical purposes. However, some problems are associated with the use of polymeric colloidal particles in the drug delivery system i.e. the slow release profile of its drug load. Owing to the fact that each polymer has its own specific physicochemical properties, it becomes difficult to obtain desired drug release profile from these polymer matrixes that involved slow degradation or dissolution of the polymer matrix (Gemeinhart, 2006). As shown in the earlier studies, it may take up to a few weeks for a total *in vivo* degradation or dissolution of the polymer matrix (D'Souza and DeLuca, 2006; Gupta et al., 2001; Gutowska et al., 1995; Hiremath et al., 2013). Also, some polymeric materials were cytotoxic after phagocytosis that caused irritation *in vivo* and could only be partially overcome by incorporating anti-inflammatory drugs (Müller et al., 1996; Smith and Hunneyball, 1986). The polymeric colloidal particles were also found to have a limited drug loading capacity. As a result, large excessive amounts of

the polymeric colloidal particles were needed to achieve sufficient drug supply (Gemeinhart, 2006; Tan et al., 2009).

The lipid nanoparticle is another example of a colloidal particle drug carrier which was designed in the early 1990s (Blasi et al., 2013; Üner, 2006). The lipid nanoparticle drug carrier was designed as an alternative to the polymeric colloidal particle (Ekambaram et al., 2012) and oil-in-water emulsion in parenteral nutrition (Mehnert and Mäder, 2001). It could be suspended in aqueous medium and provided a higher drug loading capacity compared with the polymeric and emulsion types of drug carrier (Ekambaram et al., 2012; Mehnert and Mäder, 2001). The lipid nanoparticle drug delivery system is a perfect system for the delivery of lipophilic drugs such as retinol (Westesen et al., 1997) and doxorubicin (Cavali et al., 1993). However, the lipid nanoparticle is not entirely suitable for hydrophilic drugs. This is because of the high partition coefficient of the hydrophilic drug to the aqueous phase which results in the low entrapment efficiency of the hydrophilic drug in the lipid nanoparticle (Üner, 2006).

Liposome drug carrier (lipid-based) are widely investigated as it was discovered by Bangham et al. (1974) (Lasic, 1995; Peer et al., 2007). The higher popularity of liposome as a drug carrier compared with lipid nanoparticle and polymeric-based nanoparticle is mainly attributed to its versatile nature and ability to entrap both hydrophilic and hydrophobic drugs. Liposome can be modified easily in order to achieve passive and/or active targeting. The passive targeting system can be attained by altering the physical properties of the liposome such as size, surface charge, and membrane fluidity (Sato and Sunamoto, 1992; Takeuchi et al., 2001b). On the other hand, the active targeting system can be attained by grafting the liposome surface with targeting ligands such as antibodies (Danhier et al., 2010).

1.1.1 Liposomes in gel

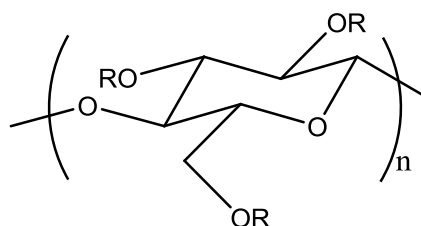
Incorporation of the liposome into a gel is the most common approach used in the preparation of topical and transdermal liposomal formulations. Most pharmaceutical formulations are prepared in gel forms as gels usually have a considerably longer contact time with the skin (Dew et al., 2009). This is an important characteristic of gel as it can prolong the release rate of the liposome from the gel matrix, and thus reduce the dosing frequency of the therapeutic drugs encapsulated within the liposome (Mourtas, Duraj et al., 2008).

Liposomes can disperse in the gel matrix and get accommodated in between the network spaces. There is strong evidence to prove the co-existence of the liposomes in the gel matrix (Dragicevic-Curic et al., 2009; Mourtas et al., 2007). Dispersion of the liposomes into the gel formulation can be visualised using the cryo-electron microscope (Dragicevic-Curic et al., 2009). The electron micrographs revealed that the liposomes were dispersed into the gel with high homogeneity. The size of the dispersed liposome was also unaffected by the presence of gels. Besides, no changes in liposome size were observed during the stability test (six months period of testing). It was also found that the liposomes dispersed in the gel are more stable when compared with the conventional liposomal solution (six months period of testing).

In this study, the liposomes were loaded into the carbohydrate-based gel prepared from a mixture of carboxymethyl cellulose (CMC) and iota carrageenan (ι C). The CMC is a derivative of cellulose with a carboxymethyl group at the hydroxyl group of its glucopyranose monomer backbone, as shown in Figure 1.1(a) (Heinze et al., 1998). It is often used as a binding, thickening, and stabilising agent of various products, especially in the cosmetic and pharmaceutical industries such as creams, lotions, and toothpaste formulations due to its biocompatibility and solubility in water (Benchabane

and Bekkour, 2008; Palmer et al., 2011; Srokova et al., 1998; Wade and Weller, 1994; Weiner, 1991). As shown in Figure 1.1(b), the ι C is a linear sulphated polysaccharide composed of alternating 3-linked β -D-galactopyranose and 4-linked 3,6-anhydro- α -pyranose residues (Gobet et al., 2009; Millane et al., 1988). The water soluble ι C is used in the preparation of food stuffs such as dairy products and jellies, due to its typical gelling strength (Gobet et al., 2009; Gupta et al., 2001). Besides the food industry, the ι C is also widely used in pharmaceutical and cosmetic formulations, in the preparation of soft gel formulations for oral drug delivery systems prescribed for patients with swallowing difficulties (Gupta et al., 2001; Miyazaki et al., 2011; Thrimawithana et al., 2011).

(a)



(b)

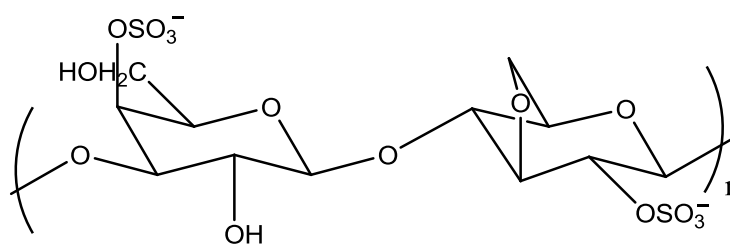


Figure 1.1: Molecular structure of (a) carboxymethyl cellulose (CMC) and (b) ι -carrageenan (ι C).

The pKa of ι C and CMC are 2 and 4.3, respectively (Gu et al., 2004; Magdassi et al., 2003). In other words, at pH levels greater than 4.3, both ι C and CMC behave as polyelectrolytes. As polyelectrolyte polymers, their internal network structure and gel strength become very sensitive to the change of the types of ions, ionic strength, and pH (Bonferoni et al., 1995; Gobet, 2009; Liu et al., 2002; Michailova et al., 1999). According to previous study, ι C formed a strong and transparent gel in the presence of divalent cations (Thrimawithana et al., 2010). This is mainly due to the ability of the divalent cations to interact electrostatically with the two sulphate groups present in the anhydro-D-galactopyranose and D-galactopyranose of the ι C polymer chains. As a result, bridges are formed between the adjacent double helices of the ι C polymer chains and thus, an even more complicated gel network structure is formed (Nijenhuis, 1996). However, the ι C gel formed in the presence of monovalent cations was relatively more flexible and soft when compared with the divalent cations (van de Velde et al., 2003), mainly because of the less inter-helical aggregation of the double helical structure of the ι C polymer chains with the monovalent cations (Gobet, 2009; Yuguchi et al., 2003). Unlike divalent cations, the monovalent cations can only interacted ionically with one of the sulphate groups of the ι C chains and is followed by the formation of secondary electrostatic interactions with the sulphate groups or the anhydro-bridge oxygen atom of the galactose unit from the adjacent double helices of the ι C polymer chains. This secondary electrostatic interaction is relatively weak when compared with the electrostatic interaction contributed by the divalent cations. Therefore, it reduced the efficacy of the monovalent cations in controlling the flexibility and rigidity of the ι C chains and resulted in the formation of a soft gel (Gobet, 2009; Thrimawithana et al., 2010).

The presence of cations also influences the physical strength of the CMC gel (Bajpai and Giri, 2003; Kästner et al., 1997). However, the physical strength of the

CMC gel was reduced in the presence of the cations, especially the divalent cations, as they induce globular aggregations of the CMC chains even at very low ionic strengths (~ 0.5 mM) thus destroying the three dimensional CMC gel network structure (Ueno et al., 2007). This is because the CMC chains that are rich in $-\text{COOH}$ groups can interact with the cations to form intra- and intermolecular linkages (Khvan et al., 2005). These interactions will be more pronounced as the cation's valency and the concentration of the used cations increase.

For pH effect, it was found that the conformational changes of the ιC chains with respect to the pH changes were negligible because the sulphate groups in the backbone of the ιC chains begin to ionise at pH 2 ($\text{p}K_a = 2$) (Gu et al., 2004). On the other hand, the physical strength of the CMC gel is highly dependent on the pH of its aqueous environment. It was found that the physical strength of the CMC gel increased with increasing pH and reached the maximum in the pH range of 6-10 depending on the degree of substitution of the CMC chains (Bajpai and Giri, 2003; Kästner et al., 1997; Lee et al., 2006). This is mainly due to the swelling behaviour of the CMC chains. The $-\text{COOH}$ groups in the CMC backbone begin to ionise as the pH increases and adopt a more extended conformation due to strong intramolecular electrostatic repulsion. These extended CMC chains interpenetrate and entangle with each other to form a good gel network. However, when the CMC chains are extensively charged at high pH ($> \text{pH } 10$), the strength of the CMC gel network decreases (Zhong and Jin, 2009). This is mainly due to the great electrostatic repulsion between the highly charged CMC chains.

1.2 Liposomes as drug carrier

Liposome has been widely used as drug delivery carrier in the pharmaceutical and medical industries due to its unique structure which consists of an aqueous core

entrapped by bilayer lipid membrane composed of lipids or lipid mixture (Figure 1.2) (Bangham and Horne 1964; Jesorka and Orwar, 2008; López-Pinto et al., 2005; Mura et al., 2007; Sato and Sunamoto, 1992). The unique structure of the liposome enables it to encapsulate both hydrophobic and hydrophilic drugs into its lipid bilayer membrane and aqueous core, respectively (Maurer et al., 2001). This could protect the drugs from degradation and increase the therapeutic efficacy of the drugs by reducing their toxicity and side effects (Torchilin, 2005; Yuan et al., 2010).

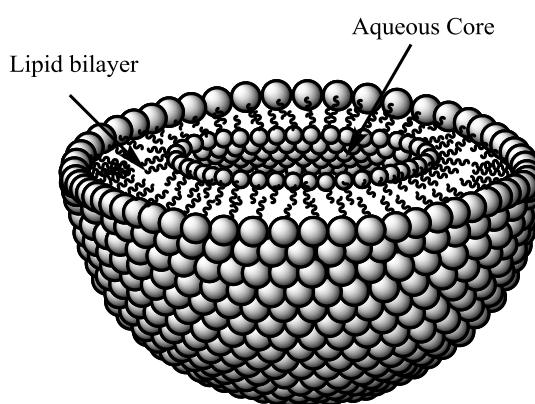


Figure 1.2: Unilamellar liposome showing the enclosed structure of the liposome.

There are many types of liposomes which can be classified based on their lamellarity and size (Figure 1.3 and Table 1.1) (Jesorka and Orwar, 2008). Liposomes formed by a single bilayer enclosing an aqueous core are termed unilamellar liposomes (Shailesh et al., 2009). The unilamellar liposomes can range in size from less than 100 nm to 1 μ m (Figure 1.3 (a)). All unilamellar liposomes less than 100 nm in size are categorised as small unilamellar liposomes, while the unilamellar liposomes larger than 100 nm in size are categorised as large unilamellar liposomes. Giant unilamellar liposomes refer to liposomes more than 1 μ m in size (Mezei and Gulasekharam, 1980; Samad et al., 2007). Liposomes also can be formed by more than one enclosed bilayer (Figure 1.3(b)). Such liposomes are termed multilamellar liposomes which are actually

several unilamellar liposomes formed one inside another, creating an onion-like structure separated by an aqueous layer (Shailesh et al., 2009). The multilamellar liposomes are normally larger than 500 nm in size. Multivesicular liposomes are another type of liposomes easily distinguished from the unilamellar liposomes and multilamellar liposomes by their unique structure. The multivesicular liposome consists of several non-concentric lipid bilayer membranes as shown in Figure 1.3(c) (Mantripragada, 2002; Zhong et al., 2005). Typically, this multivesicular liposome is larger than 1 μm in size (Table 1.1) (Samad et al., 2007).

Table 1.1: The classification of liposomes and their size (Samad et al., 2007).

Type of liposome	Diameter (nm)
Small unilamellar liposome	< 100
Large unilamellar liposome	$100 < x < 1000$
Giant unilamellar liposome	> 1000
Multilamellar liposome	> 500
Multivesicular liposome	> 1000

Liposomes with different lamellarity and size can be controlled by their preparation methods (Vemuri and Rhodes, 1995). For example, the unilamellar liposomes can be obtained by the disruption of the multilamellar liposome and multivesicular liposome using sonication or extrusion (Kepczynski et al., 2010; Schrijvers et al., 1989). Besides, unilamellar liposomes can also be prepared from the reverse-phase evaporation method (Moscho et al., 1996). The large unilamellar liposome and multilamellar liposome can be prepared using the hydration technique or thin film method, which is another commonly used method in liposome preparation (Jesorka and Orwar, 2008; Samad et al., 2007; Shailesh et al., 2009; Vemuri and Rhodes, 1995).

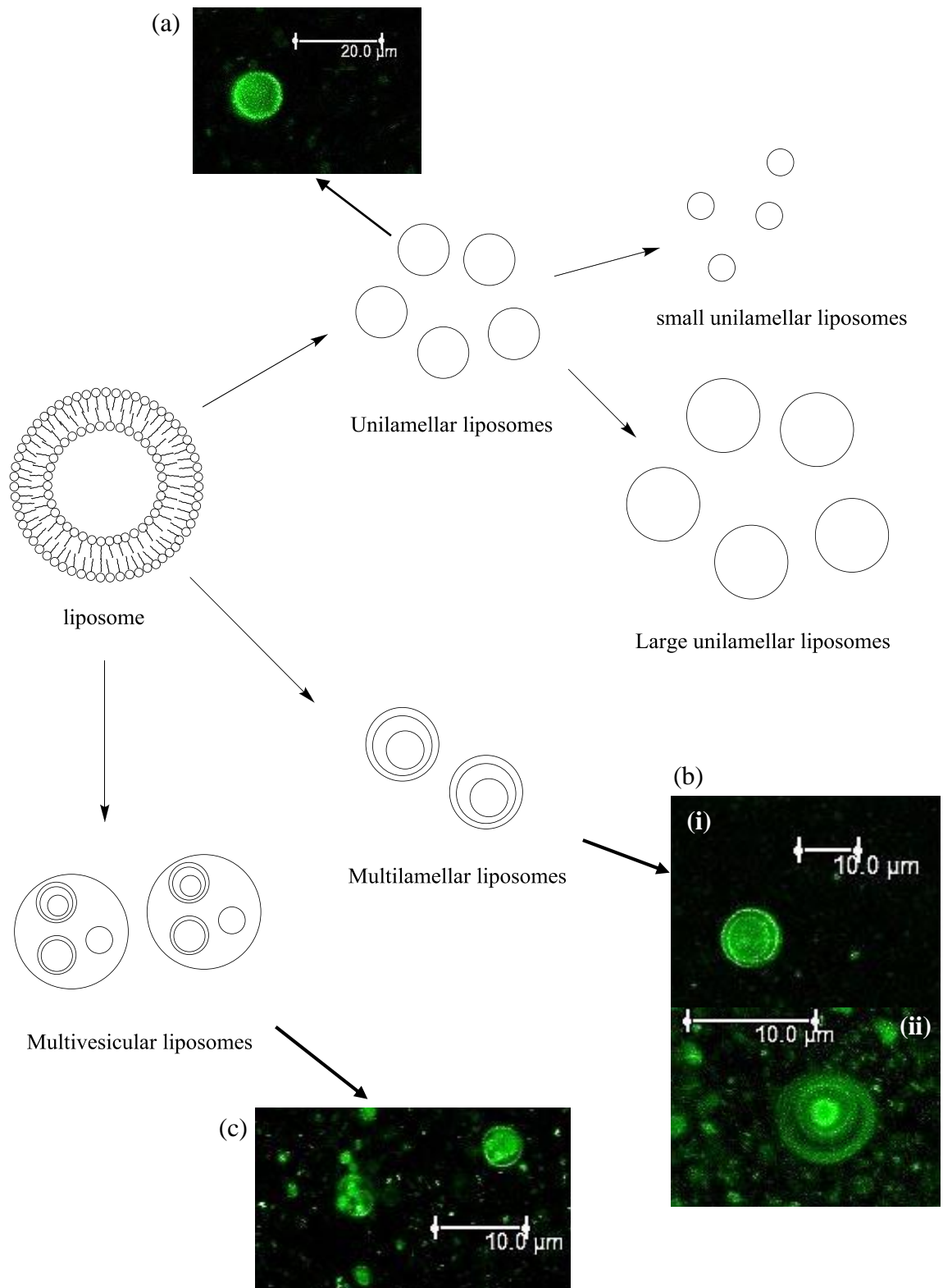


Figure 1.3: Different types of liposomes classified based on the liposomal structure and their fluorescence micrographs. (a) Fluorescence micrograph of unilamellar liposome; (b)(i) and (ii) shows the appearance of multilamellar liposomes; and (c) Fluorescence micrograph of multivesicular or oligomer liposomes.

Single type, non-surface modified liposomes were found to barely survive in the bloodstream because of their fast elimination by the mononuclear phagocyte system (Immordino et al., 2006; Maurer et al., 2001). The recognition and removal of the liposomes from the bloodstream as foreign particles was promoted by the adsorption of proteins present in the bloodstream, onto the liposome surface (Maurer et al., 2001). This disadvantage inhibited the function of the liposome as a drug carrier and reduced its circulation half-life (Immordino et al., 2006). In order to overcome this disadvantage, surface modified liposomes were developed (He et al., 2010; Klibanov et al., 1990; Takeuchi et al., 2001a; Yuan et al., 2010).

1.2.1 Surface-modified liposomes

The first attempt to modify the liposome surface was performed by Allen and Chonn (1987) using gangliosides. It was found that the bioavailability of the surface modified liposome increased with increasing concentrations of the gangliosides (Abuchowski et al., 1977; Allen, 1994; Chonn and Cullis, 1998). Another type of surface modified liposome was prepared using the derivatives of polyethylene glycol (PEG) (Abuchowski et al., 1977; Immordino et al., 2006). The PEG grafted liposome was proved to exhibit high liposome stability and bioavailability in the bloodstream compared to the unmodified liposomes, although the PEG was a synthetically produced polymer (Chonn and Cullis, 1998; Taguchi et al., 2009). This was because the grafted PEG on the liposome surface created a steric barrier which prevented the adsorption and the binding of the proteins which marked the liposome for removal by the phagocytic cells (Figure 1.4) (Lasic, 1995; Maurer et al., 2001; Veronese and Pasut, 2005).

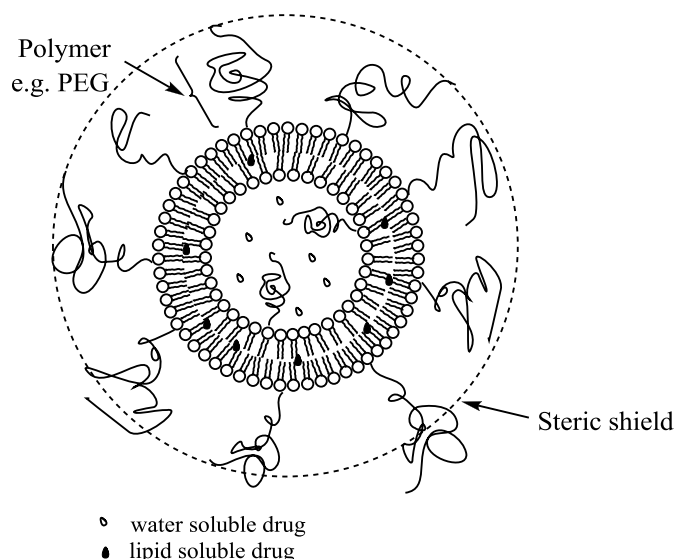


Figure 1.4: Surface modified liposome. The presence of the polymers on the liposome surface can act as a steric shield that decreases the accessibility of the proteins which mark the liposome for recognition and removal by phagocyte system.

The PEGylated-lipid liposomes have been widely used in the pharmaceutical and medical industries, such as chemotherapy of cancer, fungal infections (Mehta et al., 1987; Mills et al., 1994), vaccines (Gregoriadis et al., 1996; Steers et al., 2009), and gene therapy (Gul-Uludag et al., 2012; Jeschke and Klein, 2004; Ropert, 1999). There are several liposome-based pharmaceutical products that have been approved by the US FDA (U.S. Food and Drug Administration) for cancer and antifungal treatment, such as DOXIL, Amphotec, and AmbiSome (Barenholz, 2001; Torchilin, 2005). However, studies have revealed that the systematic administration of the PEGylated-lipid liposome can induce the Accelerated Blood Clearance (ABC) phenomenon and reduce its bioavailability (Dams et al., 2000; Ishida et al., 2005; Laverman et al., 2001). The clearance of the second dose of PEGylated-lipid liposomes from the bloodstream was triggered by the serum proteins produced in response to the first injection of the liposome (Dams et al., 2000). According to Ishida et al. (2006), IgM (Immunoglobulin M) is the protein responsible for the clearance of the PEGylated-lipid liposomes due to

its high affinity to the PEG on the liposome surface. Therefore, studies on many other liposomal systems that stabilised with various polymers, especially polysaccharides such as dextran, pullulan, amylopectin and chitosan have been conducted (Filipović-Grić et al., 2001; Mobed and Chang, 1998; Thongborisute et al., 2006).

The potential of the polysaccharides to serve as ligands in the preparation of stable and site-targeted liposomes has received wide attention because the cell surface is rich in carbohydrate moieties (Table 1.2) (Dicorleto and De La Motte, 1989; Mufamadi et al., 2011; Sato and Sunamoto, 1992; Sihorkar and Vyas, 2001; Sunamoto et al., 1992). This carbohydrate-rich layer, known as the glycocalyx, contains high amounts of polysaccharide that are involved in cellular adhesion, intercellular communication, and biological recognition (Abeygunawardana and Bush, 1991; Palte and Raines, 2012; Sihorkar and Vyas, 2001). Miyazaki et al., (1992) have successfully demonstrated the lung-targeted delivery of amphotericin B using polysaccharide-modified liposomes as the delivery vehicle. The bioavailability of the amphotericin B at the disease site was found to be higher compared to the non-encapsulated amphotericin B. Besides, the liposome can also act as a drug reservoir by coating the mucoadhesive polysaccharide such as cellulose and chitosan onto its surface (El Maghraby et al., 2005; Harrington et al., 2002; Takeuchi et al., 1994; Vinood et al., 2012; Yuan et al., 2010). The layer of the mucoadhesive polysaccharide which has a high adherence to the mucous membrane helps to prolong the residence time of the liposome and increases the bioavailability of the encapsulated drug (Nguyen et al., 2011).

Table 1.2: Polymers used for the modification of liposome surface.

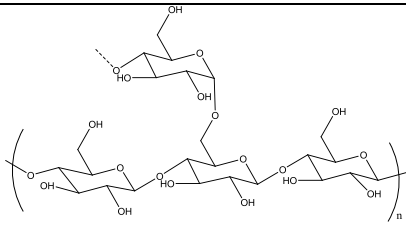
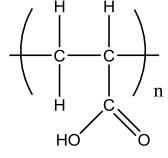
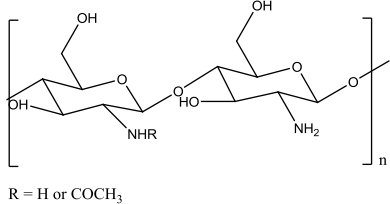
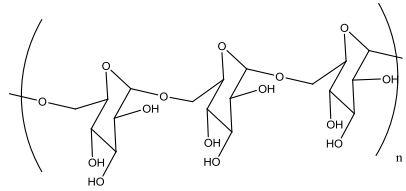
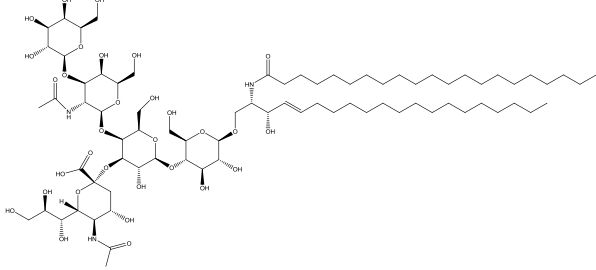
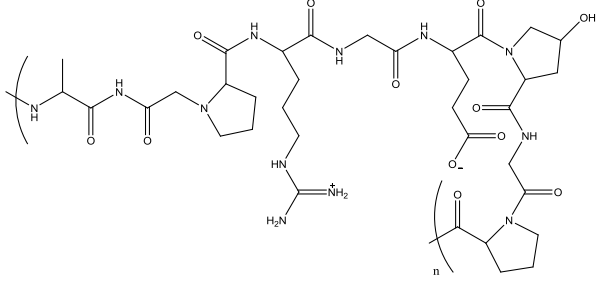
Polymer	Structure	Reference(s)
Amylopectin		(Miyazaki et al., 1992)
Carbopol		(Jain et al., 2007; Takeuchi et al., 2003)
Chitosan	 R = H or COCH ₃	(Liu et al., 2011; Mady et al., 2009)
Dextran		(Elferink et al., 1992; Sunamoto et al., 1992)
gangliosides		(Allen, and Chonn, 1987)
Gelatin		(Shende and Gaud, 2009)

Table 1.2 (continued)

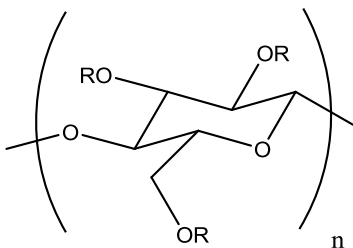
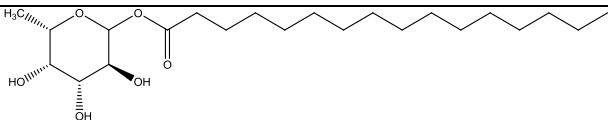
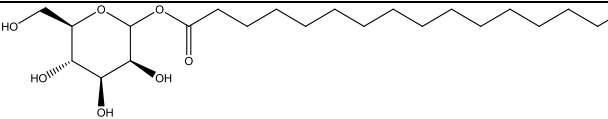
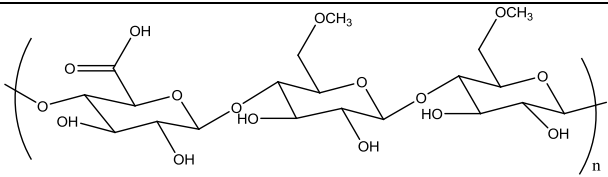
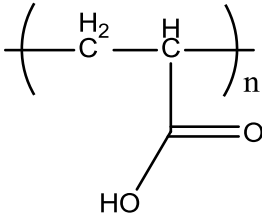
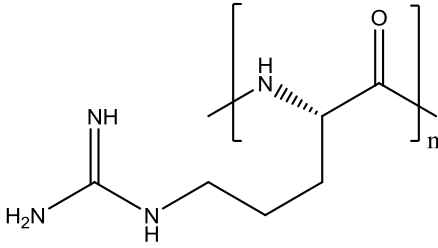
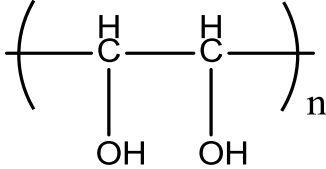
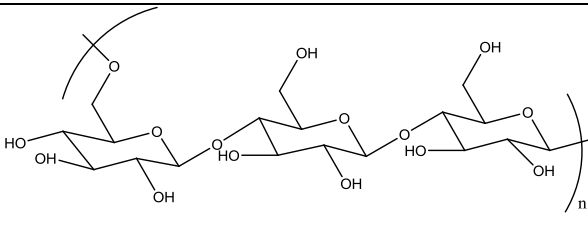
Hydroxypropyl-methyl cellulose	 <p>R = H, CH₃, OR CH₂CH(OH)CH₃</p>	(Takeuchi et al., 2001b)
O-palmitoyl fucose		(Garg et al., 2007)
O-palmitoyl mannose		(Garg et al., 2007)
Pectin		(Nguyen et al., 2011)
Poly(acrylic acid)		(Takeuchi et al., 1994; Werle et al., 2009)
Poly(asparagines)		(Park et al., 2011)
Polyethylene glycol		(Abuchowski, et al. 1977; Beugin et al., 1998; Woodle and Lasic, 1992)

Table 1.2 (continued)

Poly(vinyl alcohol)	$\left(\begin{array}{c} \text{H} \quad \text{H}_2 \\ \quad \\ \text{---C---C---} \\ \\ \text{OH} \end{array} \right)_n$	(Rescia et al., 2011; Takeuchi et al., 2000; Takeuchi et al., 2001b)
Pullulan		(Kang et al., 1997; Sehgal and Rogers, 1995)

Polysaccharide-modified liposomes are prepared using the co-incubation method. The polysaccharide chains adsorbed onto the liposome surface interact with the liposome through hydrogen bonding or hydrophobic interaction (Sato and Sunamoto, 1992). However, desorption of the polysaccharides from the liposome surface may occur during storage and transportation (Sihorkar and Vyas, 2001; Sunamoto and Iwamoto, 1986). In order to prevent desorption, the polysaccharide was further modified by introducing hydrophobic moieties such as fatty acids and cholesterol onto its backbone (Figure 1.5) (Sehgal and Rogers, 1995; Sihorkar and Vyas, 2001; Wang et al., 2010). These hydrophobic moieties are allowed to interact covalently with the lipid bilayer of the liposome, thus endowing the lipid bilayer membrane with an anchoring ability (Sihorkar and Vyas, 2001). The incorporation of the modified polysaccharide into the lipid bilayer of the liposome can reduce membrane permeability, increase the stability as well as bioavailability of the liposome and encapsulated drugs (Ge et al., 2007).

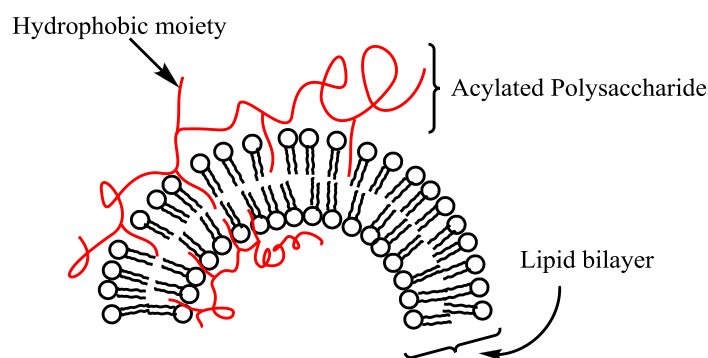


Figure 1.5: Hydrophobic moieties from the polysaccharide backbone anchored into the lipid bilayer of the liposome.

1.2.2 Chitosan modified liposomes

Chitosan-modified phospholipid liposomes are showing promise for application in gene and drug delivery (Liu et al., 2011; Parabakaran, 2008). According to Liu et al. (2011), the combination of the phospholipid liposome and chitosan-DNA complexes has enhanced the DNA delivery efficiency in the *in vitro* cell culture system as well as the *in vivo* mouse model system. The application of the chitosan-coated phospholipid liposome as a drug carrier for lung disease through nebulisation was also investigated (Zaru et al., 2009). It was found that the chitosan-coated phospholipid liposome exhibited greater stability and its drug encapsulation efficiency was relatively higher when compared to the non-coated phospholipid liposome.

The bioadhesive properties of chitosan have also shown some potential application of chitosan in the mucoadhesive drug delivery system, especially in the oral peptides and proteins delivery (Prego et al., 2005; Sonia and Sharma, 2011). The study carried out by Takeuchi et al. (1996; 2003) has shown that chitosan-coated liposomes were able to improve the bioavailability and prolong the pharmacokinetic effect of the peptides (e.g. insulin) in the gastrointestinal tract. This is mainly due to the ability of the chitosan-coated liposome to protect the drug load from enzymatic degradation in the

gastrointestinal tract and its mucoadhesive property to the intestinal tract. Besides, the chitosan-coated phospholipid liposome was also found to show muco-penetrative behaviour across the mucous layer in the intestinal epithelial cell (Thongborisute et al., 2006). Research had revealed that the orally administrated chitosan-coated phospholipid liposome could permeate the mucous layer in the small intestine and thus enhance the adsorption of the therapeutic drugs.

Chitosan-anchored phospholipid liposome is another type of liposome where the liposome surface was modified with lipid-modified chitosan. The lipid-modified chitosan can be prepared via chemically attaching the lipids such as fatty acids to either the carboxyl group at the C-6 position (esterification) or amino group at the C-2 position (acylation) of the chitosan (Qu et al., 2012; Sonia and Sharma, 2011; Wang et al., 2010). The fatty acid modified chitosan can successfully modify the liposome surface by anchoring its fatty acid alkyl chain into the phospholipid liposome bilayer, thereby improving the entrapment efficacy of the drugs by reducing the permeability of the liposome bilayer and thus, prolonging the drug releasing rate (Qu et al., 2012). This will enhance the stability of the liposome and increase its encapsulated drug circulation time. Besides fatty acids, cholesterol also has been used to modify the chitosan for the preparation of cholesterol modified chitosan-anchored phospholipid liposome for the encapsulation of epirubicin as an anticancer drug (Wang et al., 2010). It was found that the drug release rate of the Epirubicin from the chitosan-anchored phospholipid liposome decreased significantly when compared to the unmodified liposome. This slow release profile of the encapsulated epirubicin from the chitosan-anchored phospholipid liposome was mainly attributed to the decrease in the liposome membrane permeability after surface modification.

1.2.2.1 Chitosan

Chitosan is a linear polysaccharide which is composed of randomly distributed β -(1-4)-linked D-glucosamine and N-acetyl-D-glucosamine (Figure 1.6). It is also a form of N-deacetylated chitin that can be prepared from N-deacetylation of the chitin under alkaline conditions using concentrated sodium hydroxide or the enzymatic hydrolysis method in the presence of chitin deacetylase (Rinaudo, 2006). The degree of deacetylation of chitosan normally ranges from 50% to 98% whereas for the commercially available chitosan, the degree of deacetylation is generally 80% (Baldrick, 2010; Dufresne et al., 1999; Rinaudo, 2006).

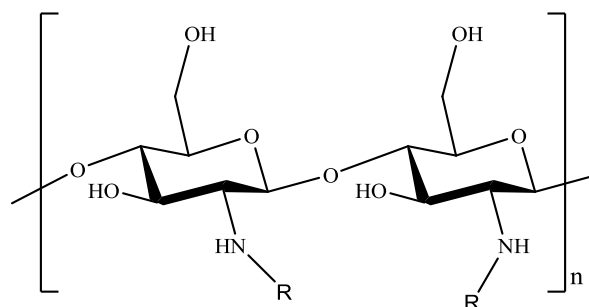


Figure 1.6: The molecular structure of chitosan with n is the number of repeating unit where $R = H$ or $COCH_3$.

Chitosan has a wide range of application in different fields such as agriculture, waste water treatment, dentistry, cosmetic, pharmaceutical, and food industries (Honarkar and Barikani, 2009; Renault et al., 2009; Zhang et al., 2006). There is a growing interest in using chitosan in biomedical application mainly due to its biocompatibility, biodegradability, non-toxic nature, bioadhesivity (Adamo and Isabella, 2003; Aranaz et al., 2010), mucoadhesive properties (Karn et al., 2011; Rengal et al., 2002) and cost effectiveness (Illum, 1998; Kean and Thanou, 2010; Sheng et al., 2009). Besides, the chitosan was also a potential haemostatic agent as it was found to have a blood clotting ability (Barnard and Millner, 2009; Gu et al., 2010; Russell et al., 2009).

Several haemostatic products such as Celox and HemCon, which contain chitosan for bleeding control in cardiothoracic surgery and bandage have been marketed in USA, as well as Europe (CDRH, 2006; Russell et al., 2009). Besides, chitosan gel membrane has also been used for wound dressing. The chitosan gel membranes showed excellent results in wound healing by promoting skin regeneration and also preventing scar tissue formation (Oshima et al., 1987; Risbud and Bhat, 2001).

However, research conducted on the chitosan-coated liposome and the chitosan-anchored liposome has been largely focused on the phospholipid-based liposome (e.g. (Abdelbary, 2011; Li et al., 2009; Zaru et al., 2009). The chitosan-coated non-phospholipid liposome such as fatty acid liposome has not been reported because the preparation of the chitosan-modified fatty acid liposome is often restricted by the poor solubility of chitosan in aqueous solution.

1.2.2.2 Solubility of chitosan in aqueous solution

In general, chitosan is insoluble in both neutral and alkaline solutions, and can only be dissolved in mild acidic solutions (Chan et al., 2007). Under acidic conditions, the solubilisation of chitosan occurs by the protonation of the $-NH_2$ group at the D-glucosamine repeating units (Rinaudo, 2006). When the pH of the aqueous phase is increased, deprotonation of chitosan at the $-NH_2$ group occurs leading to flocculation of the polymer chains. The chitosan was eventually precipitated with further increase in the pH of the solution to pH 7.5 (Rinaudo, 2006). However, the aqueous solubility of chitosan can be improved by reducing its molecular weight (Li et al., 2006; Rinaudo, 2006). This is attributed to the decreasing intermolecular interaction such as van der Waals forces between the chitosan chains (Kubota et al., 2000). Besides, increasing the degree of the *N*-deacetylation of chitosan and the distribution type of *N*-acetyl-D-

glucosamine and the D-glucosamine copolymers in the chitosan chains also influence the aqueous solubility of the chitosan (Aiba, 1991; Fan et al., 2009; Rinaudo, 2006).

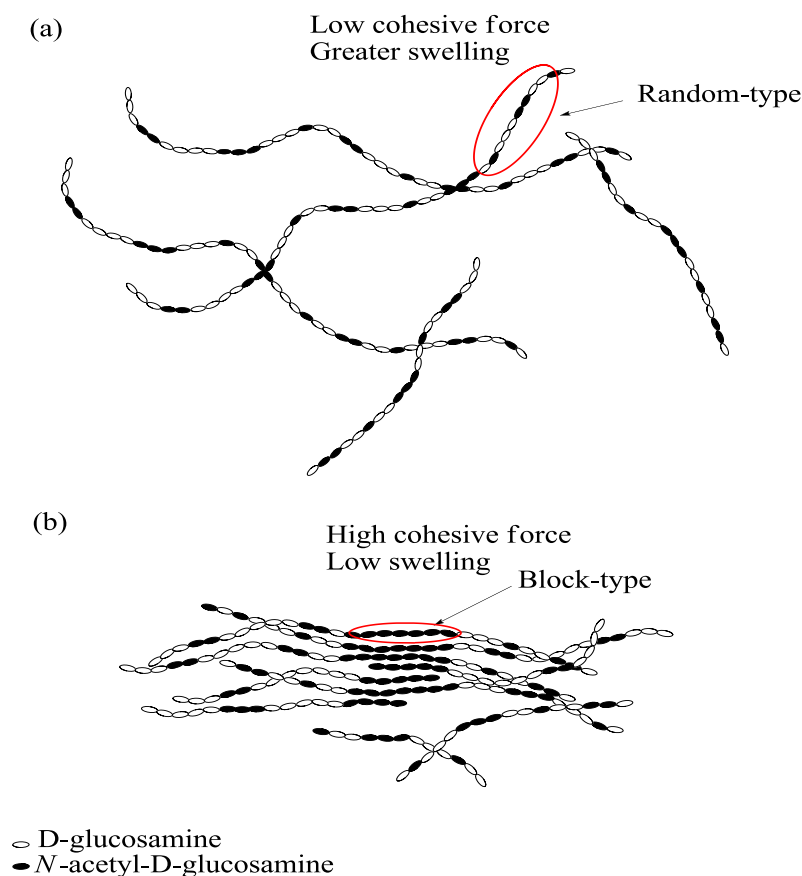


Figure 1.7: The sequence of the *N*-acetyl-D-glucosamine and D-glucosamine residues in the chitosan chains. (a) Random-type distribution of *N*-acetyl-D-glucosamine and D-glucosamine residues which can be prepared from alkaline treatment in the dissolved state. (b) Block-type distribution of *N*-acetyl-D-glucosamine and D-glucosamine residues which can be prepared at high temperatures under solid-state reaction conditions.

It has been reported that chitosan with the random-type distribution of *N*-acetyl-D-glucosamine and D-glucosamine residues have higher aqueous solubility when compared with the block-type distribution as depicted in Figure 1.7 (Aiba, 1991; Tolaimate et al., 2000). This is because the block-type distribution of the *N*-acetyl-D-glucosamine and D-glucosamine residues has a higher cohesive force between the

chitosan chains than the random-type which limits the swelling behaviour of the chitosan and consequently decreases its solubility. Besides the degree of deacetylation, chemical modification can also improve the aqueous solubility of chitosan (Sogias et al., 2010). Modifying the chitosan by introducing hydrophilic or hydrophobic groups in the chitosan chains will reduce its crystallinity and thus, improve its aqueous solubility (Fan et al., 2009; Ge et al., 2007; Hirano et al., 2002).

1.3 Fatty acid liposomes

Much interest is being generated in developing non-phospholipid liposomes in recent years due to the relatively higher costs associated with phospholipid preparation (Bastiat et al., 2007; Gupta et al., 1996). Non-phospholipid liposomes can be prepared from amphiphiles such as fatty acids (Bastiat et al., 2007). The preparation of liposomes using fatty acids was first reported by Gebicki and Hicks (Gebicki and Hicks, 1973; Morigaki and Walde, 2007). The formation of fatty acid liposomes is often restricted to a narrow pH range as it required the coexistence of both the ionic and neutral forms of the fatty acid in critical ratio (Cistola et al., 1988). In other words, the fatty acid liposome is formed when the fatty acid is at or around its corresponding pK_a value (Bastiat et al., 2007). In order to determine the correct pH range to produce the fatty acid liposome, a titration curve can be constructed (Figure 1.8). The titration curve can be divided into five regions (Cistola et al., 1988):

- at the (I) region, the pH of the mixture was high (i.e. highly alkaline) and contained micelles in the aqueous phase;
- region (II) is a three-phase region containing a mixture of micelles, with liposomes in the aqueous phase;
- region (III), a two-phase region containing liposomes in the aqueous phase;

- further increase in the volume of hydrochloric acid and the degree of protonation of the fatty acid increase led to the formation of emulsion as shown in region (IV);
- in region (V), when the mixture became acidic, the fatty acid molecules were fully protonated and the formation of water insoluble oil droplets or fatty acid crystals was observed.

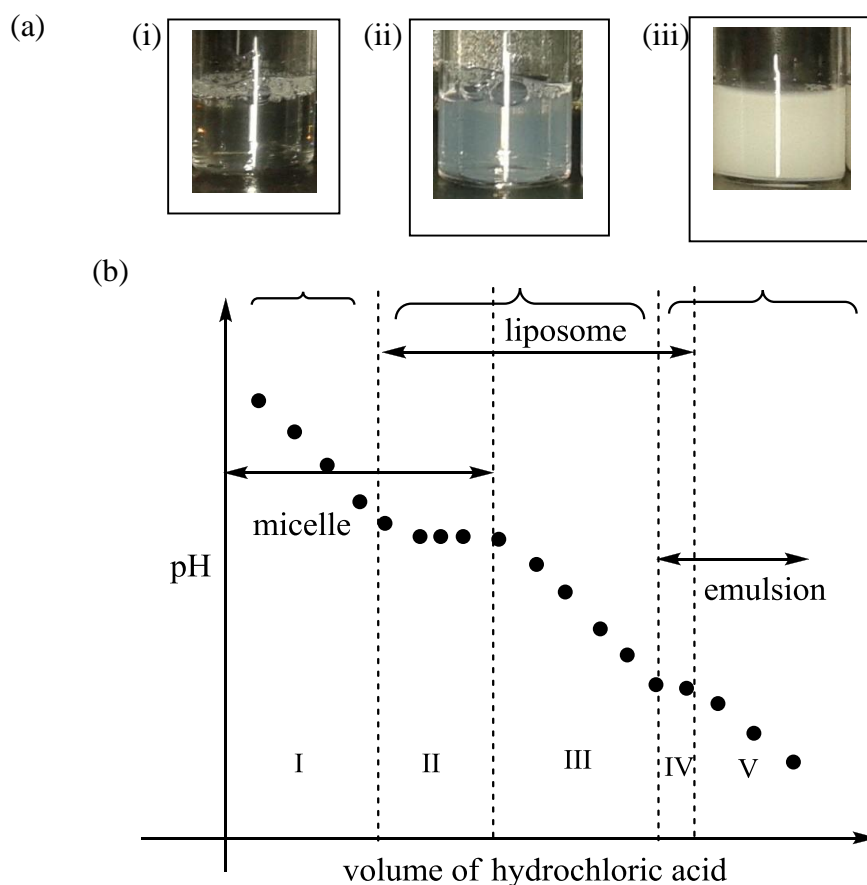


Figure 1.8: (a) Images of the physical appearance of (i) micelles, (ii) liposomes, and (iii) emulsions. (b) Titration curve indicating the regions for the formation of (I) micelles, (II) coexistence of micelle and liposomes, (III) liposomes, (IV) coexistence of liposomes and emulsion, and (V) emulsion.

It has also revealed that the saturated fatty acids composed of 8 to 16 carbons are capable of forming liposomes (Apel et al., 2002; Hargreaves and Deamer, 1978). The pH range for the formation of these fatty acid liposomes can vary from pH 7 to pH 9 depending on the chain length of the fatty acid. As demonstrated by several studies, the saturated fatty acid with 8 to 10 carbons form liposomes at pH 7 (Apel et al., 2002; Cistola et al., 1988; Hargreaves and Deamer, 1978; Morigaki et al., 2003; Namani and Walde, 2005). However, the pH for the formation of fatty acid liposomes further increases to pH 9 with the increasing fatty acid chain length from 12 to 16 carbons. The fatty acid liposomes can also be prepared using unsaturated fatty acids such as myristoleic acid, palmitoleic acid, oleic acid, linoleic acid, and docosahexanoic acid (Chen and Szostak, 2004; Morigaki and Walde, 2002; Namani et al., 2007; Rogerson et al., 2006). These unsaturated fatty acids were able to form liposomes at pH 8 – 9.

Unlike the phospholipid liposome, the concentration of the fatty acid monomers in equilibrium with the bilayer of the fatty acid liposome ($\sim 10^{-4}$ M) was significantly larger than that of the phospholipid liposome ($\sim 10^{-10}$ M). This could be due to the fact that the bilayer of fatty acid liposomes are non-covalently bound, and merely interact electrostatically between their carboxylic (COOH) and carboxylate (COO⁻) groups in the solution. Therefore, the interchange kinetic refers only to monomeric exchange and not to pairs of fatty acids, thus reflecting the higher concentration in the fatty acid liposome when compared with the phospholipid liposome. Another scenario could be due to the imbalance between the COOH to COO⁻ ratio of the fatty acid whereby the COO⁻ has a higher solubility in the aqueous bulk solution. It was also suggested that the fatty acid liposome system is a chemical system in equilibrium, because the dynamic exchange rate of the fatty acid monomer between the bulk and the monolayer of the liposome bilayer membrane was relatively higher when compared with the phospholipid liposome (Morigaki and Walde, 2007; Walde et al., 1994).

1.4 Potential application of liposomes in dermal/transdermal delivery systems

The potential application of liposomes as topical and transdermal drug delivery carriers has been extensively studied. This is because the liposomes were found to improve the drug deposition and permeation rate within the skin (El Maghraby et al., 2008). Figure 1.9 shows the proposed routes that the drug-loaded liposomes may able to penetrate the epidermal layer through the transepidermal pathway, as in paths C and D (de Jager et al., 2007; El Maghraby et al., 2008). The transepidermal pathway refers to the permeation of chemical compounds such as active therapeutic agents across the stratum corneum without altering the structure of the stratum corneum. The transepidermal pathway consists of two micro-pathways, one is the intercellular route and the other is the transcellular route (Barry, 1991). For the intercellular route, liposomes are required to diffuse deep into the dermis layer through the intercellular space (Figure 1.9(C)). Meanwhile, the transcellular route involved the diffusion of the liposomes through the keratinocytes and the lipid lamellae (Figure 1.9(D)) (Fox et al., 2011).

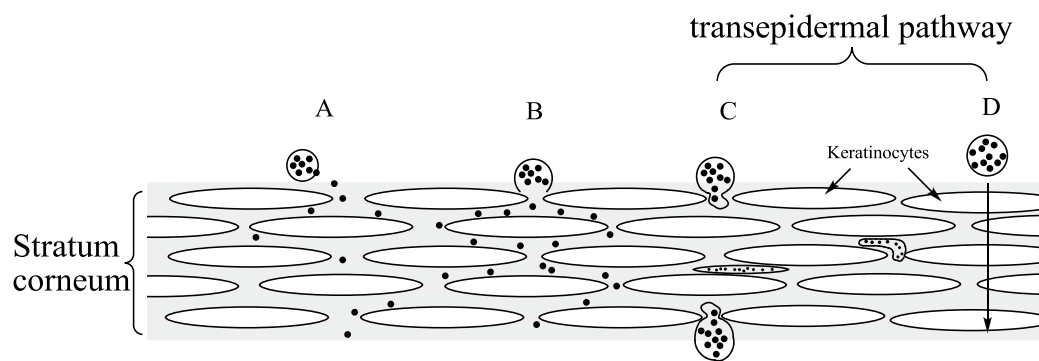


Figure 1.9: The possible penetration route of the drug-loaded liposome through the stratum corneum, (A) the loaded drug release on the surface of the stratum corneum, (B) liposome adsorption or fusion with the stratum corneum and release the drug payload, (C) liposome penetration through the intercellular diffusion in the stratum corneum, and (D) liposome penetration via transcellular diffusion through the keratinocytes and lipid lamellae.

Many studies have been carried out to investigate the efficiency of different types of liposomes as the dermal and transdermal drug delivery vehicle (El Maghraby et al., 2008; Pierre and Costa, 2011). In the dermal delivery system, the phospholipid liposomes, less than 278 nm in size, were found to penetrate deeper into the dermis layer of the skin via the intercellular penetration mechanism, which was proved by the microscopic technique (van Kujik-Meuwissen et al., 1998; Verma et al., 2003). Besides the phospholipid liposomes, the penetration of the non-phospholipid liposomes prepared from sucrose esters through the stratum corneum was also observed under the freeze-fracture electron microscope by Honeywell-Nguyen et al. (Honeywell-Nguyen et al., 2002; Honeywell-Nguyen et al., 2003). Their results showed that the liposomes, 100-200 nm in size, were present in significant amounts in the deeper layer of the stratum corneum. These liposomes were found to fill the channel-like region located within the intercellular lipid lamellae and revealed the ability of the liposome to diffuse into the deeper layer of the skin via the intercellular diffusion route.

Besides deep penetration, the liposomes can also act as a localised drug reservoir in the skin in order to avoid excessive usage of the active ingredients while minimising the side effects of the active ingredients during topical delivery (El Maghraby et al., 2005). Mezei and Gulasekharam, (1980) demonstrated the topical administration of triamcinolone encapsulated phospholipid liposomes through the anti-fungal liposomal lotion formulation. The drug concentration in the epidermis and dermis layers was four times higher than in the control sample and the urinary excretion of the drug was lowered. Besides the anti-fungal liposomal formulation, liposomal formulation was also used for the treatment of other dermatological diseases, such as acne and psoriasis (de Leeuw et al., 2009). Foong et al., (1990) found that the liposome containing retinoic acid produced higher percutaneous adsorption and greater retention of the retinoic acid compared to the conventional cream. The topical anaesthesia delivery of lidocaine using

the phospholipid liposomal formulation has also shown an improvement in its effectiveness and prolonged anaesthetic action of the drugs compared with the conventional dosage form of formulation (Glavaš-Dodov et al., 2005; Ranjit and Vyas, 1996).

For transdermal delivery, several studies have shown the ability of the liposome to enhance the drug transport across animal and human skin. The effectiveness of the liposome to deliver drugs across the skin was demonstrated by using model drugs such as oestradiol (El Maghraby et al., 2000) and diclofenac (Cevc and Blume, 2001). It was found that drug-encapsulated liposomes were able to penetrate into the skin spontaneously and were distributed throughout the whole body via the lymphatic system (Cevc et al., 1995). This finding has also shown that the transdermal administration of anti-cancer drugs into the systemic circulation using liposomes is promising. Several studies have been conducted to investigate the effectiveness of transdermal administration of 5-fluorouracil which is a type of anti-cancer drug using liposomal formulation (da Costa and Moraes, 2003; El Maghraby et al., 2001; Glavaš-Dodov et al., 2003). Besides small molecule drugs, the transdermal delivery of macromolecules such as insulin in the liposome was also investigated as demonstrated by Cerv et al., (1998) where the phospholipid liposome encapsulated insulin was successfully delivered through transdermal route into the human skin. Results also showed that the transdermal delivery of insulin using liposome can be as efficient as the injection method.

1.5 Rheology of gel and its topical applications

Rheology is a commonly used method in the characterisation of polymeric gels. In the rheological study, the gel is characterised according to its flow and viscoelastic properties. These are important properties of the gel as they provide information on the deformability, spreadability, and stability of the gel (Brummer, 2006b; Brummer, and Godersky, 1999; de Brito et al., 2005; Nishinari, 2009). Besides, the rheological behaviour of the gels could also affect the interaction between the liposome and the skin and skin feel upon application (Dragicevic-Curis et al., 2009). Flow property such as gel viscosity, especially for the topical application gels such as the liposomal gel, can directly influence the treatment consistency to the targeted site. This is because the viscosity is responsible for gel spreadability and poor spreading could reduce the homogeneity of the liposome's dispersion in the skin (Garg et al., 2002; Ueda et al., 2009). As a result, the liposome's diffusion rate from the gel into the skin is affected and this may also cause adverse effects due to the incorrect drug dosage that has been transferred (Glavaš-Dodov et al., 2003; Ivens et al., 2001; Jelvehgari et al., 2007). Besides, monitoring the rheological properties of the topical application gel would also help to control the batch-to-batch production consistency of the liposomal gel in order to ensure the efficiency of the final products.

Other than the spreading property of the gel, rheological data also helps to evaluate the skin feel of the gel upon application, especially for topical application products, as they affect sensation when the gel is rubbed against the skin (Islam et al., 2004). This can be done by studying the critical yield point and shear thinning of the gels. For example, a high yield point gel is desirable for storage as it could suspend and stabilise the loaded carrier or drugs. However, the high yield stress of the gel must occur at a low shear rate for the ease of application. Most of all, the gel should be able to

exhibit shear thinning behaviour in order to allow even spreading onto the skin for optimum adsorption of the loaded carrier or drug (Brummer, 2006b; Jelvehgari et al., 2007; Jones et al., 1997). In addition, the gel formulations used in the topical applications are expected to be able to extend their retention time on the targeted site. In order to achieve this property, gels with thixotropic behaviour are often used in the preparation of cosmetic and pharmaceutical products such as sunscreen, topical drugs and vaginal formulations. Such thixotropic type of gels extend their retention time by forming a layer of film on top of the targeted site and thus, prolonged the release of the liposome or loaded drug (Lee et al., 2009).

Apart from the physical flow properties of the gels, information on its microstructural changes with respect to the applied strain and frequency related to its physical strength can also be extracted from their rheological data (Brummer, 2006a; Grillet et al., 2012). This can be achieved by studying the viscoelastic properties of the gel. Generally, gels that exhibit high elastic property possess great internal network structure integrity and physical strength (Nishinari et al., 2000). Besides physical strength, it is also possible to estimate the thermal stability and gelling temperature of the gel by evaluating its viscoelastic behaviour as a function of temperature (Hossain et al., 2001; Tischer et al., 2006). These tests provide useful information on the study of storage and lifetime of the final gel products.

1.6 Objective

- a) To prepare and characterize chitosan- and *N*-(fatty acyl)-chitosan-coated oleic acid liposome;
- b) To prepare carbohydrate-based liposomal gel;
- c) To study the rheological properties of the liposomal gel.

CHAPTER 2

MATERIALS AND METHODS

CHAPTER 2

2.0 Materials

All solutions and samples were prepared by using deionized water with the resistivity of 18.2 Ω/cm , (Barnstead Diamond Nanopure Water Purification, Barnstead International, Iowa USA). rC was obtained from Fluka (USA). Food grade CMC with degree of substitution ranging from 0.60 to 0.70, was purchased from Dai-Ichikogyo Seiyaku Co. Ltd. (Japan). Boric acid, hydrochloric acid and acetone were obtained from Merck (Germany). Sodium hydroxide (NaOH) and sodium nitrite (NaNO_2) were purchased from Fluka (Switzerland). Potassium bromide (KBr) for IR spectroscopy was purchased from Merck (Germany). Deuterium oxide (D_2O) and deuterated acetic acid (CD_3COOD) were purchased from ARMAR Chemicals (Switzerland). GC grade oleic acid (OA) (99%), and acetic acid were purchased from Sigma (USA). Potassium chloride was purchased from R&M (UK). Palmitoyl chloride was purchased from Aldrich (Switzerland) and used as received. Chitosan with the average molecular weight of 150 kDa was obtained from Acros Organics (USA).

2.1 Preparation of depolymerized chitosan

Different molecular weights of chitosans were prepared through depolymerisation reaction. First, an appropriate amount of chitosan was dissolved in 1% acetic acid solution to yield 1% (w/v) of chitosan solution. The depolymerisation was performed by adding dropwise of 7 and 10 mL of NaNO_2 solution (0.10 mol dm^{-3}) into the solution 1% (w/v) chitosan solutions separately (Table 2.1). The reaction mixture was stirred under magnetic stirring at room temperature for 1 hour. Then, the pH of the solution was adjusted to pH 8-9 with 0.1 mol dm^{-3} of NaOH solution in order to precipitate out the non-water soluble chitosan that later was removed by filtration. The remaining

filtrate was neutralized to pH 7 using 0.1 mol dm⁻³ of hydrochloric acid solution. The remaining water soluble chitosan was precipitated by adding acetone and collected by using centrifugation method (will be discussed in section 2.6.1). The collected precipitate was dried under vacuum (Janes and Alonso, 2003; Mao et al., 2004).

Table 2.1: Volume of NaNO₂ used in the depolymerisation reaction of chitosan.

Name	Volume of NaNO ₂ added (mL)
Ch1	10
Ch2	7

2.2 Preparation of *N*-Acylated Chitosan

Two types of Ch2Ps with different degree of acylation (DA) were prepared from Ch2 (Ch2P1 and Ch2P2). First, 1% (w/v) of Ch2 solution was prepared by dissolving an appropriate amount of Ch2 into 1% of acetic acid solution. Then, the pH of the Ch2 solution was adjusted to 7. Then, 27 µL and 55 µL of palmitoyl chloride were added into two Ch2 solutions, separately. These two solutions were stirred under magnetic stirring at room temperature to yield Ch2P1 and Ch2P2, respectively. After 5 hours, the mixtures were neutralized and Ch2P1 and Ch2P2 were precipitated using acetone. The Ch2P1 and Ch2P2 were collected by centrifugation method as discussed in section 2.6.1. The collected Ch2P1 and Ch2P2 were washed several times with chloroform to eliminate any presence of free fatty acid and followed by drying under vacuum oven at 30°C (Le-Tien et al., 2003).

2.3 Preparation of OA liposome and chitosan-modified OA liposome

A liposome solution with final concentration of 30 mmol dm⁻³ was prepared by dissolving appropriate amount of OA using 50 mmol dm⁻³ of borate buffer (pH 8.8). For

Chs-modified OA liposome, series of Ch1 and Ch2 solutions with different concentrations ranging from 0.04 to 0.30% (w/v) were prepared by dissolving appropriate amount of Ch1 and Ch2 into 50 mmol dm⁻³ of borate buffer. The pH of OA liposome, Ch1 and Ch2 solutions were adjusted to 7 before mixing. Then, the liposome solution was added dropwise into Ch1 and Ch2 solutions under magnetic stirring. The mixtures were stirred for 24 hours at room temperature. Then, the pH of the mixtures was adjusted to 8.8 for the formation of Chs-coated OA liposomes (OACH1 and OACH2). With similar method, OA liposomes modified with Ch2P1 and Ch2P1 were prepared (OACH2P1 and OACH2P2). All liposome solutions were incubated at 25°C for 24 hours before analysis.

2.4 Preparation of ι C and CMC gel

1% (w/w) of ι C gel and 2% (w/w) of CMC solution were prepared individually by dispersing appropriate amount of ι C and CMC into 50 mmol dm⁻³ borate buffer (pH 8.8) that containing 0.20% (w/w) of potassium chloride. These solutions were then heated to 80 °C in a sealed vial until a clear gel system was obtained. All ι C gels and CMC solutions were kept at room temperature for 24 hours before proceed to the next preparation step. Then, a series of gel mixtures with different amount of ι C and CMC were prepared using the above mentioned ι C gel and CMC solution. These gel mixtures were further diluted with 50 mmol dm⁻³ borate buffer (pH 8.8) at the ratio of 9 to 1. The final composition of ι C and CMC was presented in mass fraction (Table 2.2). The mixtures were stored at room temperature for another 24 hours before rheological study. Prepared gel with optimum rigidity and elasticity was selected to prepare liposomal gels.

Table 2.2: The final concentration of the gel mixtures.

<i>i</i> C-CMC ratio	Mass Fraction	
	<i>i</i> C	CMC
8:2	0.8	0.2
7:3	0.7	0.3
5:5	0.5	0.5
4:6	0.4	0.6
3:7	0.3	0.7

2.5 Preparation of liposomal gels

Liposomal gels were prepared by dispersing 10% (^w/_w) of the prepared OA, OACH1, OACH2, OACHP1, and OACHP2 liposomes into the selected gel with the ratio of 1:9 by weight using a Vortex mixer (Uzusio VTX-3000L, Japan). The mixtures were vortexed for 3 minutes and store at room temperature for 24 hours prior to analysis.

2.6 Instrumentation

2.6.1 Centrifugation

The Chs and Ch2Ps precipitates that were obtained from section 2.2.2 and 2.2.3 were collected by centrifugation method. The centrifugation was performed at 5000 rpm for 2 minutes using a CT15RT TechComp Versatile Refrigerated Centrifuge equipped with a TA15-6-50 angle rotor at 25°C. (Janes and Alonso, 2003; Mao et al., 2004).

2.6.2 Chitosan structural analysis

2.6.2.1 Fourier transform infrared spectroscopy (FT-IR) analysis

The FT-IR spectra for Ch1, Ch2, Ch2P1 and Ch2P2 in KBr disc were obtained using Perkin Elmer spectrometer (model RX-1, USA). For the sample preparation, these Ch1, Ch2, Ch2P1, and Ch2P2 were mixed with KBr (1:100) and compressed into pellets. The

resolution of the IR spectra was 4 cm⁻¹ and was recorded in 8 accumulations from 400 – 4000 cm⁻¹ in transmittance mode. The degree of acylation (DA) of Ch1, Ch2, Ch2P1 and Ch2P2 was calculated from FT-IR spectra using the following equation (Kasaai, 2008),

$$DA(\%) = \left(\frac{A_{1655}}{A_{3450}} \right) \times \frac{100}{1.33} \quad \text{Eq. 2.1}$$

A_{1655} and A_{3450} are the intensity of the 1655cm⁻¹ and 3450 cm⁻¹ peaks in FT-IR spectra, respectively.

2.6.2.2 ¹H-NMR

The sample for ¹H-NMR analysis was prepared by dissolving 10 mg of each Ch1, Ch2, Ch2P1, and Ch2P2 into 1 ml of 1 % of CD₃COOD/D₂O solution. ¹H-NMR spectra for all samples were acquired using a JEOL JNM-GSX 270 FT NMR spectrometer (270 MHz) at 70 °C. The ¹H-NMR measurements of the samples were performed at high temperature in order to obtain better resolution of the signals and minimized the interference from the solvent peaks with the chitosan peaks (Lavertu et al., 2003; Onesippe and Lagerfe, 2008).

2.6.3 Average molecular weight determination

The average molecular weight of Ch1, Ch2, Ch2P1, and Ch2P2 were determined by Static Light Scattering (SLS) method using a Malvern NanoSeries ZetaSizer (Malvern, UK) at 25°C. First, a series of Ch1, Ch2, Ch2P1, and Ch2P2 solutions with different concentrations was prepared. Then, the refractive index of the solutions was determined with an ATAGO refractometer (NAR-2T, Japan) at 25°C. The refractive index

increment, $\frac{dn}{dc}$ of the Ch1, Ch2, Ch2P1, and Ch2P2 was determined from the slope of the linear relationship between the refractive index and concentration (Zhao et al., 2011). A value of 0.159 of $\frac{dn}{dc}$ was used in this study in order to determine the average molecular weight of all Chs and Ch2Ps. The average molecular weight for the Chs and Ch2Ps was measured in triplicate.

In the SLS theory, the average molecular weight was determined by applying the Rayleigh equation as shown in the following equation:

$$\frac{KC}{R_\theta} = \left(\frac{1}{M} + 2A_2C\right)P(\theta) \quad \text{Eq. 2.2}$$

where C is the concentration, M is the molecular weight, A_2 is the 2nd viral coefficient which described the interaction strength between the polymer and its dispersed medium, $P(\theta)$ is the angular dependency of the analyte scattering intensity. In the Rayleigh scattering, this $P(\theta)$ is reduced to 1 by assuming that the particles are small and the multiple photon scattering was absent. Therefore, the Rayleigh equation can be rewritten as follow:

$$\frac{KC}{R_\theta} = \frac{1}{M} + 2A_2C \quad \text{Eq. 2.3}$$

where the K is an optical constant and can be defined as follow:

$$K = \frac{2\pi^2}{\lambda_o^4 N_A} \left(n_o \frac{dn}{dc}\right) \quad \text{Eq. 2.4}$$

where λ_o^4 is the wavelength of the laser, N_A is the Avogadro's number, n_o is the refractive index of the solvent, and $\frac{dn}{dc}$ is the differential refractive index increment which referred to the changes in refractive index as a function of analyte concentration.

The R_θ found in the Rayleigh equation (**Eq. 2.3**) is the Rayleigh ratio of the

analyte which is used to characterize its scattered intensity at scattering angle of θ . The R_θ of the analyte can be obtained from the relative scattering intensity of the analyte to that of a standard pure liquid and is defined as follow:

$$R_\theta = \frac{I_A n_o^2}{I_T n_T^2} R_T \quad \text{Eq. 2.5}$$

where I_A and I_T is the scattering intensity of the analyte and standard liquid, respectively; n_T is the refractive index of the standard liquid; and R_T is the Rayleigh ratio of the standard liquid. In this study, toluene was used as the standard liquid for the determination of the analyte's R_θ .

After the scattering intensity of the analyte was obtained, a Debye plot was constructed by the Zetasizer software by plotting $\frac{KC}{R_\theta}$ versus concentration of the analyte. The molecular weight of the analyte was determined from the intercept of the plot.

2.6.4 Determination of chitosan solubility by UV-Vis spectroscopy

The solubility of Ch1, Ch2, Ch2P1, and Ch2P2 in water were determined using UV-Vis spectrophotometer. First, a series of Ch1, Ch2, Ch2P1, and Ch2P2 solutions with different concentrations was prepared. Calibration curve was constructed by plotting the intensity of the absorption at the wavelength of 274 nm versus concentration. Then, saturated Ch1, Ch2, Ch2P1, and Ch2P2 solutions were prepared and their UV-Vis absorption was determined at 25°C. The solubility of the Ch1, Ch2, Ch2P1, and Ch2P2 solutions was obtained by extrapolation method from the calibration curve (Li et al., 2006).

2.6.5 Surface tension measurement

The surface tension of a series of OA, OACH1 OACH2, OACH2P1, and OACH2P2 liposome solutions with different concentrations was determined by du Noüy ring method using a Krüss Tensiometer (Model K100, Germany) at 25°C. These liposome solutions were diluted using 50 mmol dm⁻³ of borate buffer (pH 8.8) and were incubated at 25°C for overnight before measurement. Surface tension of the prepared solutions was determined using 20 successive measurements and the standard deviation was calculated.

2.6.6 Size and Zeta potential

The size and zeta potential of the OA, OACH1, OACH2, OACH2P1, and OACH2P2 liposomes were measured using a Malvern NanoSeries ZetaSizer (Malvern, UK) at a constant temperature of 25°C. The size and zeta potential of the prepared liposome were monitored over 30 days of storage time. The size and zeta potential measurements for all liposomes were measured in triplicates and the average value was reported.

2.7 Morphological study

2.7.1 Optical Polarizing Microscope imaging

The polarizing micrographs of the OA, OACH1, OACH2, OACH2P1, and OACH2P2 liposomes were captured using a Leica Polarizing Microscope equipped with Leica QWin software (Leica Microsystems, Germany). All measurements were performed at the temperature of 25°C.

2.7.2 Confocal microscope

The micrographs of the liposomes and liposomal gels were studied using a Leica TCS SP5 confocal setup mounted on a Leica DMI 6000 CFS inverted microscope (Leica Microsystems GmbH, Germany) and was operated under the Leica Application Suite Advanced Fluorescence program (LAS AF) (courtesy of Hi-Tech Instrument, Malaysia). The LGs were stained with acridine orange. The sample was equilibrated at room temperature for 5 minutes before further analysis.

2.7.3 Atomic Force Microscope (AFM) imaging

AFM images of the liposomes were captured using AFM Nanoscope III, Model MMAFM-2 (Digital Instruments, USA). All imaging was performed via tapping mode with integrated pyramidal tips aluminium cantilever (BS-Multi75Al) (Vermette et al., 2002). The samples were prepared by placing a drop of the liposome solutions onto a freshly cleaved mica surface. The dispersing medium was removed by air dry (Paleos et al., 1996).

2.7.4 Transmission Electron Microscope (TEM) imaging

An Energy Filtered TEM (EFTEM) model LIBRA 120 equipped with an Olympus SIS-iTEM (ver. 5) was employed to analyze the image of the prepared liposomes. A drop of the liposome solution was placed onto a copper-coated carbon grid followed by the removal of excess dispersed medium using a filter paper. Then, a drop of negative staining reagent (1% of phosphotungstic acid in 50 mmol dm⁻³ of borate buffer solution (pH 8.8) was added and the sample was air dried at room temperature for 25 minutes. The sample was then examined under TEM (Garg et al., 2007).

2.8 Rheological study

The rheological tests in this study were performed using a stress/rate controlled Bohlin Germini CVO-R Rheometer (Malvern, UK) which was equipped with a temperature controller. All measurements were carried out at $25.0 \pm 0.1^\circ\text{C}$ with 4°/40 mm cone and plate geometry at 0.100 mm gap in triplicates and average value was reported.

2.8.1 Dynamic oscillation measurement

The amplitude sweep test was performed at a controlled strain mode with the applied strain ranging from 0.01 to 10 units at fixed frequency of 0.5 Hz. This amplitude sweep test was performed prior to frequency sweep test in order to ensure that the selected strain was within the linear viscoelastic region (LVR) of the gels (Figure 2.1). The frequency sweep test was performed at controlled strain mode by varying the frequency from 0.01 to 5 Hz.

The viscoelastic property of the gels was studied from small deformation test using dynamic oscillatory rheometry method. In general, this oscillation method containing two main tests where both the storage elastic energy (elastic modulus, G') and the loss of energy through viscous flow (viscous modulus, G'') can be obtained as a function of strain (amplitude sweep test) and frequency (frequency sweep test). In the amplitude sweep test, the gel is subjected to sinusoidal oscillating strain at a constant angular frequency and the response stress that shifted by an amount of phase difference (δ radians) is measured (Figure 2.2). For frequency sweep test, the gel is subjected to a constant strain and the response stress is recorded as a function of frequency. This test is useful in monitoring the behavior of the gel at different time scale since frequency is inversely proportional to time.

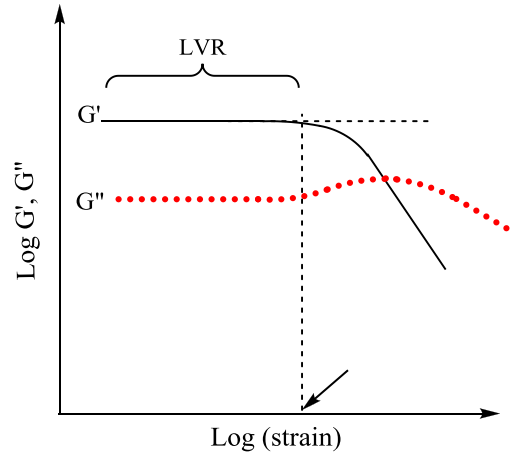


Figure 2.1: The linear viscoelastic region (LVR) of gels.

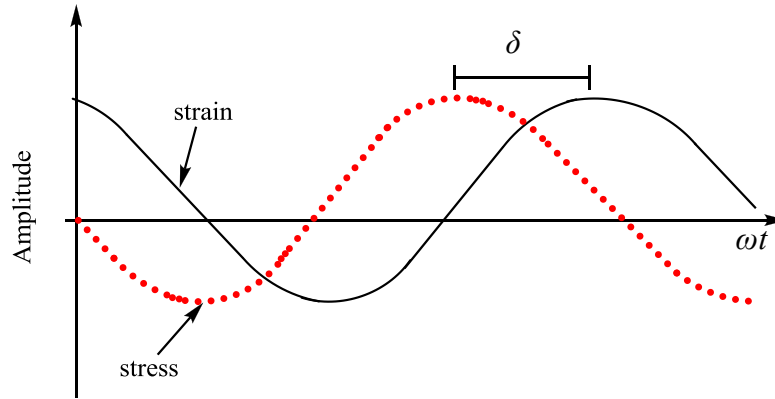


Figure 2.2: Sinusoidal stress response which shifted by an amount of δ to the sinusoidal strain deformation for viscoelastic material.

2.8.2 Temperature sweep

The temperature sweep test was performed at temperature interval of 2°C from 20°C to 60°C . The frequency was set at 0.5 Hz throughout the test and a constant strain of 0.01 units which is well within the LVR of the gels is applied.

In this test, a small and non-destructive shear stress or shear strain is applied onto the gel at a temperature range and the changes of its moduli were monitored. The gelling point of the gels was defined as the crossover point of the G' and G'' curves as shown in Figure 2.3 (MacArtin et al., 2003). The moduli of the gel will remain constant and show a plateau with $G' > G''$ when the applied temperature is below its gelling

temperature. This also indicated that there are no significant changes in the internal network structure of the gel. However, when the applied temperature reached the gelling temperature of the gel, its G'' will dominate against G' which implied the deformation of the internal gel networks structure as a result in the changes of polymer chain's mobility.

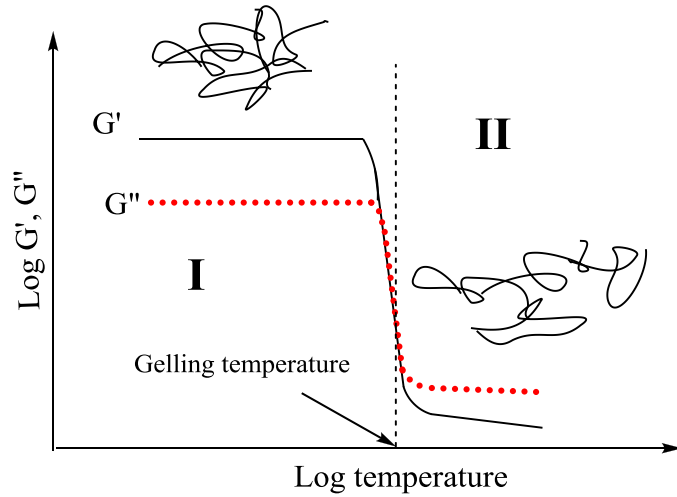


Figure 2.3: (I) Constant moduli showing the thermal stability of the gel ($G' > G''$). (II) Deformation of the internal gel network structure at high temperature ($G'' > G'$). The cross point between the G' and G'' profiles show the gelling temperature of the examined gel.

2.8.3 Creep-recovery test

The creep measurements were performed at a constant stress of 0.1 Pa for 60 s (within the range of LVR) and the changes in the strain of the gel with time were recorded. This was followed by a recovery test where the applied stress is removed. In the recovery test, the responded strain or deformation of the gel is measured for another 300 s.

The deformation from the creep and recovery test is presented as compliance, J (per unit stress). Generally, there are three types of creep and recovery curves as shown in Figure 2.4. For an ideal elastic material, it shows a constant strain response once the

material is loaded with stress and immediately returns to its original state upon removal of the applied stress (Figure 2.4(i)). On the other hand, the strain of an ideal viscous material would show a linear response to the applied stress indicating the steady flow and its strain is not able to be recovered when the applied stress is removed (Figure 2.4(ii)). A viscoelastic material would exhibit both the elastic response and followed by steady flow (Figure 2.4(iii)). However, the ability to recover its structure was mainly attributed to the magnitude of the applied stress. The viscoelastic material could fully recover if the applied stress was lower than its critical stress. Otherwise, the structure of this viscoelastic material could only be partially recovered as some of the applied stress has been dissipated in its viscous flow (Dolz et al., 2008; Goodwin and Hughes, 2008; Schramm, 2000). The creep and recovery test is also a useful method used to characterize the retardation time of the gel. This retardation time (λ_{ret}) is $\frac{\eta_1}{G_1}$ that measured the rate for the gel to reach its full deformation and it is unique for every material. The gel with large retardation time indicated that it takes a long period to reach its full deformation which implies that the gel is less elastic (Steffe, 1996).

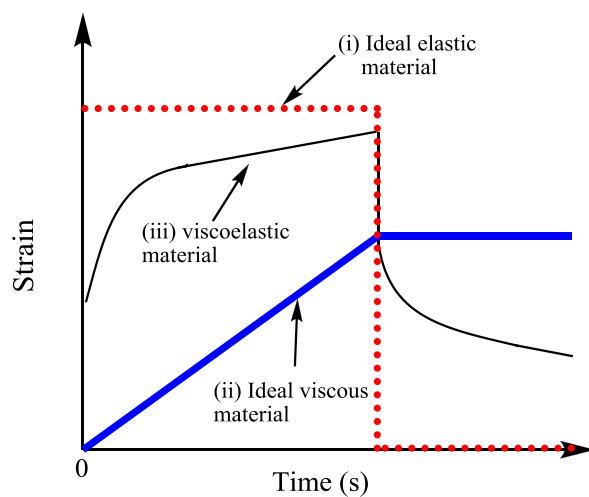


Figure 2.4: Creep and recovery curves for (i) an ideal elastic material, (ii) an ideal viscous material, and (iii) a viscoelastic material.

In this study, the creep profiles of all gels were fitted with the Burger's model which is one of the most widely used model due to its acceptable results obtained in many cases (Figure 2.5) (Dolz et al., 2008). The four-components Burger's model consisted of a Maxwell model and a Kelvin-Voigt model that are associated in series as shown in Figure 2.6 and can be expressed as follow (Dogan et al., 2012):

$$J(t) = \frac{1}{G_0} + \frac{1}{G_1} \left[1 - \exp\left(\frac{-tG_1}{\eta_1}\right) \right] + \frac{t}{\eta_0} \quad \text{Eq. 2.6}$$

where G_0 is the instantaneous elastic modulus which defines the sample resistivity to deformation. G_1 is the retarded elastic modulus, η_0 is the residual viscous flow of the gels, η_1 is the internal viscosity.

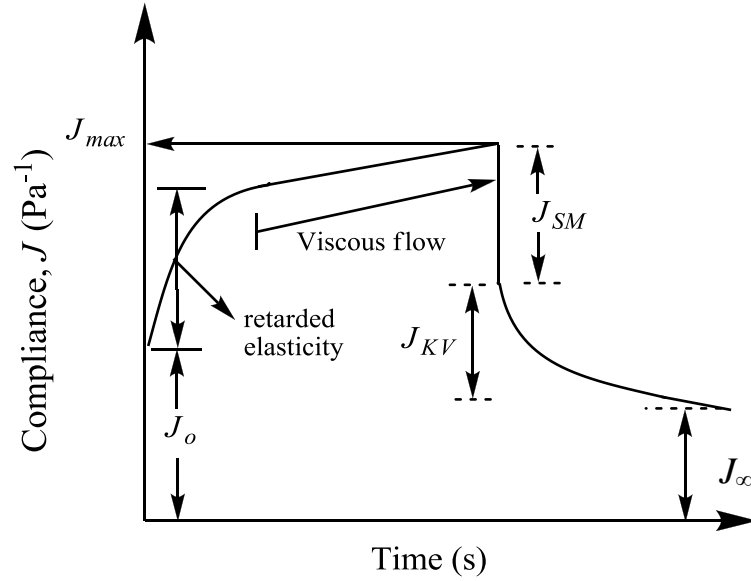


Figure 2.5: Creep and recovery profile for Burger's model.

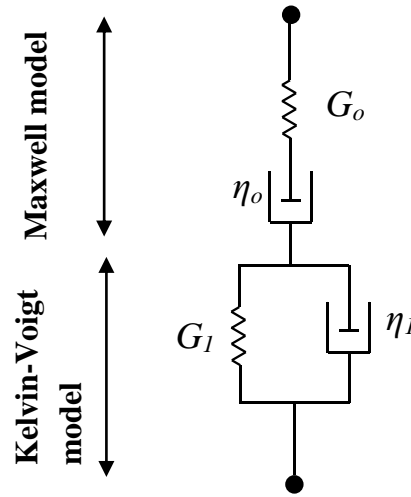


Figure 2.6: Burger's model which consists of Maxwell model and Kelvin-Voigt model in series.

For the recovery test, the obtained profile as shown in Figure 2.5 can be fitted to the following equation:

$$J = J_{\infty} + J_{KV} \exp(-Bt^C) \quad \text{Eq. 2.7}$$

where J_{∞} is the permanent deformation, J_{KV} is the retarded deformation, B and C are the parameters that define the recovery speed and can be calculated from the first derivative with respect to Eq. 2.7. Typically, the recovery profile consisted of three zones (Dolz, 2008). The first recovery zone is an instantaneous recovery (J_{SM}) which corresponds to the spring element of the Maxwell model and the second zone corresponds to the Kelvin-Voigt model (J_{KV}) which is decreasing in an exponential manner. The third zone is the permanent deformation (J_{∞}) which corresponds to the sliding of dashpot from the Maxwell model (Figure 2.6). The contributions of the four elements i.e. J_{SM} , J_{KV} , and J_{∞} from the Burger's model to the total compliance of the system can be calculated using Eq. 2.8, while the contribution of J_{SM} , J_{KV} , and J_{∞} to the total deformation ($\%J_e$) of the system is determined using Eq. 2.9. The recovery percentage ($\%R_e$) of the J_{SM} , J_{KV} , and J_{∞} and overall system recovery ($\%R_{ovr}$) of the gels were defined using Eq. 2.10 and Eq. 2.11, respectively (Dolz et al., 2008; Toro-Vazquez et al., 2010).

$$J_{SM} = J_{\max} - (J_{\infty} + J_{KV}) \quad \text{Eq. 2.8}$$

$$\%J_e = \frac{J_e}{J_{\max}} \times 100 \quad \text{Eq. 2.9}$$

$$\text{Recovery, \% } R_e = \frac{J_e}{J_{\max}} \times 100 \quad \text{Eq. 2.10}$$

$$\text{Overall System Recovery, \% } R_{ovr} = \frac{J_{\max} - J_{\infty}}{J_{\max}} \times 100 \quad \text{Eq. 2.11}$$

where J_{\max} is the maximum compliance achieved during the creep test.

2.8.4 Steady flow measurement

The steady rheological behavior of the gels was measured at a controlled rate mode varying from 0.01 to 200 s⁻¹.

Polymeric gels systems are generally non-Newtonian and exhibited shear thinning behavior which is also described as pseudoplastic. Although the polymeric gel is shear thinning, it also shows shear thickening behavior at low shear rate region as shown in Figure 2.7(a) (Goodwin and Hughes, 2008; Steffe, 1996). This is a typical behavior of a plastic type of material such as tooth paste and tomato paste. However, the pseudoplastic gel starts to flow when the applied shear exceeds its critical yield point and shows shear thinning behavior (Figure 2.7(b)). In order to study the degree of shear thinning of all gels and LGs, their shear viscosity profile were fitted with Power-Law model as shown in the following equation:

$$\eta = k\dot{\gamma}^{n-1} \quad \text{Eq. 2.12}$$

where η is shear viscosity, $\dot{\gamma}$ is shear rate, k is the consistency index, and n is the Power-Law index (PLI) (Karaman and Kayacier, 2012). The consistency index is referred to the average viscosity of the fluid and it is temperature dependent (Osswald and

Hernández-Ortiz, 2006). For a Newtonian fluid, this consistency index is equal to its Newtonian viscosity (Rauwendaal, 2001). The PLI is a measure of the degree of deviation of a fluid from Newtonian behavior (PLI for Newtonian fluid is equal to 1). A shear thinning fluid will show PLI value less than 1 and it is considered to behave strong shear thinning when its PLI is less than 0.5 (Rauwendaal, 2001). On the other hand, a shear thickening fluid showed PLI larger than 1 (Barrera et al., 2013).

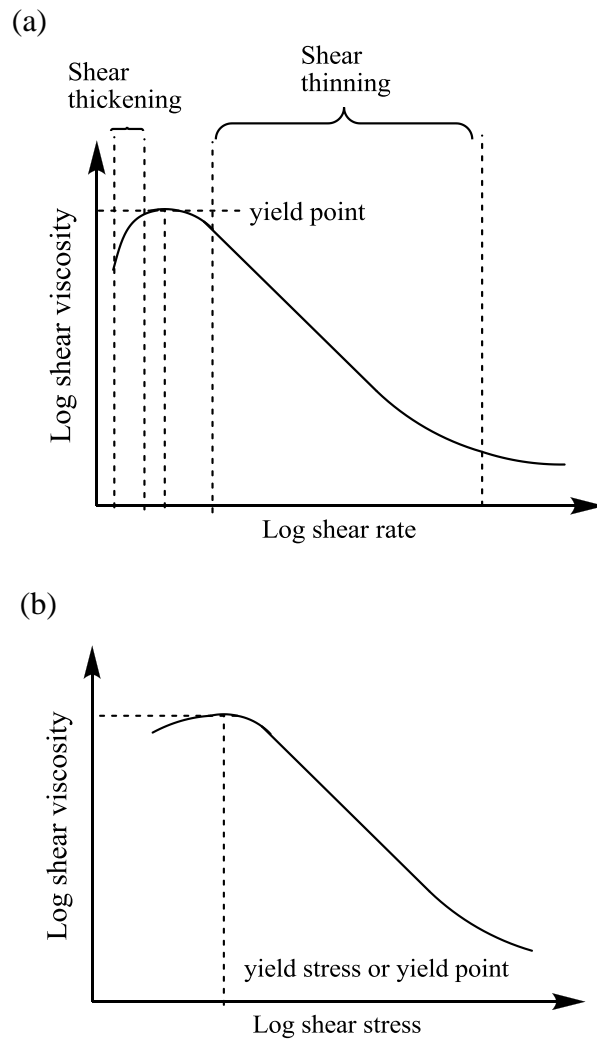


Figure 2.7: (a) A typical viscosity curve of pseudoplastic gel showing shear thickening behavior at low shear rate. When the applied shear rate exceeded the yield point, the viscosity of the gel started to decrease with increasing shear rate and shows shear thinning behavior. (b) Yield stress determination from shear viscosity versus shear stress curve.

2.8.5 Thixotropic behavior study

The thixotropic for all gels and LGs was performed within a shear rate of $0.1\text{--}10\text{ s}^{-1}$. In general, this time-dependent viscosity can be divided into rheopectic and thixotropic (Figures 2.8). The viscosity of a rheopectic gel will increase with time when it is subjected to a shear stress (Figure 2.8(a)). Meanwhile a thixotropic gel behaves like a shear thinning gel which demonstrated a decrease in viscosity with time and regained its viscosity when the applied shear is removed as a result of the ability of the gel to rebuild its network structure (Figure 2.8(b)). In this study, all the prepared gels and LGs are thixotropic gel. The degree of thixotropic for all gels was determined by performing hysteresis experiment. In this approach, the thixotropic gel is subjected to an increasing shear rate and followed by a decreasing shear rate in order to produce a hysteresis loop. The degree of thixotropic is estimated from the area of the hysteresis loop (Figure 2.8(c)) and it was admitted that the greater the hysteresis area, the stronger the thixotropic properties (Barnes, 2000; Benchabane and Bekkour, 2008; Harris, 1967).

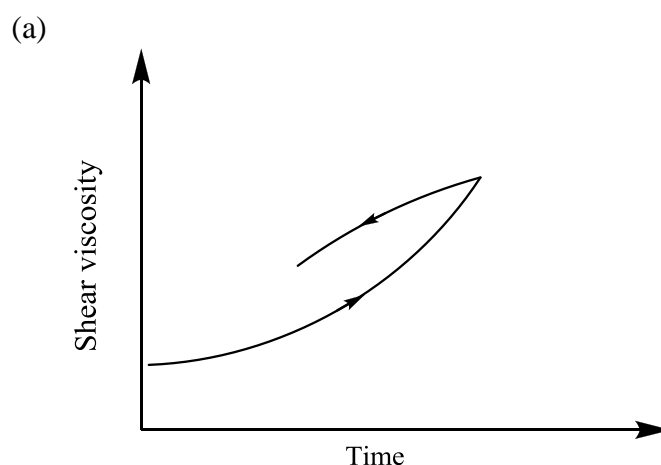


Figure 2.8: Time dependent viscosity profile of (a) rheopectic systems for shear thickening materials, (b) thixotropic for shear thinning materials, and (c) the hysteresis loop of thixotropic gel.

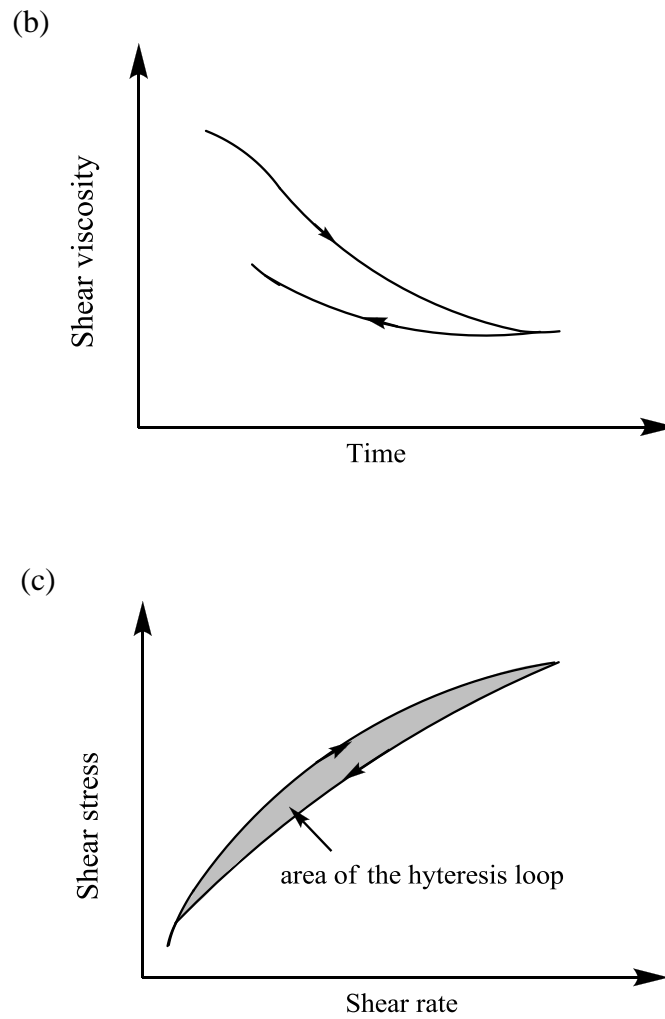


Figure 2.8 (continued)

2.9 Statistic

The statistical analyses were performed using Microsoft Excel 2010 (Microsoft Corporation, Redmond, WA). The data were analyzed with one-way analysis of variance (Moghadam). The differences in means and pairwise comparisons were considered to be statistically significant when $P < 0.05$ (Lorenzo et al., 2013; Nakauma et al., 2012).

CHAPTER 3

RESULTS AND DISCUSSION

CHAPTER 3

3.1 Characterization of chitosan

3.1.1 FT-IR analysis

As shown in the FT-IR spectrum of the Chs and Ch2Ps (Figure 3.1), absorption peak at 1555cm^{-1} and 1655 cm^{-1} assigned for the N-H bending of the amide II band and the carbonyl stretching of secondary amides from the chitosan backbone respectively (Xu, 1996). The intensity of the N-H bending of amide II was found to increase with increasing degree of acylation (DA). Other peaks that have shown similar trend are the absorption peaks at 2879 and 2929 cm^{-1} which were attributed to the $-\text{CH}$ stretching of the alkyl chains attached at the amino group at C-2 position of chitosan (Tien et al., 2003). We are using these results to confirm that the acylation reaction which was carried out using palmitoyl chloride at the amino group of chitosan has been successful.

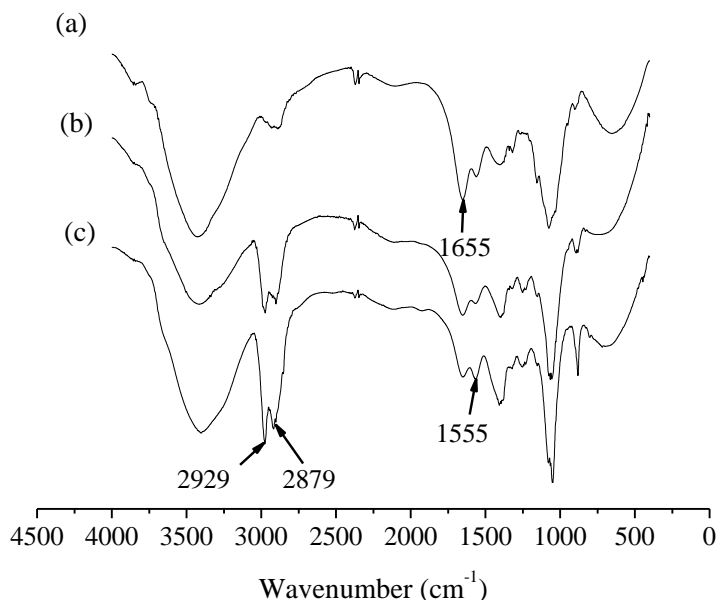


Figure 3.1: FT-IR spectra of (a) Ch2, (b) Ch2P1 (DA= $8 \pm 2\%$), and (c) Ch2P2 (DA= $18 \pm 2\%$).

3.1.2 ^1H -NMR analysis

The ^1H -NMR spectra of the Ch2 and Ch2Ps are presented in Figure 3.2. The peak assignment for the Chs and Ch2Ps were based on previous works (Li et al., 2006; Rinaudo et al., 1992). The proton of deuterated water (HOD) and deuterated acetic acid (CD_3COOD) resonated at 4.65 and 2.11 ppm, respectively. Following is the proton assignment of Chs (Figures 3.2(a)): $\delta_{1.92} = \text{CH}_3$ (acetyl group of chitosan); $\delta_{2.5-2.1} = \text{CH}$ (carbon 2 of chitosan); $\delta_{4.1-3.1} = \text{CH}$ (carbon 2-6 of chitosan); and $\delta_{4.5-4.3} = \text{CH}$ (carbon 1 of chitosan). After modification, the NMR spectrums of Ch2Ps showed two new peaks at $\delta_{1.1}$ and $\delta_{1.7}$ which refer to $-\text{CH}_3$ and $-\text{CH}_2-$ protons of the long alkyl chains, respectively (Figures 3.2(b) and (c)) (Li et al., 2006). This result confirmed the modification of Ch2 with palmitoyl chloride.

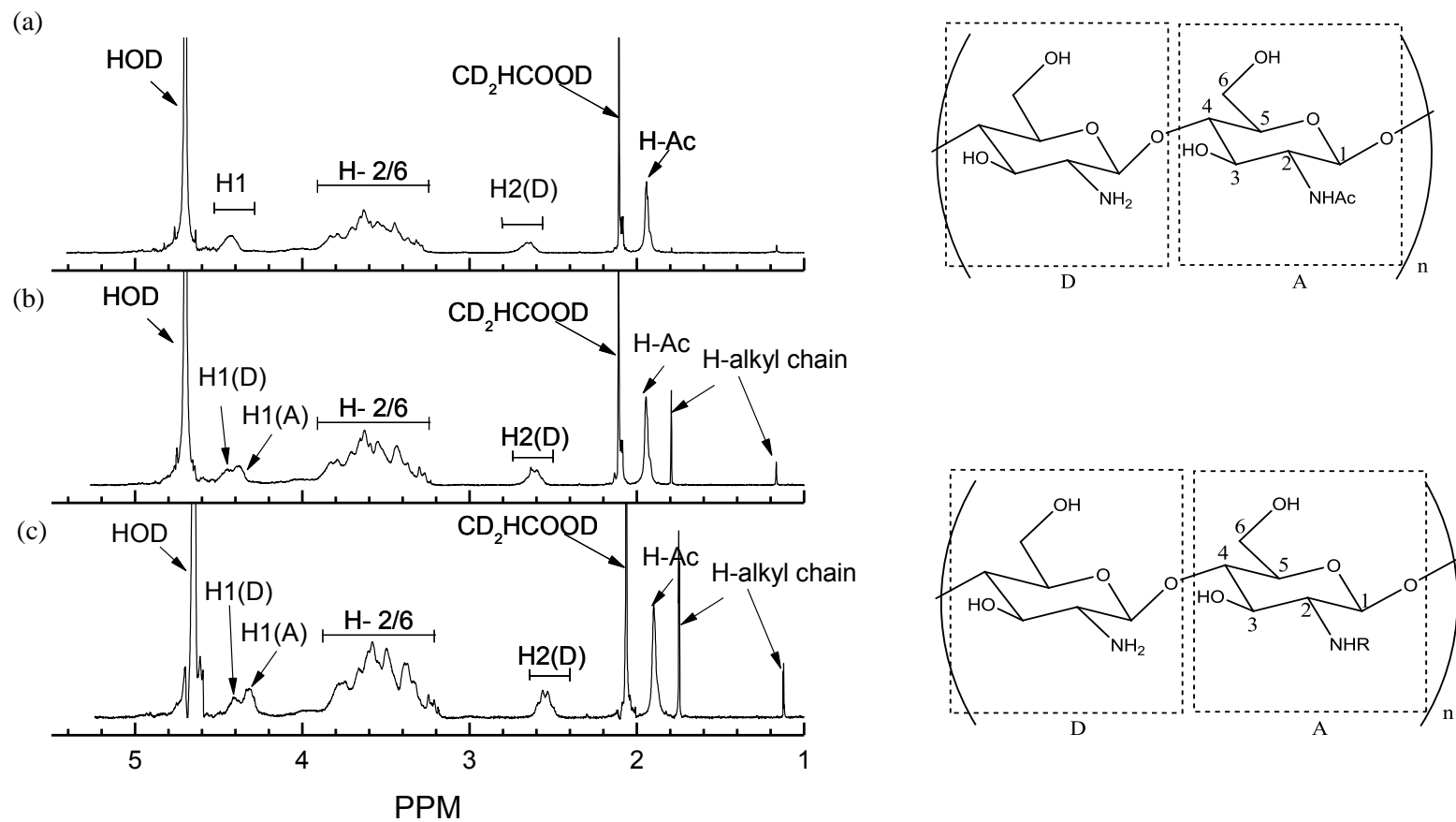


Figure 3.2: NMR spectra for (a) Ch2, (b) Ch2P1, and (c) Ch2P2 where D is the glucosamine group and A is the *N*-acetyl or *N*-acyl glucosamine group of the chitosan.

3.1.3 Average molecular weight determination

In this study, depolymerization of chitosan was performed using sodium nitrite. The average molecular weight of the original chitosan decreased from 150 kDa to 10 kDa as the amount of 0.1M sodium nitrite increased to 10 mL during depolymerization reaction (Table 3.1). The decrease in chitosan molecular weight with increasing sodium nitrite amount was mainly due to the increase in the amount of nitrosonium ion (NO^+) and eventually more β -glycosidic linkage is cleaved. The cleavage mechanism of the β -glycosidic linkage by ion NO^+ was first proposed by Allan and Peyron (1995). This NO^+ attacked the primary amine group in the chitosan molecule and resulting in the formation of 2,5-anhydro-mannose unit at the reducing end of the depolymerized chitosan (Figure 3.3). In order to produce the NO^+ , the sodium nitrite was first dissolved into deionized water to obtain nitrite ion (NO_2^-). The solution that contains NO_2^- was then added dropwise into the chitosan that dissolved in 1% acetic acid solution. Under acidic condition, the NO_2^- was converted into nitrous acid (HONO). These HONO were then rearranged to form NO^+ and uses for the depolymerization of chitosan as shown in Figure 3.4.

Table 3.1: Average molecular weight of the depolymerized chitosan with different amount of sodium nitrite and the degree of deacetylation.

Name	Volume of 0.1M sodium nitrite used (mL)	Average molecular weight, M_w (kDa)	Degree of deacetylation (%) ($\pm 2\%$)
chitosan	0	150	90
Ch2	7	25	90
Ch1	10	10	90
Ch2P1	-	29	82
Ch2P2	-	32	72

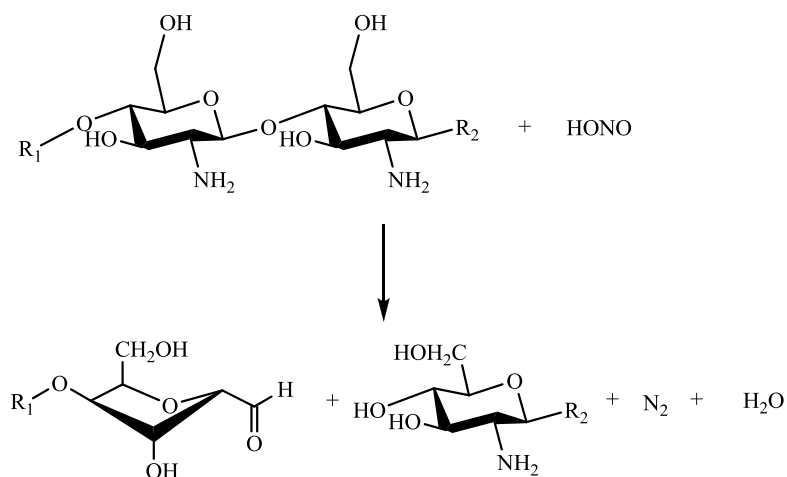


Figure 3.3: Chemical equation of the depolymerization of chitosan by sodium nitrite (Allan and Peyron 1995).

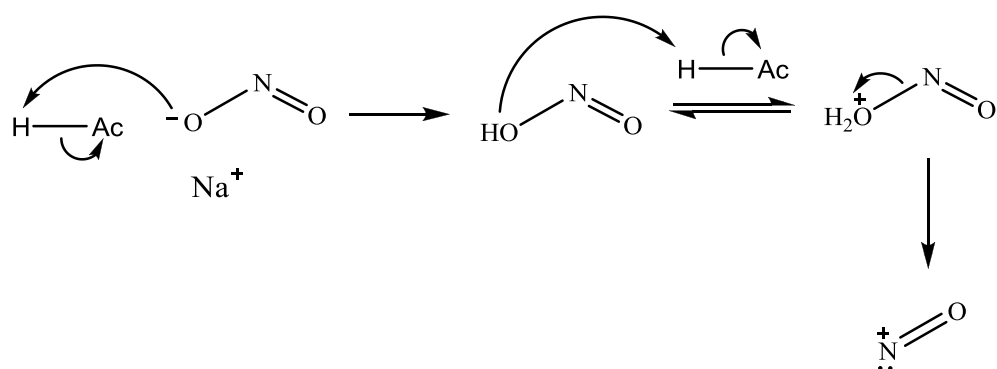


Figure 3.4: Formation of NO^+ from the salt of nitrous acid for the depolymerization process.

3.1.4 Determination of chitosan solubility

The water solubility of Ch1 and Ch2 was found to decrease with increasing molecular weight (Figure 3.5). The decrease of Ch1 and Ch2 water solubility was mainly attributed to the increase in the intermolecular interactions such as van der Waals forces between the Ch1 and Ch2 chains which restricted their swelling (Kubota et al., 2000). For the Ch2P1 and Ch2P2, the water solubility was decreased with increasing DA (Figure 3.5). This was mainly due to the increase of hydrophobic moieties at the chitosan backbone that increases the hydrophobicity of the Ch2Ps (Hirano et al., 2002).

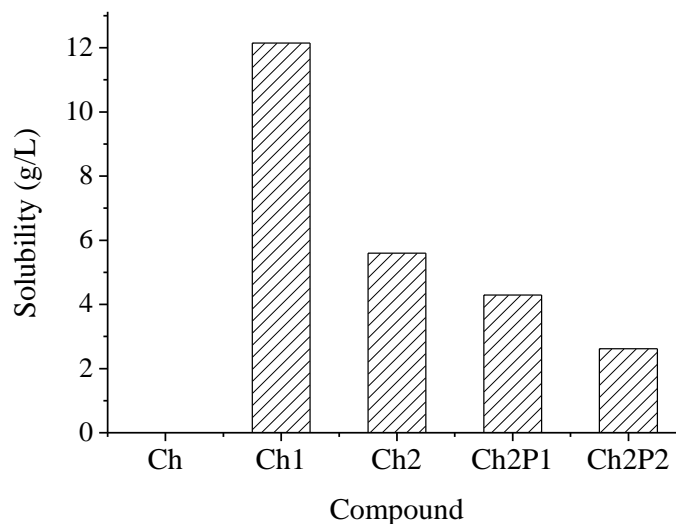


Figure 3.5: Water solubility of Ch1, Ch2, Ch2P1, and Ch2P2.

3.2 Characterization of OA and chitosan-modified OA liposomes

3.2.1 Titration curve

The formation of OA liposome and Chs or Ch2Ps modified OA liposomes were studied by evaluating their titration curves. By adding HCl into the alkaline solution of sodium oleate, some of the sodium oleate molecules were protonated and the pH of the solution was decreased (Figure 3.6 (a)(i)). Initially, when all the OA molecules were completely dissociated in high alkaline region, the solution was transparent (Figure 3.6(b)(i)). However, when the degree of protonation increases to a certain oleate/oleic ratio, the solution became turbid due to the formation of OA liposomes that scattered light (Figure 3.6(b)(ii)) and confirmed by the appearance of Maltase crosses under the Polarizing Microscope (Figure 3.6 (a)(ii)). At the liposome formation region, a buffering effect that started from pH 10.0 – 8.8 was observed. However, when the pH of the solution was decreased to pH 8.5 the solution became milky which showed the formation of emulsion droplets (Figure 3.6(b)(iii)). As the pH of the solution further

decreased to 7, phase separation was observed and a white precipitate was formed. Also, there were two plateau regions in the equilibrium titration curves in this study, one appear at the high pH (located at phase transition between micelle and liposome region (A-B)) and another at low pH (located at phase transition between liposome and emulsion region (C-D)) (Figure 3.6 (b)-(f)). The plateau that appeared at high pH region indicated the coexistence of micelles and liposomes, while the plateau located at low pH region showed coexistence of liposomes and emulsions droplets (Namani and Walde, 2005).

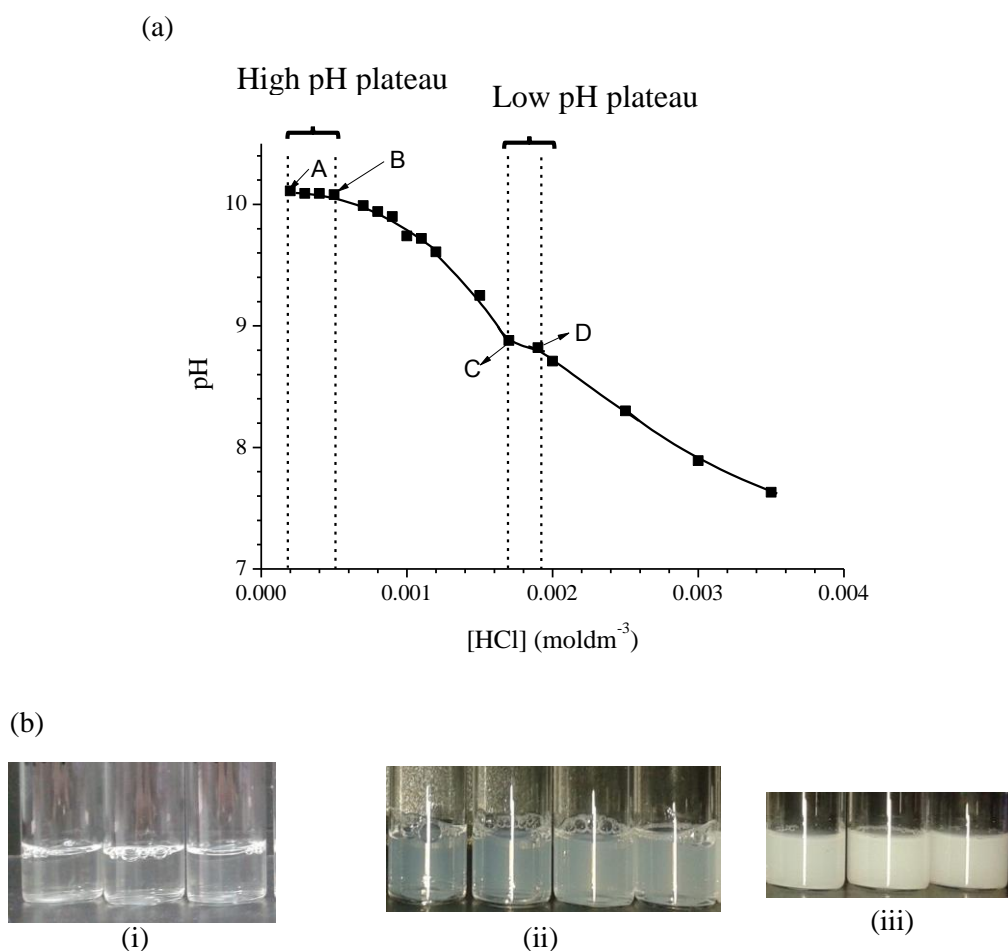


Figure 3.6: Equilibrium titration curve of oleate/OA and the buffering effect (from pH 10-9) when the oleate and OA coexist (a). The changes of the OA solution appearance with decreasing pH from (b)(i) the clear micellar region ($> \text{pH } 10$) to the formation of liposomes showing turbid appearance ($\text{pH } 10 - 8.0$) (b)(ii) and finally to milky appearance of emulsion ($< \text{pH } 8$) (b)(iii). The equilibrium titration curves for (c) OA + Ch1, (d) OA + Ch2, (e) OA + Ch2P1, and (f) OA + Ch2P2. All the titration curves were obtained at room temperature.

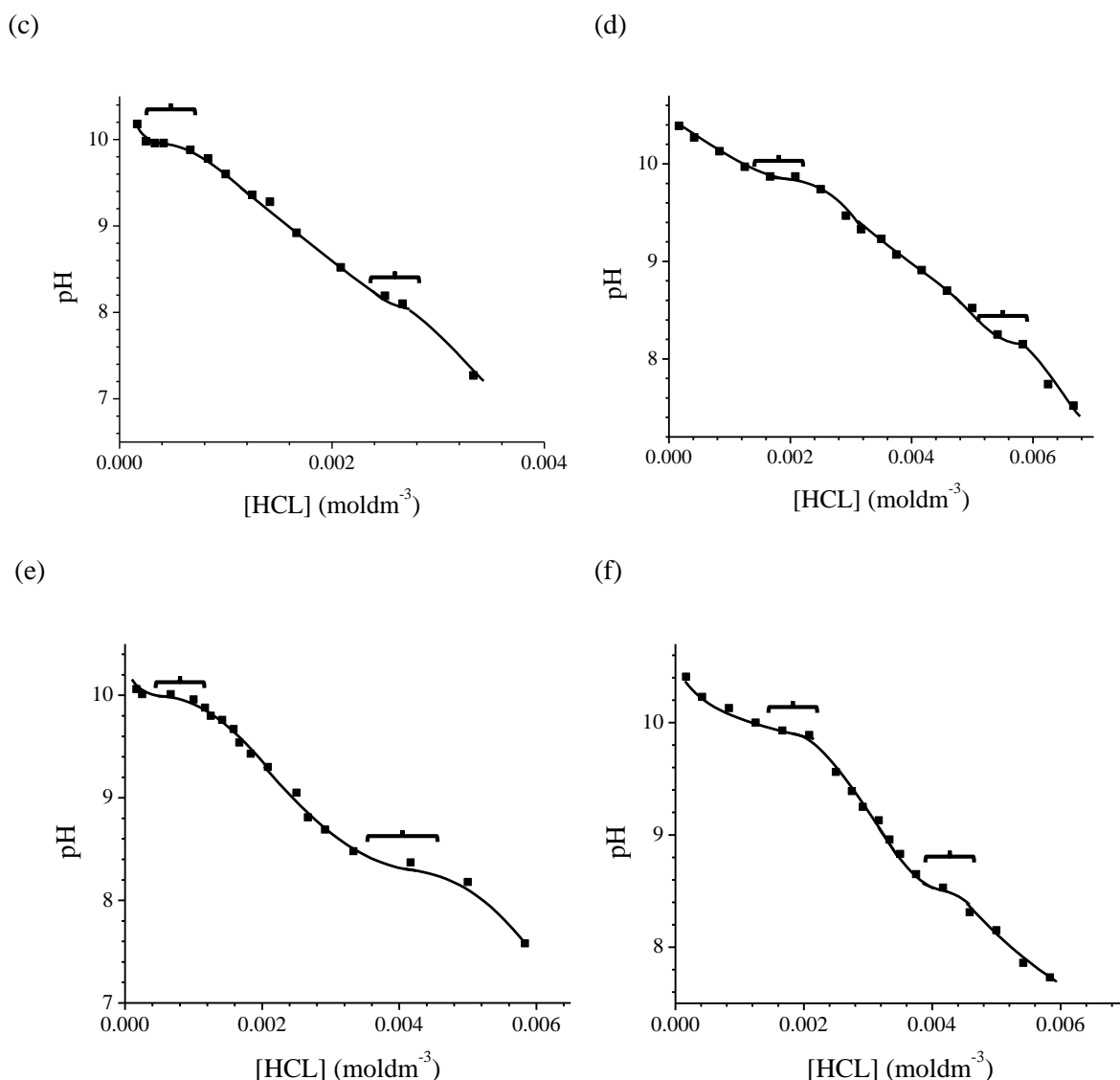


Figure 3.6 (continued)

The profiles of the titration curves for OA-Chs and OA-ChPs mixtures were found to be slightly deviated from the pure OA solution. The buffering region for OA-Chs and OA-Ch2Ps was found to shift towards lower pH region (\sim pH 8.5) as compared to the titration curve for pure OA (Figure 3.6). This result can be explained with the shift of the pK_a value for the OA-Chs or Ch2Ps mixtures. It was found that the pK_a s of OA-Chs and OA-Ch2Ps mixed systems were relatively lower than the pure OA (Table 3.2). The decrease in the pK_a of a mixed system may be attributed to the intermolecular interaction between the OA molecules and Chs or Ch2Ps. In the OA-Chs mixed systems,

Chs containing amine and hydroxyl groups could interact with the OA molecules at the membrane bilayer of the liposomes. The interaction between the OA molecules and Chs may involve hydrogen bonding by sharing the hydrogen from the amine and/or hydroxyl groups of the Chs with the OA molecules or via ion-dipole interaction with the Chs molecules since the OA dimers are negatively charged (Harris and Turner, 2002). Besides, the decrease in the pK_a of the mixed systems may also be attributed to the intermolecular distance between the OA molecules, as the pK_a value was proposed to be inversely proportional to the intermolecular distance between OA molecules (Kanicky and Shah, 2002; Kanicky et al., 2000). This may typically occur in the OA-Ch2Ps mixture as the hydrophobic moieties from its backbone could interact with the OA molecules via hydrophobic interaction and disturbed the close packing of the OA molecules.

Table 3.2: pK_a of the pure OA and its mixture with Ch1, Ch2, Ch2P1, and Ch2P2.

Samples	pK_a
OA	9.81
OA + Ch1	9.20
OA + Ch2	8.96
OA + Ch2P1	8.98
OA + Ch2P2	8.95

3.2.2 Surface tension

The surface tensions of all liposomal solutions were plotted against \ln concentration of their monomeric species at pH ~ 8.8 in 0.05 mol dm^{-3} borate buffer solution (Figure 3.7). It was found that the surface tension of all liposomal solutions decreased with increasing oleic acid concentration until reaching a concentration at which the surface tension deviate to a constant value. For the surface tension profile of the OA liposome, two inflection points were observed with the increase of OA concentration. These inflection points were characterized as the critical aggregation concentration (CAC), namely CAC_1 and CAC_2 . This result indicated that there was a difference in the decreasing rate of the surface tension with increasing OA concentration before and after CAC_1 that can be plausibly explained with the presence of the conjugate base (OA-COO^-) and conjugate acid (OA-COOH) of OA. Since the OA liposome solution was prepared at pH 8.8, more OA-COOH was present in the solution as the $\text{p}K_a$ of OA was reported to be 9.80 as discussed in previous section. This OA-COOH is more hydrophobic and more surface active at the air-water interface. On the other hand, the OA-COO^- is more polar characteristic, therefore it has higher solubility in the aqueous environment. For this reason, the OA-COOH could adsorb at the surface of the aqueous and thus, reduced its surface tension. This phenomenon is pronounced at OA concentration lower than CAC_1 . However, when the OA concentration increased and exceeded the CAC_1 , the OA liposomes started to form whereby the OA-COOH started to pair-up with the OA-COO^- of the OA molecule (Walde et al., 2007). The pair of OA-COOH and OA-COO^- with double alkyl chains is more hydrophobic, as a result the hydrophobic effect will minimized the unfavourable energy by forming aggregates (i.e. liposomes) or adsorb at the air-water interface. As a consequence, the second slope as shown in Figure 3.7 is formed. Further increase in the OA concentration led to the formation of more OA-COOH and OA-COO^- pair and eventually reached an

equilibrium condition between the bulk and the surface of the aqueous solution which explained the formation of plateau region after the CAC₂. However, this phenomenon is less pronounced in the OACHs and OACH2Ps liposomes systems.

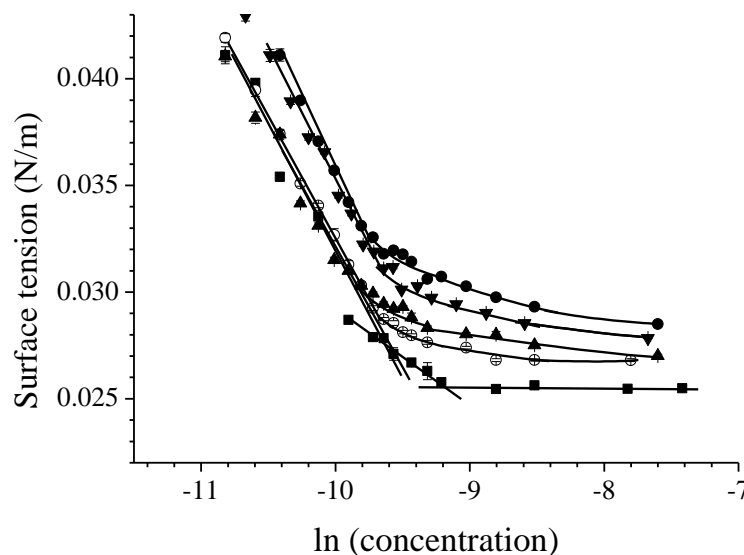


Figure 3.7: Surface tensions profile of the (■) OA, (○) OACH1 (0.20%), (▲) OACH2 (0.20%), (●) OACH2P1 (0.20%), and (▼) OACH2P2 (0.20%) liposome solutions respectively as a function of ln concentration at pH 8.8 ± 0.1 in 0.05 mol dm^{-3} borate buffer solution at 25°C .

The surface tensions of OACHs and OACH2Ps liposomes were found to be higher than the OA liposome (Figure 3.7). This could be due to the greater water solubility and less surface active property of the Chs and Ch2Ps as compared to the OA (Li et al., 2006). The critical vesicular concentration (CVC) of the liposome solutions was estimated at the crossover point by drawing two linear lines, one at low concentration region and the other one at plateau region. The CVC of all the Chs and Ch2Ps modified liposomes were found to be slightly lower than OA liposome (Table 3.3). This result showed that the formation of OACHs and OACH2Ps liposomes were more favourable as compared to the OA liposome (Teo, 2012).

Table 3.3: CVC of OA, OACH1, OACH2, OACH2P1, and OACH2P2 liposome solutions at constant temperature of 25 °C.

Sample name	Amount of chitosan (% w/v)	Critical vesicular concentration, CVC ($\mu\text{mol dm}^{-3}$)	
		1	2
OA	-	79.48	101
OACH1	0.10	74.85	-
	0.20	68.41	-
	0.30	58.88	-
OACH2	0.04	74.85	-
	0.10	74.85	-
	0.15	76.36	-
	0.20	61.28	-
	0.25	60.67	-
OACH2P1	0.03	71.46	-
	0.05	65.84	-
	0.10	57.55	-
	0.15	62.47	-
	0.20	60.01	-
	0.25	67.66	-
OACH2P2	0.03	70.00	-
	0.05	67.53	-
	0.10	54.75	-
	0.15	52.33	-
	0.20	55.71	-
	0.25	62.88	-

3.2.3 Morphology of liposomes

3.2.3.1 Optical polarizing micrographs

The morphology of OA, OACH1, OACH2, OACH2P1, and OACH2P2 was evaluated using optical polarizing microscope, TEM, and AFM. The micrographs obtained from the optical polarizing microscope showed that all liposomes are spherically shape (Figure 3.8). Unlike the OA liposome, the optical polarizing images of OACH1, OACH2, OACH2P1, and OACH2P2 liposomes do not exhibit any birefringence effect and Maltese cross at dark field. This might be due to the adsorption of chitosan onto the surface of OA liposome and disturbed the packing order of the OA molecules at the bilayer membrane since the birefringence effect of the OA liposomes arises from the ordered alignment of OA molecules at the lipid bilayer (Miyata and Hotani, 1992).

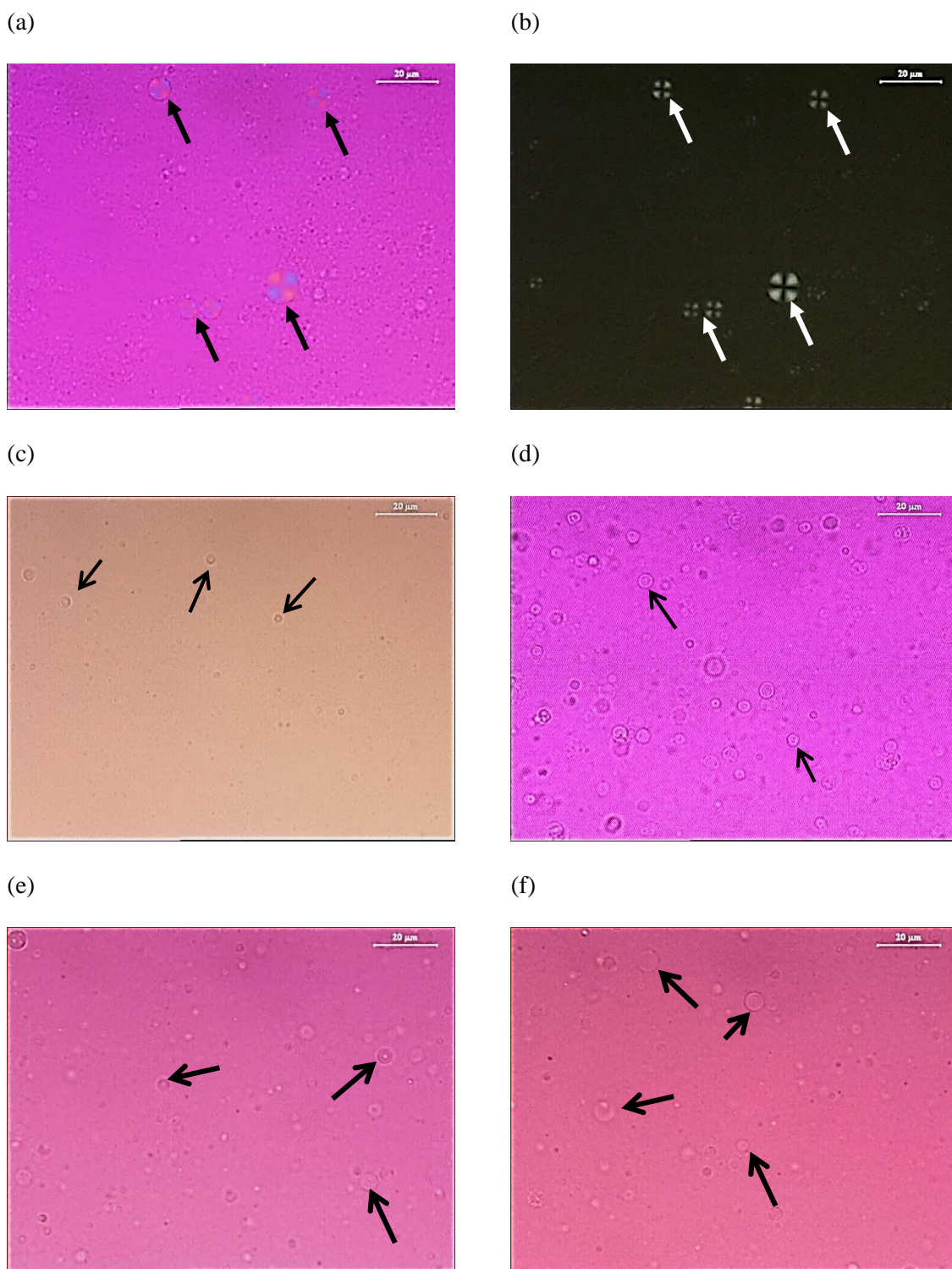


Figure 3.8: The optical polarizing micrograph of (a) OA liposome which showed birefringence effect, (b) OA liposome under dark field which showed Maltese cross, (c) OACH1 liposome, (d) OACH2 liposome, (e) OACH2P1, and (f) OACH2P2 liposome.

3.2.3.2 TEM and AFM micrographs

The TEM micrographs clearly showed that the chitosan modified OA liposomes (OACH1, OACH2, OACH2P1, and OACH2P2) were spherical in shape (Figure 3.9). The presence of the Chs and Ch2Ps on the lipid layer of the OA liposome thickened the lipid layer and increased the opacity, thus the surface of the chitosan-modified OA liposome appears to be black in colour (Wang et al., 2010). However, the OA liposome was not observed under TEM. The structure of the OA liposome was found to collapse under the TEM (Figure 3.9(a)). The collapse of the OA liposome structure might be due to the drying process or vacuum condition.

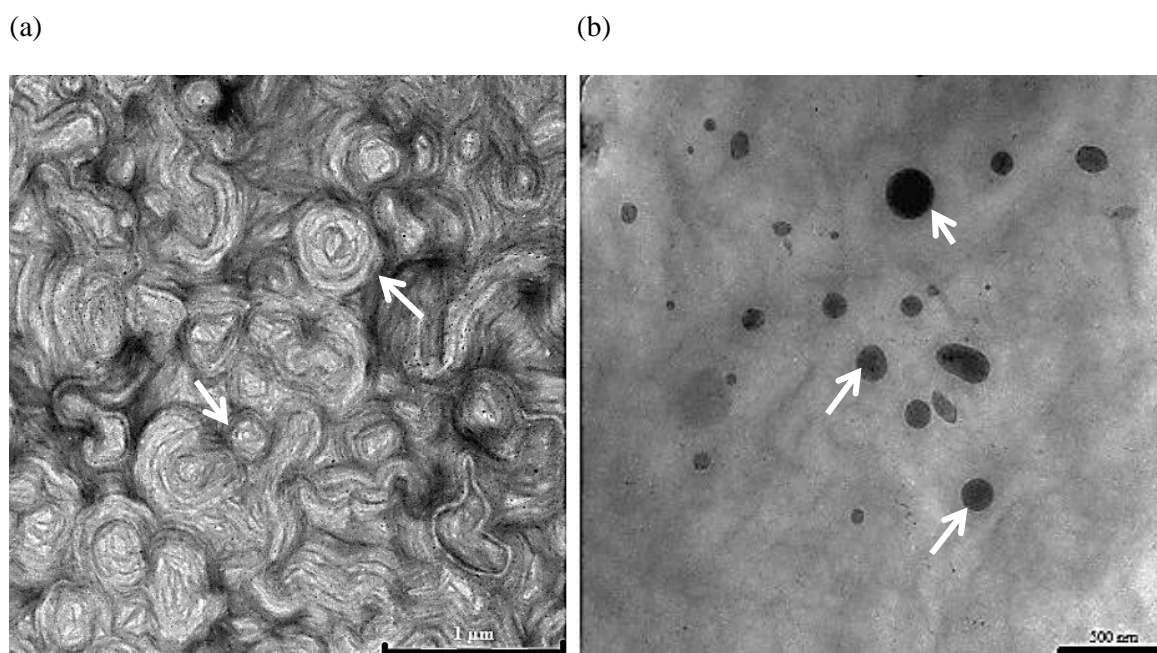


Figure 3.9: TEM image of the (a) OA liposomes, (b) OACH1 liposomes, (c) OACH2 liposomes, (d) OACH2P1 liposomes, and (e) OACH2P2 liposomes. The amount of chitosan used in the preparation of the OACH2 liposome was 0.20%.

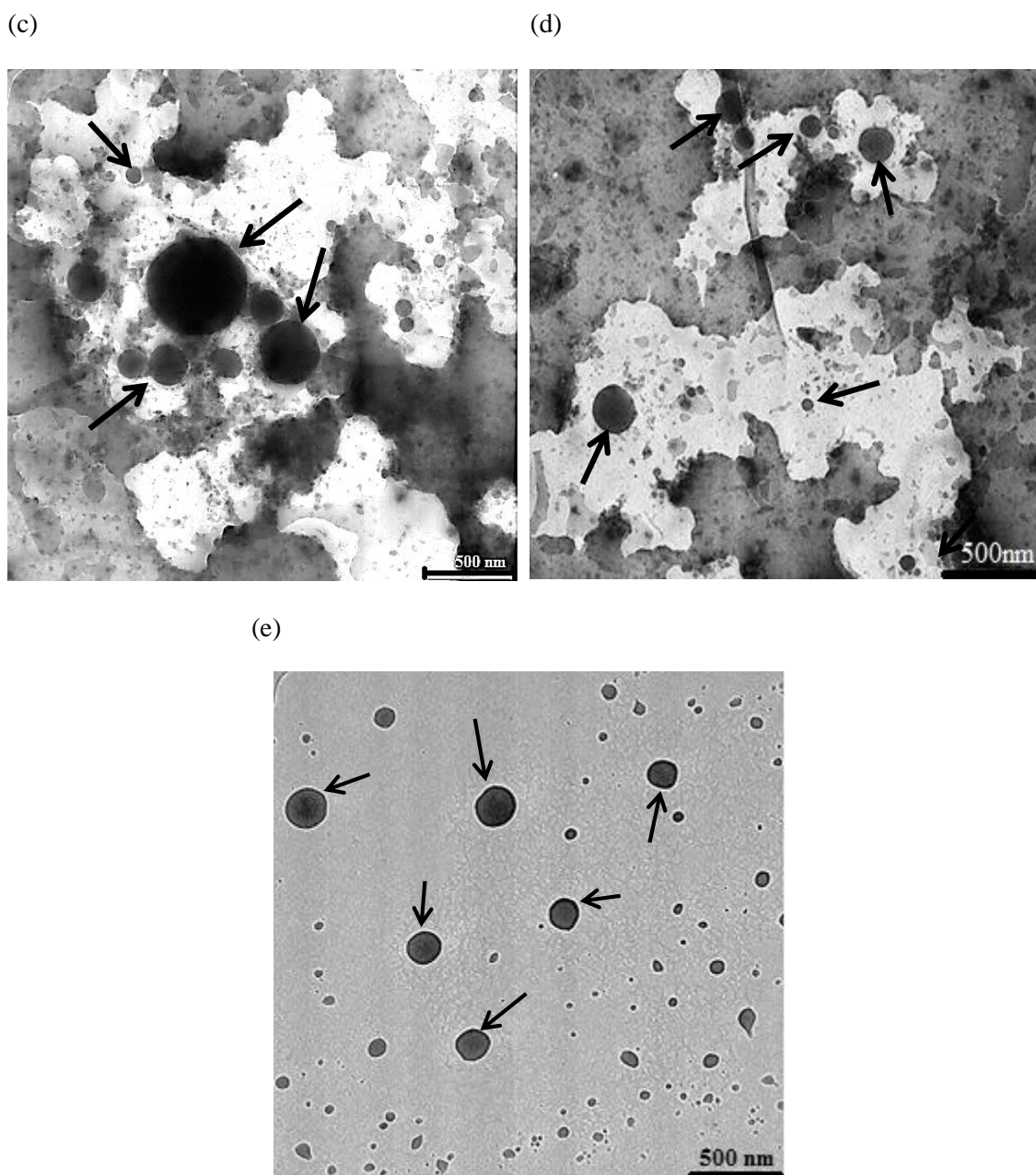


Figure 3.9 (continued)

Similarly, for the AFM micrographs, the OA liposomes were hardly seen as compared with the OACH1, OACH2, OACH2P1, and OACH2P2 liposomes (Figures 3.10). This observation further indicated that the rupture of structure of the OA liposome happen in the drying process during sample preparation, as vacuum is not required for AFM imaging. These results can be explained in terms of the rigidity of the liposome (Lipowsky, 1991; Maurer et al., 2001). Generally, rapid spreading will happen

once the liposome is in contact with the surface (Maurer et al., 2001). The membrane bilayer of liposomes tends to flatten on the surface when they come in contact with surface and eventually increase the tension of the membrane bilayer. When the stress continuously increases, the lipid membrane of the liposomes will release the stress by rupturing its structure (Lipowsky, 1991; Maurer et al., 2001). In other word, liposome with greater rigidity has higher resistance to the stress and prevents structural damage as demonstrated by the surface modified liposomes (OACH1, OACH2, OACH2P1, and OACH2P2). It was also found that the OACH1, OACH2, OACH2P1, and OACH2P2 liposomes showed “peeling off” effect on their surface and indicated that the Ch1, Ch2, Ch2P1, and Ch2P2 have modified the surface of the OA liposome.

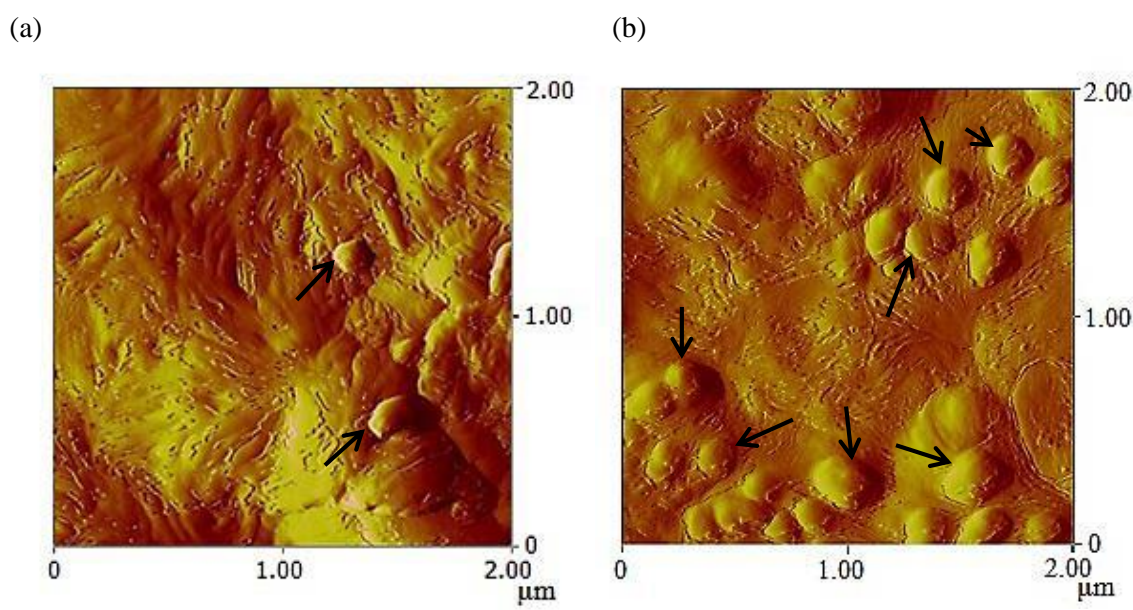


Figure 3.10: AFM image of (a) OA liposome, (b) OACH1, (c) OACH2, (d) OACH2P1, and (e) OACH2P2. All the chitosan modified OA liposomes were prepared with 0.20 % (w/v) of chitosan and its derivatives. (The liposomes were indicated by the black arrows).

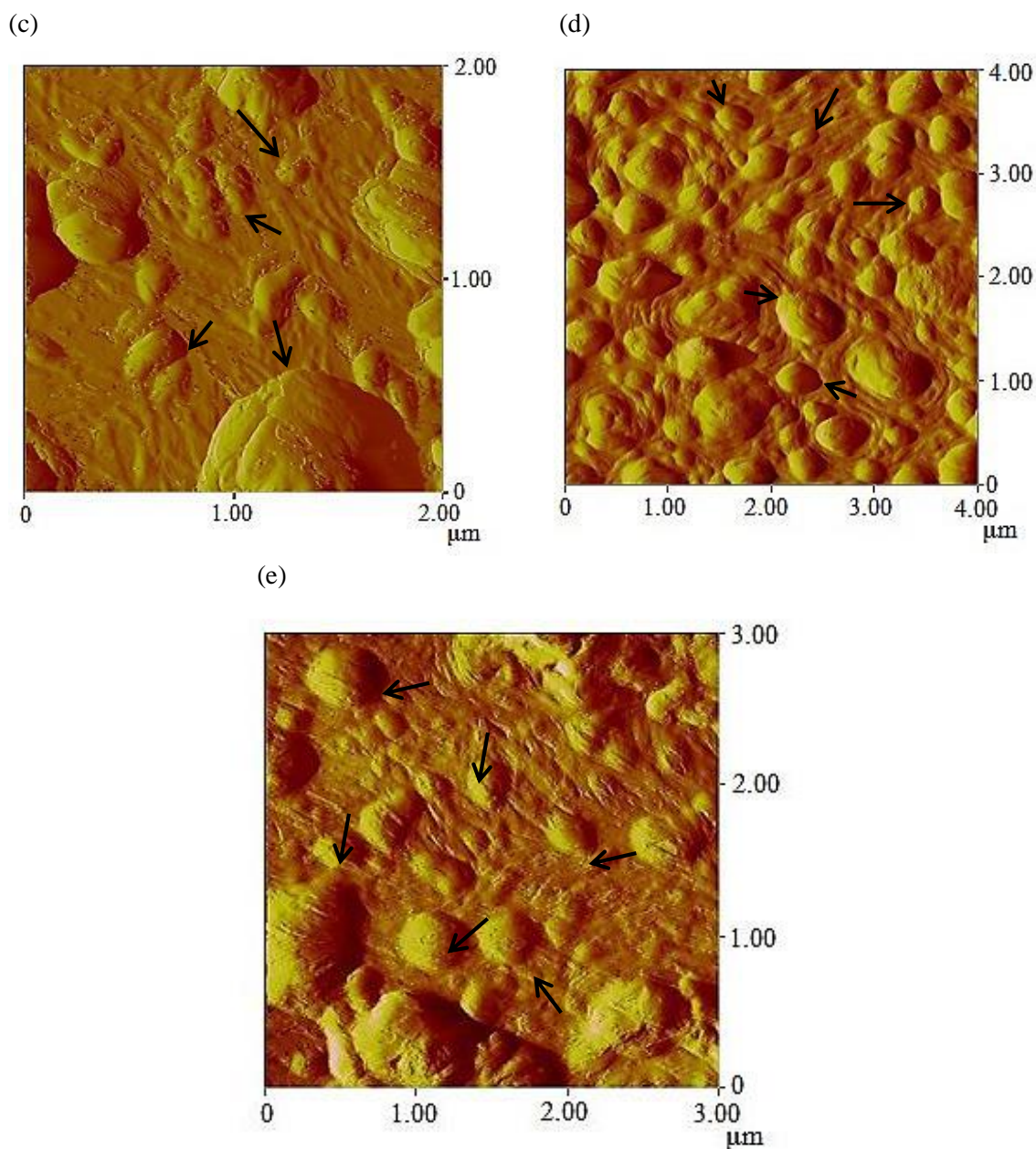


Figure 3.10 (continued)

3.2.4 Size of liposomes

The size of the OACH1 and OACH2 liposomes was found to be at least 20 nm smaller than that of the OA liposome (Figure 3.11). It was mainly due to the chitosan that formed a cage-like steric barrier that protected the liposome from aggregation and stabilized the liposomes (Morigaki and Walde, 2007). The size of OACH1 was increased

from 115 nm to 130 nm when the amount of Ch1 increased from 0.10% (w/w) to 0.30% (w/w), whereas, the size of the OACH2 increased from 105 nm to 125 nm when the amount of Ch2 increased from 0.10% (w/w) to 0.20% (w/w) (Figure 3.11). This result indicated that the formation of more chitosan layers on the surface of the liposome (Guo et al., 2003). Similar result was also reported in the characterization of chitosan-coated phospholipid liposomes (Li et al., 2009; Liu and Park, 2010; Mady et al., 2009). However, the size of the OA liposomes that are modified with Chs concentration lower than 0.10% was found to be higher as compared to the liposomes that modified with 0.30% of Chs. This result indicated that 0.04% of Chs was not sufficient to create an adequate protection layer on the surface of the liposomes (Li et al., 2009). The distributions of the prepared liposomes were found to be polydispersed (Figure 3.12). The changes in the polydispersity index of all chitosan-modified liposomes were not significant as compared to the OA liposome (Figure 3.12(b)).

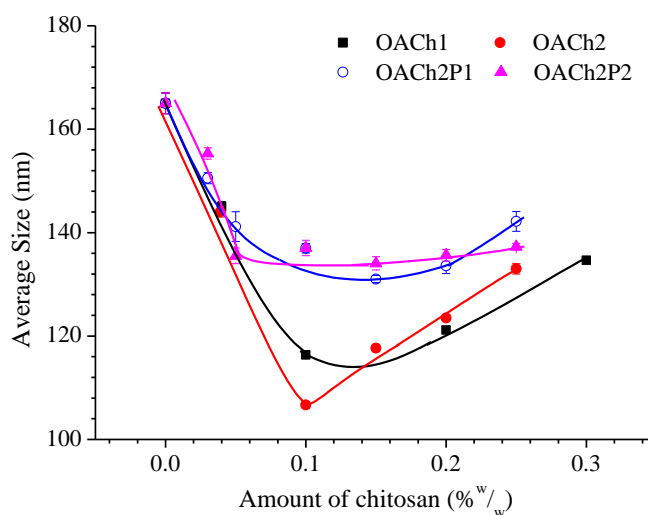


Figure 3.11: Effect of the amount of Ch1, Ch2, Ch2P1, and Ch2P2 on the size and zeta potential of the OA liposome. The data was taken at day seventh after the liposome solutions were prepared.

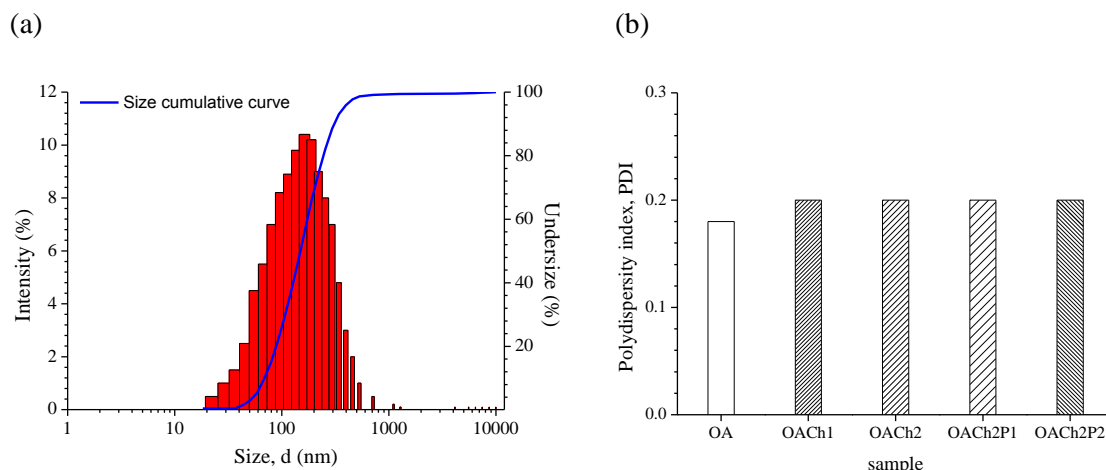


Figure 3.12: (a) The typical size distribution of the OA liposome showing its polydispersity. (b) The polydispersity index for the OA liposome and chitosan-modified OA liposomes.

The size of OACH2P1 and OACH2P2 liposomes was found to be at least 30 nm smaller than that of OA liposome (Figures 3.11). The decrease in the size of OACH2P1 and OACH2P2 liposomes was mainly due to the anchored Ch2Ps that perturbed the OA monomer arrangement at the liposome bilayer. The insertion of the hydrophobic moieties of Ch2Ps into the liposome bilayer has resulted in the increase of curvature and decrease of the size of liposomes (Park et al., 2011). The effect of the amount of Ch2P1 and Ch2P2 on the size of the OACH2Ps liposome was evaluated at day 7. The OACH2P1 and OACH2P2 liposomes were found to exhibit two different size profiles with increasing amount of Ch2Ps. The size of OACH2P1 liposome was decreased with increasing amount of Ch2P1 from 0 to 0.15% (w/w) but increased when the amount of Ch2P1 exceeded 0.15% (w/w). This result indicated that more Ch2P1 layers were attached onto the surface of the liposome (Guo et al., 2003). For the OACH2P2 liposome, the size was decreased from 165 nm to 136 nm when the amount of Ch2P2 increased from 0 to 0.05% (w/w) and the size remained unchanged when the amount of Ch2P2 exceeded 0.05% (w/w). This result indicated that 0.05% (w/w) of Ch2P2 is sufficient to enhance the physical stability of the OACH2P2 liposome. This was mainly

attributed to the higher DA of Ch2P2. Ch2P2 has more alkyl side chains that are available to be inserted into the liposome lipid bilayer and improved the liposome membrane rigidity and integrity as discussed in section 3.2.3.2.

3.2.5 Zeta potential of liposomes

The surface modification of the OA liposome by Chs and Ch2Ps was also evaluated by comparing their zeta potential before and after modification. The zeta potential of OA liposome was negatively charged. After surface modification, the zeta potential for all Chs- and Ch2Ps-modified OA liposomes were decreased by at least 20 mV. These results were attributed to the formation of a condensed coating of the chitosan layers that carried the positive charge, on the surface of the liposomes (Li et al., 2009; Liu and Park, 2010; Mady et al., 2009). The Chs and Ch2Ps layers have effectively shielded the negatively charge of the OA liposomes. The amount of Chs and Ch2Ps used also affected the zeta potential of the Chs- and Ch2Ps-modified OA liposomes. For Chs, the zeta potential increased from -86 to -64 mV when the amount of Ch1 and Ch2 increased to 0.15% and 0.05%, respectively (Figures 3.13). However, there were no significant changes in the zeta potential of OACH1 and OACH2 liposomes that are modified with > 0.15% of Ch1 and > 0.05% of Ch2, respectively. This result implied that 0.15% of Ch1 and 0.05% of Ch2 are the minimum amount required to coat and protect the surface of the OA liposome. Also, the amount of Ch2 required was significantly lesser than Ch1. This can be explained with the molecular structure of the Ch1 and Ch2. According to section 3.1.3, the molecular weight of Ch2 is greater than Ch1. In other word, the Ch2 have longer polymer chain as compared to Ch1. The longer polymer chain can coat and shield the liposome more effectively than the shorter one. As a result, less amount of Ch2 is required to reduce the zeta potential of the OA liposome. Similar result was also found in the zeta potential of OACH2P1 and OACH2P2 liposomes. The zeta potential for

OChP1 and OCh2P2 increased from -86.0 to -60.0 mV by increasing the amount of Ch2P1 and Ch2P2 to 0.05% and 0.03%, respectively (Figures 3.13). However, the difference in the minimum amounts of Ch2P1 and Ch2P2 that are required to decrease the zeta potential of the liposomes were negligible. This result was mainly due to the fact that the chain length of Ch2P1 and Ch2P2 were the same as they were prepared from the same starting material (Ch2). Besides, it was found that the effect of DA to the changes in liposome size and zeta potential were negligible.

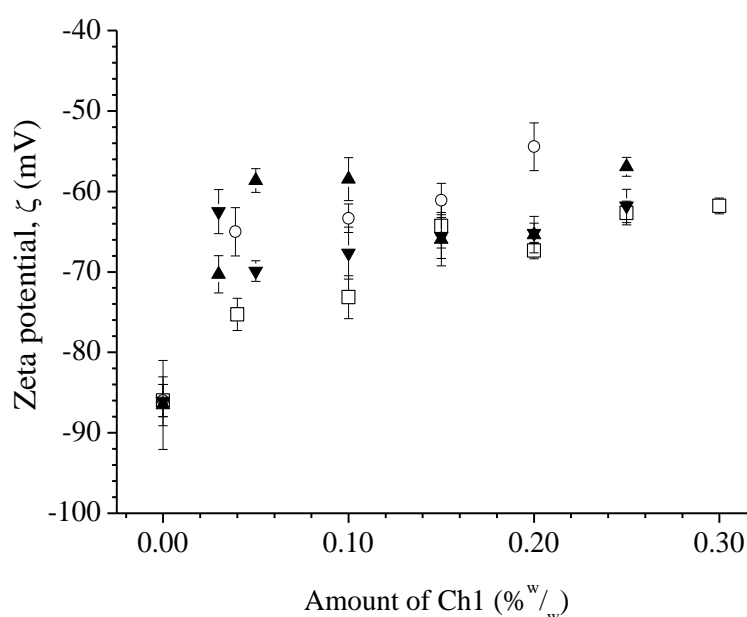


Figure 3.13: The effect of (\square) Ch1, (\circ) Ch2, (\blacktriangle) Ch2P1, and (\blacktriangledown) Ch2P2 amount of the zeta potential of the OA liposome.

3.2.6 Liposome stability

The stability of all prepared liposomes was evaluated by monitoring the changes of their size as a function of storage duration of 30 days. As compared to Chs and Ch2Ps modified liposomes (130 nm), the OA liposome can only be stable at larger liposome size (161 nm). This was mainly due to the increase in the curvature of the surface

modified OA liposomes as discussed previously in section 3.2.4. As an OA liposome, the size of the OACH1, OACH1, OACH2P1 and OACHP2 liposomes was found to increase slowly for the first 7 days of storage time. This result has been attributed to the continuous rearrangement of the Chs and Ch2Ps distribution at the surface of the liposomes (Li et al., 2009). The size of all OACH1, OACH2, OACH2P1 and OACH2P2 liposomes remained unchanged after the 7th day. However, liposomes that were modified with 0.25% of Ch2P1 and 0.30% of Ch2P2 showed slight increment in size (Figure 3.14). For the liposome that modified with 0.25% of Ch2P1 (OACH2P1), the size of the liposome was found to increase from 140 nm to 160 nm after 30 days of the storage period, while the size of liposome that was modified with 0.30% of Ch2P2 (OACH2P2) was found to increase dramatically from 125 nm to 190 nm at the 30 days of storage period. These results have showed that the OACH2P1 (0.25% Ch2P1) and OACH2P2 (0.30% Ch2P2) liposomes are relatively less stable as compared to other liposomal systems that have been prepared in this study.

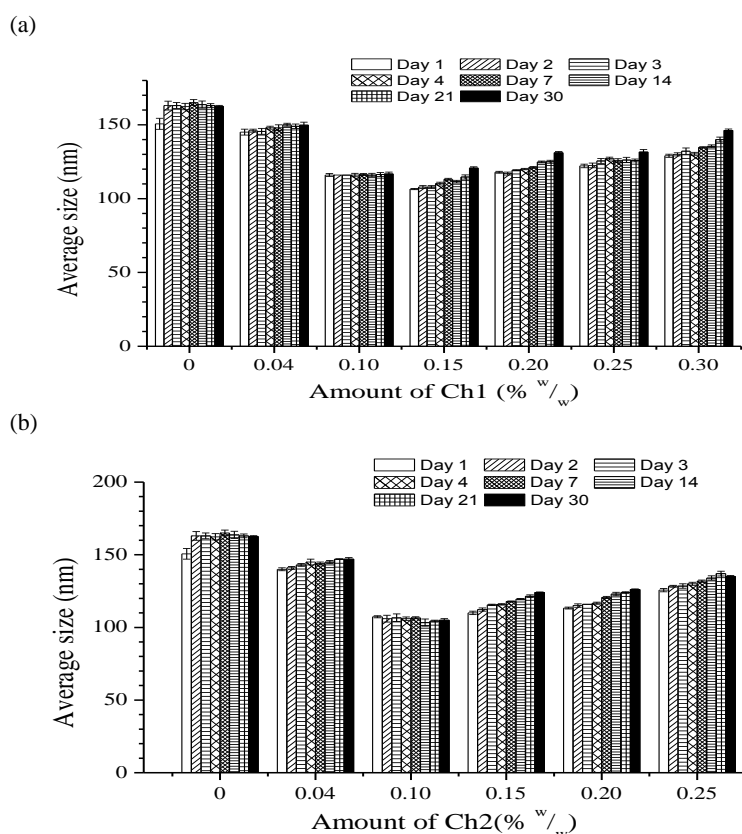
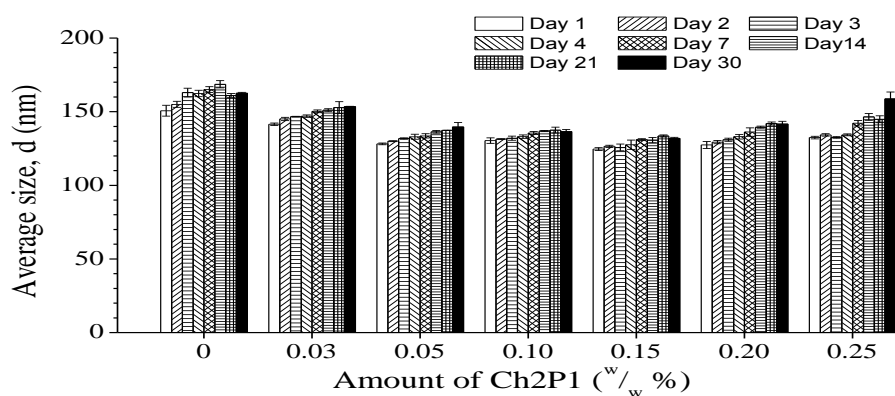


Figure 3.14: Variation of size of (a) OACH1, (b) OACH2, (c) OACH2P1, and (d) OACH2P2 liposomes.

(c)



(d)

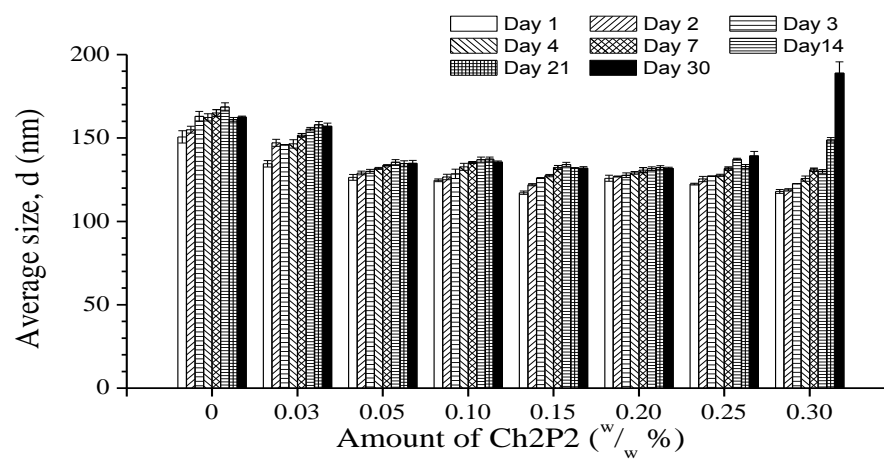


Figure 3.14 (continued)

3.3 Rheological study of ι C-CMC mixed gel

3.3.1 Rheological behaviour of ι C and CMC pure gel

All gels prepared in this study were subjected to rheological studies such as elasticity and flow behavior in order to evaluate the feasibility of these pure gels for the preparation of liposomal gels. The rheological behavior of ι C and CMC were first examined using amplitude sweep mode. In the amplitude sweep mode, the linear viscoelastic region (LVR), critical strain (γ_c), G' , and cohesive energy (CE) values were obtained. The LVR and γ_c are the parameters used to characterize the flexibility of the gels, while the G' and CE are the parameters that can be used to evaluate the

elasticity and cohesiveness of the gel (Table 3.4). The G' of the gel was determined from the LVR from the amplitude sweep profile and the γ_c is the critical strain that represents the end of the LVR (Figure 3.15(a)), whereas the CE can be determined using the following equation (Sohm and Tadros, 1989):

$$CE = \frac{1}{2} G' \gamma_c^2 \quad \text{Eq. 3.1}$$

The ιC gel exhibited high G' and CE values which indicated its high rigidity (Table 3.4 and Figure 3.15). This result was mainly attributed to the strong internal gel network structure of the ιC . The frequency sweep test of the ιC gel also showed that the G' of the ιC was found to be greater than its G'' over the studied frequency range which indicated its solid-like behavior (Figure 3.15(b)). The solid-like behavior of the ιC was also indicated by its $\tan \delta$ profile (Figure 3.15(c)). The $\tan \delta$ is defined as G''/G' . The result showed that the ιC was highly elastic since its $\tan \delta \sim 0.1$ (Tan and Misran., 2011).

Besides viscoelastic properties, the flow behavior of the ιC was also studied by measuring its shear viscosity as a function of shear rate and shear stress which provides information on the spreadability and flowability of the gel (Garg et al., 2002). The ιC gel exhibited high viscosity and large yield stress (σ_p) which indicated that higher applied stress is required to initiate the flow of ιC gel as the σ_p is the critical stress where the gels begin to flow (Table 3.4 and Figure 3.15(d)) (Brummer, 2006a). This result was also attributed to its strong internal gel network structure.

Table 3.4: The critical strain (γ_c), break point (γ_b), elastic modulus (G'), cohesive energy (CE), and yield stress (σ_p) of the ιC and CMC that determined from their dynamic and steady rheological behaviors.

	Critical strain, γ_c	Break point, γ_b	Elastic modulus, G' (Pa)	Cohesive energy, CE (Pa)	yield stress, σ_p (Pa)
ιC	0.413 ± 0.005	0.305 ± 0.005	36.41 ± 0.01	5.11 ± 0.01	38 ± 2
CMC	N/A	N/A	0.70 ± 0.02	N/A	4.72 ± 0.09

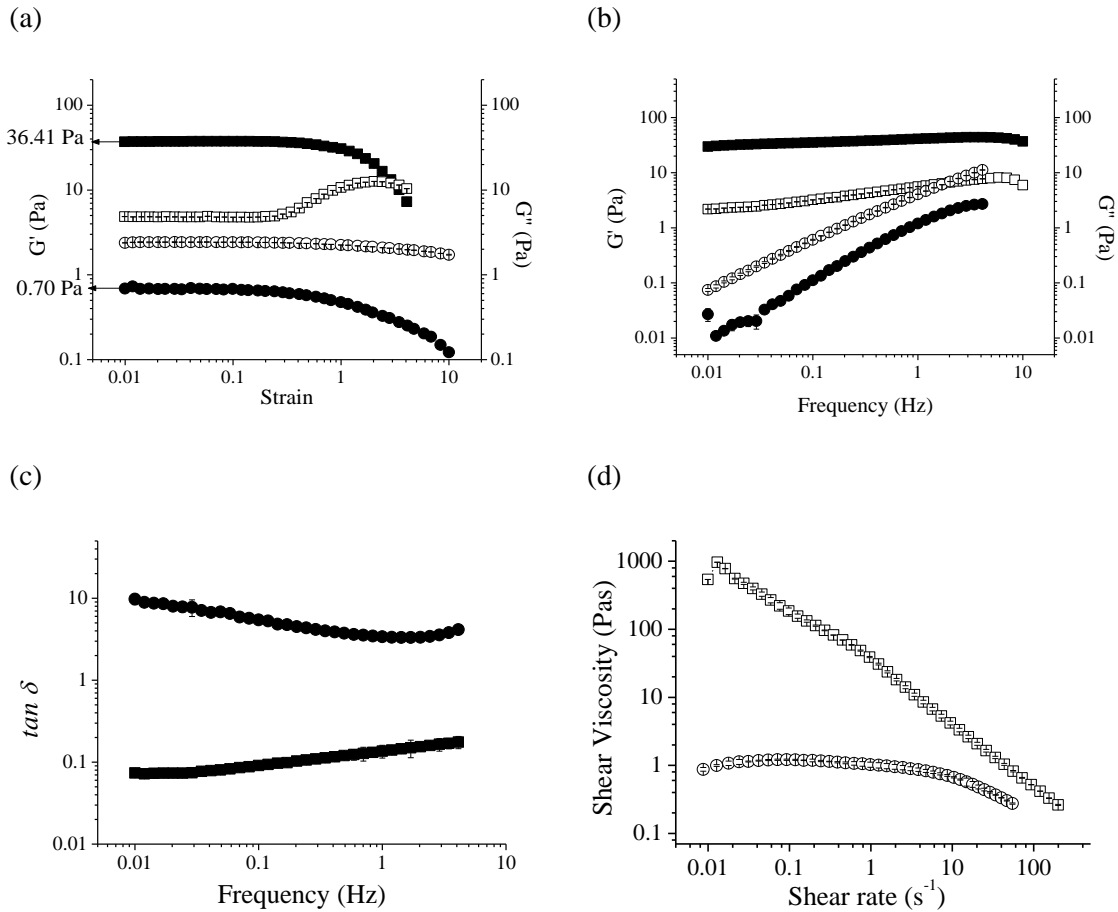


Figure 3.15: The rheological behavior of the (■) ιC and (●) CMC obtained at 25°C where (a) the strain sweep profile, (b) the variation of G' (solid symbol) and G'' (open symbol) as a function of frequency, (c) the $\tan \delta$, and (d) the flow curve.

Unlike ιC gel, the rheological analyses showed that the CMC solution exhibits different viscoelastic behavior. The amplitude and frequency sweep profile of the CMC solution have shown that the G'' curve is always dominant against G' over the studied strain and frequency range. These results indicated that the CMC is more liquid-like characteristic and does not form gel structure (Figures 3.15(a)-(c)) (Benchabane and

Bekkour, 2008; Kästner et al., 1997). In other words, there were no complicated gel network structure being formed within the CMC chains (Barbucci et al., 2000; Kästner et al., 1997; Khaled and Abdelbaki, 2012; Zhong and Jin, 2009). The G' of the CMC solution was also relatively lower than that of ιC gel. This predictably shows that the internal network structure of the CMC solution is quite weak which is due possibly to the non-entangled nature of CMC chains (Benchabane and Bekkour, 2008). It's also interesting to note that the shear viscosity of the CMC solution was 1000 time lower than ιC gel. This result indicated that the CMC solution is less resistant to flow and less entanglement of CMC chain in the network to form three dimensional network structures as discussed above.

By comparing the rheological properties that has been discussed, it can be concluded that the ιC gel in this study has a rigid structure with high G' and CE . However, the liposomes were unable to be dispersed homogeneously in the ιC gel due to its high G' and CE (Rodríguez-Hernández and Tecante, 1999). In addition, the high shear viscosity of the ιC will also result in poor spreadability at the skin which eventually affected the liposome's diffusion rate from the ιC gel into the skin during application (Garg et al., 2002; Ueda et al., 2009). This may also cause adverse effects due to the incorrect dosage of drugs that has been transferred (Glavaš-Dodov et al., 2003; Ivens et al., 2001; Jelvehgari et al., 2007; Gabrijelčič and Šentjunc, 1995). On the other hand, the weak internal structure of the CMC solution was not strong enough to entrap the dispersed liposomes in its network structure thereby reducing the liposomal gel stability. For these reasons, mixtures of ιC and CMC were prepared by mixing the ιC and CMC at different ratio (Table 2.2). In order to identify the optimum composition of the mixed gel system that is suitable for the preparation of liposomal gel system, the rheological properties of these mixed gels were evaluated.

3.3.2 Gelation temperature of ι C-CMC mixed gel

Gelling temperature (T_{gel}) of the mixed gel was studied by evaluating the variation of its moduli as a function of temperature since the gelling behavior is temperature dependent (Tischer et al., 2006). In this study, T_{gel} of the gel mixtures was determined from a graph of modulus versus temperature as shown in Figure 3.16. The T_{gel} of ι C in borate buffer (pH 8.8) was 39.63 °C (Figure 3.16(a)). The determination of the T_{gel} of CMC solution in borate buffer (pH 8.8) was not possible as the CMC did not form gel under the experimental condition as mentioned earlier in section 3.3.1 (Figure 3.16(b)). As compared to ι C gel, the T_{gel} of the ι C-CMC mixed gel has shifted to lower temperature (Figure 3.16(c)). This result showed that the CMC chains have disturbed the network structure of the ι C gel. The T_{gel} of the ι C-CMC mixed gel was also found to decrease with increasing amount of CMC used ($P < 0.05$) which indicated the decrease of the gel strength of ι C-CMC mixed gel. This was mainly attributed to the increase in the number of interaction between ι C and CMC chains which is relatively weak as compared to the interaction between the original ι C polymer chains. According to previous studies, gelling behavior of ι C gel were mainly attributed to the coil-helices transition of the polymer chains (Wang and Cui, 2005a). In other words, the ι C chains formed double helices conformation when the experimental temperature was lower than the T_{gel} where the polymer chains would associate with each other to form strong three dimensional gel network structures (Hossain, 2001; Yuguchi et al., 2002).

The moduli versus temperature profiles in Figure 3.16 show that the ι C gels showed single plateau and exhibited single step gelation behavior. The same profiles were also observed in all the mixed gel studied with the exception in CMC profile whereby no cross-over was observed. In the plateau region, both modulus (G' and G'') of the all mixed gel systems in this study were temperature independent which suggested the homogeneity of the mixed gel (Norziah et al., 2006).

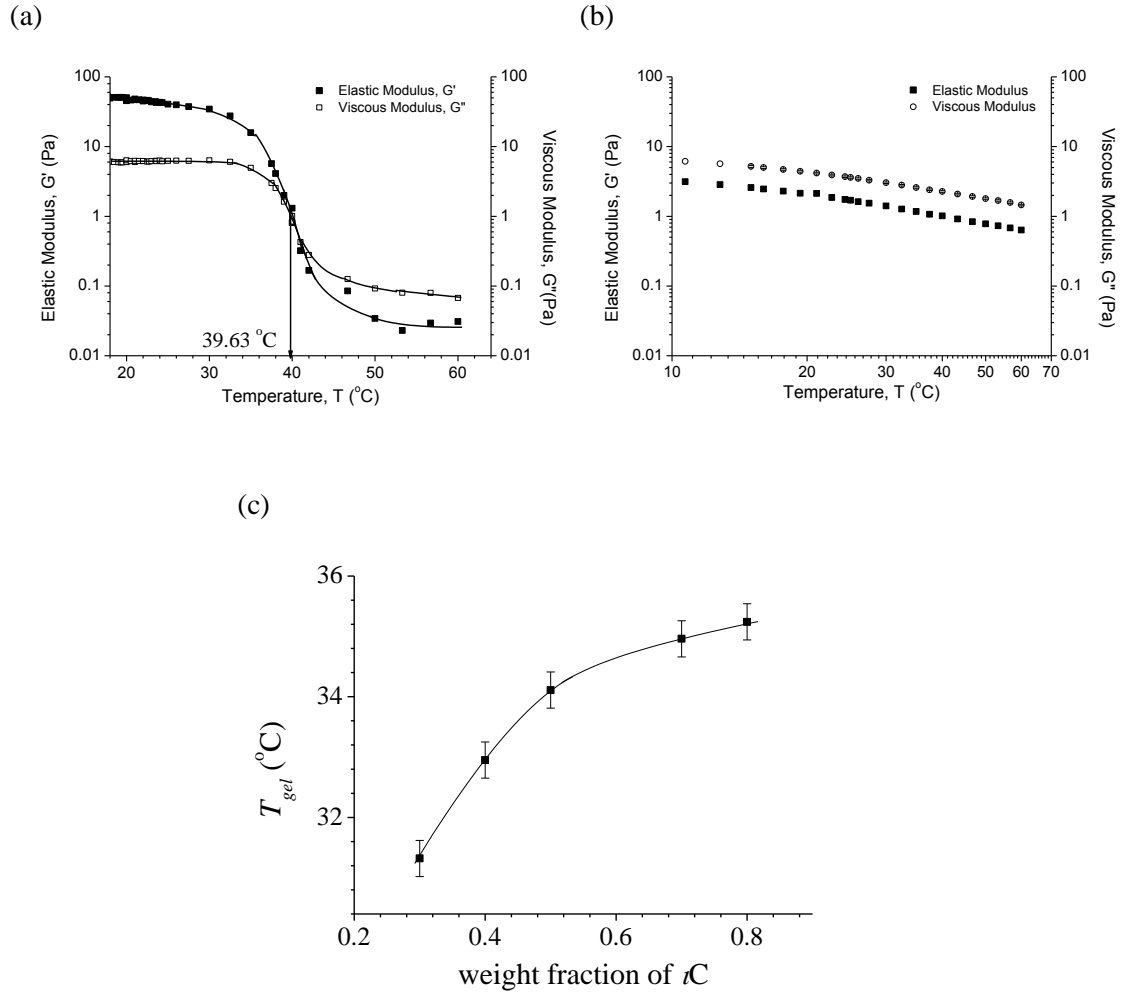


Figure 3.16: Gelation temperature of mixed gel. (a) pure ιC gel, (b) pure CMC solution, and (c) gelation temperature of the mixed gels as a function of the ιC weight fraction

3.3.3 Dynamic behavior of ιC -CMC mixed gel

In dynamic behavior test, all mixed gels were subjected to oscillating strain at an increasing manner i.e. the amplitude sweep test and the amplitude sweep profiles of these mixed gels were presented in Figures 3.17(a) and (b). The γ_c of the mixed gels was found to increase with increasing ιC concentration in the gel which indicated that the mixed gel has become more resistant to deformation. This was mainly due to the increase of ιC concentration in the gel which exerted more influence on the elasticity and flexibility of the gel mixture. As reported in previous studies (Gobet et al., 2009; Jones and Staples, 1973; Norton and Goodall, 1983), the ιC chains are in the form of

random-coil conformation and entangled with each other to form gel which promoted the formation of more flexible network structure. However, the γ_c value of the mixed gel was found to decrease when the concentration of ιC increased further and exceeded 0.54% (w/w) which indicated that the mixed gels is more sensitive to an applied strain and less flexible which might be due to the increase in the gel rigidity that is attributed from significant increase in entanglement in network structure of the mixed gels with ιC -CMC ratio of 8:2 and 7:3 as compared to the one with 5:5 of ιC -CMC ratio (Rodríguez-Hernández and Tecante 1999). The increase of physical entanglement between the polymer chains limited the mobility of the polymer chains and thus led to the formation of less flexible gel (low γ_c). Other than γ_c , the amplitude sweep profile also showed that the G' of the mixed gels were dominant over their G'' which implied the solid-like behavior of the gels. The magnitude of G' of the gels was also found to increase with increasing ιC concentration from the mixed gels with ιC -CMC ratio of 3:7 to 8:2 (Table 3.5). These results indicated the increase in the strength of the internal gel network (Shah et al., 2007). After exceeding the γ_c , the G' of the mixed gels was found to decrease with increasing applied strain until it reached the break point (γ_b). This is a characteristic point where the mixed gel started to flow ($G' < G''$). On the other hand, the γ_b was found to decrease with decreasing ιC concentration. This result indicated that the mixed gels with lower ιC concentration can easily flow. This result further supported the fact that the mixed gels with lower ιC concentration had gradually lost their elasticity as discussed above.

The changes in the CE of the mixed gels were found to be negligible for the mixed gels with ιC -CMC ratio of 8:2, 7:3, and 5:5. However, the CE of the mixed gel decreased dramatically from 1.989 Pa to 0.2497 Pa when the concentration of CMC in the mixed gel was greater than the ιC as in the mixed gel with ιC -CMC ratio of 4:6 and 3:7. This result indicated that the elastic strength of the gel network structure for the

mixed gels with ι C-CMC ratio of 4:6 and 3:7 were relatively weak as compared with the mixed gels with 8:2, 7:3, and 5:5 of ι C-CMC ratio.

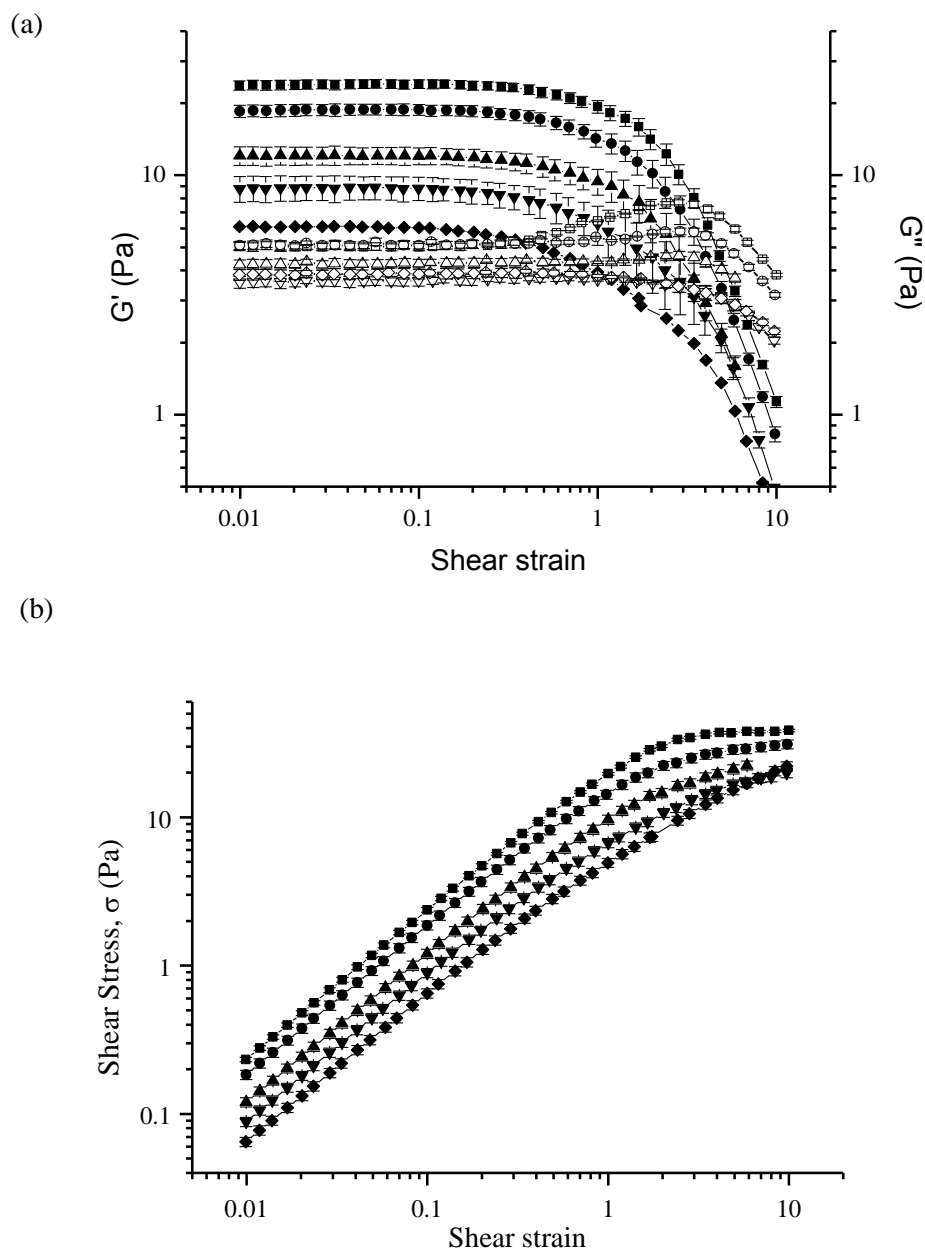
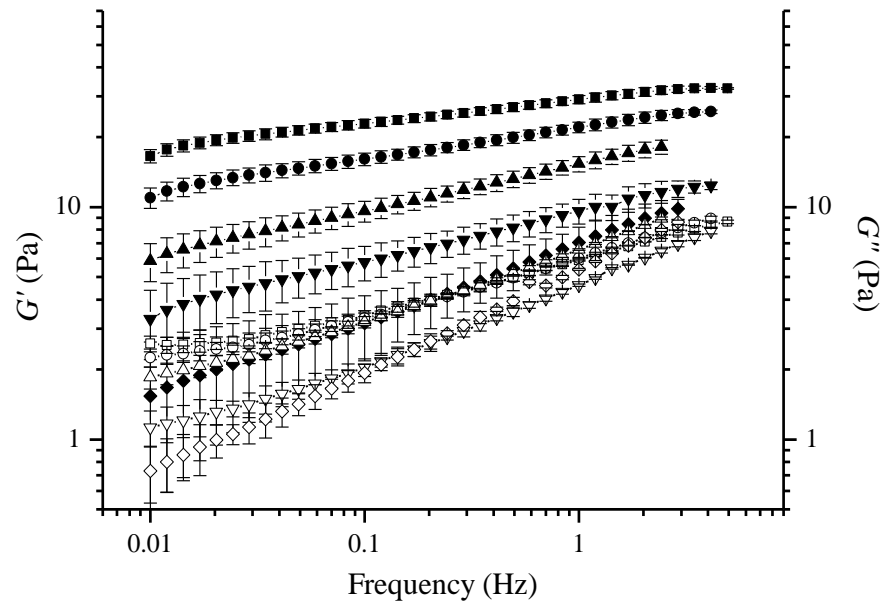


Figure 3.17: The dynamic mode rheology of the mixed gel with ι C-CMC ratio of (♦)3:7, (▼)4:6, (▲)5:5, (●)7:3, and (■)8:2 mixed gels obtained at 25°C where (a) is the strain sweep profile, (b) is the plot of shear stress versus strain to determine the γ_c , (c) is the variation of G' (solid symbol) and G'' (open symbol) as a function of frequency, and (d) is the $\tan \delta$ of the mixed gels.

(c)



(d)

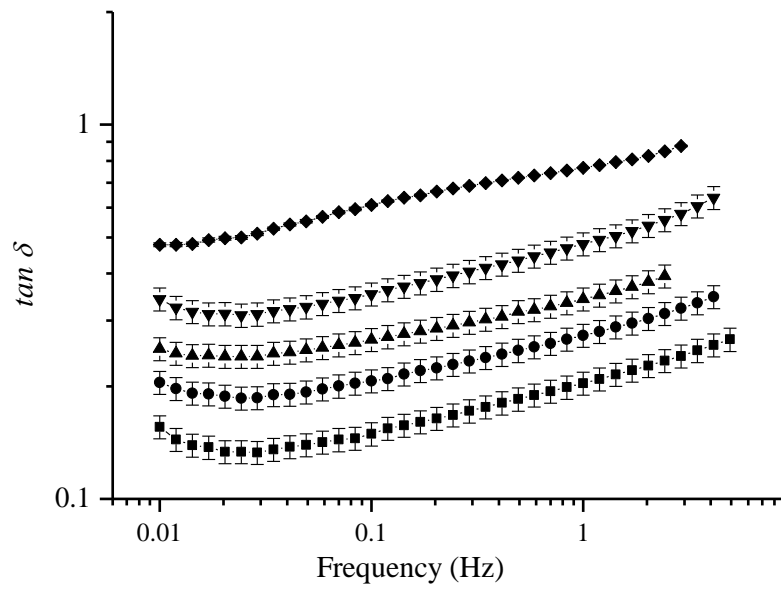


Figure 3.17 (continued)

Table 3.5: The Critical strain (γ_c), break point (γ_b), elastic modulus (G'), cohesive energy (CE), and yield stress (σ_p) of the mixed gels determined from respective dynamic rheological behaviors.

ιC -CMC ratio	Critical strain, γ_c	Break point, γ_b	Elastic modulus, G' (Pa)	CE (Pa)	Slope of G'
8:2	0.41±0.01	3.66±0.01	23.84±0.01	2.02±0.02	0.103±0.001
7:3	0.48±0.01	3.47±0.01	18.89±0.01	2.15±0.02	0.135±0.001
5:5	0.57±0.02	2.81±0.02	12±1	1.9±0.1	0.199±0.001
4:6	0.34±0.05	2.10±0.05	8.64±0.01	0.5±0.1	0.213±0.001
3:7	0.29±0.05	1.11±0.05	5.98±0.01	0.25±0.2	0.327±0.003

The viscoelastic behaviors of the mixed gels have been investigated using frequency sweep test. The frequency profiles are presented in Figure 3.17(c), all gel mixtures showed solid-like behavior with G' larger than G'' over the selected frequency range. The G' of the mixed gels was observed to be less frequency dependent when the concentration of ιC in the gel mixture was increased. The slope of G' of the gel decreases with increasing ιC concentration which indicates that the internal gel network has become stronger due to the increase of the physical entanglement between the polymer chains (Table 3.5) (Picout and Ross-Murphy, 2002). The magnitude of G' of the gels was found to increase with increasing ιC concentration in the mixed gel which implied that the applied energy can be stored more effectively in the elastic component of the gels with higher ιC concentration (Ikeda and Foregeding, 2003). Beside G' , the G'' of the gels was also increased with increasing ιC concentration. This result showed that the gels with higher ιC concentration dissipated more energy through its' viscous component. The energy dissipation that occurred in the gels was mainly due to the internal energy dissipation mechanism such as physical entanglements (Grillet et al., 2012). The increase in the ιC concentration has gradually promoted greater physical entanglement between the polymer chains and dissipated more internal energy.

The relationship and ratio between the G' and G'' of the mixed gels also can be expressed through their $\tan \delta$ profile (Figure 3.17(d)). The $\tan \delta$ of the prepared gels increased towards 1 when the concentration of CMC in the gel mixture is increased. This result indicated that the gel with higher CMC concentration was more liquid-like. An increase in the $\tan \delta$ with increasing CMC concentration also indicated that the gel has gradually lost its elasticity and rigidity (Figure 3.17(b)) (Barbucci et al., 2000).

The frequency sweep test will help to provide information on the relaxation time (τ) of the gel where τ is defined as the reciprocal frequency at the point where G' equal to G'' in the frequency sweep profile (Tan and Misran, 2011). However, the τ of all the gels was unable to determine from this study as ω did not fall within the studied frequency range. This is because the ω of the gels has shifted to lower frequency region (< 0.1 Hz) and indicated the long relaxation time of all gels.

3.3.4 Creep and recovery of ι C-CMC mixed gel

The long time scales viscoelastic behavior of the mixed gel was studied using the creep and recovery tests within the LVR. The long term viscoelastic behavior is highly related to the internal structure and realignment of the polymer chains. The information obtained from the long term viscoelastic behavior test also can be used to characterize the strength of a physical gel (Herraz et al., 2012). The formation of a physical gel was mainly attributed to the physical entanglement between the polymer chains i.e. the mixed gel system that was prepared in this study. The physical gel is reversible and the cross-links of the gel are non-covalent bond, and have finite lifetime (Fuchs et al., 1998). Since the cross-link of the physical gel is non-permanent, the physical gel tends to exhibit rheological creep behavior (Picout and Ross-Murphy, 2002).

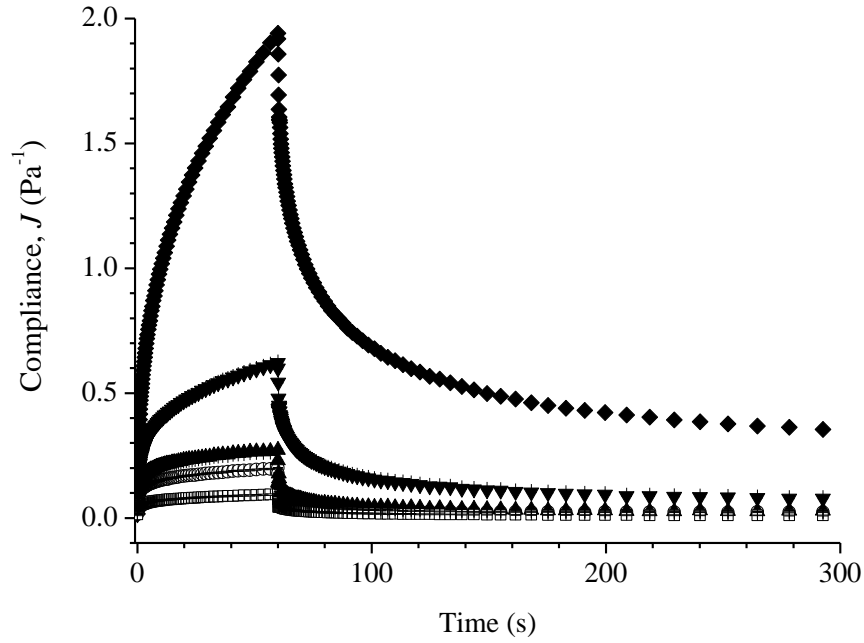


Figure 3.18: Creep and recovery profiles for the mixed gels with ιC -CMC ratio of (\blacklozenge)3:7, (\blacktriangledown)4:6, (\blacktriangle)5:5, (\circ)7:3, and (\square)8:2 performed under 0.1 Pa constant stresses at 25°C.

In this study, the creep profile was performed for 60 s and fitted to the Burger's model (Eq. 2.6 as discussed in Chapter 2) and yielded values of $r^2 \geq 0.995$. On the other hand, the recovery profile ($t \geq 60$ s) of the gels was fitted to the Eq. 2.7. All four elements, G_o , G_I , η_o , η_I , that contributed to the springs and dashpots of Maxwell and Kelvin-Voigt models were determined and shown in Table 3.6. All mixed gels were found to exhibit viscoelastic creep response (Figure 3.18). The creep and recovery compliance profile ($J(t)$) and the maximum compliance, J_{max} , of the mixed gels decreased with increasing concentration of ιC (Figure 3.18). This result indicated that the mixed gel with higher ιC concentration have become stronger as similarly observed in our previous frequency test (Herraz et al., 2012). The G_o and G_I that corresponded to the spring elements in the Burger's model of the mixed gel increased with increasing ιC concentration. Higher G_o and G_I of the mixed gel indicated the greater elasticity and higher resistance to deformation. This is in agreement with the results obtained from the

oscillatory test discussed previous section. The increased in the elastic components (G_o and G_l) of the mixed gels with higher ιC concentration was also accompanied with an increased in its viscous component (η_o and η_l). This result implied that the mixed gel with higher concentration of ιC undergoes lower structural deformation upon application of stress which could mainly be due to the greater and stronger physical entanglement between the polymer chains of the mixed gel.

The retardation time, λ_{ret} , is another characteristic parameter that can be obtained from the Kelvin-Voigt model to describe the viscoelastic behavior of the mixed gel. The λ_{ret} is defined as $\frac{\eta_l}{G_l}$ that described the rate at which the maximum strain is achieved immediately after the application of constant stress (Toro-Vazquez et al., 2010). The result showed that the λ_{ret} of the mixed gel is increased with decreasing ιC concentration which indicated that longer time is needed to achieve its maximum compliance (Table 3.6). This result was mainly due to the low elasticity in the mixed gel with lower ιC concentration (Toro-Vazquez et al., 2010).

The relaxation behavior of all mixed gels was also studied by evaluating the recovery function ($J(t)$) of the mixed gels as it can be converted into relaxation modulus ($G(t)$) in order to characterize the strength of the mixed gels. It was proposed that when the slope of the $\ln J(t)$ versus $\ln t$ plot, $m \ll 1$ (Figure 3.19), the $G(t)$ becomes reciprocal of the $J(t)$ (Eq.3.2) and can be characterized by a power-law behavior as shown in Eq. 3.3 (Fuchs et al., 1998; Herraz et al., 2012; Struik, 1987):

$$\frac{d \ln J(t)}{d \ln t} = m \approx \frac{d \ln G(t)}{d \ln t} = -n \quad \text{Eq.3.2}$$

$$G(t) = St^{-n} \quad \text{Eq. 3.3}$$

where S is describing the strength of the junction zones between the polymer chains and n is the degree of the entanglement in the gel (Gabriele et al., 2001). In this study, the S of the mixed gel was found to increase with increasing ιC . This result indicated that the mixed gel with higher ιC has stronger internal network structure (Table 3.6). On the other hand, the n value of the mixed gel exhibited a different trend as compared to the S value. The result showed that no significant changes in the n value ($\sim 7\%$) for the mixed gels with ιC -CMC ratio of 8:2, 7:3, and 5:5. However, the n value of the mixed gel was found to increase for more than 50% in the mixed gels with ιC -CMC ratio of 4:6 and 3:7. The increase in the n value implied the decrease of the physical crosslink density in the mixed gel which indicated the weak internal network of the mixed gels with ιC -CMC ratio of 4:6 and 3:7 as compared to 8:2, 7:3, and 5:5 (Herraz et al., 2012). This is in agreement with results obtained from the oscillatory test (section 3.3.3).

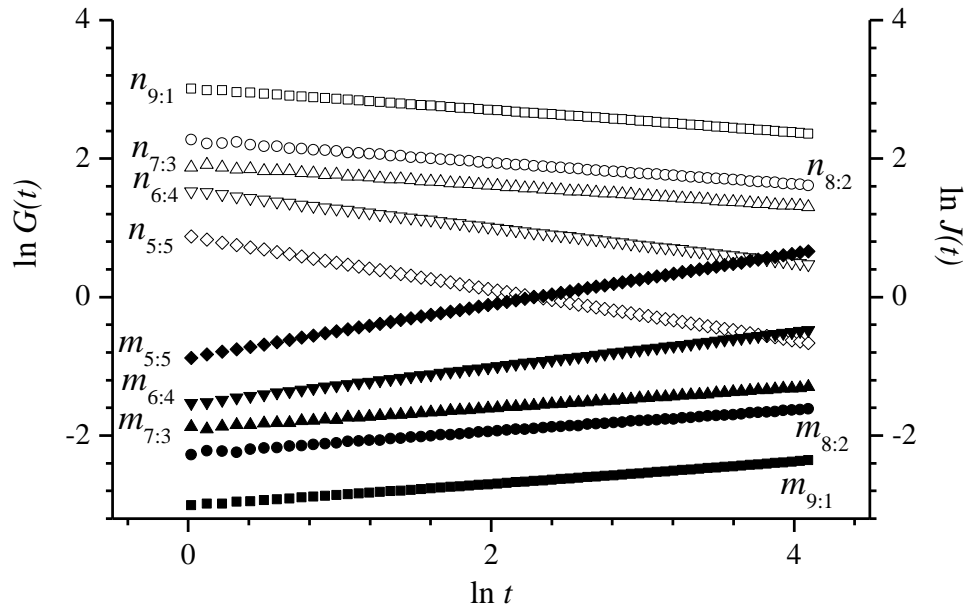


Figure 3.19: $\ln J(t)$ versus $\ln t$ plot (solid symbol) and $\ln G(t)$ versus $\ln t$ plot (open symbol) for the mixed gels with ιC -CMC ratio of (\diamond)3:7, (\blacktriangledown)4:6, (\blacktriangle)5:5, (\bullet)7:3, and (\blacksquare)8:2 mixed gels that showed the reciprocal relationship between the $J(t)$ and $G(t)$.

Table 3.6: Strain corresponded to Maxwell element (γ_0), strain correspond to Kelvin-Voigt element (γ_I), G_o , G_I , η_o , η_I , and delay time, λ_{ret} for ι C-CMC mixed gels. The percentage of deformation of each element in the Burger's model (J_{SM} , J_{KV} , and J_∞) and the percentage of recovery for the entire gel system ($R\%$) at $t=300$ s, the strength of junction zone, and degree of entanglement for ι C-CMC mixed gels.

ι C-CMC ratio		8:2	7:3	5:5	4:6	3:7
$\gamma_0 (\times 10^{-3})$		4.2 \pm 0.1	8.6 \pm 0.3	9.1 \pm 0.1	16.4 \pm 0.3	26.4 \pm 0.4
$\gamma_I (\times 10^{-3})$		3.4 \pm 0.1	7.1 \pm 0.3	6.9 \pm 0.1	27.4 \pm 0.3	105.7 \pm 0.4
G_o (Pa)		24.0 \pm 0.5	11.7 \pm 0.4	10.9 \pm 0.1	6.1 \pm 0.1	4.9 \pm 0.1
η_o (Pas)		3170 \pm 10	1390 \pm 10	340 \pm 6	227 \pm 3	55.2 \pm 0.8
G_I (Pa)		29.9 \pm 0.9	14.2 \pm 0.6	14.5 \pm 0.9	3.7 \pm 0.4	1.6 \pm 0.1
η_I (Pas)		146.7 \pm 0.1	70 \pm 4	61 \pm 2	45 \pm 6	20 \pm 6
J_{max} (Pa^{-1})		0.095	0.199	0.272	0.621	1.94
λ_{ret} (s)		4.91	4.93	4.21	12.16	12.50
Percentage of deformation	$\%J_{SM}$ (%)	51.31	47.41	49.94	36.90	17.16
	$\%J_{KV}$ (%)	38.91	40.94	40.10	51.92	65.71
	$\%J_\infty$ (%)	9.77	9.64	9.95	11.64	17.13
Percentage of recovery	R_{SM} (%)	105.9	99.7	98.50	94.65	92.24
	R_{KV} (%)	90.32	88.36	90.04	78.82	76.89
R_{ovr} (%)		90.22	90.65	89.91	88.82	82.87
Strength of junction zone, S (Pas)		20.4362 \pm 0.0004	9.5816 \pm 0.0008	6.708 \pm 0.007	4.6249 \pm 0.0005	2.3746 \pm 0.0007
Degree of entanglement, n		0.1468 \pm 0.0007	0.1580 \pm 0.0008	0.1588 \pm 0.0004	0.2588 \pm 0.0004	0.3752 \pm 0.0006

The contribution of each element to the total deformation ($\%J_e$, where $e = SM$, KV or ∞) in the Burger's model was calculated using Eq. 2.9 (Table 3.6). The $\%J_{SM}$ which is the instantaneous elastic response of the gel was found to decrease with decreasing ι C concentration. This result showed that the elasticity contributed from the Maxwell spring of the mixed gel had decreased. In other word, the ι C is the component that is responsible for the instantaneous elastic response of the mixed gels. On the other

hand, the contribution of the mixed gel to the deformation by Kelvin-Voigt element ($\%J_{KV}$) is very similar in ι C-CMC ratio of 8:2, 7:3, and 5:5. However, the $\%J_{KV}$ of the mixed gel increased dramatically ($> 10\%$) when there is less amount of ι C in the gel mixture as in the 4:6 and 3:7 of ι C-CMC ratio. The increase in the $\%J_{KV}$ indicated the decrease in the elasticity and recovery ability of the Kelvin-Voigt element since the J_{KV} is representing the delayed elasticity of the gel system. This might be due to the reduction in the strength of junction zone (S) and degree of entanglement (n) of the mixed gel with ι C-CMC ratio of 3:7 as discussed above. The contribution of the Maxwell dashpot (J_{∞}) to the deformation of the mixed gels was found to be negligible for the ι C-CMC ratio of 8:2, 7:3, 5:5, and 4:6. However, the mixed gel with 3:7 of ι C-CMC ratio showed the highest $\%J_{\infty}$ among the mixed gels. This result revealed that the mixed gel exhibited the most liquid like behavior with greatest unrecovered strain when the stress was applied (Dolz, 2008). This result was also supported by the percentage recovery ($\%R$) of the mixed gel which is the lowest among the mixed gels.

As reported by Steffe (1996), when a material that obeys the Burger's model is tested in the linear viscoelastic region, its J_o and J_l determined from the creep test will be equal to its J_{SM} and J_{KV} from the recovery test. In other words, the recovery of the Maxwell spring ($\%R_{SM}$) and the Kelvin-Voigt element ($\%R_{KV}$) will be 100% for a perfect viscoelastic material. In our mixed gel system, their J_o was $> 90\%$ recovered (Table 3.6). However, the Kelvin-Voigt element of all mixed gel was $< 90\%$ recovered especially for all the mixed gels. The $\%R_{KV}$ was found to decrease dramatically when the amount of CMC in the mixed gel increased and exceeded 50%. The decrease of the $\%R_{KV}$ of the gel mixture with ι C-CMC ratio of 3:7 and 4:6 has showed its low retarded recovery ability as compared to 8:2, 7:3, and 5:5 of ι C-CMC ratio which may be due to its low S and n values.

3.3.5 Flow behavior of ι C-CMC mixed gel

The shear viscosity of mixed gels was found to increase with increasing ι C. The increase in the viscosity of the mixed gels was highly related to its S and n values (Table 3.6). The mixed gels with higher S and n values were more resistant to flow. The viscosity profiles of the mixed gels showed shear-thickening behavior at shear rate lower than 0.02 s^{-1} (Figure 3.20(a)). The shear thickening behavior of the mixed gels at low shear rate was attributed to the stiff inner structure of the gels (Benchabane and Bekkour, 2008). However, when the shear stress increased and exceeded σ_p , the shear viscosity of the mixed gels was found to decrease with increasing shear rate and this result showed the shear thinning effect. The shear thinning behavior originated from the disentanglement of the polymer coil or increased orientation of the polymer chains in the flow direction (Benchabane and Bekkour, 2008). The PLI of the mixed gel was increased with decreasing ι C and indicated that the mixed gel has become less shear thinning. This result implied the decrease of spreadability of the mixed gels (Table 3.7). Apart from the shear thinning behavior, heterogeneous flow was also observed in the flow curve of the mixed gels (Figure 3.20).

Table 3.7: Shear viscosity, Power Law Index (PLI), and yield stress (σ_p) of the mixed gels which determined from their steady rheological behaviors.

ι C-CMC ratio	Shear Viscosity	Power Law Index, PLI	Yield stress, σ_p (Pa)
8:2	603 \pm 5	0.124 \pm 0.005	13.28
7:3	407 \pm 4	0.137 \pm 0.004	10.88
5:5	190 \pm 7	0.247 \pm 0.004	4.23
4:6	98 \pm 2	0.284 \pm 0.003	3.63
3:7	66 \pm 3	0.362 \pm 0.004	1.65

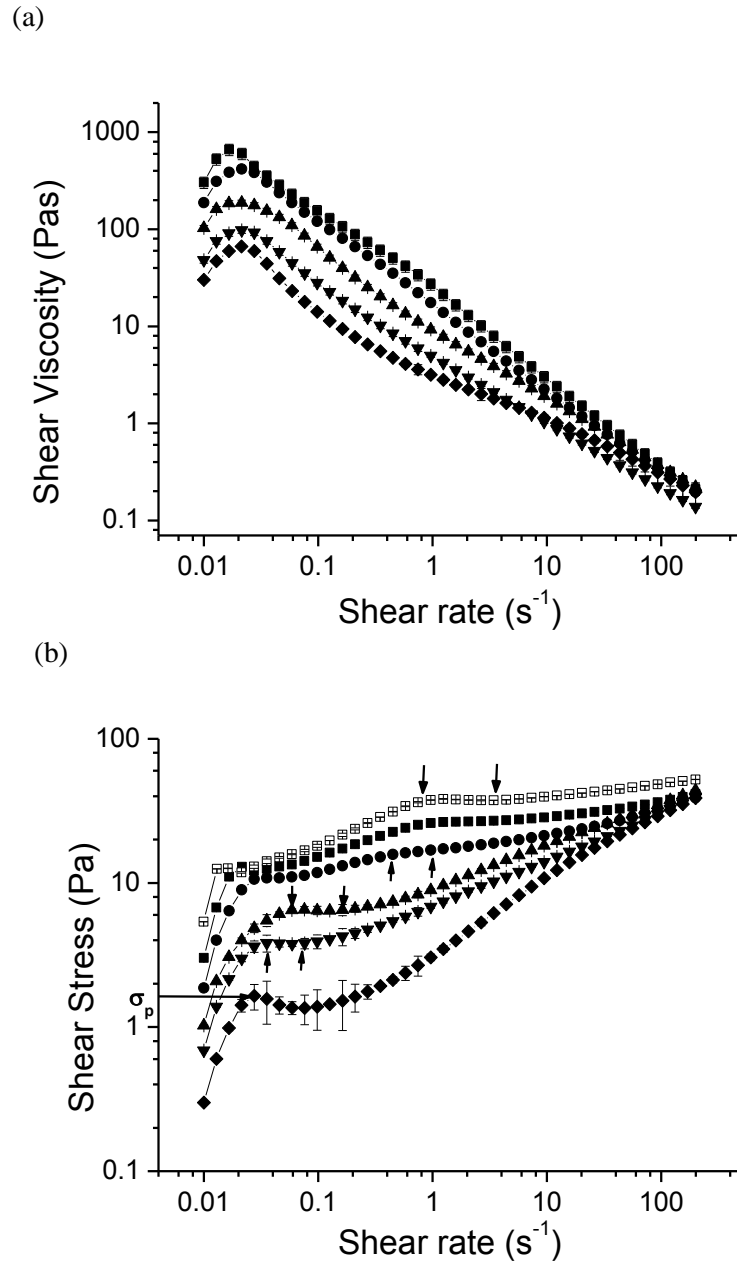


Figure 3.20: The flow behavior of the mixed gel with ι C-CMC ratio of (\blacklozenge)3:7, (\blacktriangledown)4:6, (\blacktriangle)5:5G, (\bullet)7:3, and (\blacksquare)8:2 where (a) is the shear viscosity profile of the mixed gels with increasing shear rate and (b) is the shear stress versus shear rate profile for the determination of yield stress (σ_p) of the mixed gels.

A stress peak that illustrates the shear banding transitions (indicated with arrows) (Chu and Feng, 2010) was observed for all mixed gels (Figure 3.20(b)). Initially, at low shear rate, the flow of the gels was homogeneous until it reached the σ_p of the gels. When the σ_p is reached, the flow of the gels became unstable and followed by decreasing in shear stress. A nonlinear increment of shear stress was observed when the

shear rate increased further and showed the second critical point for phase transition. This heterogeneous flow may be attributed by the relaxation of the entanglement of the polymer chain (Adams and Olmsted, 2009; Chu and Feng, 2010; Tapadia et al., 2006). The heterogeneous flow may also be attributed to the newly formed entanglements between the polymer chains which retarded the flow of the mixed gel at higher shear rate region (Wang, and Cui, 2005b). The stress banding was found to shift to lower shear stress region when the concentration of ι C in the gel decreased and eventually associated with the σ_p for 3:7 of ι C-CMC ratio. This result indicated that the gel structure has become less entangled with the decreasing of ι C concentration.

3.3.6 Thixotropic behavior of ι C-CMC mixed gel

All mixed gels prepared in this study were thixotropic gel (Figure 3.21). However, the degree of thixotropy of the mixed gels decreased with increasing CMC concentration indicating the decrease in the thixotropic properties of the gels. This result might be due to the less entanglement of the gel with higher CMC concentration since thixotropic behavior described the changes in the disentanglement-entanglement process of the gel network with time (Table 3.8). This result also explained the decrease in the strength of gel network structure with increasing CMC concentration as the degree of thixotropy was obtained from the hysteresis loop which is also describing the force that is needed to disrupt gel network structure (Benchabane and Bekkour, 2008). The structural change can also be explained with the pseudoplastic index and thixotropic index of the gel which described the rate of changes in the viscosity of the gel. These indices were obtained from the logarithmic plot of instantaneous viscosity versus shear rate. The pseudoplastic index is referred to the slope of the plot with increasing shear rate, while the thixotropic slope is referred to the slope of the reverse path (decreasing shear rate). It was found that the change in the pseudoplastic index for the mixed gels with ι C-CMC

ratio of 8:2, 7:3, and 5:5 was negligible. This result showed that the disentanglement process was similar in these mixed gel. However, the pseudoplastic index for 4:6 and 3:7 of ι C-CMC ratio was significantly lower than that of 8:2, 7:3, and 5:5. This result indicated that less structural changes occur in the mixed gel with higher CMC concentration due to its less entanglement gel structure and the polymer chains can be easily aligned along the shear direction. This was also further supported by the low shear viscosity of the mixed gels with 4:6 and 3:7 of ι C-CMC ratio as discussed in section 3.3.5.

The thixotropic index of all mixed gels was lower as compared to their pseudoplastic index. For the mixed gels with 8:2, 7:3, and 5:5 of ι C-CMC ratio, their thixotropic indices were found to be half of their pseudoplastic index. This result implied that the structural recovery for these mixed gels were relatively slower than their disentanglement process. However, the structural recovery rate for these mixed gels was found to occur at similar rate. On the other hand, the difference between the pseudoplastic index and thixotropic index of the mixed gels with ι C-CMC ratio of 4:6 and 3:7 was small. This result indicated that these mixed gels do not experience large structural change after the first cycle of stress loading.

Table 3.8: Degree of thixotropy, pseudoplastic index, and thixotropic index of the mixed gels.

ι C-CMC ratio	Degree of thixotropy	Pseudoplastic index	Thixotropic index
8:2	23.1 \pm 0.8	1.15 \pm 0.03	0.77 \pm 0.03
7:3	20.3 \pm 0.8	1.15 \pm 0.03	0.76 \pm 0.02
5:5	11.9 \pm 0.2	1.05 \pm 0.01	0.72 \pm 0.02
4:6	5.78 \pm 0.07	0.99 \pm 0.04	0.66 \pm 0.03
3:7	1.48 \pm 0.05	0.60 \pm 0.02	0.49 \pm 0.02

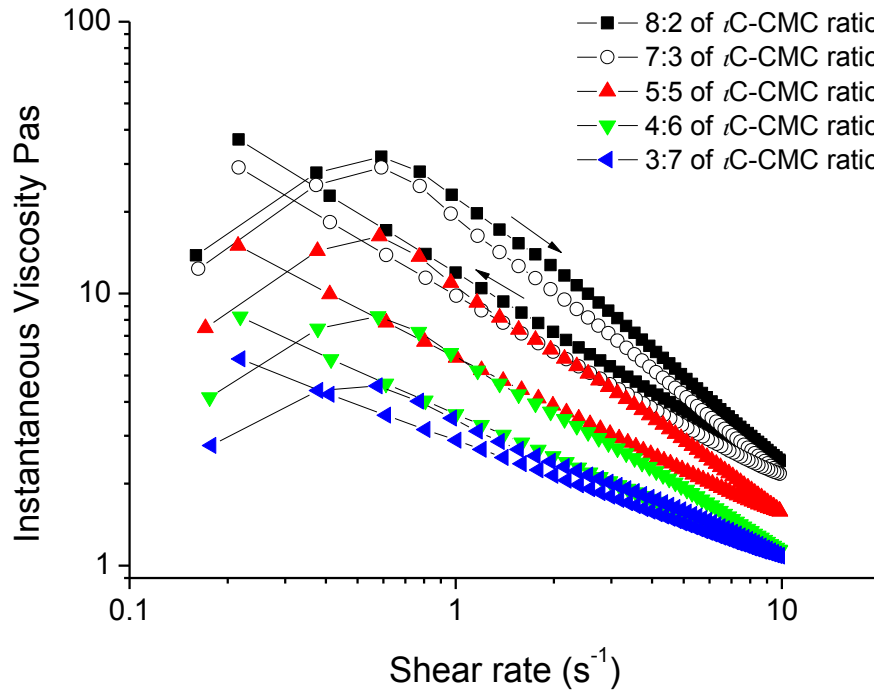


Figure 3.21: Thixotropic plot for mixed gel.

3.4 Liposomal gels

In order to produce a good dispersion of liposome in the selected gel system, the *CE* of the gel must be high enough to suspend the liposome since the *CE* is related to the work required to disrupt the dispersion (Sohm and Tadros, 1989). Another factor to be considered was the flow property of the gel, because it could affect the stability of the dispersed liposome and also the texture of the gel. The mixed gel with ι C-CMC ratio of 5:5 exhibited greatest flexibility by showing largest γ_c value among the mixed gel. The *CE* and %*R* of this mixed gel was an optimum value as there were no significant changes being observed when the concentration of ι C increased further in the mixed gels with 7:3 and 8:2 ι C-CMC ratio. In addition, the mixed gel with 5:5 ι C-CMC ratio showed medium σ_p and shear viscosity as compared to others (3:7, 4:6, 7:3, and 8:2 of ι C-CMC ratio). This is because high shear viscosity will decrease the homogeneity of the liposome dispersion, whereas low viscosity will lead to phase separation and

consequently affect the liposome stability and homogeneity in the gel. High σ_p will also affect the spreadability and texture of the mixed gel. After considering these factors, mixed gel that prepared from 5:5 ι C-CMC ratio was selected for the preparation of the liposomal gel.

In this work, five types of different liposomal gels were prepared, namely OA-in-gel (LG-OA), OACH1-in-gel (LG-OACH1), OACH2-in-gel (LG-OACH2), OACH2P1-in-gel (LG-OACH2P1), and OACH2P2-in-gel (LG-OACH2P2). Each liposomal gel was loaded with 8 mg/mL of liposomes.

3.4.1 Morphology of liposomal gels

The morphology of liposomal gels was evaluated using a confocal laser scanning microscope. All the liposomes were found to be entrapped in the 3-dimensional network of the gel. As compared with the liposome which dispersed in aqueous (Figure 3.22(a)), the liposomes entrapped in the gel matrix (5:5 ι C-CMC ratio) showed spherical morphology (Figures 3.22(b) and (c)). This result showed that the polymer chains do not disrupt the structure of the liposome, but the liposomes are accommodated into the voids of the gel network (Chieng, 2010). Similar result was also reported in a number of earlier studies (Bochot et al., 1998; Dowling et al., 2009; Dragicevic-Curic et al., 2009).

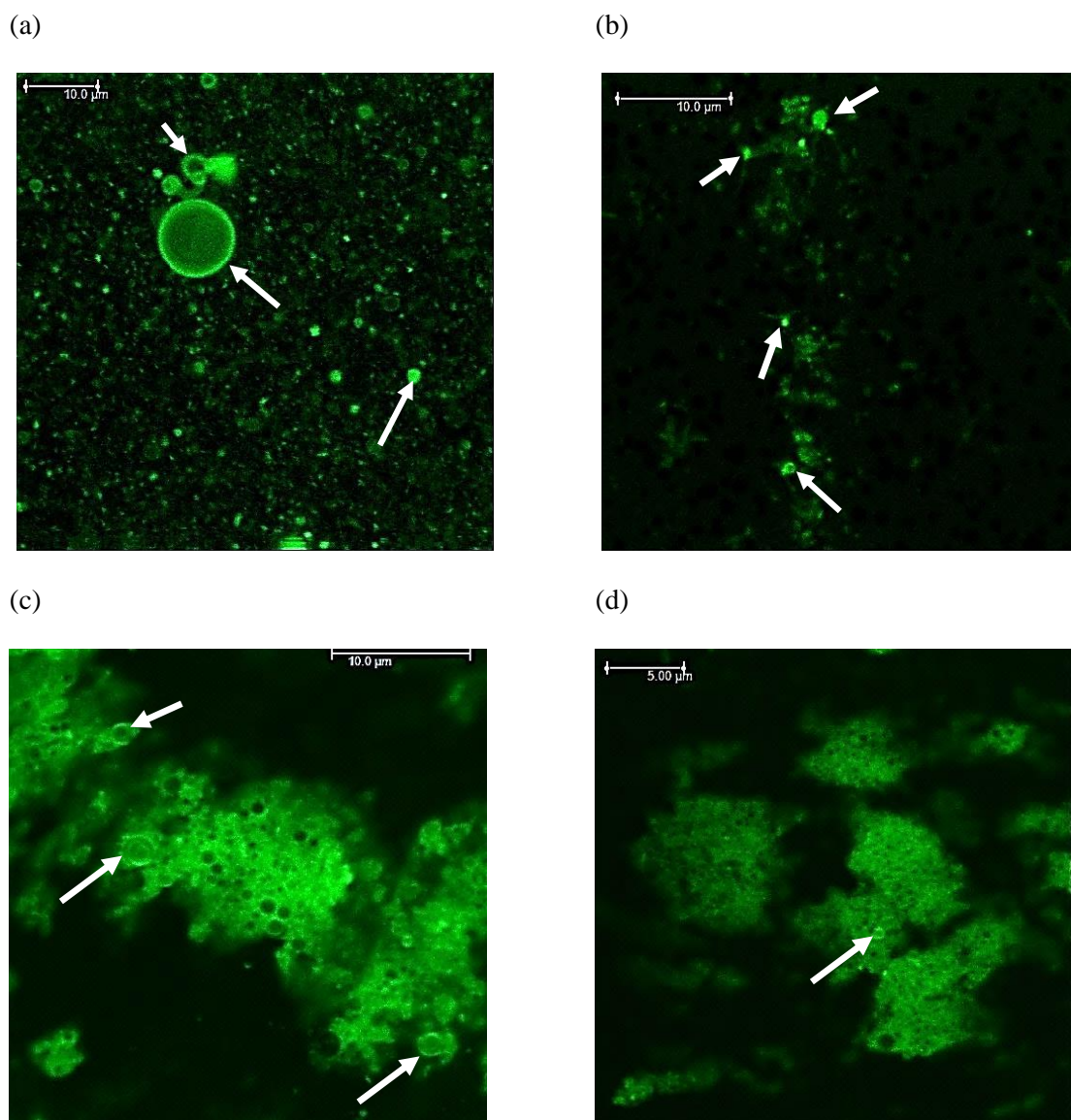


Figure 3.22: The fluorescence images of (a) OA in solution, (b) LG-OA, (c) LG-OACh1, and (d) LG-OACh2P1. The liposomes were indicated with arrows.

3.4.2 Rheological properties of the liposomal gels

3.4.2.1 Gelling temperature of the liposomal gels

The gelling temperature (T_{gel}) of all liposomal gels was 1 °C higher than the 5:5 *i*C-CMC mixed gel ($P < 0.05$) (Table 3.9). In other words, the gelation temperature of the gel increased with the presence of liposomes. This result indicated that there was an interaction between the liposomes and the polymer network. The liposomes that are

accommodated in between the network space of the gel matrix could act as bridges that link the adjacent polymer chains via intermolecular interaction such as hydrogen bonding and enhanced the integrity of internal gel network structure (Chieng and Chen, 2010). This behaviour was further proved with the S value of the liposomal gels which will be discussed in the following section. The higher T_{gel} also revealed that the liposomal gels had exhibited greater thermostability as compared to the pure 5:5 ι C-CMC mixed gel. However, the increment of the T_{gel} for all the liposomal gels was found to be independent of liposome type ($P > 0.05$).

Table 3.9: Gelation temperature of liposomal gels.

Sample	T_{gel} ($^{\circ}\text{C}$)
5:5 ι C-CMC mixed gel	34.2 ± 0.6
LG-OA	35.9 ± 0.6
LG-OACh1	35.6 ± 0.6
LG-OACh2	35.7 ± 0.6
LG-OACh2P1	35.6 ± 0.6
LG-OACh2P2	35.4 ± 0.6

3.4.2.2 Dynamic behavior of liposomal gels

The G' value of the liposomal gels increased from 12 Pa to 13.7 Pa after liposomes were added into the 5:5 ι C-CMC mixed gel indicating the increase in its elasticity (Figure 3.23). This result was mainly due to the rigidity of the liposomes (Mourtas, Haikou et al., 2008). Under applied shear, the liposomes could effectively store the applied stress in its elastic component and thus increased the G' of the liposomal gels (Table 3.10). This result is further supported by the γ_b of the liposomal gels. The γ_b of the liposomal gels was one unit higher than the 5:5 ι C-CMC mixed gel and indicated that the liposomal gels' strength were slightly higher than the pure gel and can withstand larger deformation strain before they started to flow like a liquid. However,

the γ_c for all liposomal gels were found to be lower than 5:5 ι C-CMC mixed gel and indicated that these liposomal gels exhibited shorter LVR. This was accompanied with the decrease in the CE of the liposomal gels which indicated the decrease of cohesiveness of the gel structure. This result is favorable as the cohesiveness within the liposomal gels is directly proportional to the flowability and spreadability of the liposomal gels. High CE retarded the flow of the liposomal gels and limited the spreadability of the gel. This result will influence the homogeneity and consistency of the gel upon application (Garg et al., 2002).

The contribution of liposomes to the elastic component of the 5:5 ι C-CMC mixed gel is also shown in the frequency sweep (Figure 3.24). According to the frequency sweep profile, all liposomal gels exhibited viscoelastic behavior with G' larger than G'' over the selected frequency range. The G' profile of all liposomal gels was shifted to higher value as compared to the pure 5:5 ι C-CMC mixed gel ($P < 0.05$). This result showed the increase in the elasticity of the liposomal gels (Ikeda and Foregeding, 2003). The slope of G' of the liposomal gels was also found to decrease as compared to the pure 5:5 ι C-CMC mixed gel. The decrease in the G' slope implied that the liposomal gels are more solid-like behavior than that of the 5:5 ι C-CMC mixed gel (Picout and Ross-Murphy, 2002). The increase in the elasticity of liposomal gels was also expressed through their $\tan \delta$ profile (Figure 3.25). The $\tan \delta$ of the liposomal gels was significantly lower than the blank gel which showed that the liposomal gels were more solid-like. The decrease of $\tan \delta$ for liposomal gels also shows that the presence of liposomes have enhanced the elasticity of the gel (Barbucci et al., 2000). On the other hand, the changes of the G'' for the liposomal gels were negligible as compared to the 5:5 ι C-CMC mixed gel which implied that the amount of dissipation energy of the liposomal gels was similar to the 5:5 ι C-CMC mixed gel. This result indicated that the presence of liposomes does not affect the physical entanglements in the 5:5 ι C-CMC

mixed gel and can be proved with the n value of the liposomal gels (will be discuss in section 3.4.2.3) (Grillet et al., 2012).

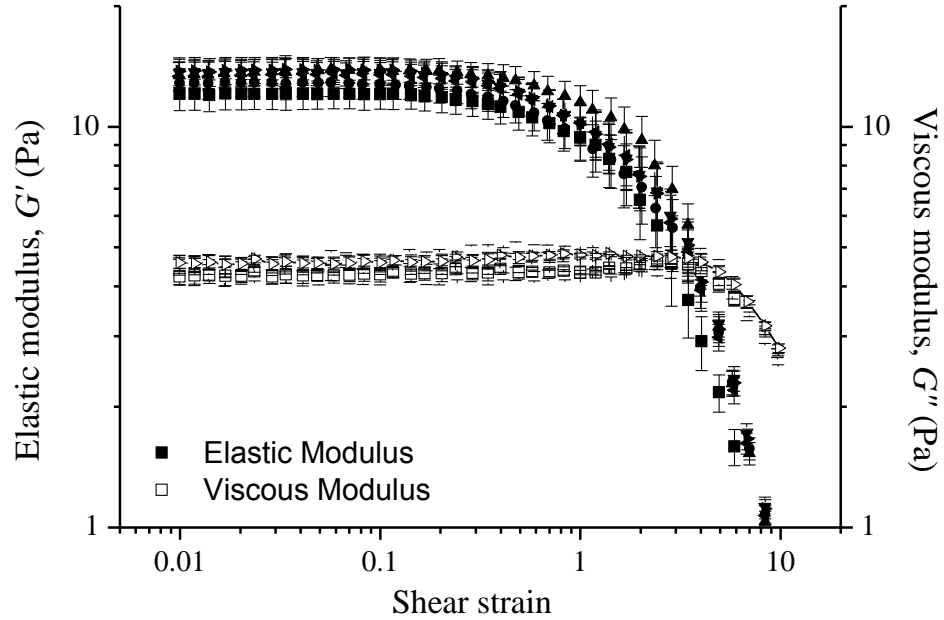


Figure 3.23: The strain sweep profile of the (■)5:5 *i*C-CMC mixed gel where (●)LG-OA, (▲)LG-OACh1, (▼)LG-OACh2, (◄)LG-OACh2P1, and (►)LG-OACh2P2 that obtained at 25°C.

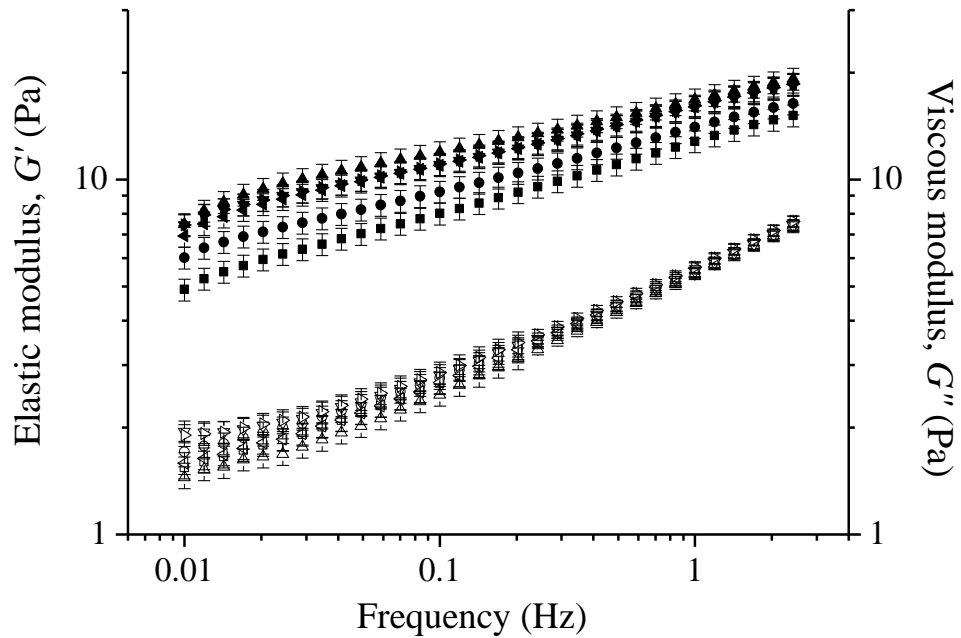


Figure 3.24: The variation of G' (solid symbol) and G'' (close symbol) as a function of frequency of the (■)5:5 *i*C-CMC mixed gel where (●)LG-OA, (▲)LG-OACh1, (▼)LG-OACh2, (◄)LG-OACh2P1, and (►)LG-OACh2P2 that obtained at 25°C.

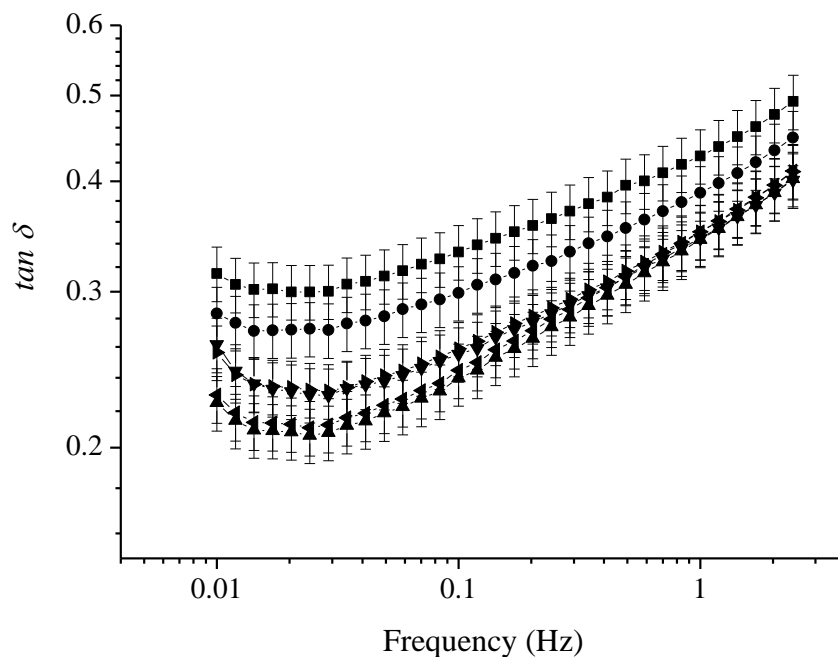


Figure 3.25: The $\tan \delta$ of the (■)5:5 ι C-CMC mixed gel where (●)LG-OA, (▲)LG-OACh1, (▼)LG-OACh2, (◄)LG-OACh2P1, and (►)LG-OACh2P2 that obtained at 25°C.

Table 3.10: The critical strain (γ_c), break point (γ_b), elastic modulus (G'), cohesive energy (CE), and yield stress (σ_p) of the liposomal gels which determined from their dynamic rheological behaviors.

Name	Critical strain, γ_c	Break point, γ_b	Elastic modulus, G' (Pa)	CE (Pa)	Slope of G'
5:5 ι C-CMC mixed gel	0.57 ± 0.02	2.81 ± 0.02	12 ± 1	1.9 ± 0.1	0.199 ± 0.001
LG-OA	0.41 ± 0.01	3.67 ± 0.01	12.31 ± 0.04	1.039 ± 0.006	0.178 ± 0.001
LG-OACh1	0.43 ± 0.01	3.79 ± 0.01	13.38 ± 0.04	1.243 ± 0.007	0.147 ± 0.001
LG-OACh2	0.42 ± 0.01	3.76 ± 0.01	13.62 ± 0.04	1.184 ± 0.007	0.159 ± 0.001
LG-OACh2P1	0.44 ± 0.01	3.79 ± 0.01	13.45 ± 0.04	1.28 ± 0.01	0.163 ± 0.001
LG-OACh2P2	0.44 ± 0.02	3.67 ± 0.02	13.85 ± 0.04	1.33 ± 0.01	0.161 ± 0.001

3.4.2.3 Creep and recovery of liposomal gels

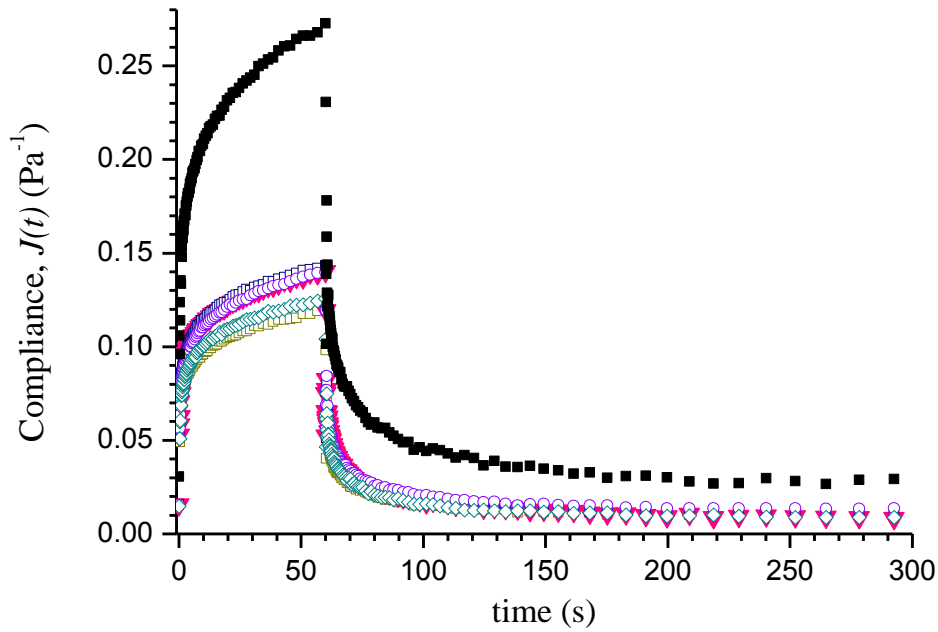


Figure 3.26: Creep and recovery profiles for (■)5:5 ι C-CMC mixed gel, (□)LG-OA, (▼)LG-OACh1, (○)LG-OACh2, (◇)LG-OACh2P1, and (□)LG-OACh2P2 that performed at 0.1 Pa constant stresses at 25 °C.

The $J(t)$ results showed that all liposomal gels exhibited viscoelastic creep response (Figure 3.26). The $J(t)$ profile and J_{max} of the liposomal gels were found to be lower than the 5:5 ι C-CMC mixed gel. The result indicated that the elastic response of liposomal gels had become stronger in the presence of liposomes. However, the changes of the G_o value for the liposomal gels which corresponded to the Maxwell's spring element in the Burger's model were negligible as compared to the pure 5:5 ι C-CMC mixed gel (Table 3.11). This result showed that only the gel matrix of the liposomal gels was responsible for the instantaneous elastic response. In other words, the contribution of the liposomes to the G_o of the liposomal gels was negligible. The presence of liposomes was found to contribute to the Kelvin-Voigt elements as the G_I value of liposomal gels was found to be two times higher than the pure 5:5 ι C-CMC mixed gel (Table 3.11). The increase in the G_I of the liposomal gels was also accompanied with an

increase in their viscous component, η_I which increased the liposomal gels' retarded elasticity. The results also indicate that the liposomal gels can sustain greater deformation stress as compared to the 5:5 ι C-CMC mixed gel. This behavior could be due to the small and more rigid liposomes that could not easily deform (as easy as the 5:5 ι C-CMC mixed gel) under applied stress and thus, increased the G_I and η_I values of the liposomal gels (Figure 3.27) (Mourtas, Haikou et al., 2008). The λ_{ret} for the liposomal gels was increased as compared to the pure 5:5 ι C-CMC mixed gel as a result of the increase in the η_I value (Table 3.11). The increase in the η_I of the liposomal gel had delayed the response of the elastic component in its Kelvin-Voigt element, thus increased the time taken for the strain of the liposomal gels to accumulate and reached J_{max} .

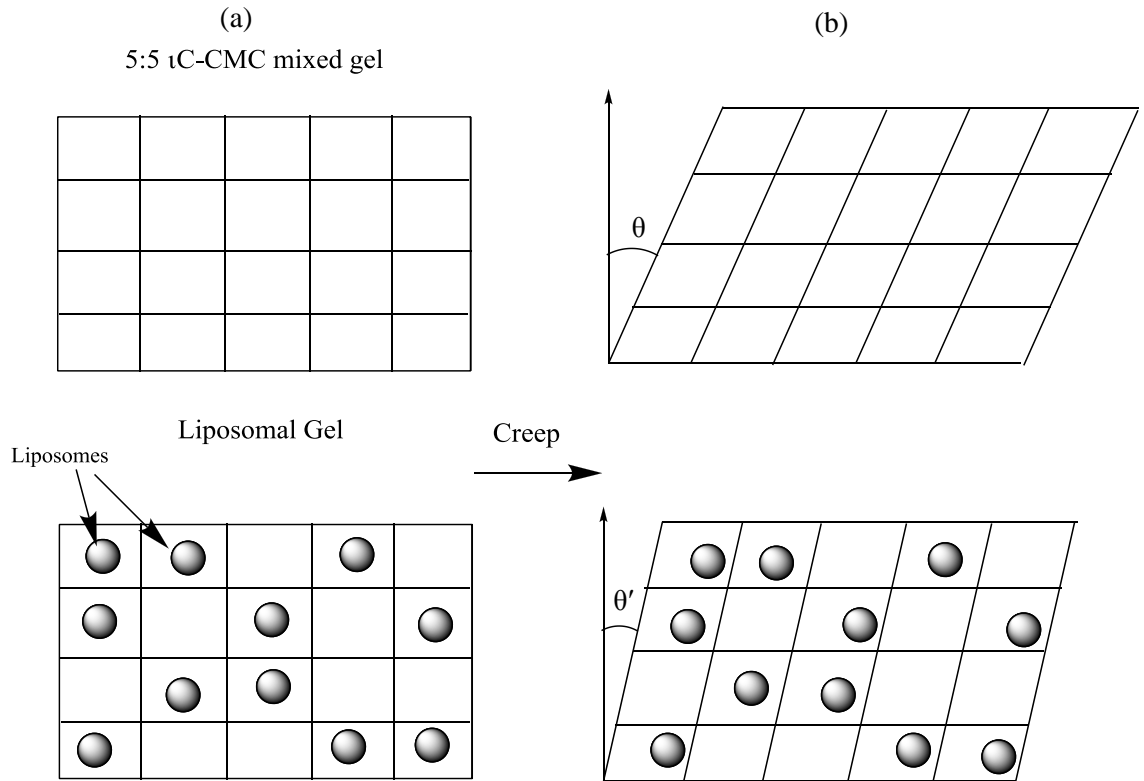


Figure 3.27: (a) Gel matrix representing internal network structure of blank gel and liposomal gel before creep; (b) during creep, the pure 5:5 ι C-CMC mixed gel deformed more as compared to the liposomal gel where the $\theta > \theta'$.

The $J(t)$ functions of the liposomal gels obtained from the creep test were also converted to the $G(t)$ function in order to study their S and n (Figure 3.28). According to the result (Table 3.11), the changes in the n value for all liposomal gels were found to be negligible as compared to the pure 5:5 ι C-CMC mixed gel which indicated that the degree of entanglement (n) in the liposomal gels was similar with the pure 5:5 ι C-CMC mixed gel. However, the S value of the liposomal gels increased significantly and indicated their greater gel strength. This was mainly due to the presence of liposomes in the gel matrix that plays a role in enhancing the elasticity of the gel. The result is in good agreement with the result obtained from the frequency sweep profile of the liposomal gels.

(a)

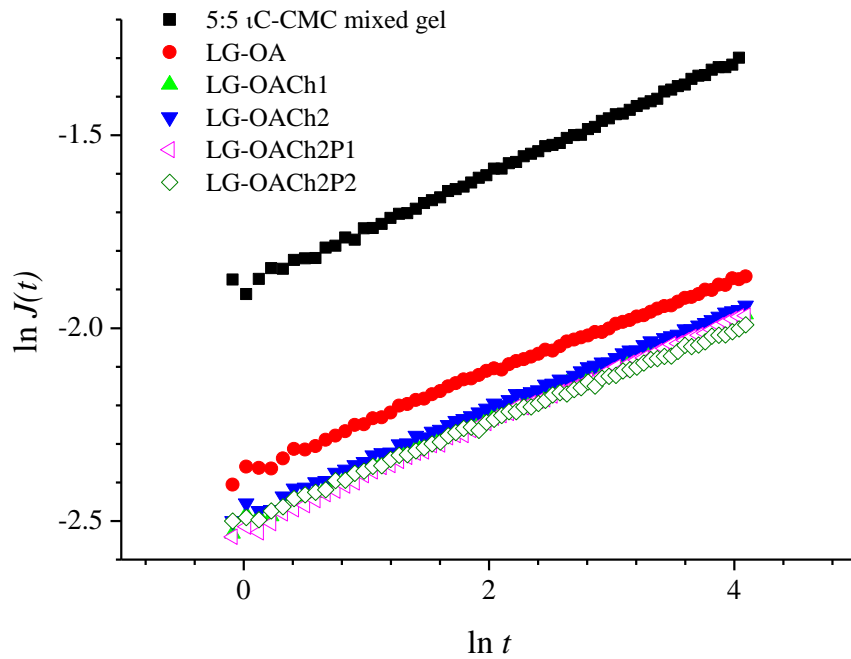
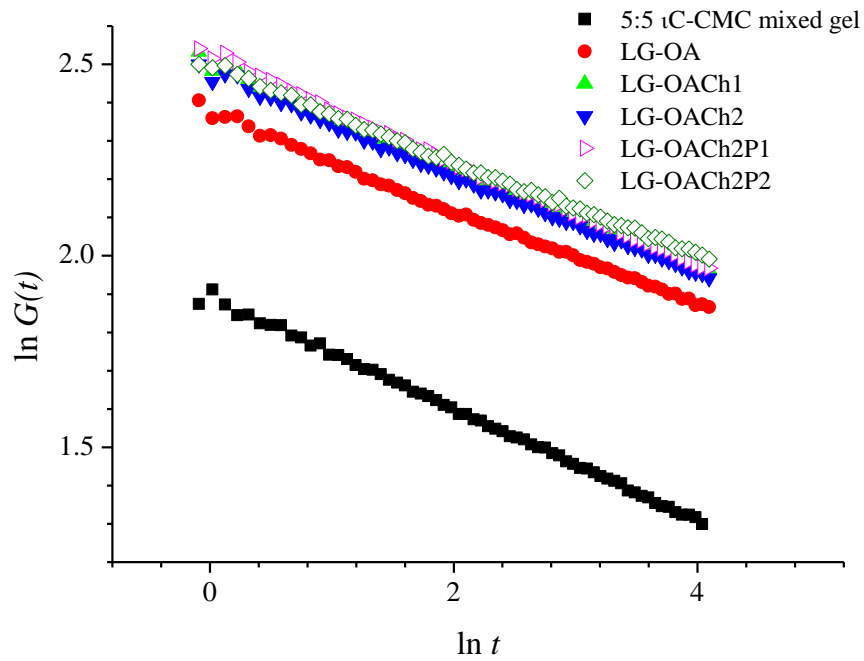


Figure 3.28: The (a) $\ln J(t)$ versus $\ln t$ plot and (b) $\ln G(t)$ versus $\ln t$ plot of the pure 5:5 ι C-CMC mixed gel and liposomal gels showing the reciprocal relationship between the $J(t)$ and $G(t)$.

(b)

**Figure 3.28** (continued)

For the recovery profiles of the liposomal gels, its percentage of deformation ($\%J_{SM}$) was found to be 20% higher than the pure 5:5 ι C-CMC mixed gel. However, the J_{SM} for all the liposomal gels recovered is 100% after the load was removed (Table 3.11) (Steffe, 1996). On the other hand, the $\%J_{KV}$ of the liposomal gels which represents the retarded elasticity was found to be 30% lower than the pure 5:5 ι C-CMC mixed gel. The lower $\%J_{KV}$ of liposomal gels was mainly due to its higher internal viscosity (η_I) than that of the pure 5:5 ι C-CMC mixed gel. As discussed above, the η_I of the liposomal gels was tenfold greater than the η_I of the pure 5:5 ι C-CMC mixed gel. The higher η_I has decreased the deformation of the Kelvin-Voigt elements of the liposomal gels and resulted in the decrease of the $\%J_{KV}$. It was found that the deformation contributed by the Kelvin-Voigt elements ($\%R_{KV}$) was not fully recovered as compared to the $\%R_{SM}$. This unrecovered strain from the Kelvin-Voigt elements contributed to the permanent deformation of the gels (J_∞) (Table 3.11). The $\%J_\infty$ of the liposomal gels was slightly

lower than the pure 5:5 ι -C-CMC gel. This result showed that the recovery ability of the liposomal gels was higher than that of pure 5:5 ι -C-CMC gel. This was further supported by the overall recovery percentage ($\%R_{ovr}$) of the liposomal gels. The $\%R_{ovr}$ of the liposomal gels was found to be higher than the pure 5:5 ι -C-CMC gel. This result might be attributed to the presence of the liposomes that added an extra “bridging” effect which linked the adjacent polymer chains in the gel beside the physical entanglement between the polymer chains (Figure 3.29) (Chieng and Chen, 2010). It was suggested that this bridging effect originated from the hydrogen bonding between the O-H at the backbone of the polymer chains from the gel matrix and the oxygen atom of fatty acid or the oxygen atom or nitrogen atom of the chitosan molecules at the surface of the liposomes as the molecules were rich with –OH groups. Since the hydrogen bond is weak and non-permanent, it could break during creep process, but reformed when the applied stress was removed, leading to the high recovery of the liposomal gels. This result further indicates that the loaded liposomes do not contribute to the permanent deformation of gel, but enhanced the recovery of the liposomal gels. The permanent deformation was mainly attributed to the disentanglement of some entangled polymer chains during creep.

The CMC chains present in the 5:5 ι -C-CMC mixed gel might also be partially coated on the chitosan-modified liposomes (Figure 3.29(b)). This is because the –OH group in the CMC chains as its pK_a value is 4.3 and will interact ionically with the –NH group in the chitosan molecules (Magdassi et al., 2003). However, this does not significantly affect the elastic property of the gel matrix as the changes in the G_0 of the liposomal gel was found to be negligible as compared to the pure 5:5 ι -C-CMC mixed gel (Table 3.11).

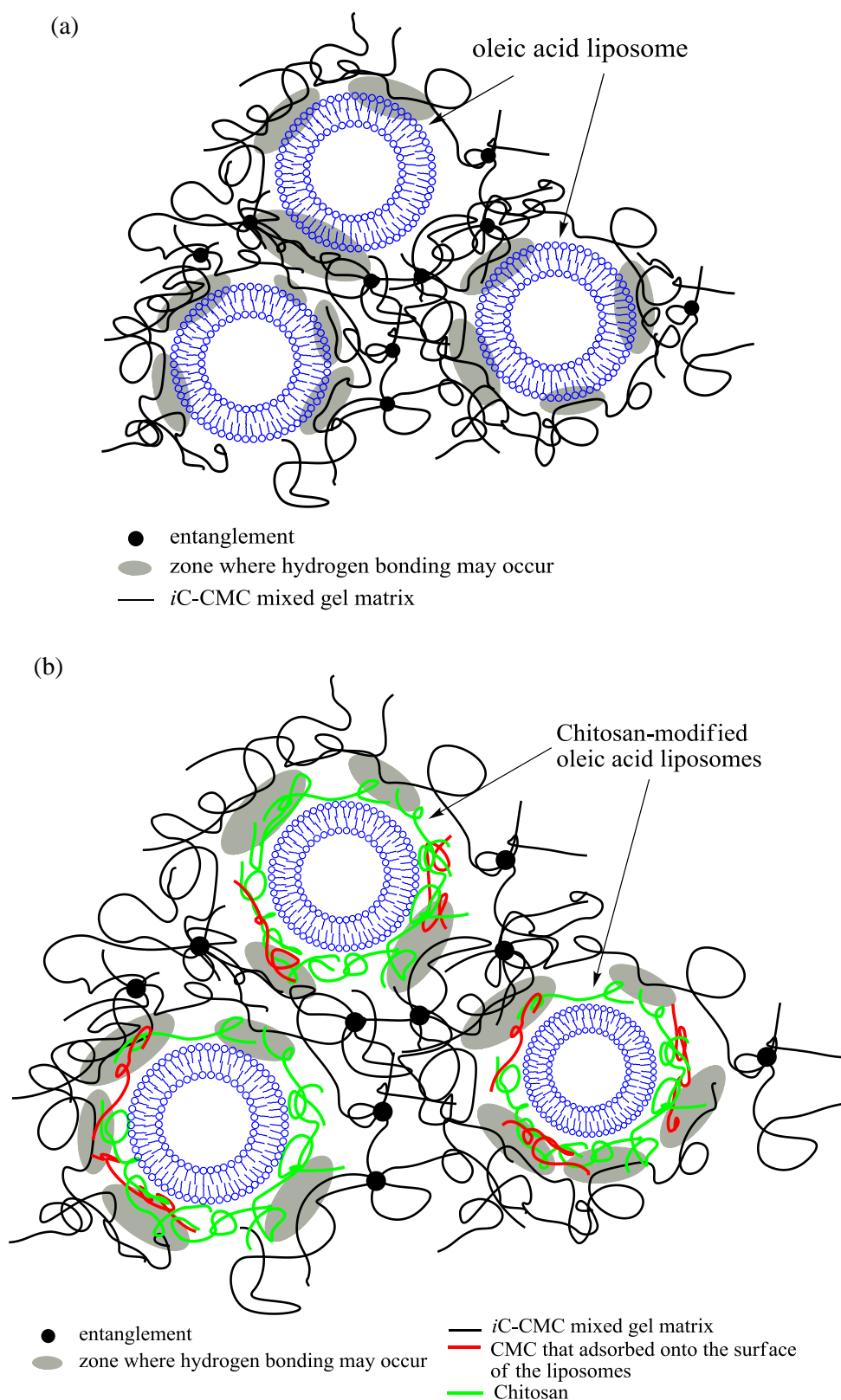


Figure 3.29: Schematic network structure of the 5:5 *iC*-CMC mixed gel matrix (a) loaded with OA liposome and (b) chitosan-modified OA liposomes. The grey area is the possible hydrogen bonding zone between the gel network structure and the liposomes.

Table 3.11: Strain corresponds to Maxwell element (γ_0), strain corresponds to Kelvin-Voigt element (γ_I), G_o , G_I , η_o , η_I , and delay time, λ_{ret} for the liposomal gels. The percentage of deformation of each element in the Burger's model (J_{SM} , J_{KV} , and J_∞), the percentage of total recovery ($R\%$) at $t=300$ s, the strength of junction zone, and degree of entanglement for liposomal gels.

	5:5 ι C-CMC mixed gel	LG-OA	LG-OACh1	LG-OACh2	LG-OACh2P1	LG-OACh2P2
$\gamma_0 (\times 10^{-3})$	9.1 \pm 0.1	7.5 \pm 0.1	7.9 \pm 0.1	7.9 \pm 0.1	8.2 \pm 0.3	7.4 \pm 0.2
$\gamma_I (\times 10^{-3})$	6.9 \pm 0.1	3.49 \pm 0.06	3.29 \pm 0.04	4.29 \pm 0.04	3.6 \pm 0.02	3.55 \pm 0.05
G_o (Pa)	10.9 \pm 0.1	13.3 \pm 0.2	12.7 \pm 0.2	12.7 \pm 0.2	12.3 \pm 0.5	13.4 \pm 0.4
η_o (Pas) ($\times 10^3$)	0.340 \pm 0.006	3.13 \pm 0.02	2.78 \pm 0.02	2.63 \pm 0.05	2.38 \pm 0.04	2.92 \pm 0.02
G_I (Pa)	14.5 \pm 0.9	28.6 \pm 0.2	30.4 \pm 0.2	23.3 \pm 0.2	27.8 \pm 0.2	28.2 \pm 0.2
η_I (Pas) ($\times 10^2$)	0.61 \pm 0.02	3.1 \pm 0.2	3.3 \pm 0.3	3.0 \pm 0.2	2.9 \pm 0.4	2.6 \pm 0.3
J_{MAX} (Pa $^{-1}$)	0.2723	0.1398	0.1404	0.1435	0.128	0.1276
λ_{ret} (s)	4.21	10.84	10.85	12.88	10.43	9.22
Percentage of deformation	J_{SM} (%)	49.94	63.89	62.18	84.28	64.83
	J_{KV} (%)	40.10	27.62	32.41	28.61	28.59
	J_∞ (%)	9.95	8.49	5.41	7.11	6.58
Percentage of recovery	R_{SM} (%)	98.5	102	99.54	99.75	101
	R_{KV} (%)	90.04	91.51	94.57	92.89	91.42
R_{ovr} (%)		89.91	91.31	94.20	92.64	93.42
Strength of junction zone, S (Pas)	6.71 \pm 0.01	14.4 \pm 0.9	12.8 \pm 0.9	12.5 \pm 0.9	13.1 \pm 0.9	13.4 \pm 0.2
Degree of entanglement, n	0.159 \pm 0.001	0.124 \pm 0.001	0.131 \pm 0.001	0.129 \pm 0.003	0.135 \pm 0.003	0.131 \pm 0.004

3.4.2.4 Flow behavior of liposomal gels

At low shear rate, the shear viscosity profile of the liposomal gels was shifted to higher value as compared to the 5:5 ι C-CMC mixed gel (Table 3.12). Beside the shear viscosity, the yield stress (σ_p) of the liposomal gels was also found to be greater than the pure 5:5 ι C-CMC mixed gel. The increase of the shear viscosity and σ_p might be due to the rigidity of the loaded liposomes or the liposomes' bridging effect as discussed in

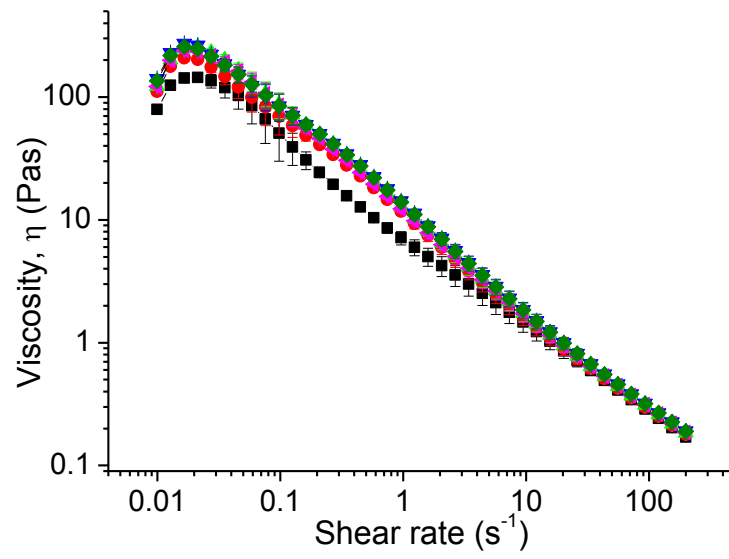
previous section (Chieng and Chen, 2010; Mourtas, Haikou et al., 2008). The viscosity and flow curves of the liposomal gels showed that they are shear thinning gels (Figure 3.30). The *PLI* of liposomal gels was significantly lower than that of 5:5 ι C-CMC mixed gel. This result indicated that the liposomal gels were more shear thinning and had better spreading ability as compared to the 5:5 ι C-CMC mixed gel (Garg et al., 2002). The effect of liposomes on the flow behavior of the gel was also found to be independent of the loaded liposome types (Table 3.12).

Table 3.12: Shear viscosity, Power Law Index (*PLI*), and yield stress (σ_p) of the liposomal gels which determined from their steady rheological behaviors.

Name	Shear viscosity (Pas)	Power Law Index, <i>PLI</i>	Yield stress, σ_p (Pa)
5:5 ι C-CMC mixed gel	132 \pm 7	0.247 \pm 0.004	4.23
LG-OA	202 \pm 9	0.200 \pm 0.004	4.32
LG-OACh1	256 \pm 2	0.169 \pm 0.005	5.48
LG-OACh2	264 \pm 5	0.179 \pm 0.005	5.65
LG-OACh2P1	222 \pm 2	0.175 \pm 0.005	5.58
LG-OACh2P2	248 \pm 4	0.179 \pm 0.005	5.28

The heterogeneous flow that was initially found in the 5:5 ι C-CMC mixed gel was still present in the liposomal gels (Figure 3.30(b)). The shear banding region of the liposomal gels has shifted to higher shear rate region as compared with 5:5 ι C-CMC mixed gel. The shift of the shear banding region was mainly due to the combinations of different stress relaxation response from different component of the liposomal gel (i.e. the gel and liposomes) (Ovarlez et al., 2009). The increase in the shear banding might also be due to the localization of stress in the region where the loaded liposomes rearrange themselves to the flow direction. When all the liposomes were orientated in the flow direction, the stress is responding linearly with the shear rate again.

(a)



(b)

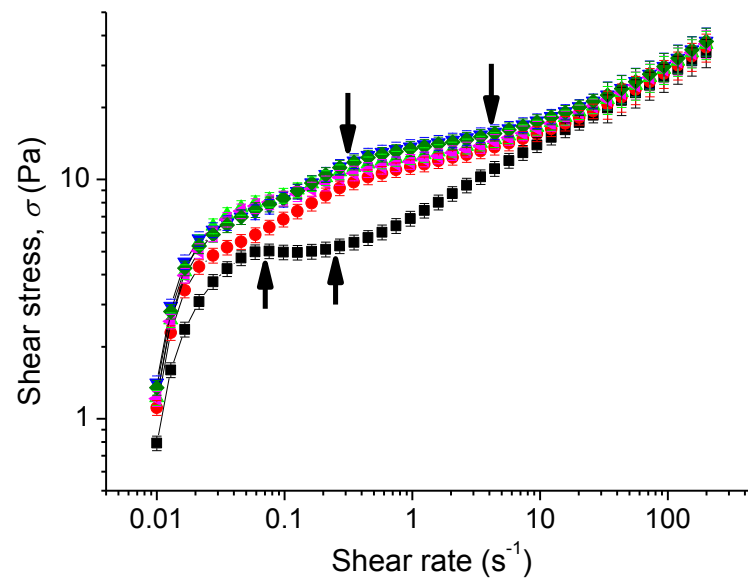


Figure 3.30: (a) Viscosity curves of the liposomal gels. (b) The flow curve of the (■)5:5 ι C-CMC mixed gel, (●)LG-OA, (▲)LG-OACh1, (▼)LG-OACh2, (◆)LG-OACh2P1, and (◆)LG-OACh2P2.

3.4.2.5 Thixotropic behavior of liposomal gels

All the prepared liposomal gels showed thixotropic properties (Figure 3.31). However, their degree of thixotropic was found to be slightly higher than the pure 5:5 ι -CMC mixed gel (Table 3.13). This result indicated that the presence of liposomes enhanced the strength of the gel network structure which was further supported by the higher elastic response of the liposomal gels as discussed in sections 3.4.2.2 and 3.4.2.3. The pseudoplastic index of all liposomal gels was significantly lower than the pure 5:5 ι -CMC mixed gel which indicated the slower structural change of the liposomal gels with respect to shear rate as compared to the pure 5:5 ι -CMC mixed gel. This might due to the greater elasticity of the liposomal gels as discussed previously. The change in the thixotropic index of the all liposomal gels was negligible and these results implied that the structural rebuilt process occurred at similar rate and independent of loaded liposome types (Table 3.13).

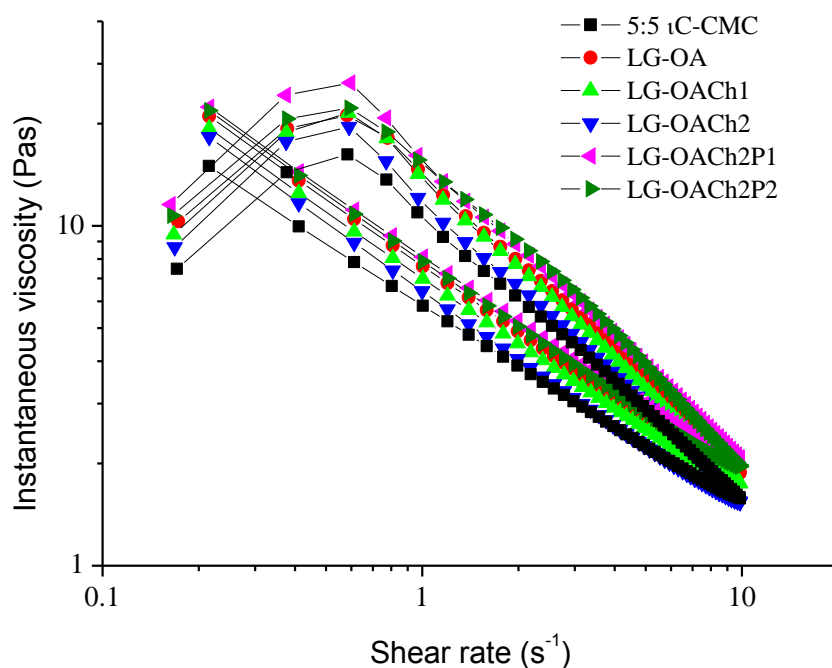


Figure 3.31: Thixotropic plot for liposomal gels.

Table 3.13: Degree of thixotropy, pseudoplastic index, and thixotropic index of liposomal gels.

Name	Degree of thixotropy	Pseudoplastic index	Thixotropic index
5:5 <i>ι</i> C-CMC mixed gel	11.9±0.2	1.05±0.01	0.72±0.02
LG-OA	15.9±0.2	0.67±0.02	0.70±0.01
LG-OACh1	16.2±0.3	0.63±0.05	0.66±0.06
LG-OACh2	13±1	0.68±0.03	0.66±0.04
LG-OACh2P1	19±2	0.64±0.03	0.65±0.05
LG-OACh2P2	18±2	0.69±0.04	0.67±0.04

CHAPTER 4

CONCLUSION

CHAPTER 4

4.0 Conclusion

This study demonstrated the preparation of surface modified OA liposomes using Chs- and Ch2Ps. The pK_a of the OA-Chs and OA-Ch2Ps mixtures was found to decrease by 1 unit and this result indicated that the interaction between the OA molecules and the Chs and Ch2Ps molecules were favourable. The size of the Chs- and Ch2Ps-modified liposomes was found to be lower than the unmodified OA liposome. In addition, the zeta potentials of these surface modified liposomes were decreased and indicated that the Chs and ChPs have successfully coated on the surface of the OA liposome. The stability and rigidity of the surface modified OA liposomes was also improved. This result can be observed from the TEM and AFM micrographs of the surface modified liposomes whereby these surface modified OA liposomes are able to retain their spherical shape unlike the unmodified OA liposome that showed structural rupture under the microscope.

The surface modified liposomes were then mixed into carbohydrate based gel for the preparation of LG. The carbohydrate gel was prepared using a mixture of ι C and CMC, this is because the individual pure gels were not suitable to be used for the preparation of LG. The high G' (36.4 Pa), CE (5.11 Pa) and shear viscosity (1000 Pas) of the ι C gel reduced the dispersity and homogeneity of the liposomes in the gel. On the other hand, the weak internal structure of the CMC gel (100 times lower than the ι C) which is due to its non-entangled nature was not strong enough to suspend the liposomes. Therefore, a series of the mixture of ι -C and CMC gels were prepared. The results showed that the presence of CMC in ι C gel managed to improve the flexibility and CE of the gel. The mixture with 5:5 ι C-CMC was used to prepare the LG due to its optimum viscoelastic properties and moderate flow behavior. The γ_c of the mixed gel with ι C-CMC ratio of 5:5 was the highest among all prepared gels which was also an

indication of more elastic nature of the gel. The CE of this mixed gel was also found to be an optimum value among the mixed gels. These properties can enhance the homogeneity, stability, and liposome dispersion in the gel. The LGs were prepared by mixing the prepared liposomes into the mixed gel with ι C-CMC ratio of 5:5. The presence of liposomes in the gel matrix has slightly modified the elastic property of the gel and this was explained with the rigidity of the loaded liposomes that could not be easily deformed. Similar results were also showed in the creep profile of the LGs as the J_{max} of all LGs were significantly lower than the pure gel matrix which indicated the stronger elastic response of the LGs. The increase in the elastic response was mainly contributed by the retarded elasticity of the LGs as the retarded elasticity of the LGs was ten folds higher than the pure 5:5 ι C-CMC mixed gel. Besides elasticity, the presence of liposomes in the gel has also enhanced its shear viscosity. The shear thinning behavior of the LGs was also found to be greater than the pure 5:5 ι C-CMC mixed gel and indicated the better spreading ability of the LGs. The G'' and σ_p values of the LGs revealed that the addition of liposomes into the gel formulation do not affect the physical entanglement of the original mixed gel with ι C-CMC ratio of 5:5. At the same time, the prepared gel system could provide the liposomes with a better protection environment towards disruptive effects and thus, improved the stability of the liposomes.

4.1 Future work

As previous researches have revealed that the liposomes have a huge potential application especially in cosmetics and topical drug delivery system. Our liposome in gel systems can be further developed for application such as delivery of anesthesia drugs and other drugs for dermatological diseases. Besides topical applications, the liposomal systems that were prepared in this study can also be used for transdermal delivery of small drugs molecules as well as macromolecules. In order to obtain an

optimum performance from liposomal system prepared in this study in transdermal delivery application, the study of biological interaction between the targeted cells and the liposomal system is relatively important. This is because it provides better understanding on the mechanism of this liposomal drug delivery system to the targeted cell and the therapeutic efficacy of the drug loaded into the liposomal system can also be predicted.

REFERENCES

References

- Abdelbary, G. (2011). Ocular ciprofloxacin hydrochloride mucoadhesive chitosan-coated liposomes. *Pharmaceutical Development and Technology*, 16, 44-56.
- Abeygunawardana, C. and Bush, C.A. (1991). Complete structure of the cell surface polysaccharide of *Streptococcus oralis* ATCC 10557: A receptor for lectin-mediated interbacterial adherence. *Biochemistry*, 30, 6528-6540.
- Abraham, G., McCarroll, J., Byrne, F., Saricilar, S., Kavallaris, M., and Bulmus, V. (2011). Block co-polymer nanoparticles with degradable cross-linked core and low-molecular-weight PEG corona for anti-tumour drug delivery. *Journal of Biomaterials Science*, 22, 1001-1022.
- Abuchowski, A., van Es, T., Palczuk, N.C., and Davis, F.F. (1977). Alteration of immunological properties of bovine serum albumin by covalent attachment of polyethylene glycol. *The Journal of Biological Chemistry*, 252, 3578-3581.
- Adamo, F. and Isabella O. (2003). The role of chitosan in drug delivery: Current and Potential Applications. *American Journal of Drug Delivery*, 1, 43-59.
- Adams, J.M. and Olmsted, P.D. (2009). Nonmonotonic models are not necessary to obtain shear banding phenomena in entangled polymer solutions. *Physical Review Letters*, 102, 067801.
- Aiba, S. (1991). Studies on chitosan: 3.Evidence for the presence of random and block copolymer structure in partially N-acetylated chitosans. *Journal of Biological Macromolecules*, 13, 40-44.
- Ajayaghosh, A., Praveen, V.K., and Vijayakumar, C. (2008). Organogels as scaffolds for excitation energy transfer and light harvesting. *Chemical Society Reviews*, 37, 109-122.

- Allan, G.G. and Peyron, M. (1995). Molecular weight manipulation of chitosan I: Kinetics of depolymerization by nitrous acid. *Carbohydrate Research*, 277, 257-272.
- Allen, T.M. (1994). Long-circulating (sterically stabilized) liposomes for targeted drug delivery. *Trends in Pharmacological Science*, 15, 215-220.
- Allen, T.M. and Chonn, A. (1987). Large unilamellar liposomes with low uptake into the reticuloendothelial system. *FEBS Letters*, 223, 42-46.
- Anitha, A., Maya, S., Deepa, N., Chennazhi, K.P., Nair, S.V., and Jayakumar, R. (2012). Curcumin-loaded N,O-carboxymethyl chitosan nanoparticles for cancer drug delivery. *Journal of Biomaterials Science*, 23, 1381-1400.
- Apel, C.L., Deamer, D.W., and Mautner, M.N. (2002). Self-assembled vesicles of monocarboxylic acids and alcohols: conditions for stability and for the encapsulation of biopolymers. *Biochimica et Biophysica Acta*, 1559, 1-9.
- Aranaz, I., Harris R, and Heras A (2010). Chitosan amphiphilic derivatives. Chemistry and applications. *Current Organic Chemistry*, 14, 308-330.
- Bajpai, A.K. and Giri, A. (2003). Water sorption behavior of highly swelling (carboxymethylcellulose-g-polyarylamide) hydrogels and release of potassium nitrate as agrochemical. *Carbohydrate Polymers*, 53, 271-279.
- Baldrick, P. (2010). The safety of chitosan as a pharmaceutical excipient. *Regulatory Toxicology and Pharmacology*, 56, 290-299.
- Bangham, A.D. and Horne, R.W. (1964). Negative staining of phospholipids and their structured modification by surface active agents as observed in the electron microscope *Journal of Molecular Biology*, 8(660-668).
- Bangham, A.D., Hill, M.W., and Miller, G.A. (1974). Preparation and use of liposomes as models of biological membranes *Methods in Membrane Biology* (Vol. 1, pp. 61-68). New York: Plenum Press.

- Barbucci, R., Magnani, A., and Consumi, M. (2000). Swelling behavior of carboxymethylcellulose hydrogels in relation to cross-linking, pH, and charge density. *Macromolecules*, 33, 7475-7480.
- Barenholz, Y. (2001). Liposome application: problems and prospects. *Current Opinion in Colloid and Interface Science*, 6, 66-77.
- Barlett, P., Teece, L.J., and Faers, M.A. (2012). Sudden collapse of a colloidal gel. *Physical Review E*, 85, 201404-201401-201404-201413.
- Barnard, J. and Millner, R. (2009). A Review of Topical Hemostatic Agents for Use in Cardiac Surgery. *The Annals of Thoracic Surgery*, 88(4), 1377-1383.
- Barnes, H.A. (2000). *A handbook of elementary rheology*. Wales: The University of Wales Institute of Non-Newtonian Fluid.
- Barrera, G.N., Bustos, M.C., Iturriaga, L., Flores, S.K., León, A.E., and Ribotta, P.D. (2013). Effect of damaged starch on the rheological properties of wheat starch suspensions. *Journal of Food Engineering*, 116, 233-239.
- Barry, B.W. (1987). Mode of action of penetration enhancers in human skin. *Journal of Controlled Release*, 6, 85-97.
- Barry, B.W. (1991). Lipid-protein-partitioning theory of skin penetration enhancement. *Journal of Controlled Release*, 15, 237-248.
- Bastiat, G., Oliger, P., Karlsson, G., Edwards, K., and Lafleur, M. (2007). Development of Non-phospholipid liposomes containing a high cholesterol concentration. *Langmuir*, 23, 7695-7699.
- Benchabane, A. and Bekkour, K. (2008). Rheological properties of carboxymethyl cellulose (CMC) solutions. *Colloid and Polymer Science*, 286, 1173-1180.

- Beugin, S., Edwards, K., Karlsson, G., Ollivon, M., and Lesieur, S. (1998). New sterically stabilized vesicles based on nonionic surfactant, cholesterol, and poly(ethylene glycol)-cholesterol conjugates. *Biophysical Chemistry*, 74, 3198-3210.
- Bianco, A., Kostarelos, K., and Prato, M. (2005). Applications of carbon nanotubes in drug delivery. *Current Opinion in Chemical Biology*, 9, 674-679.
- Blasi, P., Schoubben, A., Romano, G.V., Giovagnoli, S., Di Michele, A., and Ricci, M. (2013). Lipid nanoparticles for brain targeting II. Technological characterization. *Colloid and Surfaces B: Biointerfaces*, 110, 130-137.
- Bochot, A., Fattal, E., Grossiord, J.L., and Puisieux, F. (1998). Characterization of a new ocular delivery system based on a dispersion of liposomes in a thermosensitive gel. *International Journal of Pharmaceutics*, 162, 119-127.
- Bonferoni, M.C., Rossi, S., Ferrari, F., Bertoni, M., and Caramella, C. (1995). Influence of medium on dissolution-erosion behaviour of Na carboxymethylcellulose and on viscoelastic properties of gels. *International Journal of Pharmaceutics*, 117, 41-48.
- Brummer, R. (2006a). *Rheology essentials of cosmetic and food emulsions*. Germany: Springer-Verlag Berlin Heidelberg.
- Brummer, R. (2006b). *Rheology Essentials of Cosmetic and Food Emulsions*. Germany: Springer-Verlag Berlin Heidelberg.
- Brummer, R. and Godersky, S. (1999). Rheological studies to objectify sensations occurring when cosmetic emulsions are applied to the skin. *Colloids and Surfaces A: Physicochemical and Engineering Aspects*, 152, 89-94.
- Cavali, R., Caputo, O., and Gasco, M.R. (1993). Solid lipospheres of doxorubicin and idarubicin. *International Journal of Pharmaceutics*, 89, R9-R12.

- CDRH. (2006). Center for Devices and Radiological Health (CDRH)'s approval of Celox Topical Hemostatic Granules as a medical device (K061079). Retrieved December 05, 2009, from www.accessdata.fda.gov/cdrh_docs/pdf6/K061079
- Cevc, G. and Blume, G. (2001). New, highly efficient formulation of diclofenac for the topical, transdermal administration in ultradeformable drug carriers, Transfersomes. *Biochimica et Biophysica Acta*, 1514, 191-205.
- Cevc, G., Schätzlein, A., and Blume, G. (1995). Transdermal drug carriers: basic properties, optimization and transfer efficiency in the case of epicutaneously applied peptides. *Journal of Controlled Release*, 36, 3-16.
- Chan, P., Kurisawa, M., Chung, J.E., and Yang, Y.Y. (2007). Synthesis and characterization of chitosan-g-poly(ethylene glycol)-folate as a non-viral carrier for tumor-targeted gene delivery. *Biomaterials*, 28, 540-549.
- Chen, I.A. and Szostak, J.W. (2004). Membrane growth can generate a transmembrane pH gradient in fatty acid vesicles. *PNAS*, 101, 7965-7970.
- Chieng, Y.Y. and Chen, S.B. (2010). Rheological study of hydrophobically modified hydroxymethyl cellulose and phospholipid vesicles. *Journal of Colloid and Interface Science*, 349, 236-245.
- Choi, J.S., Seo, K.H., and Yoo, J.W. (2012). Recent advances in PLGA particulate systems for drug delivery. *Journal of Pharmaceutical Investigation*, 42, 155-163.
- Chonn, A. and Cullis P.R. (1998). Recent advances in liposome technologies and their applications for systemic gene delivery. *Advanced Drug Delivery Reviews*, 30, 73-83.
- Chu, Z. and Feng, Y. (2010). Amidosulfobetaine surfactant gels with shear banding transitions. *Soft Matter*, 6, 6065-6067.

- Cistola, D.P., Hamilton, J.A., Jackson, D., and Small, D.M. (1988). Ionization and phase behavior of fatty acids in water: application of the Gibbs phase rule. *Biochemistry*, 27, 1881-1888.
- D'Souza, S.S. and DeLuca, P.P. (2006). Methods to assess *in vitro* drug release from injectable polymeric particulate systems. *Pharmaceutical Research*, 23, 460-474.
- da Costa, C.A.M. and Moraes, Â.M. (2003). Encapsulation of 5-fluorouracil in liposomes for topical administration. *Acta Scientiarum Technology*, 25, 53-61.
- Dams, E.T.M., Laverman, P., Oyen, W.J.G., Strom, G., Scherphof, G.L., Van Der Meer, J.W.M., Corstens, F.H.M., and Boerman, O.C. (2000). Accelerated blood clearance and altered biodistribution of repeated injection of sterically stabilized liposomes. *Journal of Pharmacology and Experimental Therapeutics*, 292, 1071-1079.
- Danhier, F., Feron, O., and Pr  at, V. (2010). To exploit the tumor microenvironment: Passive and active tumor targeting of nanocarriers for anti-cancer drug delivery. *Journal of Controlled Release*, 148, 135-146.
- Dayan, N. (2005). Pathways for skin penetration *Cosmetics & Toiletries magazine*, 120, 67-76.
- de Brito, A.C.F., Sierakowski, M.R., Reicher, F., Feitosa, J.P.A., and de Paula, R.C.M. . (2005). Dynamic rheological study of *Sterculia striata* and karaya polysaccharides in aqueous solution. *Food Hydrocolloids*, 19, 861-867.
- de Jager, M.W., Ponc  , M., and Bouwstra, J.A. (2007). The lipid organization in stratum corneum and model systems based on ceramides. In E. Touitou, and Barry, B.W. (Ed.), *Enhancement in drug delivery* (pp. 217-232). New York: CRC Press.
- de Leeuw, J., de Vijlder, H.C., Bjerring, P., and Neumann, H.A.M. . (2009). Liposomes in dermatology today. *Journal compilation European Academy of Dermatology and Venereology*, 23, 505-516.

- Dew, N., Edwards, K., and Edsman, K. (2009). Gel formation in systems composed of drug containing cationic vesicles and oppositely charged hydrophobically modified polymer. *Colloid and Surfaces B: Biointerfaces*, 70, 187-197.
- Dicorleto, P.E. and De La Motte, C. (1989). Role of cell surface carbohydrate moieties in monocyte cell adhesion to endothelium in vitro. *The Journal of Immunology*, 143, 3666-3672.
- Dogan, M., Kayacier, A., Toker, Ö.S., Yilmaz, M.T., and Karaman, S. (2012). Steady, dynamic, creep, and recovery analysis of ice cream mixes added with different concentrations of xanthan gum. *Food Bioprocess Technology*, 6, 1420-1433.
- Dolz, M., Hernández, M.J., and Delegido, J. (2008). Creep and recovery experimental investigation of low oil content food emulsions. *Food Hydrocolloids*, 22, 421-427.
- Dowling, M.B., Lee, J.H., and Raghavan, S.R. (2009). pH-responsive jello: gelatin gels containing fatty acid vesicles. *Langmuir*, 25, 8519-8525.
- Dragicevic-Curic, N., Winter, S., Stupar, M., Milic, J., Krajišnik, D., Gitter, B., and Fahr, A. (2009). Temoporfin-loaded liposomal gel: Viscoelastic properties and *in vitro* skin penetration. *International Journal of Pharmaceutics*, 373, 77-84.
- Dufresne, A., Cavaillé, J., Dupeyre, D., Gracia-Ramirez, M., and Romero, J. (1999). Morphology, phase continuity and mechanical behavior of polyamide 6/chitosan blends. *Polymer Physics*, 40, 1657-1666.
- Ekambaram, P., Sathali, A.A.H., and Priyanka, K. (2012). Solid lipid nanoparticles: A review. *Scientific Reviews & Chemical Communications*, 2, 80-102.
- El Maghraby, G.M., Barry, B.W., and Williams, A.C. (2008). Liposomes and skin : From drug delivery to model membranes. *European Journal of Pharmaceutical Sciences*, 34, 203-222.

- El Maghraby, G.M., Williams, A.C., and Barry, B.W. (2000). Skin delivery of oestradiol from lipid vesicles: importance of liposome structure. *International Journal of Pharmaceutics*, 204, 159-169.
- El Maghraby, G.M., Williams, A.C., and Barry, B.W. (2001). Skin delivery of 5-fluorouracil from ultradeformable and standard liposomes in-vitro. *Journal of Pharmacy and Pharmacology*, 53, 1069-1077.
- El Maghraby, G.M.M., Barry, B.W. , and Williams, A.C. (2008). Liposomes and skin: From drug delivery to model membranes. *European Journal of Pharmaceutical Sciences*, 34, 203-222.
- El Maghraby, G.M.M., Williams, A.C., and Barry, B.W. (2005). Can drug-bearing liposomes penetrate intact skin? *Journal of Pharmacy and Pharmacology*, 58, 415-429.
- Elferink, M.G.L., de Wit, J.G., Veld, G.I., Reichert, A., Driessen, A.J.M., Ringsoorf, H., and Konings, W.N. (1992). The stability and functional properties of proteoliposomes mixed with dextran derivatives bearing hydrophobic anchor groups. *Biochimica et Biophysica Acta*, 1106, 23-30.
- Estroff, L.A. and Hamilton, A.D. (2003). Water gelation by small organic molecules. *Chemical Reviews*, 104, 1201-1217.
- Fan, M., Hu, Q.L., and Shen, K. (2009). Preparation and structure of chitosan soluble in wide pH range. *Carbohydrate Polymers*, 78, 66-71.
- Filipovicâ-Grcićâ, J., Škalko-Basnet, N., and Jalšenjak, I. (2001). Mucoadhesive chitosan-coated liposomes: characteristics and stability. *Journal of Microencapsulation*, 18, 3-12.
- Foong, W.C., Harsany, B.B., and Mezei, M. (1990). Biodisposition and histological evaluation of topically applied retinoic acid in liposomal, cream and gel dosage forms. In I. Hanin, and Pepeu, G. (Ed.), *Phospholipids* (pp. 279-282). New York: Plenum Press.

- Fox, L.T., Gerber, M., Plessis, J.D., and Hamman, J.H. (2011). Transdermal drug delivery enhancement by compounds of natural origin. *Molecules*, *16*, 10507-10540.
- Fuchs, T., Richtering, W., Burchard, W., Kajiwarra, K., and Kitamura, S. (1998). Gel point in physical gels: rheology and light scattering from thermoreversibly gelling schizophyllan. *Polymer Gels and Networks*, *5*, 541-559.
- Fuji, M., Takai, Chika, Tarutani, Y., Takei, T., and Takahashi, M. (2007). Surface properties of nanosize hollow silica particles on the molecular level. *Advanced Powder Technology*, *18*, 81-91.
- Gabriele, D., de Cindio, B., and D'Antona, P. (2001). A weak gel model for foods. *Rheologica Acta*, *40*, 120-127.
- Gabrijelčič, V. and Šentjerc, M. (1995). Influence of hydrogels on liposome stability and on the transport of liposome entrapped substances into skin. *International Journal of Pharmaceutics*, *118*, 207-212.
- Garg, A., Aggarwal, D., Garg, S., and Singla, A.K. (2002). Spreading of semisolid formulations-An update. *Pharmaceutical Technology*(September), 84-105.
- Garg, M., Dutta T, and Jain NK. (2007). Stability study of Stavadin-loaded O-palmitoyl-anchored carbohydrate-coated liposomes. *AAPS PharmSciTech*, *8*, Article 38.
- Gaumet, M., Vargas, A., Gurny, R., and Delie, F. (2008). Nanoparticles for drug delivery: The need for precision in reporting particle size parameters. *European journal of Pharmaceutics and Biopharmaceutics*, *69*, 1-9.
- Ge, L., Zhu, J.B., Xiong, F., and Ni, B. (2007). Preparation, characterization and pharmacokinetics of N-palmitoyl chitosan anchored docetaxel liposomes. *Journal of Pharmacy and Pharmacology*, *59*, 661-667.

- Gebicki, J.M. and Hicks, M. (1973). Ufasomes are stable particles surrounded by unsaturated fatty acid membranes. *Nature*, 243, 232-234.
- Gemeinhart, R.A. (2006). Polymeric systems for oral protein and peptide delivery. In M. J. Groves (Ed.), *Pharmaceutical biotechnology* (pp. 282-306). New York: CRC Press.
- Glavaš-Dodov, M., Fredro-Kumbaradzi, E., Goračinova, K., Calis, S., Simonoska, M., and Hincal, A.A. (2003). 5-Fluorouracil in topical liposome gels for anticancer treatment--formulation and evaluation. *Acta Pharmaceutica*, 53, 241-250.
- Glavaš-Dodov, M., Simonoska, M., and Goračinova, K. (2005). Formulation and characterization of topical liposome gel bearing lidocaine HCl. *Bulletin of the Chemists and Technologists of Macedonia*, 24, 59-65.
- Gobet, M., Mouaddab, M., Cayot, N., Bonny, J., Guichard, E., Le Quéré, J., Moreau, C., and Foucat, L. (2009). The effect of salt content on the structure of iota-carrageenan systems: ²³Na DQF NMR and rheological studies. *Magnetic Resonance in Chemistry*, 47, 307-312.
- Goodwin, J.W. and Hughes, R.W. (2008). *Rheology for chemists: an introduction*. UK: The Royal Society of Chemistry.
- Gregoriadis, G., Gursel, I., Gursel, M., and McCormack, B. (1996). Liposomes as immunological adjuvants and vaccine carriers. *Journal of Controlled Release*, 41, 49-56.
- Grillet, A.M., Wyatt, N.B., and Gloe, L.M. (2012). Polymer gel rheology and Adhesion. In J. De Vicente (Ed.), *Rheology* (pp. 350): InTech.
- Gruber, J.V. (1999). Polysaccharide-based polymers in cosmetics. In E. D. Goddard, and Gruber J.V. (Ed.), *Principles of Polymer science and technology in cosmetics and personal care* (pp. 325-389). New York: Marcel Dekker, Inc.

- Gu, R., Sun, W., Zhou, H., Wu, Z., Meng, Z., Zhu, X., Tang, Q., Dong, J., and Dou, G. (2010). The performance of a fly-larva shell-derived chitosan sponge as an absorbable surgical hemostatic agent. *Biomaterials*, 31, 1270-1277.
- Gu, Y.S., Decker, E.A., and McClements, D.J. (2004). Influence of pH and ι -carrageenan concentration on physicochemical properties and stability of β -lactoglobulin-stabilized oil-in-water emulsions *Agricultural and Food Chemistry*, 52, 3626-3632.
- Gul-Uludag, H., Xu, P., Marquez-Curtis, L.A., Xing, J., Janowska-Wieczorek, A., and Chen, J. (2012). Cationic liposome-mediated CXCR4 gene delivery into hematopoietic stem/progenitor cells: Implications for clinical transplantation and gene therapy. *Stem Cells and Development*, 21, 1587-1596.
- Guo, J., Pin, Q., Jiang, G., Huang, L., and Tong, Y. (2003). Chitosan-coated liposomes: characterization and interaction with leuprolide. *International Journal of Pharmaceutics*, 260, 167-173.
- Gupta, R.K., Hariharan, M., Wheatley, T.A., and Price, J.C. (2001). Controlled-release tablets from carragennans: effect of formulation, storage and dissolution factors. *European journal of Pharmaceutics and Biopharmaceutics*, 51, 241-248.
- Gupta, R.K., Varanelli, C.L., Griffin, P., Wallach, D.F.H., and Siber, G.R. (1996). Adjuvant properties of non-phospholipid liposome (Novasomes) in experimental animals for human vaccine antigen. *Vaccine*, 14, 219-225.
- Gutowska, A., Bae, Y.H., Jacobs, H., Mohammad, F., Mix, D., Feijen, J., and Kim, S.W. (1995). Heparin release from thermosensitive polymer coatings: *in vivo* studies. *Journal of Biomedical Materials Research*, 29, 811-821.
- Gwak, H.S. and Chun, I.K. (2002). Effect of vehicles and penetration enhancers on the *in vitro* percutaneous absorption of tenoxicam through hairless mouse skin. *International Journal of Pharmaceutics*, 236, 57-64.

- Hargreaves, W.R. and Deamer, D.W. (1978). Liposomes from ionic, single-chain amphiphiles. *Biochemistry*, 17, 3759-3768.
- Harrington, K.J., Syrigos, K.N., and Vile, R.G. (2002). Liposomally targeted cytotoxic drug for the treatment of cancer. *Journal of Pharmaceutical and Pharmacology*, 54, 1573-1600.
- Harris, J. (1967). Hysteresis experiment in rheology. *Nature*, 214, 796-797.
- Harris, T.K. and Turner, G.J. (2002). Structural basic of perturbed pK_a values of catalytic groups in enzyme active sites. *IUBMB Life*, 53, 85-98.
- He, Q.J., Gao, Y., Zhang, L.X., Zhang, Z.W., Gao, F., Ji, X.F., Li, Y.P., and Shi, J.L. (2011). A pH-responsive mesoporous silica nanoparticles-based multi-drug delivery system for overcoming multi-drug resistance. *Biomaterials*, 32, 7711-7720.
- He, S.J., Zhu, J.B., and Xie, F.M. (2010). Preparation and characterization of tramadol EG-coated multivesicular liposomes for sustained release. *Pharmazie*, 6, 467-470.
- Heinze, T. (1998). New ionic polymers by cellulose functionalization. *Macromolecular Chemistry and Physics*, 199, 2341-2364.
- Herraz, B., Tovar, C.A., Zolo-de-Zaldívar, B., and Borderias, A.J. (2012). Effect of alkalis on konjac glucomannan gels for use as potential gelling agents in restructures seafood products. *Food Hydrocolloids*, 27, 145-153.
- Hirano, S., Yamaguchi, Y., and Kamiya, M. (2002). Novel *N*-saturated-fatty-acyl derivatives of chitosan soluble in water and in aqueous acid and alkaline solutions. *Carbohydrate Polymers*, 48, 203-207.
- Hiremath, J.G., Khamar, N.S., Palavalli, S.G., Rudani, C.G., Aitha, R., and Mura, P. (2013). Paclitaxel loaded carrier based biodegradable polymeric implants:

- preparation and *in vivo* characterization. *Saudi Pharmaceutical Journal*, 21, 85-91.
- Honarkar, H. and Barikani, M. (2009). Applications of biopolymers I: chitosan. *Monatshefte für Chemie*, 140, 1403-1420.
- Honeywell-Nguyen, P.L., de Graaff, A.M., Groenink, H.W.W., and Bouwstra, J.A. (2002). The *in vivo* and *in vitro* interactions of elastic and rigid vesicles with human skin. *Biochimica et Biophysica Acta*, 1573, 130-140.
- Honeywell-Nguyen, P.L., Groenink, H.W.W., de Graaff, A.M., and Bouwstra, J.A. (2003). The *in vivo* transport of elastic vesicles into human skin: effects of occlusion, volume and duration of application. *Journal of Controlled Release*, 90, 243-255.
- Hossain, K.S., Miyanaga, K., Meada, H., and Nemoto, N. (2001). Sol-gel transition behavior of pure ι-carrageenan in both salt-free and added salt states *Biomacromolecules*, 2, 442-449.
- Ikeda, S. and Foegeding, E.A. (2003). Measurement of Gel Rheology: Dynamic Tests. In R. E. Wrolstad, Acree, T.E., Decker, E.A., Penner, M.H., Reid, D.S., Schwartz, S.J., Shoemaker, C.F., Smith, D.M., and Sporns, P. (Ed.), *Current Protocols in Food Analytical Chemistry*: John Wiley & Sons, Inc.
- Ilg, P. and Gado, E.D. (2011). Non-linear response of dipolar colloidal gels to external fields. *Soft Matter*, 7, 163-171.
- Illum, L. (1998). Chitosan and its use as a pharmaceutical excipient. *Pharmaceutical Research*, 15, 1326-1331.
- Im, S.H., Jeong, U.Y., and Xia, Y.N. (2005). Polymeric hollow particles with controllable holes in their surface. *Nature Materials*, 4, 671-675.
- Immordino, M.L., Dosio, F., and Cattel, L. (2006). Stealth liposomes: review of basic science, rationale, and clinical applications, existing and potential *International Journal of Nanomedicine*, 1, 297-315.

- Ishida, T., Harada, M., Wang, X.Y., Ichihara, M., Irimura, K., and Kiwada, H. (2005). Accelerated blood clearance of PEGylated liposomes following preceding liposome injection: Effects of lipid dose and PEG surface-density and chain length of the first-dose liposomes. *Journal of Controlled Release*, 105, 305-317.
- Ishida, T., Ichihara, M., Wang, X.Y., Yamamoto, K., Kimura, J., Majima, E., and Kiwada, H. (2006). Injection of PEGylated liposomes in rats elicits PEG-specific IgM, which is responsible for rapid elimination of a second dose of PEGylated liposomes. *Journal of Controlled Release*, 112, 15-25.
- Islam, M.T., Rodríguez-Hornedo, N., Ciotti, S., and Ackermann, C. (2004). Rheological characterization of topical carbomer gels neutralized to different pH. *Pharmaceutical research*, 21, 1192-1199.
- Ivens, U.I., Steinkjer, B., Serup, J., and Tetens, V. (2001). Ointment is evenly spread on the skin, in contrast to creams and solutions. *British Journal of Dermatology*, 145, 264-267.
- Jain, A.K., Chalasani, K.B., Khar, R.K., Ahmed, F.J., and Diwan, P.V. (2007). Muco-adhesive multivesicular liposomes as an effective carrier for transmucosal insulin delivery. *Journal of Drug Targeting*, 15, 417-427.
- Janes, K.A. and Alonso, M.J. (2003). Depolymerized chitosan nanoparticles for protein delivery: preparation and characterization. *Journal of Applied Polymer Science*, 88, 2769-2776.
- Jelvehgari, M., Rashidi, M.R., and Mirza, M.S.H. (2007). Adhesive and spreading properties of pharmaceutical gel composed of cellulose polymer. *Jundishapur, Journal of Natural Pharmaceutical Products*, 2, 45-58.
- Jen, C.P., Chen, Y.H., Fan, C.S., Yeh, C.S., Lin, Y.C., Shieh, D.B., Wu, C.L., Chen, D.H., and Chou, C.H. (2004). A nonviral transfection approach in Vitro: The design of a gold nanoparticle vector joint with microelectromechanical systems. *Langmuir*, 20, 1369-1374.

- Jeschke, M.G. and Klein, D. (2004). Liposomal gene transfer of multiple genes is more effective than gene transfer of a single gene. *Gene Therapy*, 11, 847-855.
- Jesorka, A. and Orwar, O. (2008). Liposomes: Technologies and analytical applications. *Annual Review of Analytical Chemistry*, 1, 801-832.
- Jiang, X.M. and Brinker, C.J. (2006). Aerosol-assisted self-assembly of single-crystal core/nanoporous shell particles as model controlled release capsules. *Journal of The American Chemical Society*, 128, 4512-4513.
- Jones, D.S., Woolfson, D.A., and Brown, A.F. (1997). Textural analysis and flow rheometry of novel, bioadhesive antimicrobial oral gels. *Pharmaceutical research*, 14, 450-457.
- Jones, R.A. and Staples, E.J. (1973). A study of the Helix-Coil transition of i-carrageenan segments by light scattering and membrane osmometry. *Journal of the Chemical Society, Perkin Transactions* 2(12), 1608-1612.
- Kang, E.C., Aklyoshi, K., and Sunamoto, J. (1997). Surface coating of liposomes with hydrophobized polysaccharides. *Journal of Bioactive and Compatible Polymers*, 12, 14-26.
- Kanicky, J.R. and Shah, D.O. (2002). Effect of degree, type, and position of Unsaturation on the pK_a of long-chain fatty acids. *Journal of Colloid and Interface Science*, 256, 201-207.
- Kanicky, J.R., Poniatowski, A.F., Mehta, N.R., and Shah, D.O. (2000). Cooperativity among molecules at interfaces in relation to various technological processes: Effect of chain length on the pK_a of fatty acid salt solutions. *Langmuir*, 16, 172-177.
- Karaman, S. and Kayacier, A. (2012). Rheology of ice cream mix flavored with black tea or herbal teas and effect of flavoring on the sensory properties of ice cream. *Food Bioprocess Technology*, 5, 3159-3169.

- Karande, P., Jain, A., Ergun, K., Kispersky, V., and Mitragotri, S. (2005). Design principles of chemical penetration enhancers for transdermal drug delivery. *PNAS*, *102*, 4688-4693.
- Karn, P.R., Vanić, Z., Pepić, I., and Škalko-Basnet, N. (2011). Mucoadhesive liposomal delivery systems: the choice of coating material. *Drug development and Industrial Pharmacy*, *37*, 482-488.
- Kasaai, M.R. (2008). A review of several reported procedures to determined the degree of N-acetylation for chitin and chitosan using infrared spectroscopy. *Carbohydrate Polymers*, *71*, 497-508.
- Kästner, U., Hoffmann, H., Dönges, R., and Hilbig, J. (1997). Structure and solution properties of sodium carboxymethyl cellulose. *Colloid and Surfaces*, *123-124*, 307-328.
- Kean, T. and Thanou, M. (2010). Biodegradation, biodistribution and toxicity of chitosan. *Advanced Drug Delivery Reviews*, *62*, 3-11.
- Kepczynski, M., Bednar, J., Kuźmich, D., Wydro, P., and Nowakowska, M. (2010). Spontaneous formation of densely stacked multilamellar vesicles in Dioctadecyldimethylammonium Bromide/Oleosiloxane mixtures. *Langmuir*, *26*, 1551-1556.
- Khaled, B. and Abdelbaki, B. (2012). Rheological and electrokinetic properties of carboxymethylcellulose-water dispersions in the presence of salts. *International Journal of Physical Science*, *7*, 1790-1798.
- Khvan, A.M., Madzhidova, V.E., and Turaev, A.S. (2005). Ionic linking of carboxymethylcellulose. *Chemistry of Natural Compounds*, *41*, 88-90.

- Kim, J.H., Kim, S.I., Kwon, I.B., Kim, M.H., and Lim, J.I. (2013). Simple fabrication of silver hybridized porous chitosan-based patch for transdermal drug-delivery system. *Materials Letters*, 95, 48-51.
- Klein, S. (2009). Polysaccharides in oral drug delivery- recent applications and future perspectives. In K. J. Edgar, Heinze, T., and Buchanan, C.M. (Ed.), *Polysaccharide materials: performance by design*. New York: American Chemical Society.
- Klibanov, A.L., Maruyama, K., Torchilin, V.P., and Huang, L. (1990). Amphipathic polyethyleneglycols effectively prolong the circulation time of liposomes. *FEBS Letters*, 268, 235-237.
- Klose, D., Siepmann, F., Elkharraz, K. and Siepmann, J. (2008). PLGA-based drug delivery systems: Importance of the type of drug and device geometry. *International Journal of Pharmaceutics*, 354, 95-103.
- Koike, N., Ikuno, T., Okubo, T., and Shimojima, A. (2013). Synthesis of monodisperse organosilica nanoparticles with hollow interiors and porous shells using silica nanospheres as templates. *Chemical Communications*, 49, 4998-5000.
- Kubota, N., Tatsumoto, N., Sano, T., and Toya, K. (2000). A simple preparation of half N-acetylated chitosan highly soluble in water and aqueous organic solvents. *Carbohydrate Research*, 324, 268-274.
- Kumar, J.A., Pullakandam, N., Prabu, S.L., and Gopal, V. (2009). Transdermal drug delivery system: An overview. *International Journal of Pharmaceutical Science Reviews and Research*, 3, 49-54.
- Kwon, H.J. and Gong, J.P. (2006). Negatively charged polyelectrolyte gels as bio-tissue model system and for biomedical application. *Current Opinion in Colloid and Interface Science*, 11, 345-350.
- Lasic, D.D. (1995). Applications of Liposomes. In R. Lipowsky, and Sackman, E. (Ed.), *Handbook of Biological Physics* (Vol. 1, pp. 419-519): Elsevier Science.

- Laverman, P., Carstens, M.G., Boerman, O.C., Dams, E.Th.M., Oyen, W.J.G., Van Rooijen, N., Corstens, F.H.M., and Strom, G. (2001). Factor affecting the accelerated blood clearance of Polyethylene Glycl-liposomes upon repeated injection. *The journal of Pharmacology and Experimental Therapeutics*, 298, 607-612.
- Lavertu, M., Xia, Z., Serreqi, A.N., Berranda, M., Rodrigues, A., Wang, D., Buschmann, M.D., and Gupta, A. (2003). A validated ¹H-NMR method for the determination of the degree of deacetylation of chitosan. *Journal of Pharmaceutical and Biomedical Analysis*, 32, 1149-1158.
- Le-Tien, C., Lacroix, M., Ispas-Szabo, P., and Mateescu, M.A. (2003). N-acylated chitosan: hydrophobic matrices for controlled drug release. *Journal of Controlled Release*, 93, 1-13.
- Lee, C.H., Moturi, V., and Lee, Y. (2009). Thixotropic propety in pharmaceutical formulations. *Journal of Controlled Release*, 136, 88-98.
- Lee, J.H., Choi, Y.M., Paik, U., and Park, J.G. (2006). The effect of carboxymethyl cellulose swelling on the stability of natural graphate particulates in an aqueous medium for lithium ion battery anodes. *Journal of Electroceramic*, 17, 657-660.
- Leong, K.H., Chung, L.Y., Noordin, M.I., Mohamad, K., Nishikawa, M.,m Onuki, Y., Morishita, M., and Takayama, K. (2011). Carboxymethylation of kappa-carrageenan for intestinal-targeted delivery of bioactive macromolecules. *Carbohydrate Polymers*, 83, 1507-1515.
- Li, J., Du, Y., and Liang, H. (2006). Low molecular weight water-soluble chitosans: Preparation with the aid of cellulase, characterization, and solubility. *Journal of Applied Polymer Science*, 102, 1098-1105.
- Li, N., Zhuang, C.Y., Wang, M., Sun, X.Y., Nie, S.F., and Pan, W.S. (2009). Liposome coated with low molecular weight chitosan and its potential use in ocular drug delivery. *International Journal of Pharmaceutics*, 379, 131-138.

- Lipowsky, R. (1991). The conformation of membranes. *Nature*, 349, 475-481.
- Liu, J.W., Stace-Naughton, A., Jiang, X.M., and Brinker, C.J. (2009). Porous nanoparticle supported lipid bilayers (Protocells) as delivery vehicles. *Journal of American Chemical Society*, 131, 1354-1355.
- Liu, N. and Park, H.J. (2010). Factors effect on the loading efficiency of Vitamin C loaded chitosan-coated nanoliposomes. *Colloids and Surfaces B: Biointerfaces*, 76, 16-19.
- Liu, P., Zhao, M., Li, J., Peng, J., and Wu, J. (2002). Radiation preparation and swelling behavior of sodium carboxymethyl cellulose hydrogels. *Radiation Physics and Chemistry*, 63, 525-528.
- Liu, R.Z., Gan, L., Yang, X.L., and Xu, H. (2011). Chitosan as a condensing agent induces high gene transfection efficiency and low cytotoxicity of liposome. *Journal of Bioscience and Bioengineering*, 111, 98-103.
- López-Pinto, J.M., González-rodríguez, M.L., and Rabasco, A.M. (2005). Effect of cholesterol and ethanol on dermal delivery from DPPC liposomes. *International Journal of Pharmaceutics*, 298, 1-12.
- Lorenzo, G., Zaritzky, N., and Califano, A. (2013). Rheological analysis of emulsion-filled gels based on high acyl gellan gum. *Food Hydrocolloids*, 30, 672-680.
- Lou, X.W., Archer, L.A., and Yang, Z.C. (2008). Hollow micro-/nanostructures: Synthesis and applications. *Advanced Materials*, 20, 3987-4019.
- MacArtin, P., Jacquier, J.C., and Dawson, K.A. (2003). Physical characteristics of calcium induced κ -carrageenan networks. *Carbohydrate Polymers*, 53, 395-400.
- Mady, M.M., Darwish, M.M., Khalil, S., and Khalil, W.M. (2009). Biophysical studies on chitosan-coated liposomes. *European Biophysics Journal* 38, 1127-1133.

- Magdassi, S., Bassa, A., Vinetsky, Y., and Kamyshny, A. (2003). Silver nanoparticles as pigments for water-based ink-jet inks. *Chemistry of Materials*, 15, 2208-2217.
- Mantripragada, S. (2002). A lipid based depot (DepoFoam[®] technology) for sustained release drug delivery. *Progress in Lipid Research*, 41, 392-406.
- Mao, S., Shuai, X., Unger, F., Simon, M., Bi, D., and Kissel, T. (2004). The depolymerization of chitosan: effects on physicochemical and biological properties. *International Journal of Pharmaceutics*, 281, 45-54.
- Maurer, N., Fenske, D.B., and Cullis, P.R. (2001). Developments in liposomal drug delivery systems. *Expert Opinion on Biological Therapy*, 1, 923-947.
- Mehnert, W. and Mäder, K. (2001). Solid lipid nanoparticles: production, characterization and applications. *Advanced Drug Delivery Reviews*, 47, 165-196.
- Mehta, R.T., Hopfer, R.L., McQueen, T., Juliano, R.L., and Lopez-Berestein, G. (1987). Toxicity and therapeutic effects in mice of liposome-encapsulated Nystatin for systemic fungal infections. *Antimicrobial Agents and Chemotherapy*, 31, 1901-1903.
- Mezei, M. and Gulasekharam, V. (1980). Liposomes- A selective drug delivery system for the topical route of administration. I. Lotion dosage form. *Life Sciences*, 26, 1473-1477.
- Michailova, V., Titeva, St., Kotsilkova, R., Krusteva, E., and Minkov, E. (1999). Influence of aqueous medium on viscoelastic properties of carboxymethylcellulose sodium, hydroxypropylmethyl cellulose, and thermally per-gelatinized starch gels. *Colloids and Surfaces A: Physicochemical and Engineering Aspects*, 149, 515-520.
- Millane, R.P., Chandrasekaran, R., and Arnott, S. (1988). The molecular structure of Kappa-carrageenan and comparison with iota-carrageenan. *Carbohydrate Research*, 182, 1-17.

- Mills, W., Chopra, R., Linch, D.C., and Goldstone, A.H. (1994). Liposome amphotericin B in the treatment of fungal infections in neutropenic patients: a single-centre experience of 133 episodes in 116 patients. *British Journal of Haematology*, 86, 754-760.
- Miyata, H. and Hotani, H. (1992). Morphological changes in liposomes caused by polymerization of encapsulated actin and spontaneous formation of actin bundles *Proceedings of the National Academy of Sciences*, 89, 11547-11551.
- Miyazaki, S., Ishitani, M., Takahashi, A., Shimoyama, T., Itoh, K., and Attwood, D. (2011). Carrageenan gels for oral sustained delivery of acetaminophen to Dysphagic patients. *Biological and Pharmaceutical Bulletin*, 34, 164-166.
- Miyazaki, T., Kohno, S., Sasayama, K., Inoune, Y., Hara, K., Ogasawara, M., Sato, T., and Sunamoto, J. (1992). Polysaccharide-coated liposomal amphotericin B for the treatment of murine pulmonary candidiasis. *Tohoku Journal of Experimental Medicine*, 168, 483-490.
- Mobed, M. and Chang, T.M.S. (1998). Adsorption of chitin derivatives onto liposomes: optimization of adsorption conditions. *Journal of Microencapsulation*, 15, 595-607.
- Moghadam, S.H., Saliaj, E., Wettig, S.D., Dong, C., Ivanova, M.V., Huzil, J.T., and Foldvari, M. (2013). Effect of chemical permeation enhancers on stratum corneum barrier lipid organizational structure and interferon alpha permeability. *Molecular Pharmaceutics*, 10, 2248-2260.
- Morigaki, K. and Walde P. (2002). Giant vesicle formation from oleic acid/sodium oleate on glass surfaces induced by adsorbed hydrocarbon molecules. *Langmuir*, 18, 10509-10511.
- Morigaki, K. and Walde P. (2007). Fatty acid vesicles. *Current Opinion in Colloid and Interface Science*, 12, 75-80.

- Morigaki, K., Walde, P., Misran, M., and Robinson, B.H. (2003). Thermodynamic and kinetic stability. Properties of micelles and vesicles formed by the decanoic acid/decanoate system. *Colloids and Surfaces A: Physicochemical and Engineering Aspects*, 213, 37-44.
- Morris, G. A., Kök, M.S., Harding, S.E., and Adams, G.G. (2010). Polysaccharide drug delivery systems based on pectin and chitosan. *Biotechnology and Genetic Engineering Reviews*, 27, 257-284.
- Moscho, A., Orwar, O., Chiu, D.T., Modi, B.P., and Zare, R.N. (1996). Rapid preparation of giant unilamellar vesicles. *Proceedings of the National Academy of Sciences*, 93, 11443-11447.
- Mourtas, S., Aggelopoulos, C.A., Klepetsanis, P., Tsakiroglou, C.D., and Antimisiaris, S.G. (2009). Complex hydrogel systems composed of polymers, liposomes, and cyclodextrins: Implications of composition on rheological properties and aging. *Langmuir*, 25, 8480-8488.
- Mourtas, S., Duraj, S., Fotopoulou, S., and Antimisiaris, S.G. (2008). Integrity of liposomes in presence of various formulation excipients, when dispersed in aqueous media and in hydrogels. *Colloids and Surfaces B: Biointerfaces*, 61, 270-276.
- Mourtas, S., Fotopoulou, S., Duraj, S., Sfika, V., Tsakiroglou, C., and Antimisiaris, S.G. (2007). Liposomal drugs dispersed in hydrogels effect of liposome, drug and gel properties on drug release kinetics. *Colloids and Surfaces B: Biointerfaces*, 55, 212-221.
- Mourtas, S., Haikou, M., Theodoropoulou, M., Tsakiroglou, C., and Antimisiaris, S.G. (2008). The effect of added liposomes on the rheological properties of a hydrogel: A systematic study. *Journal of Colloid and Interface Science*, 317, 611-619.

- Mufamadi, M.S., Pillay, V., Choonara, Y.E., Tolt, L.C.D., Girish, M., Naidoo, D., and Ndesendo, V.M.K. (2011). A review on composite liposomal technologies for specialized drug delivery. *Journal of Drug Delivery*, 2011, Article ID 939851.
- Müller, R.H., Maaßen, S., Weyhers, H., Specht, F., and Lucks, J.S. (1996). Cytotoxicity of magnetite-loaded polylactide, polylactide/glycolide particles and solid lipid nanoparticles. *International Journal of Pharmaceutics*, 138, 85-94.
- Munarin, F., Tanzi, M.C., and Petrini, P. (2012). Advances in biomedical applications of pectin gels. *International Journal of Biological Macromolecules*, 51, 681-689.
- Mura, P., Maestrelli, F., González-Rodríguez, M.L., Michelacci, I., Ghelardini, C., and Rabasco, A.M. (2007). Development, characterization and in-vivo evaluation of benzocaine-loaded liposomes. *European journal of Pharmaceutics and Biopharmaceutics*, 67, 86-95.
- Nakauma, M., Tanaka, R., Ishihara, S., Funami, T., and Nishinari, K. (2012). Elution of sodium caseinate from agar-based gel matrixes in simulated gastric fluid. *Food Hydrocolloids*, 27, 427-437.
- Namani, T. and Walde, P. (2005). From decanoate Micelles to decanoic acid/dodecylbenzenesulfonate vesicles. *Langmuir*, 21, 6210-6219.
- Namani, T., Ishikawa, T., Morigaki, K., and Walde, P. (2007). Vesicles from docosahexaenoic acid. *Colloids and Surfaces B: Biointerfaces*, 54, 118-123.
- Nguyen, S., Alund, S.J., Hiorth, M., Kjøniksen, A., and Smistad, G. (2011). Studies on pectin of liposomes for drug delivery. *Colloids and Surfaces B: Biointerfaces*, 88, 664-673.
- Nijenhuis, K.T. (1996). Carrageenan *Thermoreversible networks: viscoelastic properties and structure of gels*: Springer.

- Nishinari, K. (2009). Some thoughts on the definition of a gel. In M. Tiokita, and Nishinari, K. (Ed.), *Gels: Structures, Properties, and Functions: Fundamental and applications* (Vol. 136, pp. 87-94). German: Springer-Verlag Berlin Heidelberg.
- Nishinari, K., Zhang, H., and Ikeda, S. (2000). Hydrocolloid gels of polysaccharides and proteins. *Current Opinion in Colloid and Interface Science*, 5, 195-201.
- Norton, I.T. and Goodall, D.M. (1983). Dynamics of cation-induced conformational ordering in solutions of segmented iota carrageenan. *Journal of Chemical Society, Faraday Transactions I*, 79, 2501-2515.
- Norziah, M.H., Foo, S.L., and Karim, A.A. (2006). Rheological studies on mixtures of agar (*Gracilaria changii*) and κ -carrageenan. *Food Hydrocolloids*, 20, 204-217.
- Onesippe, C. and Lagerfe, S. (2008). Study of the complex formation between sodium dodecyl sulfate and hydrophobically modified chitosan. *Carbohydrate Polymers*, 74, 648-658.
- Osborne, J.L., Sanchez, I.C., and Paul, D.R. (2013). An asymptotic analysis of drug delivery from transdermal patches. *Journal of Membrane Science*, 442, 27-30.
- Oshima, Y., Nishino, K., Yonekura, Y., Kishimoto, S., and Wakabayashi, S. (1987). Clinical application of chitin non-woven fabric as wound dressing. *European Journal of Plastic Surgery*, 10, 66-69.
- Osswald, T. and Hernández-Ortiz, J.P. (2006). *Polymer processing: modelling and simulation*. Germany: Carl Hanser Verlag.
- Ovarlez, G., Rodts, S., Chateau, X., and Coussot, P. (2009). Phenomenology and physical origin of shear localization and shear banding in complex fluids. *Rheologica Acta*, 48, 831-844.

- Paleos, C.M., Sideratou, Z., and Tsiourvas, D. (1996). Mixed Vesicles of Didodecyldimethylammonium Bromide with Recognizable Moieties at the Interface. *Journal of Physical Chemistry*, 100, 13989-13900.
- Palmer, D., Levina, M., Nokhodchi, A., Douroumis, D., Farrellm, T., and Rajabi-Siahboomi, A. (2011). The influence of sodium carboxymethylcellulose on drug release from polyethylene oxide extended release matrices. *AAPS PharmSciTech*, 12, 862-871.
- Palte, M.J. and Raines, R.T. (2012). Interaction of nucleic acids with the glycocalyx *Journal of the American Chemical Society*, 134, 6218-6223.
- Parabaharan, M. (2008). Review paper: Chitosan derivatives as promising materials for controlled drug delivery. *Journal of Biomaterials Applications*, 23, 5-36.
- Park, S.I., Lee, E.O., Kim, J.W., Kim, Y.J., Han, S.H., and Kim, J.D. (2011). Polymer-hybridized liposomes anchored with alkyl grafted poly(asparagine). *Journal of Colloid and Interface Science*, 364, 31-38.
- Partlow, D.P. and Yoldas, B.E. (1981). Colloidal versus polymer gels and monolithic transformation in glass-forming systems. *Journal of Non-Crystalline Solids*, 46, 153-161.
- Peer, D., Karp, J.M., Hong, S., Farokhzad, O.C., Margalit, R., and Langer, R. (2007). Nanocarriers as an emerging platform for cancer therapy. *Nature Nanotechnology*, 2, 751-760.
- Pemetti, M., van Malssen, K.F., Flöter, E., and Bot, A. (2007). Structuring of edible oil by alternatives to crystalline fat. *Current Opinion in Colloid and Interface Science*, 12, 221-231.
- Peppas, N.A. and Huang, Y.B. (2002). Polymers and gels as molecular recognition agents. *Pharmaceutical Research*, 19, 578-587.

- Picout, D.R. and Ross-Murphy, S.B. (Ed.). (2002). *Thermoreversible and irreversible physical gels from biopolymers*. New York: Marcel Dekker, Inc.
- Pierre, M.B.R. and Costa, I.d.S. (2011). Liposomal systems as drug delivery vehicles for dermal and transdermal applications. *Archives of Dermatological Research*, 303, 607-621.
- Prakash, S., Malhotra, M., Shao, W., Tomaro-Duchesneau, C., and Abbasi, S. (2011). Polymeric nanohybrids and functionalized carbon nanotubes as drug delivery carriers for cancer therapy. *Advanced Drug Delivery Reviews*, 14-15, 1340-1351.
- Prego, C., Torres, D., and Alonso, M.J. (2005). The potential of chitosan for the oral administration of peptides. *Expert Opinion on Drug Delivery*, 2, 843-854.
- Qiu, Y. and Park, K. (2001). Environment-sensitive hydrogels for drug delivery. *Advanced Drug Delivery Reviews*, 53, 321-339.
- Qu, G.W., Wu, X.L., Yin, L.F., and Zhang, C. (2012). N-octyl-O-sulfate chitosan-modified liposomes for delivery of docetaxel: Preparation, characterization, and pharmacokinetics. *Biomadicine & Pharmacotherapy*, 66, 46-51.
- Ranjit, S. and Vyas, S.P. (1996). Topical liposomal system for localized and controlled drug delivery. *Journal of Dermatological Science*, 13, 107-111.
- Rauwendaal, C. (2001). *Polymer extrusion*. Germany: Carl Hanser Verlag.
- Renault, F., Sancey, B., Badot, P.-M., and Crini, G. (2009). Chitosan for coagulation/flocculation processes - An eco friendly, approach. *European Polymer Journal*, 45, 1337-1348.
- Rengal, R.G., Barišić, K., Pavelić, Ž., Grubišić, T.Ž., Čepelak, I., and Filipović-Grčić, J. (2002). High efficiency entrapment of superoxide dismutase into mucoadhesive chitosan-coated liposomes. *European Journal of Pharmaceutical Sciences*, 15, 441-448.

- Rescia, V.C., Takata, C.S., de Araujo, P.S., and da Costa, B.M.H. (2011). Dressing liposomal particles with chitosan and poly(vinyl alcohol) for oral vaccine delivery. *Journal of Liposome Research*, 21, 38-45.
- Rinaudo, M. (2006). Chitin and chitosan: Properties and applications. *Progress in Polymer Science*, 31, 603-632.
- Risbud, M.V. and Bhat, S.V. (2001). Properties of polyvinyl pyrrolidone/ β -chitosan hydrogel membranes and their biocompatibility evaluation by haemorheological method. *Journal of Materials Science: Materials in Medicine*, 12, 75-79.
- Rodríguez-Hernández, A.I. and Tecante, A. (1999). Dynamic viscoelastic behavior of gellan-i-carrageenan and gellan-xanthan gels. *Food Hydrocolloids*, 13, 59-64.
- Rogerson, M.L., Robinson, B.H., Bucak, S., and Walde, P. (2006). Kinetic studies of the interaction of fatty acids with phosphatidylcholine vesicles (liposomes). *Colloids and Surfaces B: Biointerfaces*, 48, 24-34.
- Roport, C. (1999). Liposomes as a gene delivery system. *Brazilian Journal of Medical and Biological Research* 32, 163-169.
- Russell, W.J., S. Lockhart, A., Bird, H., and Alexiou, C. (2009). A New Hemostatic Agent: Initial Life-Saving Experience With Celox (Chitosan) in Cardiothoracic Surgery. *The Annals of Thoracic Surgery*, 87(2), e13-e14.
- Saha, D. and Bhattacharya, S. (2010). Hydrocolloids as thickening and gelling agents in food: a critical review. *Journal of Food Science Technology*, 47, 587-597.
- Samad, A., Sultana, Y., and Aqil, M. (2007). Liposomal drug delivery systems: An update review. *Current Drug Delivery*, 4, 297-305.
- Samadder, A., Das, S., Das, J., and Khuda-Bukhs, A.R. (2013). Relative efficacies of insulin and poly (lactic-co-glycolic) acid encapsulated nano-insulin in modulating certain significant biomarkers in arsenic intoxicated L6 cells. *Colloids and Surfaces B: Biointerfaces*, 109, 10-19.

- Sato, T. and Sunamoto, J. (1992). Recent aspects in the use of liposomes in biotechnology and medicine. *Progress in Lipid Research*, 31, 345-372.
- Schramm, G. (2000). *A practical approach to rheology and rheometry*. Germany: Gebrueder HAAKE GmbH.
- Schrijvers, A.H.G.J., Frederik, P.M., Stuart, M.C.A., Burger, K.N.J., Heijnen, V.V.Th., Van Der Vusse, G.J., and Reneman, R.S. (1989). Formation of multilamellar vesicles by addition of Tannic acid to Phosphatidylcholine-containing small unilamellar vesicles. *The Journal of Histochemistry and Cytochemistry*, 37, 1635-1643.
- Sehgal, S. and Rogers, J.A. (1995). Polymer-coated liposomes: improved liposome stability and release of cytosine arabinoside (Ara-C). *Journal of Microencapsulation*, 12, 37-47.
- Shah, A.J. and Donovan, M.D. (2007). Rheological characterization of neutral and anionic polysaccharides with reduced mucociliary transport rates. *AAPS PharmSciTech*, 8, Article 32.
- Shailesh, S., Neelam, S., Sandeep, K., and Gupta, G.D. (2009). Liposome: A review. *Journal of Pharmacy Research*, 2, 1163-1167.
- Shende, P. and Gaud, R. (2009). Formulation and comparative characterization of chitosan, gelatin, and chitosan-gelatin-coated liposomes of CPT-11-HCl. *Drug development and Industrial Pharmacy*, 35, 612-618.
- Sheng, Y., Liu, C.S., Yuan, Y., Tao, X.Y., Yang, F., Shan, X.Q., Zhou, H.J., and Xu, F. (2009). Long-circulating polymeric nanoparticles bearing a combinatorial coating of PEG and water-soluble chitosan. *Biomaterials*, 30, 2340-2348.
- Sihorkar, V. and Vyas, S.P. (2001). Potential of polysaccharide anchored liposomes in drug delivery, targeting and immunization. *Journal of Pharmacy & Pharmaceutical Sciences*, 4, 138-158.

- Singh, A.V. (2011). Biopolymers in drug delivery: a review. *Pharmacologyonline*, 1, 666-674.
- Smith, A. and Hunneyball, L.M. (1986). Evaluation of poly(lactic acid) as biodegradable drug delivery system for parenteral administration. *International Journal of Pharmaceutics*, 30, 215-220.
- Sogias, I.A., Khutoryanskiy, V.V., and Williams, A.C. (2010). Exploring the factors affecting the solubility of chitosan in water. *Macromolecular Chemistry and Physics*, 211, 426-433.
- Sohm, R. and Tadros, Th. F. (1989). Viscoelastic properties of Sodium Montmorillonite (Gelwhite H) suspensions. *Journal of Colloid and Interface Science*, 132, 62-71.
- Sonia, T.A. and Sharma, C.P. (2011). Chitosan and its derivatives for drug delivery perspective. *Advances in Polymer Science*, 243, 23-54.
- Srokova, I., Talaba, P., Hodul, P., and Balazova, A. (1998). Emulsifying agents based on o-(carboxymethyl)cellulose. *Tenside, surfactants, detergents*, 35, 342-344.
- Steers, N.J., Peachman, K.K., McClain, S., Alving, C.R., and Rao, Mangala. (2009). Liposome-encapsulated HIV-1 Gag p24 containing lipid A induces effector CD4⁺ T-cells, memory CD8⁺ T-cells, and pro-inflammatory cytokines. *Vaccine*, 27, 6939-6949.
- Steffe, J.F. (1996). *Rheological methods in food process engineering*. USA: Freeman Press.
- Struik, L.C.E. (1987). The accuracy of some formulae for the interconversion of creep and stress-relaxation data. *Rheologica Acta*, 26, 7-13.
- Sunamoto, J. and Iwamoto, K. (1986). Protein anchored and polysaccharide-anchored liposomes as drug carriers. *Critical Reviews in Therapeutic Drug Carrier Systems*, 2, 117-136.

- Sunamoto, J., Sato, T., Taguchi, T., and Hamazaki, H. (1992). Naturally occurring polysaccharide derivatives which behave as an artificial cell wall on an artificial cell liposome. *Macromoleculars*, 25, 5665-5670.
- Taguchi, K., Urata, Y., Anraku, M., Watanabe, H., Kadowaki, D., Sakai, H., Horinouchi, H., Kobayashi, K., Tsuchida, E., Maruyama, T., and Otagiri, M. (2009). Hemoglobin Vesicles, Polyethylene Glycol (PEG)ylated Liposomes Developed as a Red Blood Cell Substitute, Do Not Induce the Accelerated Blood Clearance Phenomenon in Mice. *Drug Metabolism and Disposition*, 37, 2197-2203.
- Takeuchi, H., Kojima, H., Yamamoto H, and Kawashima Y. (2000). Polymer coating of liposomes with a modified polyvinyl alcohol and their systemic circulation and RES uptake in rats. *Journal of Controlled Release*, 68, 195-205.
- Takeuchi, H., Kojima, H., Yamamoto, H., and Kawashima, Y. (2001a). Evaluation of circulation profiles of liposomes coated with hydrophilic polymers having different molecular weights in rats. *Journal of Controlled Release*, 75, 83-91.
- Takeuchi, H., Kojima, H., Yamamoto, H., and Kawashima, Y. (2001b). Passive targeting of Doxorubicin with polymer coated liposomes in tumor bearing rats. *Biological and Pharmaceutical Bulletin*, 24, 795-799.
- Takeuchi, H., Matsui, Y., Yamamoto, H., and Kawashima, Y. (2003). Mucoadhesive properties of carbopol or chitosan-coated liposomes and their effectiveness in the oral administration of calcitonin to rats. *Journal of Controlled Release*, 86, 235-242.
- Takeuchi, H., Yamamoto, H., Niwa, T., Hino, T., and Kawashima Y. (1994). Mucoadhesion of polymer-coated liposomes to rat intestine *in vitro*. *Chemical and Pharmaceutical Bulletin*, 42, 1954-1956.
- Takeuchi, H., Yamamoto, H., Niwa, T., Hino, T., and Kawashima, Y. (1996). Enteral absorption of insulin in rats from mucoadhesive chitosan-coated liposomes. *Pharmaceutical Research*, 13, 896-901.

- Tan, H.W. and Misran, M. (2011). Viscoelastic Behavior of Olive oil-in-water Emulsion Stabilized by Sucrose Fatty Acid Esters. *Applied Rheology*, 21, article no. 54599.
- Tan, L.P., Hidayat, A., Lao, L.L., and Quah, L.F. (2009). Release of hydrophilic drug from biodegradable polymer blends. *Journal of Biomaterials Science*, 20, 1381-1392.
- Tapadia, P., Ravindranath, S., and Wang, S.Q. (2006). Banding in entangled polymer fluids under oscillatory shearing. *Physical Review Letters*, 96, 196001.
- Temprana, C.F., Duarte, E.L., Taria, M.C., Lamy,T., and Alonso, S.del.V. (2010). Structural Characterization of Photopolymerizable Binary Liposomes Containing Diacetylenic and Saturated Phospholipids. *Langmuir*, 26, 10084-10092.
- Teng, Z., Luo, Y.C., and Wang, Q. (2013). Carboxymethyl chitosan–soy protein complex nanoparticles for the encapsulation and controlled release of vitamin D3. *Food Chemistry*, 141, 524-532.
- Teo, Y.Y. (2012). *Effect of 1,2-dipalmitoyl-sn-glycero-3-phosphoethanolamine (DPPE)-PEG2000 and 1,2-dipalmitoyl-sn-glycero-3-phosphoethanolamine (DPPE)-PEG5000 on fatty acid nanoliposomes and their Langmuir monolayer.* University of Malaya, Kuala Lumpur, Malaysia.
- Thongborisute, J., Tsuruta, A., Kawabata, Y., and Takeuchi, H. (2006). The effect of particle structure of chitosan-coated liposomes and type of chitosan on oral delivery of calcitonin. *Journal of Drug Targeting* 14, 147-154.
- Thrimawithana, T.R., Young, S., and Alany, R.G. (2011). Effect of cations on the microstructure and in-vivo drug release of κ - and ι - carrageenan liquid and semi-solid aqueous dispersions. *Journal of Pharmacy and Pharmacology*, 63, 11-18.

- Thrimawithana, T.R., Young, S., Dunstan, D.E., and Alany, R.G. (2010). Texture and rheological characterization of kappa and iota carrageenan in the presence of counter ions. *Carbohydrate Polymers*, 82, 69-77.
- Tischer, P.C.S.F., Nosedá, M.D., de Freitas, R.A., Sierakowski, M.S., and Duarte, M.E.R. (2006). Effects of iota-carrageenan on the rheological properties of starches. *Carbohydrate Polymers*, 65, 49-57.
- Tolaimate, A., Desbrières, J., Rhazi, M., Alagui, A., Vincendon, M., and Vettero, P. (2000). On the influence of deacetylation process on the physicochemical characteristics of chitosan from squid chitin. *Polymer*, 41, 2463-2469.
- Torchilin, V.P. (2005). Recent advances with liposomes as pharmaceutical carriers. *Nature Reviews Drug Discovery*, 4, 145-160.
- Toro-Vazquez, J.F., Morales-Rueda, J., Mallia, V.A., and Weiss, R.G. (2010). Relationship between molecular structure and thermo-mechanical properties of Candelilla wax and amides derived from (*R*)-12-hydroxystearic acid as gelators of Safflower oil. *Food Biophysics*, 5, 193-202.
- Touitou, E. and Godin, B. (2007). Vesicular carriers for enhanced delivery through the skin. In E. Touitou, and Barry, B.W. (Ed.), *Enhancement in drug delivery* (pp. 255-278). New York: CRC Press.
- Ueda, C.T., Shah, V.P., Derdzinski, K., Ewing, G., Flynn, G., Maibach, H., Marques, M., Rytting, H., Shaw, S., Thakker, K., and Yocobi, A. (2009). Topical and transdermal drug products. *Pharmaceutical Forum*, 35, 750-764.
- Ueno, T., Yokota, S., Kitaoka, T., and Wariishi, H. (2007). Conformational changes in single carboxymethylcellulose chains on a highly oriented pyrolytic graphite surface under different salt conditions. *Carbohydrate Research*, 342, 954-960.
- Üner, M. (2006). Preparation, characterization and physico-chemical properties of solid lipid nanoparticles (SLN) and nanostructured lipid carriers (NLC): their benefits as colloidal drug carrier systems. *Pharmazie*, 61, 375-386.

- van de Velde, F., Rollema, H.S., and Tromp, R.H. (2003). Coil-helix transition of γ -Carrageenan as a function of chain regularity: the effect of counterion valency. In E. Dickinson, and van Vliet, T. (Ed.), *Food colloids, biopolymers and materials* (pp. 256-264). UK: The Royal Society of Chemistry.
- van Kujik-Meuwissen, M.E., Junginger, H.E., and Bouwstra, J.A. (1998). Interactions between liposomes and human skin in vitro, a confocal laser scanning microscopy study. *Biochimica et Biophysica Acta*, 1371, 31-39.
- Vemuri, S. and Rhodes, C.T. (1995). Preparation and characterization of liposomes as therapeutic delivery system: a review. *Pharmaceutica Acta Helvetiae*, 70, 95-111.
- Verma, D.D., Verma, S., Blume, G., and Fahr, A. (2003). Particle size of liposomes influences dermal delivery of substances into skin. *International Journal of Pharmaceutics*, 258, 141-151.
- Vermette, P., Meagher, L., Gagnon, E., and Griesser, H.J. (2002). Immobilized liposome layers for drug delivery applications: inhibition of angiogenesis. *Journal of Controlled Release*, 80, 179-195.
- Veronese, F.M. and Pasut, G. (2005). PEGylation, successful approach to drug delivery. *Drug Discovery Today*, 10, 1451-1458.
- Vinood, K.R., Rohit, R.T., Sandhya, S., David, B., and Venkatram, R.B. (2012). Critical review on mucoadhesive drug delivery systems. *Hygeia Journal of Drugs & Medicines*, 4, 7-28.
- Wade, A. and Weller, P.J. (Ed.). (1994). *Handbook of Pharmaceutical Excipients* (2nd ed.). Wallingford Oxon, U.K.: The Pharmaceutical Press.

- Walde, P., Namani, T., Morigaki, K., and Häuse, H. (2007). Formation and properties of fatty acid vesicles (Liposomes). In G. Gregoriadis (Ed.), *Liposome Technology: Liposome preparation and related technique* (Vol. 1). New York: Informa Healthcare.
- Walde, P., Wick, R., Fresta, M., Mangone, A., and Luisi, P.L. (1994). Autopoietic self-reproduction of fatty acid vesicles. *Journal of the American Chemical Society*, 116, 11649-11654.
- Wang, Q. and Cui, S.W. (2005a). Understanding the conformation of polysaccharides. In S. W. Cui (Ed.), *Food carbohydrates: chemistry, physical properties, and applications* (pp. 432). USA: CRC press.
- Wang, Q. and Cui, S.W. (2005b). Understanding the physical properties of food polysaccharides. In S. W. Cui (Ed.), *Food carbohydrates: chemistry, physical properties, and applications* (pp. 432). USA: CRC press.
- Wang, Y.S., Tu, S.L., Li, R.S., Yang, X.Y., Liu, G., and Zhang, Q.Q. (2010). Cholesterol succinyl chitosan anchored liposomes: preparation, characterization, physical stability, and drug release behavior. *Nanomedicine: Nanotechnology, Biology, and Medicine*, 6, 471-477.
- Weiner, M.L. (1991). Toxicological properties of carrageenan. *Agents and Actions*, 32, 46-51.
- Werle, M., Hironaka, K., Takeuchi, H., and Hoyer, H. (2009). Development and in vitro characterization of liposomes coated with thiolated poly(acrylic acid) for oral drug delivery. *Drug Development and Industrial Pharmacy*, 35, 209-215.
- Westesen, K., Bunjes, H., and Koch, H.J. (1997). Physicochemical characterization of lipid nanoparticles and evaluation of their drug loading capacity and sustained release potential. *Journal of Controlled Release*, 48, 223-236.
- Williams, A.C. and Barry, B.W. (2004). Penetration enhancers. *Advanced Drug Delivery Reviews* 56, 603-618.

- Wokovich, A.M., Prodduturi, S., Doub, W.H., Hussain, A.S., and Buhse, L.F. (2006). Transdermal drug delivery system (TDDS) adhesion as a critical safety, efficacy and quality attribute. *European journal of Pharmaceutics and Biopharmaceutics*, 64, 1-8.
- Woodle, M.C. and Lasic, D.D. (1992). Sterically stabilized liposomes. *Biochimica et Biophysica Acta*, 1113, 171-199.
- Xi, H.L., Yang, Y.G., Zhao, D.M., Fang, L., Sun, L., Mu, L.W., Liu, J., Zhao, N.X., Zhao, Y.Y., Zheng, N., and He, Z.G. (2013). Transdermal patches for site-specific delivery of anastrozole: In vitro and local tissue disposition evaluation. *International Journal of Pharmaceutics*, 391, 73-78.
- Xu, J., McCarthy, S.P., and Gross, R.A. (1996). Chitosan film acylation and effects on biodegradability *Macromolecules*, 29, 3436-3440.
- Yang, D.D., Wei, K.W., Liu, Q., Yang, Y., Guo, X., Rong, H.R., Cheng, M.L., and Wang, G.X. (2013). Folic acid-functionalized magnetic ZnFe₂O₄ hollow microsphere core/mesoporous silica shell composite particles: Synthesis and application in drug release. *Materials Science and Engineering: C*, 33, 2879-2884.
- You, J., Wang, Z.H., Du, Y.Z., Yuan, H., Zhang, P.Z., Zhou, J.L., Liu, F., Li, C., and Hu, F.Q. (2013). Specific tumor delivery of paclitaxel using glycolipid-like polymer micelles containing gold nanospheres. *Biomaterials*, 34, 4510-4519.
- Yuan, Z.H., Cheng, D.W., Zhang, S.T., and Zheng, Z.D. (2010). Preparation, characterization and evaluation of docetaxel-loaded, folate-conjugated PEG-liposomes. *Yakugaku Zasshi*, 130, 1353-1359.
- Yuguchi, Y., Thuy, T.T.T., Urakawa, H., and Kajiwarra, K. (2002). Structural characteristics of carrageenan gels: temperature and concentration dependence *Food Hydrocolloids*, 16, 515-522.

- Yuguchi, Y., Urakawa, H., and Kajiwara, K. (2003). Structural characteristics of carrageenan gels: various types of counter ions. *Food Hydrocolloids*, 17, 481-485.
- Zamiri, C. and Gemeinhart, R.A. (2006). Pulmonary drug delivery systems for biomacromolecules. In G. M.J. (Ed.), *Pharmaceutical biotechnology* (pp. 259-281). New York: CRC Press.
- Zaru, M., Manca, M.L., Fadda, A.M., and Antimisiaris, S.G. (2009). Chitosan-coated liposomes for delivery to lungs by nebulisation. *Colloids and Surfaces B: Biointerfaces*, 71, 88-95.
- Zeng, X.W., Tao, W., Mei, L., Huang, L.Q., Tan, C.Y., and Feng, S.S. (2013). Cholic acid-functionalized nanoparticles of star-shaped PLGA-vitamin E TPGS copolymer for docetaxel delivery to cervical cancer. *Biomaterials*, 34, 6058-6067.
- Zhang, J.X. and Ma, P.X. (2013). Cyclodextrin-based supramolecular systems for drug delivery: Recent progress and future perspective. *Advanced Drug Delivery Reviews*, *In press*.
- Zhang, L.J., D'Acunzi, M., Kappl, M., Anuernhammer, G.K., Vollmer, D., van Kats, C.M., and van Blaaderen, A. (2009). Hollow silica spheres: synthesis and mechanical properties. *Langmuir*, 25, 2711-2717.
- Zhang, Y.Q., Xue, C.H., Li, Z.J., Zhang, Y.N., and Fu, X.Y. (2006). Preparation of half-deacetylated chitosan by forced penetration and its properties. *Carbohydrate Polymers*, 65, 229-234.
- Zhao, H.Y., Brown, P.H., and Schuck, P. (2011). On the distribution of protein refractive index increments. *Biophysical Journal*, 100, 2309-2317.
- Zhong, H., Deng, Y., Wang, X., and Yang, B. (2005). Multivesicular liposome formulation for the sustained delivery of breviscapine. *International Journal of Pharmaceutics*, 301, 15-24.

Zhong, Q. and Jin, M. (2009). Zein nanoparticles produced by liquid-liquid dispersion. *Food Hydrocolloids*, 23, 2380-2387.

Zhu, Y.F., Meng, W.J., and Hanagata, N. (2011). Cytosine-phosphodiester-guanine oligodeoxynucleotide (CpG ODN)-capped hollow mesoporous silica particles for enzyme-triggered drug delivery. *Dalton Transactions*, 40, 10203-10208.

APPENDIX

RESEARCH ARTICLE

Characterization of fatty acid liposome coated with low-molecular-weight chitosan

Hsiao Wei Tan and Misni Misran

Department of Chemistry, Faculty of Science, University of Malaya, Kuala Lumpur, Malaysia

Abstract

Preparation of chitosan-coated fatty acid liposomes is often restricted by the solubility of chitosan under basic conditions. In this experiment, the preparation of chitosan-coated oleic acid (OA) liposomes using low molecular weight (LMW) chitosan (10 and 25 kDa) was demonstrated. These selected LMW chitosans are water soluble. The coating of the chitosan layer on OA liposomes was confirmed by its microscope images and physicochemical properties, such as zeta potential and the size of the liposomes. The “peeling off” effect on the surface of chitosan-coated OA liposomes was observed in the atomic force microscope images and showed the occurrence of the chitosan layer on the surface of OA liposomes. The size of the chitosan-coated liposomes was at least 20 nm smaller than the OA liposomes, and the increase of zeta potential with the increasing amount of LMW chitosan further confirmed the presence of the surface modification of OA liposomes.

Keywords: Oleic acid vesicle, surface tension, atomic force microscope, drug delivery

Introduction

Over the past few decades, focus has been given to drug targeting in pharmaceutical industries to prevent the usage of excessive drugs during medication to reduce the toxicity and side effects caused by undesired drug localization (Yuan et al., 2010). Currently, liposomes have drawn much attention in the pharmaceutical industry as a drug delivery vehicle. The ability of the liposome to encapsulate and protect active drugs enabled it to deliver drugs to the desired disease sites. Commercially available liposome and liposome-like pharmaceutical products, such as DOXIL, have been developed and successfully applied for the delivery of anticancer drug, such as doxorubicin, for the treatment of breast cancer (Torchilin, 2005). However, researches have revealed that conventional liposome hardly survive in the bloodstream because it can be easily detected and destroyed by the immune system. This disadvantage has limited the application of conventional liposome as a drug carrier (Immordino et al., 2006). Consequently, PEGylated liposomes with longer circulation times (He et al., 2010) have been developed to overcome this

problem. PEG (polyethylene glycol) is a synthetic, nontoxic polymer that has been used to modify the surface of the liposome for the enhancement of liposome stability in the bloodstream (Chonn and Cullis, 1998; Taguchi et al., 2009). Again, studies have revealed that repeated injections of the PEGylated liposome can induce the accelerated blood clearance phenomenon and reduce the bioavailability of the PEGylated liposome (Laverman et al., 2001; Ishida et al., 2005). Therefore, various polymers, especially polysaccharides, have been used to replace PEG (Mobed and Chang, 1998; Filipovicâ-Grciicâ et al., 2001; Thongborisute et al., 2006). Among polysaccharides, chitosan has been the most widely used coating material for liposomes because of its biocompatibility, biodegradability, nontoxicity, bioadhesivity (Adamo and Isabella, 2003; Aranaz et al., 2010), and mucoadhesive properties (Karn et al., 2011). Takeuchi et al. (1996, 2003) reported that chitosan-coated liposomes were able to prolong the pharmacokinetic effect of peptides (e.g., insulin) as a result of the mucoadhesion of the liposome to the intestinal tract. Chitosan can also increase the stability and prolong the blood-circulation time of the

Address for Correspondence: Hsiao Wei Tan, Department of Chemistry, Faculty of Science, University of Malaya, 50603 Kuala Lumpur, Malaysia. Fax: +603-79674193. E-mail: weith83@gmail.com

(Received 04 January 2012; revised 30 April 2012; accepted 02 June 2012)

liposome as well as decrease the leakage of encapsulated drugs (Garg et al., 2007; Dong and Rogers, 1991; Wang et al., 2010).

So far, research on chitosan-coated liposomes has been largely focused on phospholipid-based liposomes (Zaru et al., 2009; Li et al., 2009; Abdelbary, 2011), and chitosan-coated nonphospholipid liposomes have not been reported on. There has been continuous interest in developing the nonphospholipid liposome because of the instability of phospholipids, their reactivity in the biological environment, and the relatively higher cost associated with phospholipid preparation (Bastiat et al., 2007). Nonphospholipid materials, especially oleic acid (OA), are self-assembled into closed bilayers to form liposomes in an aqueous solution at basic conditions (pH 9) (Morigaki et al., 2003). The application of chitosan in the preparation of chitosan-coated nonphospholipid liposomes, such as chitosan-coated OA liposomes, is restricted because of the poor solubility of chitosan in water under basic conditions. Therefore, the main aim of this study was to prepare chitosan-coated nonphospholipid liposomes using low molecular weight LMW chitosan (10–25 kDa), and the OA liposome was selected as a model for nonphospholipid liposomes. The selected LMW chitosan is well soluble in water under neutral and basic conditions. The coating of LMW chitosan on the surface of the OA liposome was confirmed by its microscope images and physicochemical properties, such as zeta potential and the size of the liposome.

Methods

Method and materials

All solutions and samples were prepared by using deionized water (with the resistivity of 18.2 Ω/cm) from a Barnstead Diamond Nanopure Water Purification unit coupled with a Barnstead Diamond™ reverse osmosis RO unit (Barnstead International, Dubuque, Iowa, USA). Gas-chromatography-grade OA (99%) and acetic acid (99%) were purchased from Sigma-Aldrich (St. Louis, Missouri, USA). Boric acid, hydrochloric acid, and acetone were obtained from Merck KGaA (Darmstadt, Germany). Sodium hydroxide and sodium nitrite were purchased from Fluka AG (Buchs, Switzerland). Chitosan, with an average molecular weight of 150 kDa, was obtained from Acros Organics (Fair Lawn, New Jersey, USA) and used as received.

Sample preparation

Preparation of LMW chitosan

For this experiment, two types of chitosans (Ch1 and Ch2) with different molecular weights (MWs) were prepared. Depolymerization of chitosan was started by preparing a 1% (w/v) chitosan solution in 1% acetic acid solution. Next, 10 mL of sodium nitrite solution (0.10 M) was then added dropwise into the chitosan solution under magnetic stirring at room temperature (25°C) for 1 hour. Then, the pH of the solution was adjusted to pH 8–9 with 1 M of sodium

hydroxide solution. The reaction mixture containing Ch1 was then neutralized with 1 M of hydrochloric acid solution. Ch1 was then precipitated using acetone and collected using centrifugation. With a similar method, Ch2 was prepared by using 7 mL of 0.10 M sodium nitrite solution.

Preparation of chitosan-coated OA liposomes

First, 30 mM of OA liposome solution was prepared by dissolving an appropriate amount of OA using 50 mM of borate buffer (pH 8.8). Ch1 and Ch2 solutions, with concentration ranging from 0.04 to 0.30% (w/v), were prepared by dissolving an appropriate amount of Ch1 and Ch2 into 50 mM of borate buffer. pH levels of both OA liposome and Ch1 or Ch2 solutions were adjusted to 7 before mixing. Then, the liposome solution was added dropwise into Ch1 and Ch2 solutions under magnetic stirring to produce OACH1 and OACH2 solution, respectively. OACH1 and OACH2 were stirred for 24 hours at room temperature. Then, pH levels of OACH1 and OACH2 were adjusted to 8.8 for the formation of chitosan-coated liposomes. These liposome solutions were incubated at 25°C for 24 hours before analysis.

Characterization of liposomes and liposome solutions

Average MW determination

Average MWs of Ch1 and Ch2 were determined by the dynamic light scattering method using a Malvern NanoSeries ZetaSizer (Malvern Instruments Ltd., Malvern, UK).

Estimation of chitosan solubility

Water solubility of Ch1 and Ch2 was determined by the turbidity method (Li et al., 2006). Briefly, 0.10% of Ch1 and Ch2 were dissolved separately into deionized water and 50 mM of borate buffer (pH 8.8). Then, the transmittance of these solutions was recorded using a Cary 50 Conc UV-Vis spectrophotometer (Varian, Melbourne, Victoria, Australia) with a quartz cell with an optical path length of 1 cm at 600 nm. The above-described method was repeated by changing the concentration of Ch1 and Ch2.

Size and zeta potential

Size and zeta potential of OA, OACH1, and OACH2 liposomes were measured using a Malvern NanoSeries ZetaSizer (Malvern Instruments) at a constant temperature of 25°C. Size and zeta potential of prepared liposomes were over 30 days of storage time.

Optical polarizing microscope (OPM) imaging

OPM images of OA, OACH1, and OACH2 liposomes were captured using a Leica Polarizing Microscope equipped with Leica QWin software (Leica Microsystems, Buffalo Grove, Illinois, USA). All measurements were performed at the temperature of 25°C.

Transmission Electron Microscope (TEM) imaging

An EFTEM model LIBRA 120 (Carl Zeiss Microscopy GmbH, Oberkochen, Germany) equipped with an Olympus SIS-iTEM (ver. 5) was employed to analyze the

image of the prepared liposomes. A drop of liposome solution was placed onto a copper-coated carbon grid, followed by the removal of excess dispersed medium using a filter paper. Then, a drop of negative staining reagent (1% of phosphotungstic acid in 50 mM of borate buffer solution; pH 8.8) was added and the sample was air-dried at room temperature for 25 minutes. The sample was then examined under a TEM.

Atomic force microscope (AFM) imaging

AFM imaging of liposomes was captured by using an AFM Nanoscope III (Model MMAFM-2; Digital Instruments,

Tonawanda, New York, USA). All imaging was performed by tapping mode with an integrated pyramidal tips aluminium cantilever (BS Multi75Al; NanoAndMore GmbH, Wetzlar, Germany) (Vermette et al., 2002). Samples were prepared by placing a drop of the liposome solutions onto a freshly cleaved mica surface. The dispersing medium was removed by air drying (Paleos et al., 1996).

Surface tension

The rigidity of the vesicle was investigated by studying the effect of Ch1 and Ch2 on the critical vesicular concentration (CVC) of liposome solutions. Surface tension

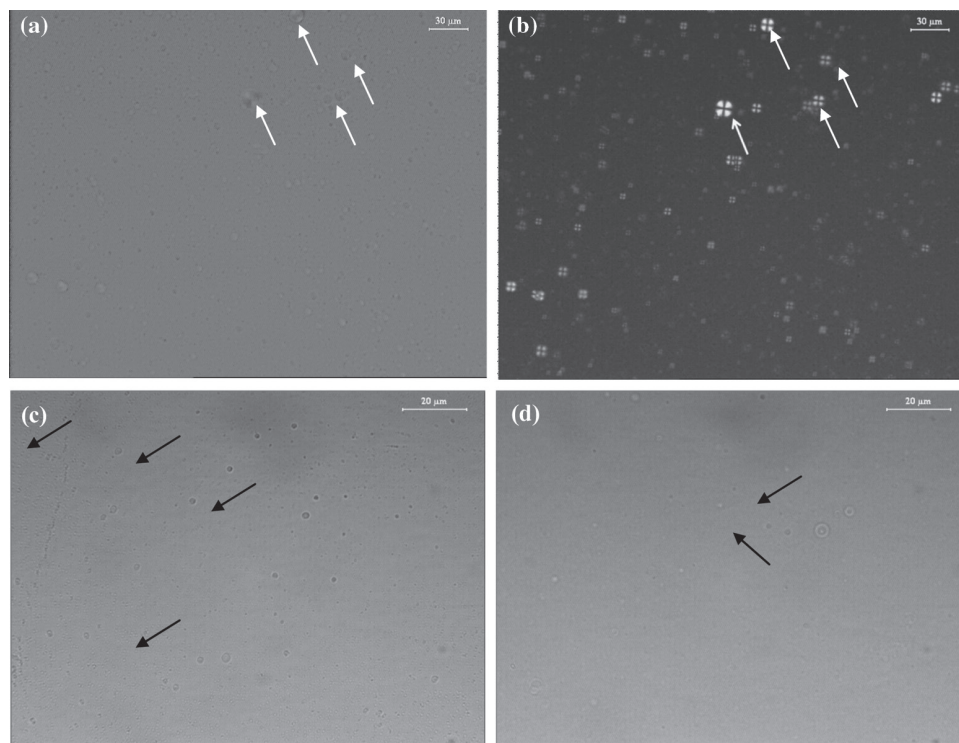


Figure 1. Image of liposomes obtained using OPM. (a) Birefringence effect of OA liposome, (b) maltase cross structure of OA liposome under dark field, (c) the OACH1 liposome (0.20% of Ch1), and (d) the OACH2 liposome (0.20% of Ch2).

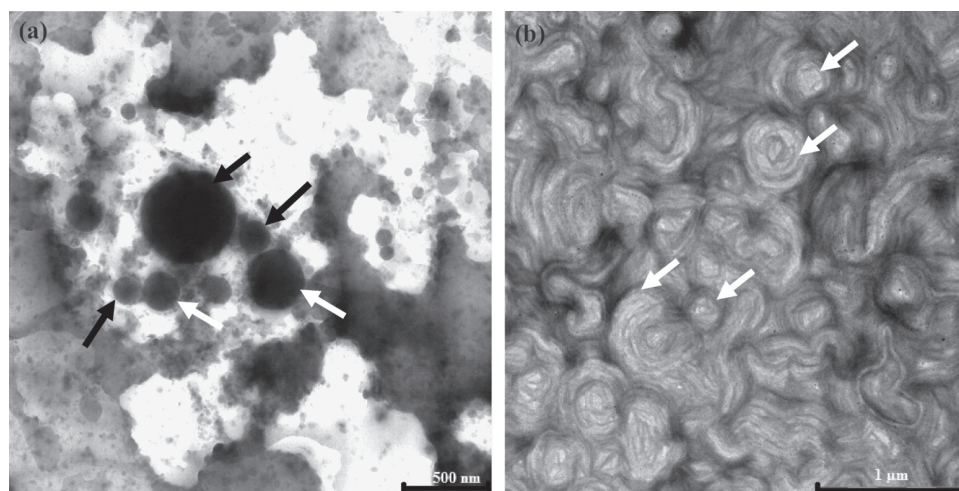


Figure 2. TEM image of (a) OACH2 liposome and (b) OA liposome. The amount of chitosan used in the preparation of the OACH2 liposome was 0.20%.

of a series of OA, OACH1, and OACH2 liposome solutions with different concentrations were determined by the du Noüy ring method using a Krüss Tensiometer (Model K100; Krüss, Hamburg, Germany) at 25°C. OA, OACH1, and OACH2 liposome solutions were diluted using 50 mM of borate buffer (pH 8.8) and were incubated at 25°C overnight before measurement. Surface tension of the prepared solution was determined using 20 successive measurements, and the standard deviation was calculated.

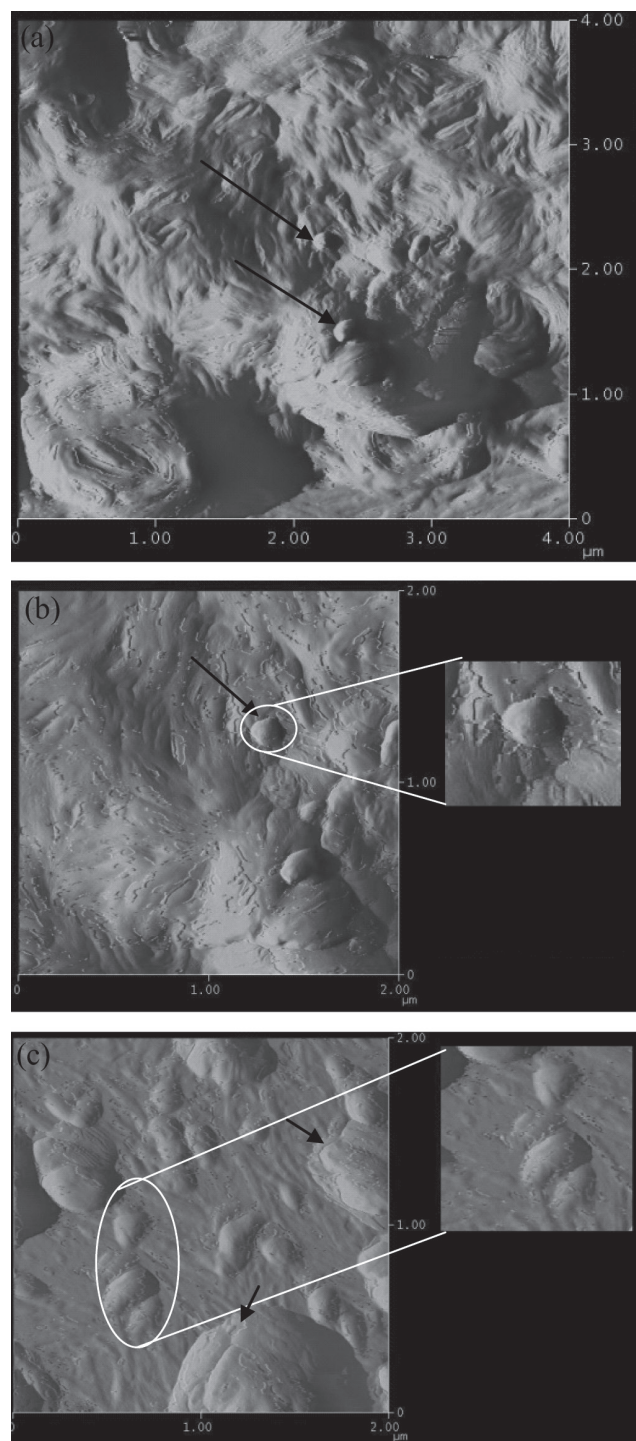


Figure 3. AFM image of (a) OA liposome, (b) magnified OA liposome, and (c) OACH2 (0.20% Ch2). Liposomes were indicated by black arrows.

Results and discussion

Characterization of LMW chitosan (Ch1 and Ch2)

The average MW of Ch1 and Ch2 was 10 and 25 kDa, respectively, and Ch1 and Ch2 have been found to be soluble in deionized water and borate buffer (pH 9).

Appearance of chitosan-coated liposomes

Ch1- and Ch2-coated OA liposomes were prepared and labeled as OACH1 and OACH2, respectively. The appearance of OACH1 and OACH2 was evaluated using an OPM, a TEM, and AFM. According to the micrographs obtained from the OPM, all liposomes (OA, OACH1, and OACH2) showed a spherical morphology (Figure 1). Compared with the OA liposome, OACH1 and OACH2 liposomes do not exhibit any birefringence effect (Figure 1C and 1D) and Maltese cross at dark field.

The TEM image clearly shows that the chitosan-coated OA liposome was spherical in shape (Figure 2A). The presence of the chitosan layer on the lipid layer of the OA liposome thickened the lipid layer and increased the opacity, thus the surface of the chitosan-coated OA liposome appears to be black in color (Wang et al., 2010).

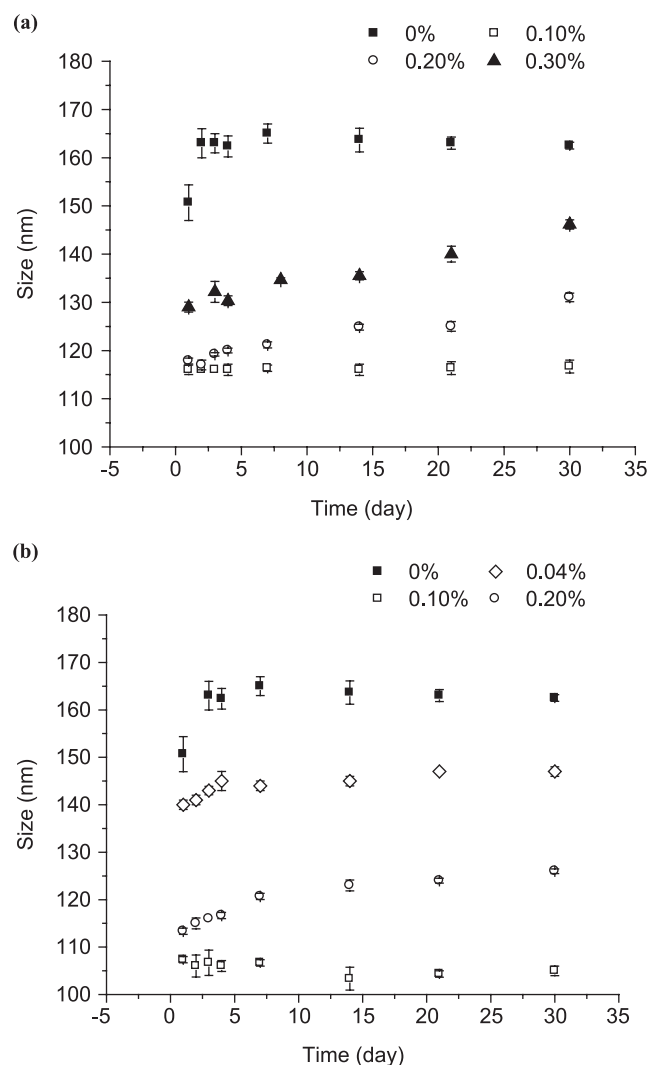


Figure 4. Variation of the size of (a) OACH1 and (b) OACH2 liposomes.

However, the OA liposome was not observed under the TEM. The structure of the OA liposome was found to collapse under the TEM (Figure 2B). The collapse of the structure of the OA liposome might be the result of the drying process or vacuum condition and indicates less rigidity of the OA liposome bilayer. This result also indicated that the chitosan modification of the OA liposome has enhanced the stability and bilayer rigidity of OA liposomes. For the AFM image, compared with the chitosan-coated OA liposome, the OA liposomes were hardly seen (Figure 3A and 3B). This result further indicated that the structure of the OA liposome was damaged as a result of the dry condition, because a vacuum is not required for AFM imaging. By comparison with the OA liposome, the chitosan-coated liposome showed a “peeling off” effect on the surface. This result showed that Ch1 and Ch2 have been coated on the surface of the OA liposome.

In terms of stability of the prepared liposomes, there was no flocculation observed throughout the 30 days of storage time, except for the OACH2 liposome solution that contained 0.30% of Ch2. A white precipitate was observed in the OACH2 liposome solution after 3 days of storage time. It was suggested that the presence of excess Ch2 has promoted the coagulation process of liposomes. Therefore, the size and zeta potential analysis of the OACH2 liposome are not presented.

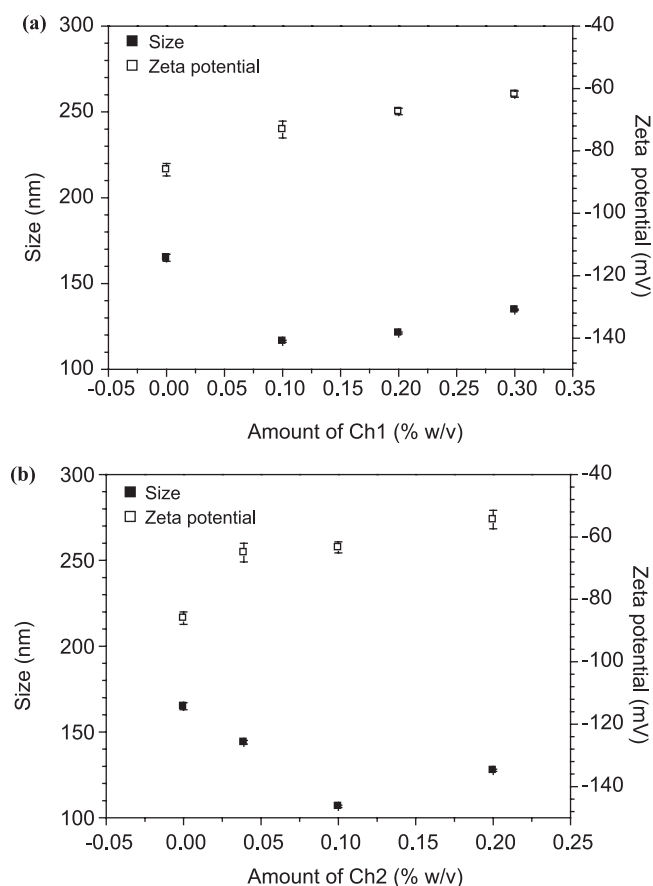


Figure 5. Effect of the amount of (a) Ch1 and (b) Ch2 chitosan on the size and zeta potential of the OA liposome. The reading plotted was taken at 7 days after liposome solutions were prepared.

Liposome size and zeta potential

The size of the OACH1 and OACH2 liposomes was found to be at least 20 nm smaller than that of the OA liposome (Figure 4). It was the result of the chitosan that formed a cage-like steric barrier that protected the liposome from aggregation and also prevented the uptake of the OA monomer from the bulk (Morigaki and Wald, 2007). As an OA liposome, the size of OACH1 and OACH2 was also found to increase slowly for the first 7 days of storage time, and this result has been attributed to the chitosan-coating process that happens on the surface of liposomes (Li et al., 2009). The size of OACH1 was increased from 115 to 130 nm when the amount of Ch1 increased from 0.10 (w/v) to 0.30% (w/v), whereas the size of the OACH2 increased from 105 to 125 nm when the amount of Ch2 increased from 0.10 (w/v) to 0.20% (w/v). This result indicated the formation of more chitosan layers on the surface of the liposome (Figure 5) (Guo et al., 2003). A similar result was also reported in the characterization of chitosan-coated phospholipid liposomes (Li et al., 2009; Liu and Park, 2010; Mady et al., 2009). For OACH2 liposomes, the size of liposomes was found to decrease from 140 to 100 nm when the amount of Ch2 increased from 0.04 (w/v) to 0.10% (w/v). This result indicated that 0.04% of Ch2 was not sufficient to create an adequate protection layer on the surface of the liposomes, as compared with the OACH2 liposome coated with 0.10 and 0.20% of Ch2 (Li et al., 2009).

The surface modification of the OA liposome by Ch1 and Ch2 was also evaluated by comparing its zeta potential before and after coating (Takeuchi et al., 2003). The zeta potential of OA was negatively charged. The zeta potential increased from -86.0 to -61.8 and -54.4 mV with the increasing amount of Ch1 and Ch2 coating, respectively (Figure 6). This result was attributed to the formation of a condensed coating of the Ch1 and Ch2 layers, which carried the positive charge, on the surface of the liposomes (Li et al., 2009; Liu and Park, 2010; Mady et al., 2009). Among the chitosan-coated liposomes, the zeta potential of the OACH2 liposome was smaller, compared

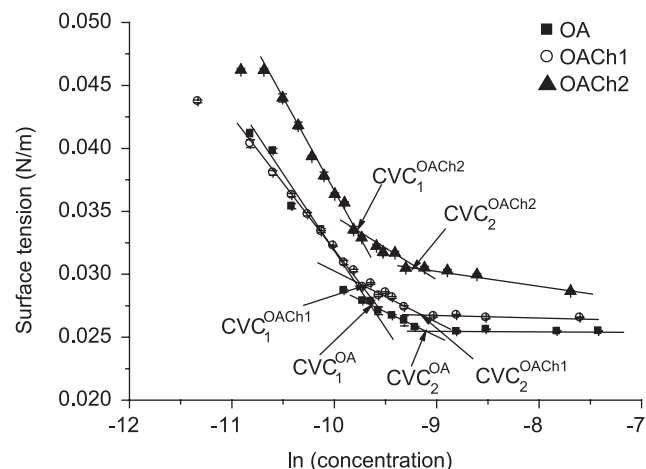


Figure 6. Surface tensions profile of the OA, OACH1 (0.20% of Ch1), and OACH2 (0.20% of Ch2) liposome solutions.

with the OACH1 liposome, thus suggesting that the longer chain length of Ch2 effectively shielded the surface of the liposome.

Surface tension

A surface tension (γ) versus $\ln(\text{OA})$ was plotted for the determination of the CVC of the liposome (Leclercq et al., 2009). All the plots exhibited two break points and indicated two CVC values (Figure 6). To investigate the formation of the two CVC values, the size of the liposome for the solution with the concentration greater than CVC_1 and CVC_2 was evaluated (Figure 7). By using the OA liposome solution as an example, the OA liposome was formed after CVC_1 (71.6 μM). The size of the OA liposome was found to decrease from 620 to 161 nm when the concentration of OA increased from CVC_1 to CVC_2 (100 μM). The decrease of the size of the OA liposome was also accompanied with a decreasing γ of the OA liposome solution. After CVC_2 , there were no significant changes in the γ of the OA liposome solution and also the size of the OA liposome. Therefore, it was suggested that the rearrangement of the OA liposome into a smaller size led to the formation of CVC_2 .

The CVC_1 of the OACH1 and OACH2 liposomes were significantly lower, compared with the OA liposome. However, there was no significant difference in CVC_2 . To explain this result, the minimum surface area occupied by the OA at the air/water interface (A_{\min}) and the surface excess concentration (Γ_{\max}) were calculated. Because the liposome started forming at CVC_1 , A_{\min} and Γ_{\max} were

obtained using the first slope before CVC_1 . A_{\min} values were determined using Gibbs' adsorption isotherm, as described by Equation 1:

$$A_{\min} = \frac{1}{N_A \cdot \Gamma_{\max}} \quad (1)$$

where N_A is Avogadro's number. The Γ_{\max} was calculated using Gibbs' adsorption equation as shown in Equation 2:

$$\Gamma_{\max} = \left(\frac{1}{nRT} \right) \left(\frac{d\gamma}{d \ln C} \right) \quad (2)$$

where n is the number of molecular species involved, and C is the concentration of OA. Liposome solutions were prepared at pH 9, where the OA was partially ionized; therefore, n is equal to 2 was used in the calculation of Γ_{\max} .

The A_{\min} value obtained from the OA liposome solution was lower than that of OACH1 and OACH2 (Table 1). This result suggested that the OA monomers in the OA liposome solution were more closely packed at the air/water interface, compared with the OACH1 and OACH2 liposome solutions (Ghosh et al., 2010). This result shows that Ch1 and Ch2 that were adsorbed on the surface of the OA monolayer had disturbed the packing of the OA molecules and decreased the number of adsorbed OA monomers at the air/water interface, thus resulting in the increase of A_{\min} as well as γ (Figure 7). The effect of the amount of Ch1 and Ch2 used to prepare OACH1 and OACH2 liposomes on the γ was negligible.

Conclusion

This study demonstrated the preparation of chitosan-coated nonphospholipid liposomes, where basic conditions are required. The OA liposome was selected as a model for this study. The result indicated that the depolymerized water-soluble chitosan was successfully coated on the surface of the OA liposomes. Modification of water-soluble chitosan on the surface of the OA liposome also improved the stability and rigidity of liposomes. A different combination of liposomes and water-soluble chitosan may produce liposomes with specific size and surface charge.

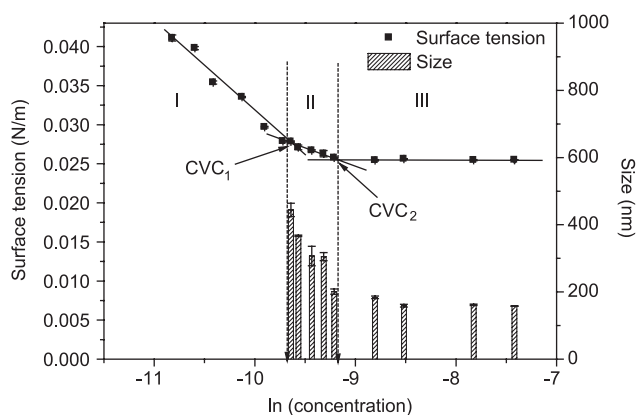


Figure 7. Liposome size and surface tension of the OA liposomes.

Table 1. Γ_{\max} , A_{\min} , and γ at CVC of OA, OACH1, and OACH2 liposome solutions at constant temperature of 25°C.

Sample name	Amount of chitosan (% w/v)		Surface excess concentration, $\Gamma_{\max} \times 10^{-6}$ (molm ⁻²)	Minimum surface area per head group, A_{\min} (Å ²)	Critical vesicular concentration, CVC (μM)		Surface tension at CVC, γ (mNm ⁻¹)	
	Ch1	Ch2			CVC ₁	CVC ₂	CVC ₁	CVC ₂
OA	—	—	3.03	54.9	71.6	100.0	28.3	25.6
OACH1	0.10	—	2.02	80.2	58.3	105	29.5	26.8
	0.20	—	2.32	71.6	53.1	101	30.9	27.2
	0.30	—	2.50	66.6	45.4	107	31.3	27.8
	—	0.04	2.61	63.5	61.3	102	30.6	28.9
OACH2	—	0.10	2.70	61.1	56.0	94.2	33.5	30.7
	—	0.20	2.50	65.7	54.9	108	31.6	30.2

Declaration of interest

The authors extend their gratitude to the University of Malaya and the Ministry of Higher Education Malaysia for providing us financial support (PPP, no. PS437/2010A; FRGS, no. FP017/2010A).

References

- Abdelbary, G. (2011). Ocular ciprofloxacin hydrochloride mucoadhesive chitosan-coated liposomes. *Pharmaceut Dev Technol* 16:44–56.
- Adamo, F., Isabella, O. (2003). The role of chitosan in drug delivery: current and potential applications. *Am J Drug Deliv* 1:43–59.
- Aranaz, I., Harris, R., Heras, A. (2010). Chitosan amphiphilic derivatives. Chemistry and applications. *Curr Org Chem* 14:308–330.
- Bastiat, G., Oliger, P., Karlsson, G., Edwards, K., Lafleur, M. (2007). Development of non-phospholipid liposomes containing a high cholesterol concentration. *Langmuir* 23:7695–7699.
- Chonn, A., Cullis, P. R. (1998). Recent advances in liposome technologies and their applications for systemic gene delivery. *Adv Drug Deliv Rev* 30:73–83.
- Dong, C., Rogers, J. A. (1991). Polymer-coated liposomes: stability and release of ASA from carboxymethyl chitin-coated liposomes. *J Control Release* 17:217–224.
- Filipović-Grić, J., Škalco-Basnet, N., Jalšenjak, I. (2001). Mucoadhesive chitosan-coated liposomes: characteristics and stability. *J Microencapsul* 18:3–12.
- Garg, M., Dutta, T., Jain, N. K. (2007). Stability study of stavadin-loaded O-palmitoyl-anchored carbohydrate-coated liposomes. *AAPS PharmSciTech* 8:E86–E93.
- Ghosh, A., Shrivastava, S., Dey, J. (2010). Concentration and pH-dependent aggregation behavior of an L-histidine based amphiphile in aqueous solution. *Chem Phys Lipids* 163:561–568.
- Guo, J., Pin, Q., Jiang, G., Huang, L., Tong, Y. (2003). Chitosan-coated liposomes: characterization and interaction with leuprolide. *Int J Pharmaceut* 260:167–173.
- He, S. J., Zhu, J. B., Xie, F. M. (2010). Preparation and characterization of tramadol EG-coated multivesicular liposomes for sustained release. *Pharmazie* 6:467–470.
- Immordino, M. L., Dosio, F., Cattel, L. (2006). Stealth liposomes: review of basic science, rationale, and clinical applications, existing and potential. *Int J Nanomed* 1:297–315.
- Ishida, T., Harada, M., Wang, X. Y., Ichihara, M., Irimura, K., Kiwada, H. (2005). Accelerated blood clearance of PEGylated liposomes following preceding liposome injection: effects of lipid dose and PEG surface-density and chain length of the first-dose liposomes. *J Control Release* 105:305–317.
- Karn, P. R., Vanić, Z., Pepić, I., Škalco-Basnet, N. (2011). Mucoadhesive liposomal delivery systems: the choice of coating material. *Drug Dev Ind Pharm* 37:482–488.
- Laverman, P., Carstens, M. G., Boerman, O. C., Dams, E. Th. M., Oyen, W. J. G., van Rooijen, N., et al. (2001). Factor affecting the accelerated blood clearance of polyethylene glycol-liposomes upon repeated injection. *J Pharmacol Exp Ther* 298:607–612.
- Leclercq, L., Nardello-Rataj, V., Turmine, M., Azaroual, N., Aubry, J. (2009). Stepwise aggregation of dimethyl-di-n-actylammonium chloride in aqueous solutions: from dimer to vesicles. *Langmuir* 26:1716–1723.
- Li, J., Du, Y., Liang, H. (2006). Low molecular weight water-soluble chitosan: preparation with the aid of cellulose, characterization, and solubility. *J Appl Polym Sci* 102:1098–1105.
- Li, N., Zhuang, C. Y., Wang, M., Sun, X. Y., Nie, S. F., Pan, W. S. (2009). Liposome coated with low molecular weight chitosan and its potential use in ocular drug delivery. *Int J Pharmaceut* 379:131–138.
- Liu, N., Park, H. J. (2010). Factors effect on the loading efficiency of vitamin C loaded chitosan-coated nanoliposomes. *Colloids Surf B Biointerfaces* 76:16–19.
- Mady, M. M., Darwish, M. M., Khalil, S., Khalil, W. M. (2009). Biophysical studies on chitosan-coated liposomes. *Eur Biophys J* 38:1127–1133.
- Mobed, M., Chang, T. M. S. (1998). Adsorption of chitin derivatives onto liposomes: optimization of adsorption conditions. *J Microencapsul* 15:595–607.
- Morigaki, K., Walde, P. (2007). Fatty acid vesicles. *Curr Opin Colloid Interface Sci* 12:75–80.
- Morigaki, K., Walde, P., Misran, M., Robinson, B. H. (2003). Thermodynamic and kinetic stability. Properties of micelles and vesicles formed by the decanoic acid/decanoate system. *Colloids Surf A: Physicochem Eng Aspects* 213:37–44.
- Paleos, C. M., Sideratou, Z., Tsiourvas, D. (1996). Mixed vesicles of didodecyltrimethylammonium bromide with recognizable moieties at the interface. *J Phys Chem* 100:13989–13990.
- Taguchi, K., Urata, Y., Anraku, M., Watanabe, H., Kadowaki, D., Sakai, H., et al. (2009). Hemoglobin vesicles, polyethylene glycol (PEG) ylated liposomes developed as a red blood cell substitute, do not induce the accelerated blood clearance phenomenon in mice. *Drug Metab Dispos* 37:2197–2203.
- Takeuchi, H., Matsui, Y., Yamamoto, H., Kawashima, Y. (2003). Mucoadhesive properties of carbopol or chitosan-coated liposomes and their effectiveness in the oral administration of calcitonin to rats. *J Control Release* 86:235–242.
- Takeuchi, H., Yamamoto, H., Niwa, T., Hino, T., Kawashima, Y. (1996). Enteral absorption of insulin in rats from mucoadhesive chitosan-coated liposomes. *Pharmaceut Res* 13:896–901.
- Thongborisute, J., Tsuruta, A., Kawabata, Y., Takeuchi, H. (2006). The effect of particle structure of chitosan-coated liposomes and type of chitosan on oral delivery of calcitonin. *J Drug Target* 14:147–154.
- Torchilin, V. P. (2005). Liposomes as pharmaceutical carriers. *Nat Rev Drug Discov* 4:145–160.
- Vermette, P., Meagher, L., Gagnon, E., Griesser, H. J. (2002). Immobilized liposome layers for drug delivery applications: inhibition of angiogenesis. *J Control Release* 80:179–195.
- Wang, Y. S., Tu, S. L., Li, R. S., Yang, X. Y., Liu, G., Zhang, Q. Q. (2010). Cholesterol succinyl chitosan anchored liposomes: preparation, characterization, physical stability, and drug release behavior. *Nanomed Nanotechnol Biol Med* 6:471–477.
- Yuan, Z., Cheng, D. W., Zhang, S. T., Zheng, Z. D. (2010). Preparation, characterization, and evaluation of docetaxel-loaded, folate-conjugated PEG-liposomes. *Yakugaku Zasshi* 130:1353–1359.
- Zaru, M., Manca, M. L., Fadda, A. M., Antimisiaris, S. G. (2009). Chitosan-coated liposomes for delivery to lungs by nebulisation. *Colloids Surf B Biointerfaces* 71:88–95.



Polysaccharide-anchored fatty acid liposome

Hsiao Wei Tan*, Misni Misran

Department of Chemistry, Faculty of Science, University of Malaya, 50603 Kuala Lumpur, Malaysia

ARTICLE INFO

Article history:

Received 7 September 2012
Received in revised form 14 October 2012
Accepted 9 November 2012
Available online 19 November 2012

Keywords:

Oleic acid vesicle
Surface tension
Atomic force microscope
Drug delivery
Chitosan

ABSTRACT

In this study, the preparation of *N*-palmitoyl chitosan (ChP) anchored oleic acid (OA) liposome was demonstrated. Two different types of water-soluble ChPs with different degrees of acylation (DA) were selected for this study. The presence of ChPs on the surface of OA liposome was confirmed with their micrographs and physicochemical properties. The “peeling off” effect on the surface of the ChP-anchored OA (OACHP) liposomes was observed on the atomic force microscope micrographs and confirmed the presence of the ChPs layer on the liposome surface. The surface tension of the OACHPs liposome solution was found to be higher than that of the OA liposome solution. This result indicated the removal of OA monomer by ChPs from the air–water interface. The increase in the minimum area per headgroup (A_{min}) of the OA with the presence of ChPs has further proved the interaction between OA monomer and the hydrophobic moieties of the ChPs. The ChPs anchored onto the OA monolayer increased the curvature of the OACHP liposomes monolayer and reduced the liposome size. The size of the OACHP liposomes was reduced by 30 nm as compared with the unmodified OA liposome. Results revealed that the anchored ChPs can improve the integrity and rigidity of the OA liposome.

© 2012 Elsevier B.V. All rights reserved.

1. Introduction

The surface of cells is rich in carbohydrate moieties that are attached to both membrane glycolipids and glycoproteins (Dicorleto and De La Motte, 1989). This carbohydrate-rich layer is known as glycocalyx (Palte and Raines, 2012). Glycocalyx contains a high amount of polysaccharide and is involved in cellular adhesion, intercellular communication, and biological recognition (Abeygunawardana and Bush, 1991; Sihorkar and Vyas, 2001). Therefore, the potential of polysaccharides to serve as ligand in the preparation of site-targeted liposomes has received wide attention (e.g. Mufamadi et al., 2011; Sihorkar and Vyas, 2001; Sunamoto et al., 1992). Among polysaccharides, the combination of chitosan with liposome has been a promising approach in the gene and drug delivery systems (e.g. Liu et al., 2011; Parabakaran, 2008; Riva et al., 2011; Zaru et al., 2009). Chitosan has been extensively used in the drug delivery system due to its biocompatibility, biodegradability, non-toxic nature, and cost effectiveness (e.g. Illum, 1998; Sheng et al., 2009). However, the use of chitosan in the biomedical field is often restricted by its poor solubility in water. Chitosan only dissolves in acidic condition (Chan et al., 2007). Previous studies have suggested that the solubility of chitosan in neutral and high pH condition can be improved by reducing its molecular weight (MW) (Illum, 1998; Kubota et al., 2000). The solubility of chitosan also

can be improved by introducing the hydrophobic moiety at the primary amino group of the chitosan through acylation (Illum, 1998; Lee et al., 2005; Mourya et al., 2010; Ortona et al., 2008). The presence of hydrophobic moieties at the backbone of the chitosan can destroy the crystalline structure of chitosan and improve the solubility of chitosan in aqueous solution (Ge et al., 2007; Wu et al., 2006).

The hydrophobized chitosan can integrate with the lipid bilayer membrane as well as be used to prepare polysaccharide-anchored liposomes. The coating of hydrophobized chitosan on the surface of the liposome can enhance the liposome stability, structural rigidity, and membrane integrity (Ge et al., 2007). The preparation of chitosan-coated liposome with hydrophobized chitosan has its advantage compared with the unmodified chitosan. The hydrophobic moieties of the hydrophobized chitosan such as the palmitoyl group can be anchored onto the monolayer (outer layer) of the liposome bilayer through hydrophobic interactions (Wang et al., 2010). This method can prevent the desorption of the coated hydrophobized chitosan from the surface of liposome during storage and transportation (Sunamoto and Iwamoto, 1986; Sihorkar and Vyas, 2001).

So far, research conducted on the hydrophobized chitosan-anchored liposomes has been largely focused on the phospholipid-based liposomes (e.g. Garg et al., 2007; Ge et al., 2007; Wang et al., 2010, 2012; Qu et al., 2012), and the study on non-phospholipid liposomes has not been reported. There is continuous interest in the development of the non-phospholipid liposomes due to the disadvantages of phospholipids, such as reactivity in the

* Corresponding author. Tel.: +60 3 79676776; fax: +60 3 79674193.
E-mail address: weith83@gmail.com (H.W. Tan).

biological milieu and high production cost (Gupta et al., 1996; Bastiat et al., 2007). Non-phospholipid liposomes can be prepared from several amphiphiles such as fatty acids (Bastiat et al., 2007) and the derivatives of polymers (Battaglia and Ryan, 2009; Discher and Eisenberg, 2002). In this study, the main objective is to prepare hydrophobized chitosan-anchored non-phospholipid liposomes using water-soluble *N*-palmitoyl chitosans (ChPs) with different DA. OA was selected as a model for non-phospholipid liposomes.

2. Methods and materials

2.1. Materials

All solutions and samples were prepared by using deionized water with a resistivity of 18.2 Ω /cm, from Barnstead Diamond Nanopure water Purification unit coupled with a Barnstead Diamond™ RO unit (Barnstead International, USA). GC grade OA (99%), palmitoyl chloride, and acetic acid (99%) were purchased from Sigma (USA). Boric acid, hydrochloric acid (HCl), potassium bromide, and acetone were obtained from Merck (Germany). Sodium hydroxide (NaOH) and sodium nitrite (NaNO₂) were purchased from Fluka (Switzerland). Deuterated acetic acid (CD₃COOD) and water (D₂O) were purchased from Armar Chemicals (Switzerland). Chitosan with an average molecular weight (MW_{avg}) of 150 kDa was obtained from Acros Organics (USA) and used as received.

2.2. Sample preparation

2.2.1. Preparation of water-soluble chitosan

The preparation of water-soluble chitosan was reported in previous works (Tan and Misran, in press). Briefly, 1% (w/v) of chitosan (MW_{avg} = 150 kDa) in 1% of acetic acid solution was prepared. 7 ml of 0.10 M of NaNO₂ was added dropwise into the chitosan solution under mechanical stirring. Then, the reaction mixture was stirred for 1 h. After that, the pH of the reaction mixture was adjusted to 8–9 in order to precipitate the undissolved chitosan. These undissolved chitosans were removed by filtration. The filtrate was neutralized to pH 7, and the remaining water soluble chitosan was precipitated by adding acetone. The precipitate was collected by using the centrifugation method at 5000 rpm for 2 min at 25 °C. The collected precipitate was washed with chloroform and dried overnight under vacuum.

2.2.2. Preparation of *N*-palmitoyl chitosans (ChPs)

Two types of ChPs with different DA (ChP1 and ChP2) were prepared from the water-soluble chitosan. First, 1% (w/v) of water-soluble chitosan solution was prepared. Then, the pH of the chitosan solution was adjusted to 7 using 1 M of NaOH. 27 μ l and 55 μ l of palmitoyl chloride were added to the chitosan solution under magnetic stirring at room temperature to prepare ChP1 and ChP2, respectively. After 5 h, the mixtures were neutralized. ChP1 and ChP2 were precipitated using acetone. ChP1 and ChP2 were collected by the centrifugation method at 5000 rpm for 2 min. ChP1 and ChP2 were washed repeatedly with chloroform to eliminate free fatty acid. Finally, the products were dried overnight under vacuum.

2.2.3. Preparation of ChP-coated OA liposomes

30 mM of OA liposome solution was prepared by dissolving an appropriate amount of OA in 50 mM of borate buffer (pH 8.8). ChP1 and ChP2 solutions with their concentration ranging from 0.05 to 0.30% (w/w) were prepared by dissolving an appropriate amount of ChP1 and ChP2 into 50 mM of borate buffer (pH 8.8). Then, the pH of OA liposome, ChP1 and ChP2 solutions was adjusted to 7 using 1 M

of HCl. The liposome solution was added dropwise into ChP1 and ChP2 solutions individually under magnetic stirring. These mixtures were stirred for 24 h at room temperature (25 °C). Then, the pH of the mixtures was adjusted to pH 8.8 for the formation of ChP-coated liposomes, OACHP1, and OACHP2. These liposome solutions were incubated at 25 °C for 24 h before analysis.

2.3. Characterization of ChP1, ChP2, and liposome solutions

2.3.1. Average molecular weight determination

The average molecular weight (MW) of chitosan was determined by the Static Light Scattering (SLS) method using a Malvern NanoSeries ZetaSizer (UK) (Wu et al., 1995).

2.3.2. Fourier-transform infrared (FT-IR) spectroscopy

FT-IR spectra for chitosan, ChP1, and ChP2 in the form of KBr disc were obtained using the Perkin Elmer spectrometer (model RX-1, USA). Water-soluble chitosan, ChP1, and ChP2 were mixed with KBr (1:100) and compressed into pellets before analysis. The resolution of the IR spectra was 4 cm⁻¹ and was recorded in 8 accumulations from 400 to 4000 cm⁻¹ in the transmittance mode. The DA of ChP1 and ChP2 was calculated from FT-IR spectra using the following equation (Kasaai, 2008):

$$DA(\%) = \left(\frac{A_{1655}}{A_{3450}} \right) \times \frac{100}{1.33}$$

A_{1655} and A_{3450} are the intensity of the peak at 1655 cm⁻¹ and 3450 cm⁻¹ in FT-IR spectra, respectively.

2.4. ¹H NMR spectroscopy

The sample for ¹H NMR analysis was prepared by dissolving 10 mg of chitosan and ChP into 1 ml of 2% of CD₃COOD in D₂O solution. ¹H NMR spectra for all samples were acquired using a JEOL JNM-GSX 270 FT NMR spectrometer (270 MHz) at 20 °C.

2.5. Estimation of chitosan solubility

The solubility of water-soluble chitosan, ChP1, and ChP2 in water was determined using a UV-Vis spectrophotometer. First, a series of the water-soluble chitosan, ChP1, and ChP2 solutions with different concentrations was prepared. Calibration curves for the water-soluble chitosan, ChP1, and ChP2 were constructed by plotting the intensity of the absorption peak at wavelength 274 nm versus the concentration. Saturated chitosan, ChP1, and ChP2 solutions were then prepared, and their UV-Vis absorption was determined. The solubility of the chitosan, ChP1, and ChP2 solutions was estimated by the extrapolation method of the calibration curve.

2.6. Size and zeta potential

The size and zeta potential of the prepared liposomes were measured using a Malvern NanoSeries ZetaSizer (Malvern, UK) at a constant temperature of 25 °C. Size and zeta potential of the prepared liposome were monitored over 30 days of storage time.

2.7. Optical polarizing microscope imaging (OPM)

The OPM micrographs of the prepared liposomes were captured using a Leica Polarizing Microscope equipped with a Leica QWin software. All measurements were performed at a temperature of 25 °C.

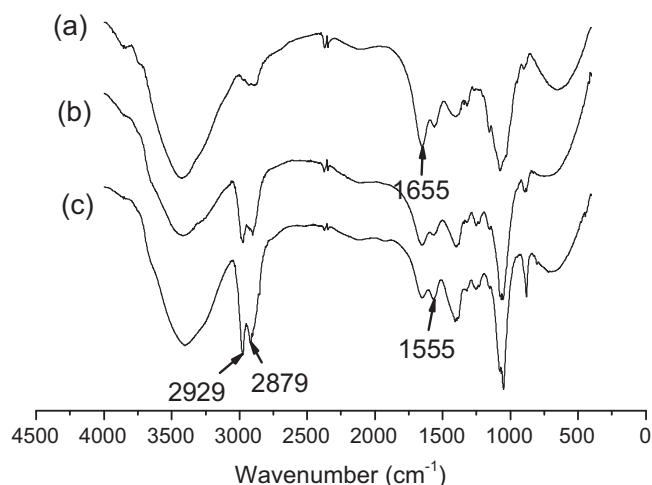


Fig. 1. FT-IR spectra of (a) chitosan, (b) ChP1 (DA=18±2%), and (c) ChP2 (DA=28±2%).

2.8. Transmission electron microscope imaging (TEM)

An Energy-filtered TEM model LIBRA 120 equipped with an Olympus SIS-iTEM (ver. 5) was employed to analyze the image of the prepared liposomes. A drop of the liposome solution was placed onto a copper-coated carbon grid followed by the removal of excess dispersed medium using a filter paper. Then, a drop of negative staining reagent (1% of phosphotungstic acid in 50 mM of borate buffer solution (pH 8.8)) was added, and the sample was air dried at room temperature for 25 min. The sample was then examined under TEM.

2.9. AFM imaging

AFM micrographs of the liposomes were captured by using an AFM Nanoscope III, Model MMAFM-2 (Digital Instruments, USA). All imaging was performed via the tapping mode with an integrated pyramidal-tip aluminum cantilever (BS-Multi75Al) (Vermette et al., 2002). The samples were prepared by placing a drop of the liposome solutions onto a freshly cleaved mica surface.

The dispersing medium was removed by air drying (Paleos et al., 1996).

2.10. Surface tension

The rigidity of the liposomes was investigated by studying the effect of ChP1 and ChP2 on the critical vesicular concentration (CVC) of the liposome solutions. The surface tension of a series of liposome solutions with different concentrations was determined by du Noüy ring method using a Krüss Tensiometer (Model K100, Germany) at 25 °C. The prepared liposome solutions were diluted using 50 mM of borate buffer (pH 8.8) and were incubated overnight at 25 °C before measurement. Surface tension of the prepared solution was determined using 20 successive measurements, and the standard deviation was calculated.

3. Results and discussion

3.1. Characterization of water-soluble chitosan, ChP1, and ChP2

The average molecular weight, solubility and DA of the water-soluble chitosan, ChP1, and ChP2 was listed in Table 1. The solubility of hydrophobized chitosan was decreased by increasing DA. This was due to the increase in the number of hydrophobic moieties, which reduced the solubility of the ChPs (Hirano et al., 2002).

3.2. FT-IR analysis

The absorption peak at 1655 cm⁻¹ was assigned as the carbonyl stretching of secondary amides, and the peak at 1555 cm⁻¹ was attributed to the N–H bending vibration of the amide II band (Xu et al., 1996). Referring to the FT-IR spectra of chitosan and ChPs (Fig. 1), the intensity of the absorption peak for N–H bending of amide II was increased by increasing DA. In addition, the absorption peaks at 2879–2929 cm⁻¹ were assigned as the –CH stretching of the alkyl chain (Tien et al., 2003). These results clearly confirmed that the chitosan was successfully modified.

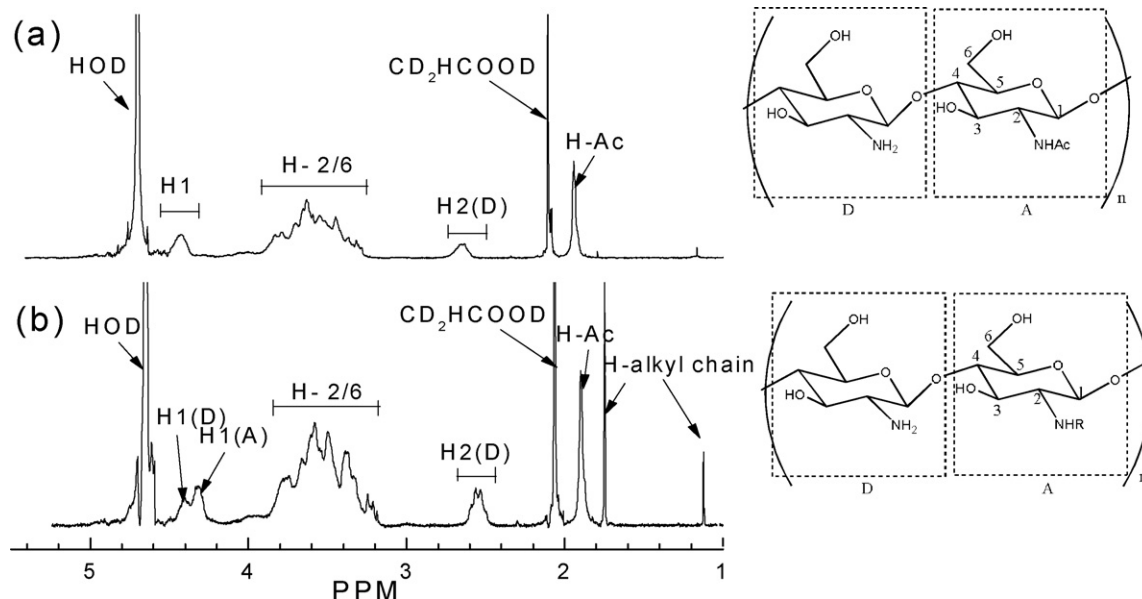


Fig. 2. NMR spectra for (a) water soluble chitosan and (b) ChP2 where D is the glucosamine group and A is the N-acetyl or N-acyl glucosamine group of the chitosan.

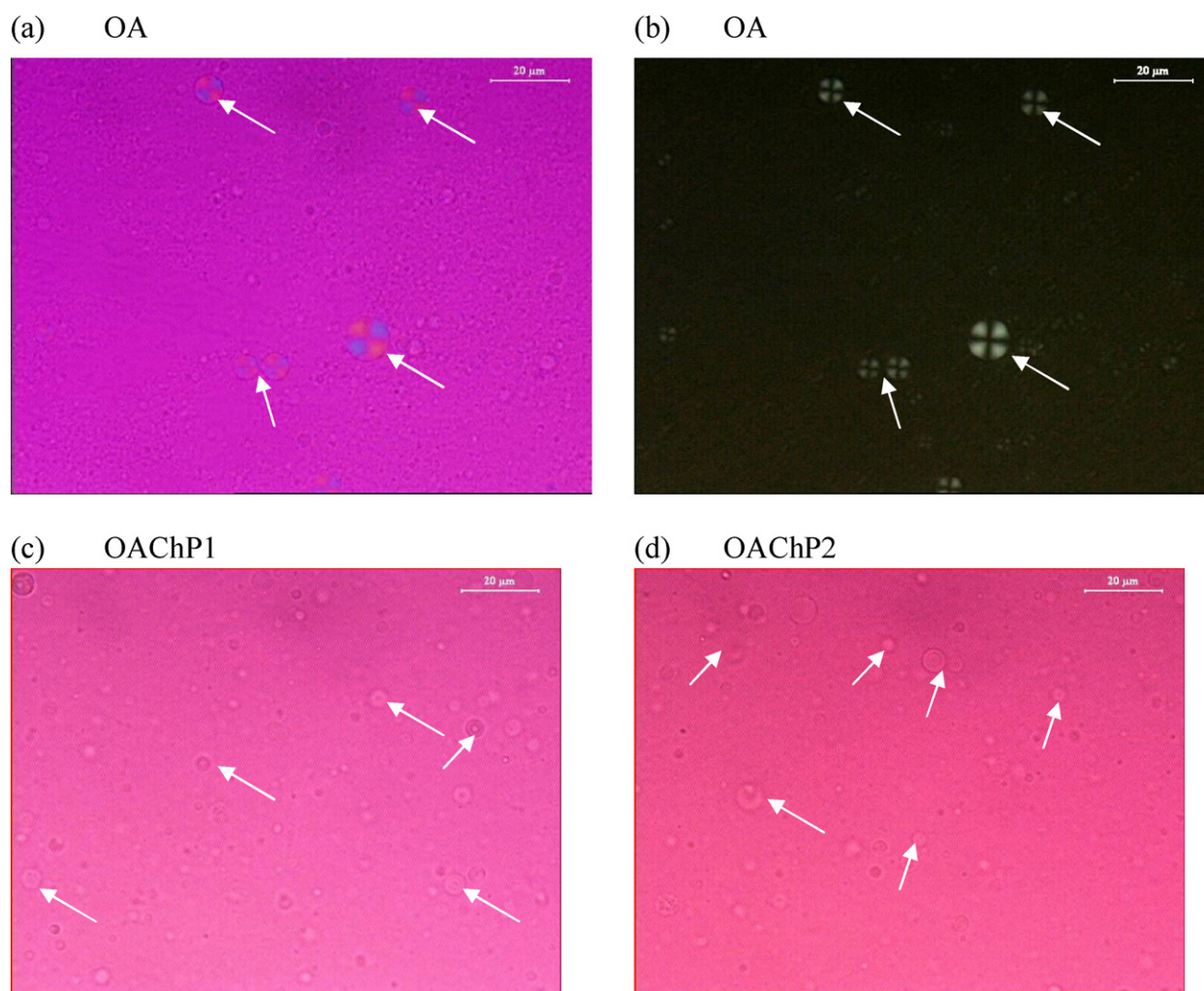


Fig. 3. The OPM micrograph of (a) OA liposome which showed birefringence effect, (b) OA liposome under dark field which showed Maltese cross, (c) OACHP1 liposome, and (d) OACHP2 liposome.

3.3. ^1H NMR analysis

The ^1H NMR spectra of the water-soluble chitosan and ChP2 are presented in Fig. 2. The proton of solvent (HOD) and acetic acid resonates at 4.65 and 2.11 ppm, respectively. The proton assignment of water-soluble chitosan (Fig. 2(a)): $\delta_{1.92} = \text{CH}_3$ (acetyl group of chitosan); $\delta_{2.5-2.1} = \text{CH}$ (carbon 2 of chitosan); $\delta_{4.1-3.1} = \text{CH}$ (carbon 2–6 of chitosan); and $\delta_{4.5-4.3} = \text{CH}$ (carbon 1 of chitosan). The proton assignment of ChP (Fig. 2(b)): $\delta_{1.1} = \text{CH}_3$ (alkyl chain); $\delta_{1.7} = \text{CH}_2$ (alkyl chain); $\delta_{1.92} = \text{CH}_3$ (acetyl group of chitosan); $\delta_{2.5-2.1} = \text{CH}$ (carbon 2 of chitosan); $\delta_{4.1-3.1} = \text{CH}$ (carbon 2–6 of chitosan); and $\delta_{4.5-4.3} = \text{CH}$ (carbon 1 of chitosan) (Li et al., 2006). The peak assignment was based on previous works (Li et al., 2006; Rinaudo et al., 1992). The NMR spectrum of ChP confirmed the modification of water-soluble chitosan with palmitoyl chloride. New peaks at 1.10

and 1.7 ppm that were observed from the ^1H NMR spectra of ChP2 were due to the $-\text{CH}_2-$ and $-\text{CH}_3$ protons of the long alkyl chain.

3.4. Micrographs of chitosan-coated liposomes

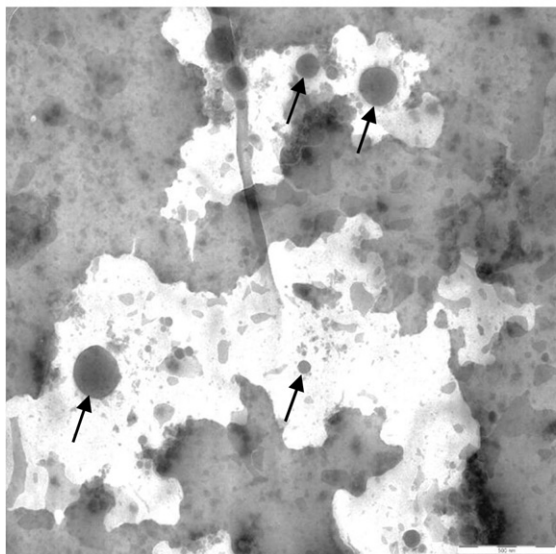
The appearance of OACHP1 and OACHP2 was evaluated using OPM, TEM, and AFM. According to the micrographs obtained from the OPM, all liposomes exhibited a spherical morphology (Fig. 3). Compared with the OA liposome, OACHP1 and OACHP2 liposomes do not exhibit any birefringence effect (Fig. 3(c) and (d)) and Maltese cross at dark field. The hydrophobic moieties anchored into the monolayer of the liposome bilayer and disturbed the arrangement of the OA monomers (Sessa and Weissmann, 1968).

The TEM micrographs clearly showed that the OACHP1 and OACHP2 were spherical in shape (Fig. 4(a) and (b)). The presence

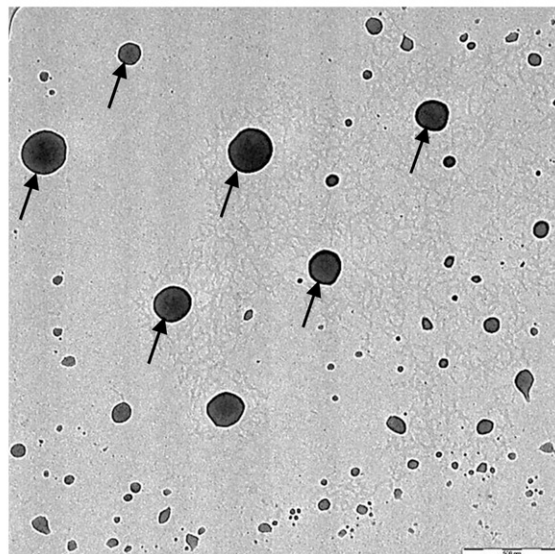
Table 1
Average molecular weight, water solubility and DA of the water soluble chitosan, ChP1 and ChP2.

Sample	Average molecular weight, MW_{avg} (kDa)	Water solubility (g/L)	DA (%)
Water soluble chitosan	25	5.60	10
ChP1	29	4.29	18
ChP2	32	2.62	28

(a) OACHP1



(b) OACHP2



(c) OA

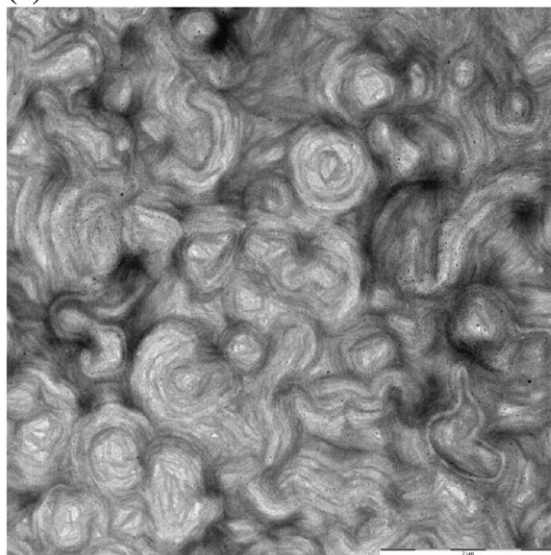


Fig. 4. TEM micrograph of (a) OACHP1, (b) OACHP2, and (c) OA liposome. The amount of hydrophobized-chitosan used in the preparation of the OACHPs liposome was 0.15%.

of the hydrophobized-chitosan layer on the lipid layer of the OA liposome thickened the lipid layer and increased the opacity. Thus, the surface of OACHP1 and OACHP2 liposomes appeared to be black in color (Wang et al., 2010). However, the OA liposome was not observed under TEM. The structure of the OA liposome was found to collapse under TEM (Fig. 4(c)) (Tan and Misran, in press). The collapse of the structure of the OA liposome might be due to the drying process or vacuum. This result indicated that the OA liposome bilayer is less rigid as compared with the OACHP liposomes (Tan and Misran, in press). For the AFM image, the OA liposome was hardly seen (Fig. 5(a)). The breakdown of the OA liposome under AFM imaging further indicated that the structure of the liposome was damaged due to the drying condition, as vacuum is not required for AFM imaging. These results revealed that the presence of ChP on the surface of the OA liposome enhanced the stability and rigidity of liposomes (Sihorkar and Vyas, 2001). As compared with the OA liposome, the ChP-coated liposomes can be seen as being spherical in shape. In addition, the ChP-coated liposomes showed “peeling off” effect on the surface (Fig. 5). This

result showed that ChP1 and ChP2 were anchored on the surface of liposomes.

3.5. Liposome size and zeta potential

The size of OACHP1 and OACHP2 liposomes was found to be at least 30 nm smaller than that of the OA liposome (Fig. 6). The decrease in the size of OACHP1 and OACHP2 liposomes was mainly due to the anchored ChPs that perturbed the OA monomer arrangement at the liposome bilayer. The insertion of the hydrophobic moieties of ChP into the liposome bilayer has resulted in increased curvature and decreased size of the liposomes (Fig. 7) (Park et al., 2011). The effect of the amount of ChP1 and ChP2 on the size of the OACHPs liposome was evaluated at day 7 (Fig. 6). The OACHP1 and OACHP2 liposomes was found to exhibit two different size profiles with increasing amount of ChPs. The size of OACHP1 liposome was decreased with increasing amount of ChP1 from 0 to 0.15% (w/w) but increased when the amount of ChP1 exceeded 0.15% (w/w) (Fig. 6(a)). This result indicated that more ChP1 layers were

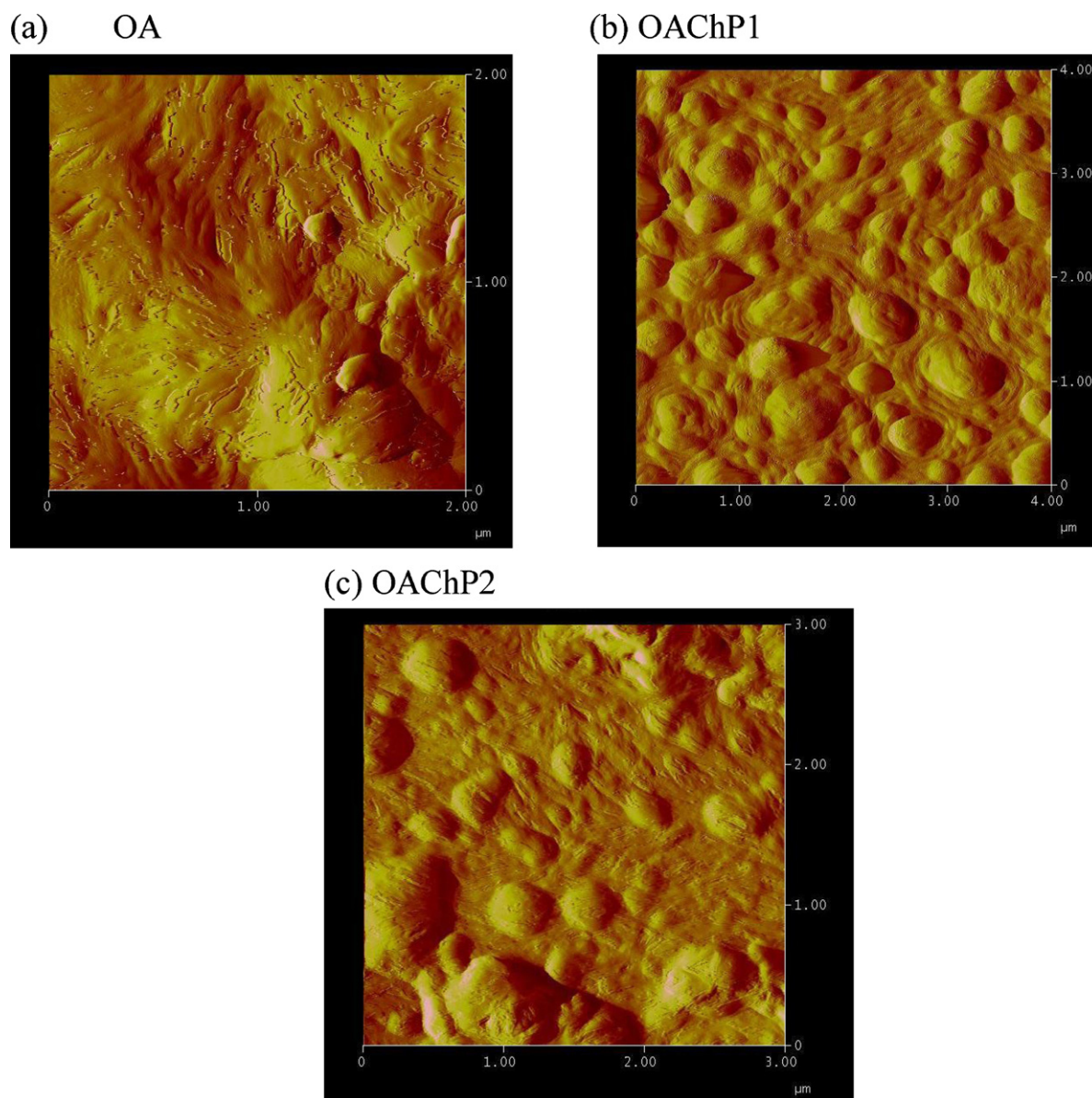


Fig. 5. AFM image of (a) OA liposome, (b) OACHP1 liposome (0.20% ChP1), and (c) OACHP2 liposome (0.15% ChP2).

Table 2

Γ_{max} , A_{min} , γ , and CVC of OA, OACHP1, and OACHP2 liposome solution obtained at controlled temperature of 25 °C.

Sample	Surface excess concentration, $\Gamma_{max} (\times 10^{-6})$	Molecular area per head group, $A_{min} (\text{\AA}^2)$	Surface tension obtained at 100 μM , γ , (mN/m)	CVC (μM)
OA	3.03	54.90	25.60	100
OACHP1-3	3.04	54.46	29.82	71.46
OACHP1-5	2.67	62.21	31.02	65.84
OACHP1-10	2.56	65.14	32.15	57.55
OACHP1-15	2.66	62.42	30.64	62.47
OACHP1-20	2.55	65.23	31.42	60.01
OACHP1-25	2.59	64.12	31.43	67.66
OACHP2-3	2.88	57.72	27.76	70.00
OACHP2-5	2.79	59.48	29.50	67.53
OACHP2-10	2.42	68.62	30.19	54.75
OACHP2-15	2.40	69.30	29.92	52.33
OACHP2-20	2.43	68.21	30.40	55.71
OACHP2-25	2.35	70.69	31.54	62.88

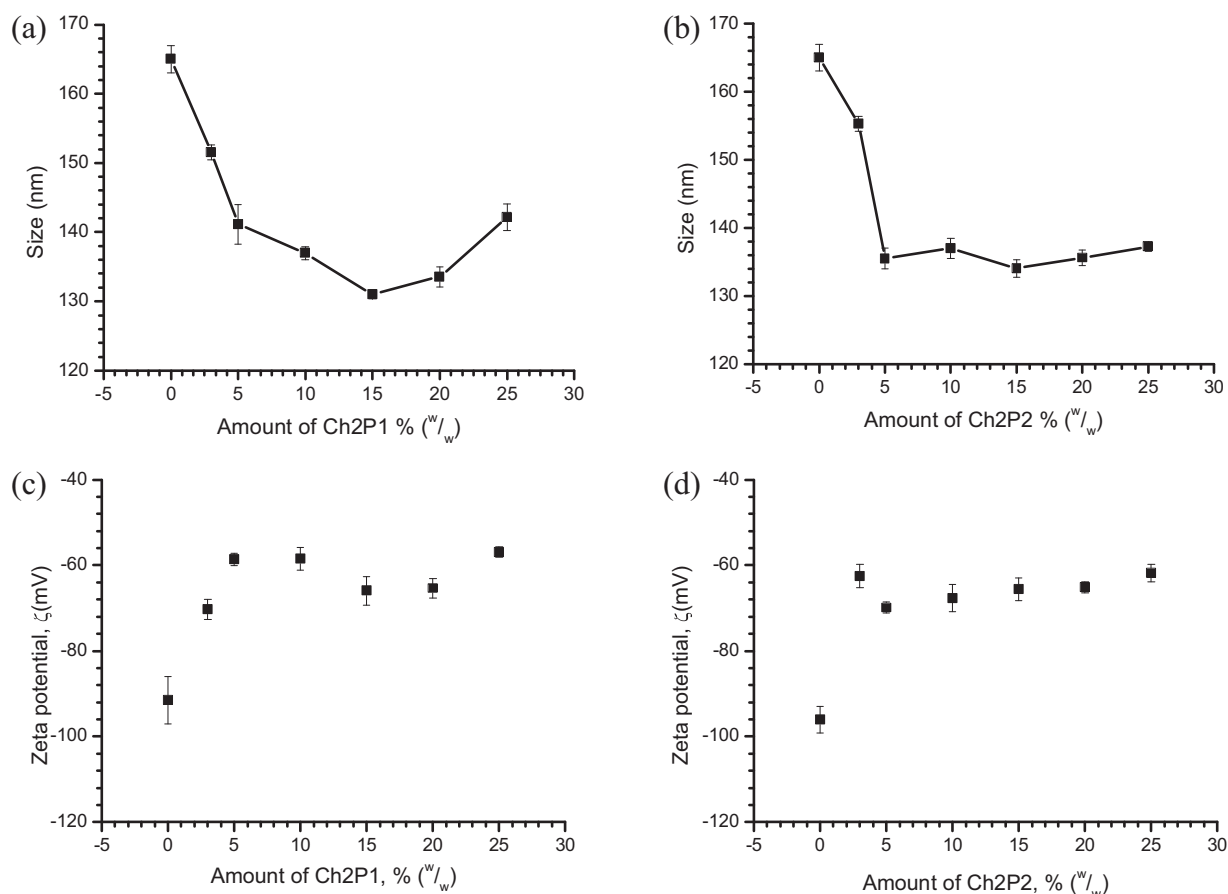


Fig. 6. Effect of (a) ChP1 and (b) ChP2 amount on the size of the OA liposome. The effect of (c) ChP1 and (d) ChP2 amount of the zeta potential of the OA liposome.

condensed onto the surface of the liposome (Guo et al., 2003). Similar results were also reported in the previous studies on the characterization of chitosan modified phospholipid liposome (Li et al., 2009; Liu and Park, 2010; Mady et al., 2009). For the OACHP2 liposome, the size was decreased from 165 nm to 136 nm when the amount of ChP2 increased from 0 to 0.05% (w/w) and the size remained unchanged when the amount of ChP2 exceeded 0.05% (w/w) (Fig. 6(b)). This result indicated that 0.05% (w/w) of ChP2 is sufficient to enhance the physical stability of the OACHP2 liposome. This was mainly attributed to the higher DA of ChP2. ChP2 has more alkyl side chains which are available to be inserted into the liposome lipid bilayer and improved the liposome membrane rigidity and integrity (Fig. 7) (Li et al., 2006).

Surface modification of the OA liposome by ChP1 and ChP2 was also evaluated by comparing its zeta potential before and after the

ChP incorporation (Takeuchi et al., 2003). The zeta potential of OA liposome was negatively charged. The zeta potential of OACHP1 and OACHP2 liposomes increased from -90.0 to -60.0 mV by increasing the amount of ChPs (Fig 6(c) and 6(d)). This result was attributed to the formation of a condensed coating of the ChP1 and ChP2 layers on the surface of the liposomes that has shielded the negative charge of the OA liposome (Li et al., 2009; Liu and Park, 2010; Mady et al., 2009).

3.6. Liposome stability

The stability of OACHP liposomes was evaluated through the monitoring of their size for 30 days of the storage period at 25°C . As an OA liposome, the size of the OACHP1 and OACHP2 liposomes was found to increase slowly for the first 7 days of storage time,

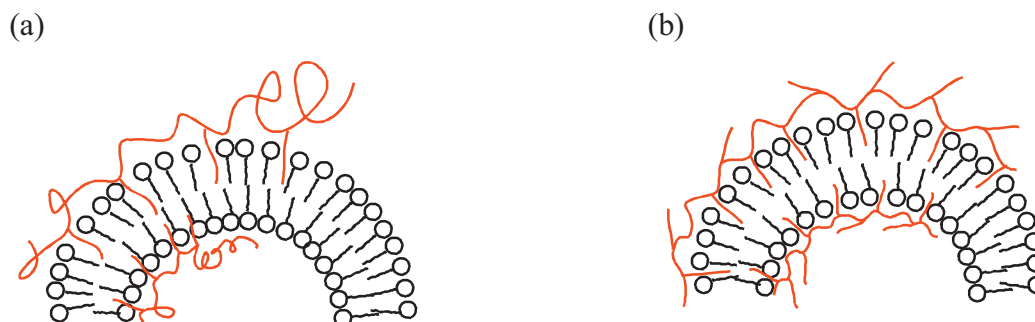


Fig. 7. Schematic illustration of the hydrophobic moieties of (a) ChP1 and (b) ChP2 anchored into the liposome lipid bilayer.

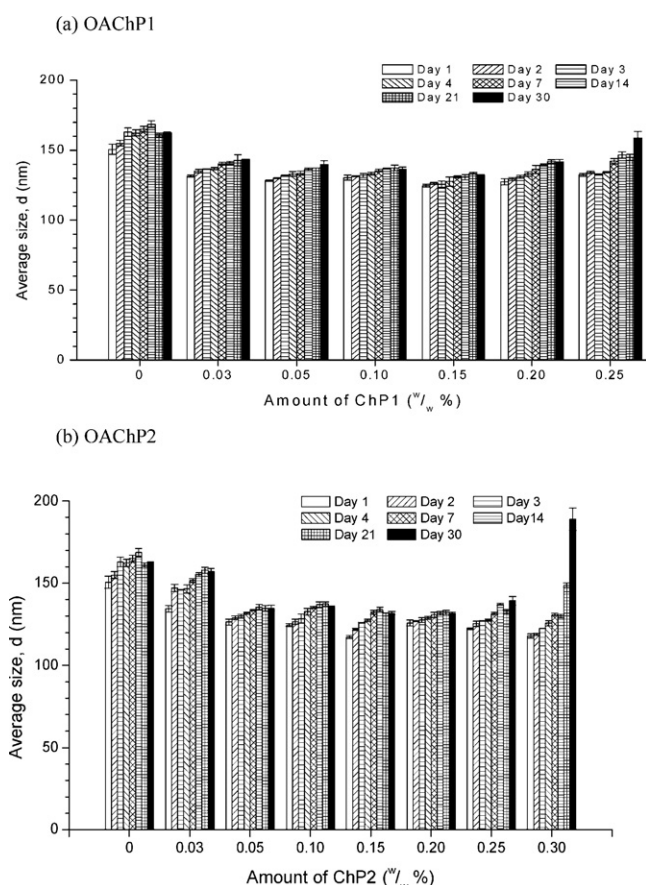


Fig. 8. Variation of size of (a) OACHP1 and (b) OACHP2 liposomes.

and this result has been attributed to the ChPs coating process that occurred at the surface of the liposome (Li et al., 2009). The size of all OACHP1 and OACHP2 liposomes remained unchanged after the 7th day of storage time except for the liposomes coated with 0.25% of ChP1 and 0.30% of ChP2 (Fig. 8). For the OACHP1 liposome that was coated with 0.25% of ChP1, the size of the liposome was found to increase from 140 nm to 160 nm after 30 days of the storage period, while the size of OACHP2 liposome that coated with 0.30% of ChP2 was found to increase dramatically from 125 nm to 190 nm after 30 days of the storage period. These results might due to the presence of excess ChPs that promote the coagulation process of liposomes (Tan and Misran, in press).

3.7. Surface tension

A surface tension (γ) versus \ln [concentration] was plotted for the determination of CVC of the prepared liposomes (Leclercq et al., 2009). Two different surface tension profiles were observed for the OA and OACHPs liposomes. The γ profile for the OA liposome exhibited two inflection points (Fig. 9(a)). These inflection points were characterized as the critical aggregation concentration (CAC). The CAC₁ is considered the CVC, because it corresponds to the formation of the OA liposome. A previous work has proposed that the formation of these inflection points was mainly due to the rearrangement of the OA monomer at the liposome bilayer (Tan and Misran, in press). For the OACHPs liposome, the γ profile of OACHPs liposomes showed only one inflection point (Fig. 9(a) and (b)). The changes in the profile of the OACHPs liposome as compared with the OA liposome were mainly attributed to the presence of ChPs. A strong hydrophobic interaction between the alkyl side chains of the ChPs with OA promotes the tighter

lipid layer arrangement and increases the membrane rigidity (Park et al., 2011). The increase in the membrane rigidity of OACHPs liposomes has limited the rearrangement of the OA monomer, resulting in the slower dynamic exchange rate of the OA monomer in the membrane with the OA monomer in the bulk phase (Fig. 9).

By comparing the γ of OA, OACHP1, and OACHP2 liposomes, the γ of OACHP1 and OACHP2 liposomes was found to be slightly higher than that of the OA liposome (Fig. 9(a)). The increase in the γ with the presence of ChPs in the solution suggested that the OA monomers are bound to the ChPs and are further removed from the surface into the bulk phase (Asnacios et al., 2000). As compared with the OACHP1 liposome, the γ of the OACHP2 was found to be lower after the CVC. This result was mainly due to the difference in the surface activity of ChP1 and ChP2. According to the experimental result, the γ decreased with an increase in DA (ChP1 = 0.0696 ± 0.0005 N/m and ChP2 = 0.0674 ± 0.0008 N/m). This result indicated that ChP2 has greater surface activity as compared with ChP1 (Li et al., 2006).

The CVCs of the OACHPs were slightly decreased as compared with the OA liposome (Table 2). In order to explain this result, the A_{min} that was occupied by OA at the air–water interface and the surface excess concentration (Γ_{max}) were calculated. Since the liposome started forming at CVC₁, A_{min} and Γ_{max} were obtained using the first slope before CVC₁. A_{min} values were determined using Gibbs adsorption isotherm as described by the following equation (Goddard, 2002):

$$A_{min} = \frac{1}{N_A \cdot \Gamma_{max}} \quad (1)$$

where N_A is the Avogadro's number. The Γ_{max} was calculated using the Gibbs adsorption equation as described by the following equation (Goddard, 2002):

$$\Gamma_{max} = \left(\frac{1}{nRT} \right) \left(\frac{d\gamma}{d \ln C} \right) \quad (2)$$

where n is the number of molecular species involved, and C is the concentration of OA. The liposome solutions were prepared at pH 9, where the OA was partially ionized; therefore, n equal to 2 was used in the calculation of Γ_{max} .

The A_{min} value obtained from the OA liposome solution was lower than the values of OACHP1 and OACHP2 (Table 2). This result suggested that the OA monomers in the OA liposome solution were more closely packed at the air–water interface as compared with OACHP1 and OACHP2 liposome solutions (Ghosh et al., 2010). This result showed that the ChP1 and ChP2 that anchored to the OA monolayer have disturbed the packing of the OA molecules, thus resulting in an increase in A_{min} (Fig. 9 and Table 2).

The effect of the amount of ChP1 and ChP2 used to prepare OACHP1 and OACHP2 liposomes on the γ at CVC was negligible except for the liposome coated with 0.03% (w/w) of ChPs (Table 2). In average, the γ of OACHP1 and OACHP2 were 31.3 ± 0.5 mN/m and 29.7 ± 0.5 mN/m, respectively. However, the γ of the OACHP1 and OACHP2 liposome coated with 0.03% (w/w) ChP1 and ChP2 was 2 mN/m lower as compared with those coated with higher amount of ChP1 and ChP2. This result indicated that there were more OA monomers adsorbed at the air–water interface. Greater amounts of OA monomers present at the air–water interface showed that 0.03% of ChPs are insufficient to bind to the OA monomers and to further remove the OA monomer from the air–water interface.

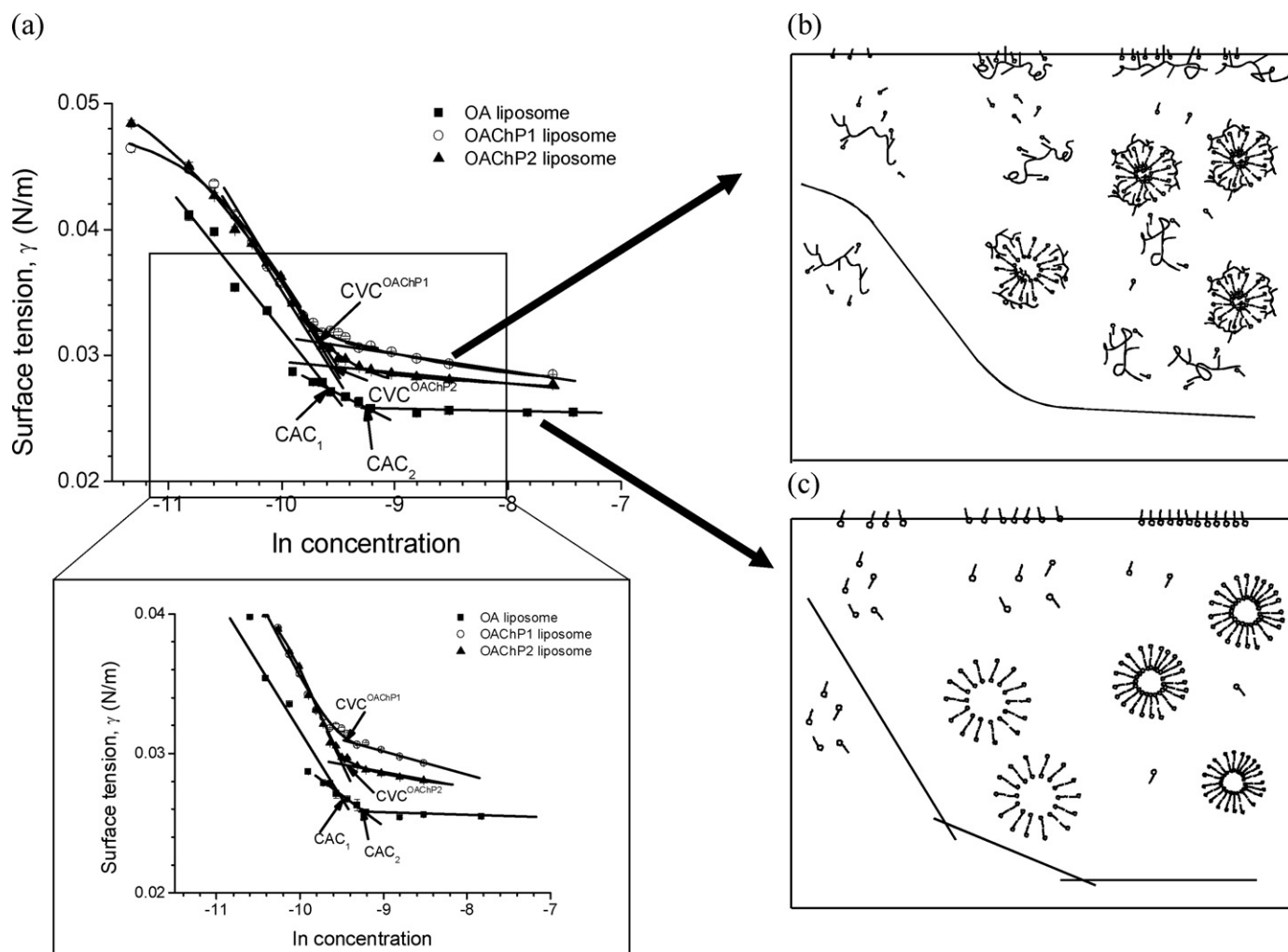


Fig. 9. Surface tension profile of the (a) OA, OACHP1 (0.15% ChP1), and OACHP2 (0.15% ChP2) liposome solutions (a). Schematic illustration on the bulk and surface conditions of (b) OACHP liposome solution and (c) OA liposome solution.

4. Conclusion

This study demonstrated the preparation of ChP-anchored OA liposomes. The decrease in the size and zeta potential of the OACHP1 and OACHP2 liposomes indicated that the ChPs successfully modified the surface of the OA liposome. According to the micrographs obtained from AFM and TEM, the OACHP1 and OACHP2 liposomes retained their spherical shape. Results also indicated that the anchored ChPs can improve the integrity and rigidity of the OA liposome. The γ of the OACHPs liposome solutions was increased as compared with the OA liposome solution. The increase in the γ of the OACHPs liposome solutions indicated that the ChPs was bound to the OA monomer. The increase in the A_{min} of the OA in the presence of ChPs has further proved the interaction between the OA monomer and the hydrophobic moieties of the ChPs.

Acknowledgement

We would like to extend our gratitude to University of Malaya for providing us financial support (PPP, No. PS437/2010A, and PV004/2012A).

References

- Abeygunawardana, C., Bush, C.A., 1991. Complete structure of the cell surface polysaccharide of *Streptococcus oralis* ATCC 10557. A receptor for lectin-mediated interbacterial adherence. *Biochemistry* 30, 6528–6540.
- Asnacios, A., Klitzing, R., Langevin, D., 2000. Mixed monolayers of polyelectrolytes and surfactants at the air–water interface. *Colloids Surf. A* 167, 189–197.
- Bastiat, G., Olliger, P., Karlsson, G., Edwards, K., Lafleur, M., 2007. Development of non-phospholipid liposomes containing a high cholesterol concentration. *Langmuir* 23, 7695–7699.
- Battaglia, G., Ryan, A.J., 2009. Pathways of polymeric vesicle formation. *J. Phys. Chem. B* 110, 10272–10279.
- Chan, P., Kurisawa, M., Chung, J.E., Yang, Y.Y., 2007. Synthesis and characterization of chitosan-g-poly(ethylene glycol)-folate as a non-viral carrier for tumor-targeted gene delivery. *Biomaterials* 28, 540–549.
- Dicorleto, P.E., De La Motte, C., 1989. Role of cell surface carbohydrate moieties in monocyte cell adhesion to endothelium in vitro. *J. Immunol.* 143, 3666–3672.
- Discher, D.E., Eisenberg, A., 2002. Polymer vesicles. *Mater. Sci. Soft Surf.* 297, 967–973.
- Garg, M., Dutta, T., Jain, N.K., 2007. Stability study of stavudine-loaded O-palmitoyl-anchored carbohydrate-coated liposomes. *AAPS PharmSciTech* 8, Article 38.
- Ge, L., Zhu, J.B., Xiong, F., Ni, B., 2007. Preparation, characterization and pharmacokinetics of N-palmitoyl chitosan anchored docetaxel liposomes. *J. Pharm. Pharmacol.* 59, 661–667.
- Ghosh, A., Shrivastava, S., Dey, J., 2010. Concentration and pH-dependent aggregation behavior of an L-histidine based amphiphile in aqueous solution. *Chem. Phys. Lipids* 163, 561–568.
- Goddard, E.D., 2002. Polymer/surfactant interaction: interfacial aspects. *J. Colloid Interface Sci.* 256, 228–235.
- Guo, J., Pin, Q., Jiang, G., Huang, L., Tong, Y., 2003. Chitosan-coated liposomes: characterization and interaction with leuprolide. *Int. J. Pharm.* 260, 167–173.

- Gupta, R.K., Varanelli, C.L., Griffin, P., Wallach, D.F.H., Siber, G.R., 1996. Adjuvant properties of non-phospholipid liposome (novasomes) in experimental animals for human vaccine antigen. *Vaccine* 14, 219–225.
- Hirano, S., Yamaguchi, Y., Kamiya, M., 2002. Novel N-saturated-fatty-acyl derivatives of chitosan soluble in water and in aqueous acid and alkaline solutions. *Carbohydr. Polym.* 48, 203–207.
- Illum, L., 1998. Chitosan and its use as a pharmaceutical excipient. *Pharm. Res.* 15, 1326–1331.
- Kasaai, M.R., 2008. A review of several reported procedures to determine the degree of N-acetylation for chitin and chitosan using infrared spectroscopy. *Carbohydr. Polym.* 71, 497–508.
- Kubota, N., Tatsumoto, N., Sano, T., Toya, K., 2000. A simple preparation of half N-acetylated chitosan highly soluble in water and aqueous organic solvents. *Carbohydr. Res.* 324, 268–274.
- Leclercq, L., Nardello-Rataj, V., Turmine, M., Azaroual, N., Aubry, J., 2009. Stepwise aggregation of dimethyl-di-n-actylammonium chloride in aqueous solutions: from dimer to vesicles. *Langmuir* 26, 1716–1723.
- Lee, M.Y., Hong, K.J., Kajiuchi, T., Yang, J.W., 2005. Synthesis of chitosan-based polymeric surfactants and their adsorption properties for heavy metals and fatty acids. *Int. J. Biol. Macromol.* 36, 152–158.
- Li, N., Zhuang, C.Y., Wang, M., Sun, X.Y., Nie, S.F., Pan, W.S., 2009. Liposome coated with low molecular weight chitosan and its potential use in ocular drug delivery. *Int. J. Pharm.* 379, 131–138.
- Li, Y.Y., Chen, X.G., Yu, L.M., Wang, S.X., Sun, G.Z., Zhou, H.Y., 2006. Aggregation of hydrophobically modified chitosan in solution and at air–water interface. *J. Appl. Polym. Sci.* 102, 1968–1973.
- Liu, N., Park, H.J., 2010. Factors effect on the loading efficiency of Vitamin C loaded chitosan-coated nanoliposomes. *Colloids Surf. B* 76, 16–19.
- Liu, R.Z., Gan, L., Yang, X.L., Xu, H., 2011. Chitosan as a condensing agent induces high gene transfection efficiency and low cytotoxicity of liposome. *J. Biosci. Bioeng.* 111, 98–103.
- Mady, M.M., Darwish, M.M., Khalil, S., Khalil, W.M., 2009. Biophysical studies on chitosan-coated liposomes. *Eur. Biophys. J.* 38, 1127–1133.
- Mourya, V.K., Inamdar, N.N., Tiwari, A., 2010. Carboxymethyl chitosan and its applications. *Adv. Mater. Lett.* 1, 11–33.
- Mufamadi, M.S., Pillay, V., Choonara, Y.E., Tolt, L.C.D., Girish, M., Naidoo, D., Ndesendo, V.M.K., 2011. A review on composite liposomal technologies for specialized drug delivery. *J. Drug Deliv.* 2011, Article ID 939851.
- Ortona, O., D'errico, G., Mangiapia, G., Ciccarelli, D., 2008. The aggregation behavior of hydrophobically modified chitosans with high substitution degree in aqueous solution. *Carbohydr. Polym.* 74, 16–22.
- Paleos, C.M., Sideratou, Z., Tsiourvas, D., 1996. Mixed vesicles of didodecyltrimethylammonium bromide with recognizable moieties at the interface. *J. Phys. Chem.* 100, 13900–13989.
- Palte, M.J., Raines, R.T., 2012. Interaction of nucleic acids with the glycocalyx. *J. Am. Chem. Soc.* 134, 6218–6223.
- Parabakaran, M., 2008. Review paper: chitosan derivatives as promising materials for controlled drug delivery. *J. Biomater. Appl.* 23, 5–36.
- Park, S.I., Lee, E.O., Kim, J.W., Kim, Y.J., Han, S.H., Kim, J.D., 2011. Polymer-hybridized liposomes anchored with alkyl grafted poly(asparagine). *J. Colloid Interface Sci.* 364, 31–38.
- Qu, G.W., Wu, X.L., Yin, L.F., Zhang, C., 2012. N-octyl-O-sulfate chitosan-modified liposomes for delivery of docetaxel: preparation, characterization, and pharmacokinetics. *Biomed. Pharmacother.* 66, 46–51.
- Rinaudo, M., Le Dung, P., Gey, C., Milas, M., 1992. Substituent distribution on ON-carboxymethylchitosans by ^1H and ^{13}C n.m.r. *Int. J. Biol. Macromol.* 14, 122–128.
- Riva, R., Ragelle, H., Des Rieux, A., Duhem, N., Jérôme, C., Préat, V., 2011. Chitosan and chitosan derivatives in drug delivery and tissue engineering. *Adv. Polym. Sci.* 244, 19–44.
- Sessa, G., Weissmann, G., 1968. Phospholipid spherules (liposomes) as a model for biological membranes. *J. Lipid Res.* 9, 310–318.
- Sheng, Y., Liu, C.S., Yuan, Y., Tao, X.Y., Yang, F., Shan, X.Q., Zhou, H.J., Xu, F., 2009. Long-circulating polymeric nanoparticles bearing a combinatorial coating of PEG and water-soluble chitosan. *Biomaterials* 30, 2340–2348.
- Sihorkar, V., Vyas, S.P., 2001. Potential of polysaccharide anchored liposomes in drug delivery, targeting and immunization. *J. Pharm. Pharm. Sci.* 4, 138–158.
- Sunamoto, J., Iwamoto, K., 1986. Protein anchored and polysaccharide-anchored liposomes as drug carriers. *Crit. Rev. Ther. Drug Carrier Syst.* 2, 117–136.
- Sunamoto, J., Sato, T., Taguchi, T., Hamazaki, H., 1992. Naturally occurring polysaccharide derivatives which behave as an artificial cell wall on an artificial cell liposome. *Macromolecules* 25, 5665–5670.
- Takeuchi, H., Matsui, Y., Yamamoto, H., Kawashima, Y., 2003. Mucoadhesive properties of carbopol or chitosan-coated liposomes and their effectiveness in the oral administration of calcitonin to rats. *J. Control. Release* 86, 235–242.
- Tan, H.W., Misran, M., 2012. Characterization of fatty acid liposome coated with low molecular weight chitosan. *J. Liposome Res.*, <http://dx.doi.org/10.3109/08982104.2012.700459>, in press.
- Tien, C.L., Lacroix, M., Ispas-Szabo, P., Mateescu, M.A., 2003. N-acylated chitosan: hydrophobic matrices for controlled drug release. *J. Control. Release* 93, 1–13.
- Vermette, P., Meagher, L., Gagnon, E., Griesser, H.J., 2002. Immobilized liposome layers for drug delivery applications: inhibition of angiogenesis. *J. Control. Release* 80, 179–195.
- Wang, Y.S., Tu, S.L., Li, R.S., Yang, X.Y., Liu, G., Zhang, Q.Q., 2010. Cholesterol succinyl chitosan anchored liposomes: preparation, characterization, physical stability, and drug release behavior. *Nanomed. Nanotechnol.* 6, 471–477.
- Wang, Y.W., Jou, C.H., Hung, C.C., Yang, M.C., 2012. Cellular fusion and whitening effect of a chitosan derivative coated liposome. *Colloids Surf. B* 90, 169–176.
- Wu, C., Zhou, S., Wang, W., 1995. A dynamic laser light-scattering study of chitosan in aqueous solution. *Biopolymers* 35, 385–392.
- Wu, Y.S., Seo, T., Sasaki, T., Irie, S., Sakurai, K., 2006. Layered structures of hydrophobically modified chitosan derivatives. *Carbohydr. Polym.* 63, 493–499.
- Xu, J., McCarthy, S.P., Gross, R.A., 1996. Chitosan film acylation and effects on biodegradability. *Macromolecules* 29, 3436–3440.
- Zaru, M., Manca, M.L., Fadda, A.M., Antimisariis, S.G., 2009. Chitosan-coated liposomes for delivery to lungs by nebulisation. *Colloids Surf. B* 71, 88–95.